Tectono-stratigraphical evolution of the Çankırı Basin (Central Anatolia, Turkey)

Nuretdin Kaymakci

TECTONO-STRATIGRAPHICAL EVOLUTION OF THE ÇANKIRI BASIN (Central Anatolia, Turkey)

TECTONO-STRATIGRAFISCHE EVOLUTIE VAN HET ÇANKIRI BEKKEN
(Centraal Anatolië, Turkije)

(met een samenvatting in het Nederlands)

ÇANKIRI HAVZASININ TEKTONO-STRATİGRAFİK EVRİMİ
(Orta Anadolu, Tűrkiye)

(Tűrkçe Őz ile birlikte)

DOOR

Nuretdin Kaymakci

Geboren 5 maart 1965 te Beysehir (Turkije)

to my daughter Dilara

Members of the examining committee:

Prof. Dr. S.B. Kroonenberg Faculty of Civil Engineering and Geosciences
Delft University of Technology, The Netherlands

Prof. Dr. C.G. Langereis Department of Geophysics
Utrecht University, The Netherlands

Prof. Dr. R.J. Lisle Department of Earth Sciences
Cardiff University, Wales, UK

Prof. Dr. J.E. Meulenkamp Department of Stratigraphy
Utrecht University, The Netherlands

Prof. Dr. A.H. Robertson Department of Geology and Geophysics
University of Edinburgh, Scotland, UK

ACKNOWLEDGEMENTS

> *"…So close no matter how far*
> *couldn't be much more from the heart*
> *forever trusting who we are*
> *nothing else matters…*
> (Metallica)"

iii

Curriculum Vitae

1965   Born in Beyşehir, Turkey

1979-1982 Beyşehir High School, Turkey

1983-1989 B.Sc. in Geological Engineering, Geological Engineering Department, Middle East Technical University (METU), Ankara, Turkey

1989-1991 M.Sc. in Geological Engineering, Geological Engineering Department, METU, Ankara, Turkey

1989-1993 Teaching and Research assistantship at METU, Ankara, Turkey.

1993-1994 Postgraduate Diploma in Geological Survey, ITC-Enschede, The Netherlands

1995-2000 Ph.D. student, Geological Survey Division, ITC-Enschede, The Netherlands

TABLE OF CONTENTS

Chapter 8   *213*

References   *239*

TECTONO-STRATIGRAPHICAL EVOLUTION OF THE ÇANKIRI BASIN (Central Anatolia, Turkey)

Abstract

The Izmir-Ankara-Erzincan Suture Zone (IAESZ) demarcates the former position of the northern Neotethys ocean, along which the Sakarya Continent of the Pontides and the Kırşehir Block of the Taurides collided and amalgamated during the Late Cretaceous to pre-latest-Early Miocene (pre-Burdigalian) time interval. The Çankırı Basin lies within the IAESZ and between the Sakarya Continent in the north and the Kırşehir Block in the south. It is a unique area to study the subduction and collisionary processes as well as post-collisional history of the region through stratigraphical and structural analysis.

The overall aim of this research is to determine the tectono-stratigraphical evolution of the Çankırı Basin, based on the integration of data sets obtained from various geological and geophysical disciplines, including remote sensing, GIS (geographic information systems), stratigraphy, structural geology (including kinematic studies based on fault slip data), paleomagnetic studies, gravity and seismics.

The results of this study indicate that the Early Tertiary lithologies of the Çankırı Basin include units formed and deposited in various tectonic/depositional settings, ranging from accretionary wedge, fore-arc, to inter-arc to collisional settings, in which the depocentre migrated southwards towards the Kırşehir Block. The collision and indentation of the Kırşehir Block with the Sakarya Continent in the Late Paleocene to Oligocene gave rise to an anticlockwise rotation of the western rim and a clockwise rotation of the eastern rim, which subsequently resulted in the Ω-shape of the Çankırı Basin. The Neogene lithologies were deposited within an extensional setting in the latest-Early Miocene to Middle Miocene (Burdigalian to Serravallian) and a transcurrent regime from the Late Miocene onwards. In detail, the basin has experienced four phases of deformation, which reflect the above tectonic development. The first phase is associated with NW-SE thrusting and is attributed to the subduction phase. The second phase is characterized by a combination of thrusting in the northern area and transpressional deformation in the southern part of the Çankırı Basin. This second phase is attributed to the collision and indentation between the Sakarya Continent and the Kırşehir Block, during which the Çankırı Basin continued to evolve as a series of piggy-back basins. The third phase was characterized by extensional deformation and is interpreted to be the result of post-orogenic collapse enhanced by the 20 Ma to Recent decrease in the Africa-Eurasia convergence rate. The last phase is characterized by transcurrent tectonics and has been active since ca. 11.1 Ma to Recent. This last phase is controlled by the North Anatolian Fault Zone (NAFZ) and commenced with the Eurasia-Arabia collision along the Bitlis-Zagros Suture in south-eastern Turkey and the subsequent expulsion of Anatolia to the west.

TECTONO-STRATIGRAFISCHE EVOLUTIE VAN HET ÇANKIRI BEKKEN
(Centraal Anatolië, Turkije)

Samenvatting

De Izmir-Ankara-Erzincan Sutuur Zone (IAESZ) markeert de vroegere positie van de noordelijke Neotethys oceaan. Langs de IAESZ werden het Sakarya continent, behorende tot de Pontiden, en het Kırşehir Blok van de Tauriden samengevoegd. Dit proces van continentbotsing vond plaats tijdens het interval van Laat Krijt tot pre-laat Vroeg Mioceen (pre-Burdigalien). Het Çankırı Bekken bevindt zich in de IAESZ, met het Sakarya continent in het noorden en het Kırşehir Blok ten zuiden. Deze tektonische positie maakt het Çankırı Bekken tot een een uniek gebied om de processen van subductie en collisie, alsmede de post-collisie ontwikkeling van de regio, te bestuderen op basis van stratigrafische en structurele analyse.

De doelstelling van dit onderzoek is om de tektono-stratigrafische evolutie van het Çankırı Bekken te ontrafelen aan de hand van integratie van gegevens afkomstig uit verschillende geologische en geofysische diciplines, waaronder: remote sensing, GIS (geografische informatie systemen), stratigrafie, structurele geologie (met kinematische studies aan de hand van wrijfspiegels ten gevolge van breukbewegingen), paleomagnetische studies, seismiek en gravimetrie.

De resultaten van dit onderzoek geven inzicht in de tectonische evolutie van het Çankırı Bekken tijdens het Vroeg Tertiair. De mariene en continentale bekkenarchitectuur weerspiegelt de verschillende tektonische fasen met sedimentatie boven de subductie zone in een accretie prisma, ontwikkeling van een externe tot centrale eilandboog en tenslotte tot continentale collisie.

Tijdens deze ontwikkeling migreerde het depocentrum zuidelijk naar het Kırşehir Blok. De collisie en indentatie van het Kırşehir Blok met het Sakarya continent tijdens het Laat Paleoceen tot midden Oligoceen veroorzaakte een rotatie tegen de klok in van de westelijke rand en een rotatie met de klok mee van de oostelijke rand van het Çankırı Bekken, resulterend in de huidige Ω-vorm van de bekkenrand. De Neogene eenheden werden afgezet in een door rek gedomineerd tecktonisch regiem tijdens het laat Vroeg Mioceen tot Midden Mioceen (Burdigalien to Serravallien), en onder overwegend transversale bewegingen vanaf het Laat Mioceen tot Recent. De onderzochte structuren in het Çankırı Bekken zijn onderverdeeld in vier fasen die de hierboven beschreven tektonische ontwikkeling weergeven.

De eerste fase staat in verband met NW-SE gerichte overschuivingen, en wordt toegeschreven aan de periode van subductie. De tweede fase wordt gekenmerkt door een combinatie van overschuivingen in het noordelijke deel van het gebied, en transpressie in het zuidelijke gedeelte van het Çankırı Bekken. Deze tweede fase wordt gerelateerd aan de collisie en indentatie van het Kırşehir Blok met het Sakarya continent. Gedurende deze fase ontwikkelde het Çankırı Bekken zich verder als een serie dakpansgewijs gestapelde bekkens tussen overschuivingen. De derde fase werd gekarakteriseerd door afschuivingen en wordt geinterpreteerd als het resultaat van post-orogene daling, versterkt door de afnemende convergentiesnelheid tussen de Afrikaanse en de Europese plaat vanaf 20 Ma tot Recent. Deze laatste fase wordt beheerst door de Noord Anatolische Breukzone, en startte met de collisie van Eurazië en Arabië langs de Bitlis-Zagros sutuurzone in zuidoost Turkije wat de daaropvolgende westwaards gerichte uitdrijving van Anatolië tot gevolg had.

ÇANKIRI HAVZASININ TEKTONO-STRATİGRAFİK EVRİMİ
(Orta Anadolu, Türkiye)

Öz

Neotetis okyanusunun eski yerin belirleyen işaret eden İzmir-Ankara-Erzincan Kenet Kuşağı (İAEKK) boyunca, Torid kuşağı içersinde yer alan, Kırşehir Bloğu ile Pontid kuşağı içersinde yer alan Sakarya Kıtası, Geç Kretase ile geç-Erken Miyosen (Burdigalian) öncesi dönemde çarpışıp bütünleşmiştir. Çankırı Havzası İAEKK içersinde, Sakarya Kıtası'nın güneyinde ve Kırşehir Bloğu'nun kuzeyinde yer alır. Havza dalma-batma, çarpışma ve çarpışma sonrası everelere ait stratigrafik ve yapısal oluşumları çalışmak açısından ender bir yere sahiptir.

Bu araştırmanın ana hedefi; uzaktan algılama, coğrafi bilgi sistemleri (CBS), stratigrafi, (fay çiziklerine dayalı kinematik analizleride içeren) yapısal jeoloji, gavite, sismik verilerin yorumlanması ve paleo-magnetizmanında içinde olduğu bir çok jeolojik ve jeofizik yöntemden elde edilen verileri birleştirerek Çankırı Havzası'nın evrimini belirlemektir.

Bu çalışma göstermiştir ki; Çankırı Havzasının Neojen öncesi dolgusu, yığışım pirizmasndan başlıyarak yay-önü, yaylar-arası havzalara ve çökelme merkezinin güneye yani Kırşehir Bloğu'na doğru göç ettiği, çarpışma tipi havzalara kadar uzanan bir çok ortamda çökelmiştir. Geç Paleosen-Oligosen dönemde Kırşehir Bloğu'nun Sakarya Kıtası'na çarpması ve onu indente etmesi, Çankırı Havzası'nın batı kenarını saatin tersi yönde ve doğu kenarını saat yönünde döndürerek bu günkü Ω-şeklini almasına neden olmuştur.

Neojen çökeleri, geç-Erken Miyosen ile Orta Miyosen (Burdigalian ile Serravallian) zaman aralığında bir genişleme tektonik rejimi, Geç Miyosenden itibaren ise bir yanal atımlı tektonik rejim içersinde çokelmişlerdir. Daha detaylıca söylemek gerekirse, Çankırı Havzası yukarda bahsi geçen tektonik oluşumları da yansıtan dört değişik deformasyon evresinden geçmiştir. İlk evre, kuzeybatıdan güneydoğuya yönelimli bindirmelerle karakterize edilmiş olup dalma-batma dönemi ile ilişkilendirilmiştir. İkinci evre, kuzeyde bindirmeler ve güneyde transpresyonal hareketlerin birleşimi ile karakterize edilir. Bu ikinci evrede Çankırı Havzası bindirme-sırtı havza serileri olarak evrilmiş ve Kırşehir Bloğu'nun Sakarya Kıtası ile çarpışması ve indentasyonu evresine atfedilmiştir. Üçüncü evre, 20 milyon yıl öncesi başlamış olan, Afrika ile Avrasya arasındaki yaklaşma hızındaki azalmanın da katkısının olduğu bir çarpışma sonrası göçmeden kaynaklanan genişleme rejimini karakterize eder. Son evre, Geç Miyosenden günümüze kadar süre gelen bir yanal artımlı tektonikle karakterize edilir. Bu son evre, Türkiye'nin güneydoğusundaki Bitlis-Zagros Kenet Kuşağı boyunca Avrasya ile Arabistan çarpışması sonucu oluşmuş olan Kuzey Anadolu Fay Kuşağı ve Anadolu Bloğu'nun batıya doğru kaçışı ile denetlenmektedir.

1

INTRODUCTION

1.1 Preamble

The Izmir-Ankara-Erzincan Suture Zone (IAESZ) demarcates the former position of the northern Neotethys ocean. Along the IAESZ, the Rhodope-Pontide fragments and Taurides collided and amalgamated in the Early Tertiary, leaving behind a number of basins with a thick in-fill that was accumulated during the subduction and collision processes. The Çankırı Basin is one of the largest of such Tertiary basins in Turkey and is located within the IAESZ. It is a unique area to study the subduction and collisionary processes and post-collisional history of central Anatolia, owing to a nearly complete sedimentary record from Late Cretaceous to Recent.

This thesis presents an integrated study concerning the Late Cretaceous to Recent tectono-stratigraphical evolution of the Çankırı Basin using stratigraphical studies, structural geology, kinematic analysis, paleomagnetic studies, 3D modeling, seismic interpretation and gravimetric analysis.

Stratigraphical studies involved detailed investigation of the lateral and vertical changes in petrographical and sedimentological characteristics, facies geometry and facies associations in relation to tectonics.

Structural analysis is aimed to unravel the characteristics, style and pattern of deformation and to reveal how it evolved spatially and temporally, especially when combined with stratigraphical information. In this regard, paleostress analyses help to understand the kinematics and dynamics of deformation. Although there is no direct way to measure the magnitudes of paleostresses, it is possible to determine the *reduced paleostress tensor* which means that the direction and relative magnitudes of the three principal stresses ($\sigma_1 > \sigma_2 > \sigma_3$) and their spatial variations can be determined (Angelier et al. 1979, 1984, and 1989, Lisle 1987).

Rotational deformation, which can cause destruction of primary collinear relationships is difficult to deal with. Paleomagnetic studies provide the best tool to overcome this problem and to determine the sense and the amount of rotation, which helps to restore geological entities to their pre-deformation state, provided that paleomagnetic signatures were acquired during or prior to deformation.

Seismic sections, combined with the surface geology, provide the means for the construction of a 3D model of the subsurface and its interpretation. The constructed 3D models can be tested and improved by the gravimetric analysis.

1.2 Aims of This Research

The overall aim of this research are to determine the tectono-stratigraphical evolution of the Çankırı Basin in relation to the subduction of northern Neotethys and the syn- to post-collisional history of the surrounding continental fragments (the Sakarya Continent to the north and the Kırşehir Block to the south). The specific aims of this thesis are:

1. To provide temporal and spatial constraints for the tectono-stratigraphical evolution of the Çankırı Basin using sedimentological, stratigraphical, structural and kinematic data for its Late Cretaceous to Recent development.

2. To determine the evolution of the Çankırı Basin from the Late Cretaceous to Recent and to model this evolution.

3. To relate the tectono-stratigraphical development of the Çankırı Basin to the adjacent microcontinents. As part of the Tethys system, the information obtained from the Çankırı Basin together with the correlation of the nearby connected basins provides a refined and up-to-date database that will further help to understand the Alpine collision system in the studied area and present-day dynamics on a regional basis.

1.3 Approach Taken

This study integrates data sets obtained from various geological disciplines. Field based data forms the backbone to this thesis. These studies involve mapping combined with processing and interpretation of satellite images and aerial photos. The interpretation of seismic sections, which were correlated with the surface geology, provide the primary tool for interpreting the subsurface extent of the stratigraphical units as well as the structures in the third dimension. Paleontological and stratigraphical studies, especially for the continental Neogene, also form a major contribution to this thesis. In order to understand the structural and kinematic history of the Çankırı Basin, a detailed structural analysis was carried out and paleostress inversion techniques were applied for the total population of measured mesoscopic faults. In order to confirm inferred rotational deformation about vertical axes, a paleomagnetic study was also conducted in the Çankırı Basin that facilitated the determination of the senses and amounts of rotations in different parts of the area.

In this study, a detailed documentation of stratigraphical and structural characteristics and interactions of sedimentation and deformation during the Late Cretaceous to Recent evolution of the Çankırı Basin are provided. The 3D geometry and the kinematics of the structures in the basin, mainly folds and faults, along with temporal constraints on their development with respect to sedimentation, provided the basis on which the evolution of the Çankırı Basin was ascertained.

In the course of this study, the results of earlier studies carried out by Akyűrek et al. (1980), Dellaloğlu et al. (1992), Özçelik (1994), Tűysűz et al. (1995), Şen et al. (1998) and some unpublished data of Turkish Petroleum Co. (TPAO; Ankara, Turkey) were used. For the regional correlations and as an aid in understanding the evolution of the Kırşehir Block, unpublished reports of Göncűoğlu et al. (1991,1992,1993 and 1994) were used.

1.4 Organization of This Thesis

This thesis consists of 8 chapters.

The first chapter provides the introduction to the thesis.

Chapter 2 presents spatial and subsurface information that serves as the basis for the other chapters. It includes surface and subsurface characteristics of the Çankırı Basin. Field based studies combined with satellite images, aerial photos, seismic and gravity data are combined to produce a 3D volume model for the basin.

Chapters 3 and 4 outline the tectono-stratigraphical evolution of the Çankırı Basin. The division of these two chapters is based on the marked changes in the style and characteristics of the tectono-stratigraphy of the Çankırı Basin at the Early Tertiary-Neogene boundary. Chapter 3 includes the stratigraphical and structural characteristics of the Çankırı Basin during its evolution in the Late Cretaceous to pre-Burdigalian. In chapter 4, Neogene stratigraphical and structural data for the Çankırı Basin are presented and their tectonic implications are discussed. This chapter provides a high precision stratigraphic division of Neogene strata which was facilitated by continental mammal paleontological analysis that enabled precise dating and ordering of the deformation events.

Chapter 5 and 6 present the spatial and temporal characteristics of the Late Cretaceous to Recent structures that played a role in the structural development of the Çankırı Basin. In addition to the mapping of structural elements and the establishment of overprinting relationships, the main contribution consists of paleostress inversion studies based on fault slip data obtained from the mesoscopic faults in the northern (chapter 5) and southern (chapter 6) parts of the Çankırı Basin.

In chapter 7, paleomagnetic data derived for the sedimentary in-fill of the Çankırı Basin is presented. From these the amount and senses of block rotations (about vertical axes) in different parts of the Çankırı Basin are presented and discussed.

Chapter 8 discusses the local and regional implications and significance of the results of all of the previous chapters. It integrates the results of this thesis with data obtained from previously published and unpublished studies. It presents a tectonic evolutionary model for the Çankırı Basin and its neighboring continental fragments with respect to the evolution of Tethys in the Eastern Mediterranean area, from the Late Cretaceous to Recent.

Each chapter has been prepared for publication as a separate paper, consequently repetition has become unavoidable.

2

SURFACE AND SUBSURFACE CHARACTERISTICS OF THE ÇANKIRI BASIN (Central Anatolia, Turkey)

Abstract

The geology of the Çankırı Basin has been studied using multi-source data including satellite images, aerial photos, gravimetric data and seismic sections, which are subsequently used to generate maps and a 3D model of that part of the basin that is covered by the seismic sections.

A geological and a lineament map of the basin were obtained using remotely sensed data together with published data and fieldwork results. The subsurface geology of the basin was interpreted from seismic sections. The lateral continuity of the units and the structures have been compiled into a 3D GIS, which was used to construct fence diagrams. In the seismic sections, buried thrust belts are recognized, one in the northern part of the Çankırı Basin and the other on the eastern margin of the Çankırı Basin. From the compilation, three different phases of deformation are recognized. The earliest phase is characterized by thrusting and took place in the Early Tertiary. The second deformation phase is characterized by extensional deformation associated with normal faulting in the latest-Early Miocene to Middle Miocene. The latest phase is characterized by compressional deformation that inverted some of the normal faults that had been developed in deformation phase 2, and has been active from the Late Miocene to Recent. It was also observed in the seismic sections and in the constructed fence diagrams that the Early Tertiary units have a wedge like geometry being thicker in the north and the east and becoming thinner towards the basement. This relationship together with regressive character of the basin in-fill, as observed in the field, is attributed to contemporaneous thrusting and sedimentation in the Early Tertiary. Growth faults have been recognized in the latest-Early Miocene to Middle Miocene units and are attributed to an extensional tectonic regime in the Middle Miocene. Some growth faults were inverted and this is interpreted to be an indication of a new compressional deformation regime after the Middle Miocene.

Note: Color figures are placed at the back of this chapter

2.1 Introduction

The Çankırı Basin is one of the largest Tertiary basins in Turkey (Figure 2.01) and has possible economical hydrocarbon and industrial mineral (mainly evaporitic) reserves. It lies within the Izmir-Ankara-Erzincan suture zone (IAESZ) (Figure 2.01), which demarcates the former position of the northern branch of the Neotethys. After consumption of the Neo-Tethyan Ocean, final collision occurred, along the IAESZ during which the Sakarya continent of the Pontides in the north amalgamated with the Kırşehir Block in the south (Şengőr and Yılmaz 1981, Gőrűr *et al.* 1984, Robertson and Dixon 1984, Koçyiğit *et al.* 1988, Koçyiğit 1991, Tűysűz and Dellaloğlu 1992, Okay *et al.* 1998, Robertson *et al.* 1996). The Çankırı Basin is a unique area in north central Anatolia to study subduction and collision processes owing to an almost 4 km thick Late Cretaceous to recent in-fill, with only minor breaks in sedimentation.

The number of geological studies in the Çankırı Basin is relatively small. This is due to difficulty in dating continental deposits as well as the geological complexity of the region with a superimposed, multi-deformational history. Recently, due to advances in digital technology and improvements in geophysical and remote sensing methods, the number of studies in the region has increased. For this purpose, the Turkish Petroleum Co. (TPAO, Ankara-Turkey) shot 24 seismic lines which amount to nearly 1000km in line length. Improved gravity measurements were made available by the General Directorate of Mineral Exploration and Research Department (MTA, Ankara-Turkey).

The aim of this paper is to study the surface and subsurface characteristics of the Çankırı Basin using multi-source data, including satellite and airborne remote sensing, reflection seismic and gravimetric data. The remotely sensed data, in combination with field data and the published literature were used to obtain an up-to-date geological map of the basin. The seismic sections were interpreted and were used to construct a 3D model for a part of the basin. The gravity data were used to obtain gravity anomaly images that were used to validate the generated 3D model.

2.2 Geological Background

The Çankırı Basin occurs between the Sakarya continent in the north and the Kırşehir Block in the south and has an Ω-shape defined in the west, north and east by an ophiolitic mélange (North Anatolian Ophiolitic Mélange, NAOM) and associated Late Cretaceous volcano-sedimentary rocks which constitute the rim. The same rocks are thought to underlie the in-fill of the Çankırı Basin. The Çankırı Basin is delimited in the south by the Sulakyurt granitoids, which represents the northernmost tip of the Kırşehir Block (Erler *and* Bayhan 1995).

The in-fill of the Çankırı Basin accumulated in 5 different cycles of sedimentation (Figure 2.02 and see chapters 3 and 4). The oldest cycle comprises Late Cretaceous to Paleocene volcano-clastics (Yaylaçayı and Yapraklı formations) and regressive shallow marine units and Paleocene mixed environment red clastics and carbonates (Dizilitaşlar, Kavak and Badiğin formations). In this paper they are referred to as the '*Late Cretaceous units*'. The second cycle is a Paleocene to Oligocene regressive flysch to molasse sequence referred to as the '*Tertiary clastics*' in this study. They are overlain by a widespread thin (<100m) '*nummulitic limestone*' of Middle Eocene age (Kocaçay Formation), which passes upwards into very thick (up to 2000m) Middle Eocene to Oligocene continental red clastics (Incik Formation) interfingering with and overlain by

6

Oligocene evaporites (Güvendik formation). The third cycle is represented by fluvio-lacustrine clastics deposited in the Early to Middle Miocene, which together with the Tortonian Tuğlu formation are referred to as the '*Middle to Late Miocene units*' in this study. The fourth cycle is represented by the strata that were deposited in Late Miocene fluvio-lacustrine conditions and frequently alternate with evaporites (Tuğlu, Süleymanlı and Bozkır formations). Plio-Quaternary alluvial fan deposits and recent alluvium locally overlay all of these units (Figure 2.02).

The structures, which have played a role in the tectonic development of the Çankırı Basin are discussed in detail in chapters 3,4,5 and 6. They are compressional faults (thrust, reverse, and transpressional faults) located mainly in the rim of the basin and dominantly NE-SW oriented strike-slip faults that have traversed the basin in-fill, the basement, as well as the rim. These include the Sungurlu Fault Zone (a sub strand of the Ezinepazarı-Sungurlu Fault Zone), Yağbasan-Faraşlı Fault Zone and the Kızılırmak Fault Zone (Figure 2.01c). Other, but less pronounced structures are the normal faults that are concentrated mainly in the central part of the basin and which have displaced some of the compressional structures in the rim (Figure 2.03).

Presently, the active tectonics of the Çankırı Basin area are dominated by regional transcurrent tectonics, controlled by splay faults (LFZ, KFZ, and ESFZ in Figure 2.01c) of the North Anatolian Fault Zone (NAFZ) (Barka 1992). This zone is approximately 1200km long structure that formed due to collision and the northwards convergence of the Arabian and Eurasian plates (Şengör and Yılmaz 1981, Jackson and McKenzie 1984, Şengör *et al.* 1985).

2.3 Remote Sensing

2.3.1 Introduction

The remote sensing methods used in this study are processing of satellite images, interpretations of analog aerial photos and processing of gravity data. In this section, these data are interpreted and the results are presented and discussed.

2.3.2 Satellite Remote Sensing

Two scenes from Landsat Thematic Mapper (TM)-5 images were used as a basis for the geological map of the Çankırı Basin (Figure 2.03a and b). The characteristics of these images are given in Table 2.01. Before any processing of the images, a radiometric enhancement (Lavreau 1992, Richard 1993) was carried out and then they were mosaiced. Subsequently, the portion of the image covering the Çankırı Basin was chosen for further analysis.
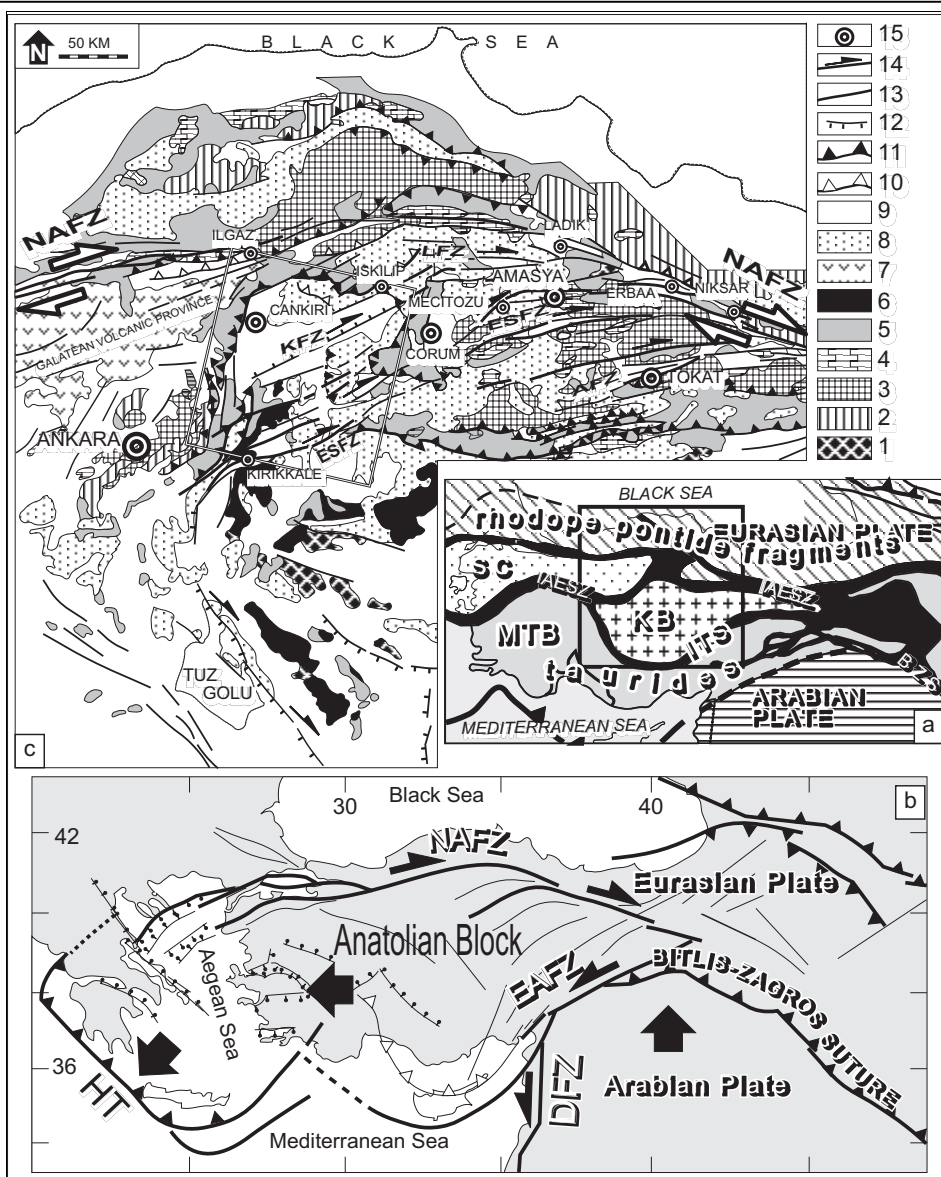
Figure 2.01 a) Inset map showing the geological outline of the Eastern Mediterranean area (Modified after Şengőr et al. 1984). BSZ: Bitlis-Zagros Suture, IAESZ: Izmir-Ankara-Erzincan Suture Zone, ITS: Inner-Tauride Suture, KB: Kırşehir Block, MTB: Menderes-Taurus Block, SC: Sakarya Continent. b) Tectonic setting of the Eastern Mediterranean area. Large black arrows indicate plate movement directions. DFZ: Dead Sea Fault zone, EAFZ: East Anatolian Fault Zone, HT: Hellenic Trench, NAFZ: North Anatolian Fault Zone (modified after Barka and Hancock 1984, Gőrűr et al. 1984, Őzçelik 1994, Kaymakci and Koçyiğit 1995). c) Tectono-stratigraphical map of central Anatolia. Box shows the location of the Çankırı Basin. AFZ: Almus Fault Zone, ESFZ: Ezinepazari-Sungurlu Fault Zone, KFZ: Kızılırmak Fault Zone, LFZ: Laçin Fault Zone, NAFZ: North Anatolian Fault Zone, 1. Pre-Late Cretaceous metamorphic basement of the Kırşehir Block, 2. Pre-Jurassic metamorphic basement of the Sakarya Continent, 3. Triassic Karakaya Complex, 4. Jurassic-Cretaceous platform carbonates on the Sakarya Continent, 5. Late Cretaceous (?) ophiolites and ophiolitic melanges, 6. Pre-Paleocene Granitoids of the Kırşehir Block, 7. Galatean Volcanic Province (Toprak et al. 1996), 8. Early Tertiary units (mainly marine), 9. Neogene and Quaternary Cover, 10. reverse faults, 11. thrust faults, 12. normal faults, 13. faults with unknown sense of movement, 14. Strike-slip faults. 15. major towns.

A number of different image enhancement techniques were performed to differentiate and map each litho-stratigraphic unit and to delineate the geological structures. These techniques include simple linear contrast enhancement (Figure 2.04), decorrelation stretch enhancement (Figure 2.05) (Soha and Schwartz 1978, Gillespie *et al.* 1986), Intensity-Hue-Saturation enhancement (HIS, Figure 2.06a) (Hayden 1982, Daily 1983, Grasso 1993) and Principal Component Analysis (PCA, Figure 2.06b) (Taylor 1974, Chavez and Kwarteng 1989). As seen in the Figures 2.05 and 2.06, only some of the units are partly distinguishable by any one method. Unfortunately, none of the techniques had the ability to discriminate all of the lithological units and structures in one scene. Therefore, during interpretation, all enhancements were used to identify the units and structures. However, the decorrelation stretching technique with band combination of Red:5, Green:3, and Blue:1 produced the optimum image to show most of the structures and almost all units. Therefore, final interpretation and tracing of the boundaries and plotting of structures were performed on this image while the other images were used in support. The image and the resultant map are presented in Figure 2.03.

2.3.4 Image Interpretation

The interpretation of the images and the aerial photos was performed in three succesive steps. In the first step, before fieldwork, published maps were to support interpretation (Akyűrek *et al.* 1980, Dellaloğlu *et al.* 1992, Özçelik and Savun 1993, Özçelik 1994, Özçelik and Öztaş 2000). The resultant interpreted map was verified in the first fieldwork season (between 07 July-25 September 1995). In areas where sufficient resolution could not be achieved, due to the small scale of the structures and/or the intensity of the deformation, field mapping was performed using 1:25.000 scale topographical maps. Then the images were re-interpreted and verified in the successive fieldwork seasons (between 01 July-06 October 1996). This procedure was repeated four times and verified in the field (between 05 July-05 November 1997 and 01 August-10 September 1998 periods) until a final map was produced (Figure 2.07). In the final map (Figure 2.03a and b), the formation boundaries, faults, folds and the photo-lineaments (O'Leary *et al.* 1976) were traced using on-screen digitizing directly onto the image using advanced cartographic techniques. Hardcopies were only utilized during field verification.

Table 2.01 Specifications of the images used in this study

Images	Landsat TM 5
Path/row	176/32 and 177/32
Date	17 August 1991 and 01 September 1984
Area covered (x,y)	10800km^2
Coordinates of studied portion (UTM ZONE 36)	
Upper left corner x	523298
Upper left corner y	4523570
Lower right corner x	630518
Lower right corner y	4422840
Aerial Photos	
Color	Black and white
Date	1960-?
Scale	1:60.000 full coverage 1:35.000 partial coverage (mainly basin margins are covered)

2.3.5 Lithological Discrimination and Formation Boundaries

In this study, twenty-eight formations, plus the alluvium, were recognized and mapped (Figure 2.3b). Six of these formations are recognized for the first time in this study. These are, in stratigraphic order, Late Cretaceous quartz-latite member of the NAOM, Late Cretaceous to Paleocene Kavak and Badiğin formations, the Middle Eocene to Oligocene Incik Formation,

which were separated into two units (Ti1 and Ti2) although in the field they could not be differentiated clearly, the Oligocene Gűvendik formation and Tortonian Tuğlu formation, which had previously mapped as a single unit (see chapters 3 and 4). In addition, the Kılçak, Altıntaş, Hancılı, and Çandır formations, which were partly recognized by previous researchers. Have been separated and mapped out for the first time in this study (Figure 2.03a).

2.3.6 Lineament Analysis

Photo-lineaments are defined as simple or composite linear features on the earth's surface which can be recognized on maps or on satellite images and must be mappable at least for a few kilometers length and which have a rectilinear or slightly curvilinear geometry and presumably reflect subsurface phenomena (O'Leary et al. 1976, Park and Jaroszewski, 1994). These lineaments (Figure 2.08) were categorized into two classes based on their quality. Only those with appreciable offset are classified as "faults" and were analyzed together with the faults that are verified in the field. The others are classified as photo-lineaments. In the analyses the Çankırı Basin was dived into 11 sub areas (Tables 2.02 and 2.03). The subdivision was based on variation in structural trends

and on the geometry of the rim of the basin. For each sub area, length weighted rose diagrams for the faults and the photo lineaments were prepared and compared.

2.3.7 Spatial Characteristics of the Lineaments

Apart from the differences in the orientations of the lineaments (Table 2.02 and 2.03), there is a difference in the distribution of the lineaments in the study area. The lineaments are concentrated mainly in the rim of the basin and in the pre-Neogene units. The southern sub areas (sub areas 3,4,5 and 9) have the highest frequency of faults, while in the western sub areas (sub areas 1 to 3) photo-lineaments have the highest frequency (see Table 2.02 and 2.03). Sub area-7 has the least frequency of faults. Considering the size of this last sub area, the photo-lineaments are also less than in other parts of the Çankırı Basin (Figure 2.08).

The dominance of the lineaments within the pre-Neogene units may indicate that these units were subjected to deformation phases (Kaymakci *et al.* 1998) that did not affected the Neogene units. It is obvious that the younger rocks are exposed to less deformation phases, which is the case for sub area-7 where mainly Late Miocene formations are exposed.

2.3.8 Tectonic Implications of the Lineaments

The rose diagrams prepared for all the faults and for the photo-lineaments display a Riedel geometral pattern (Figure 2.09b) in which all the Riedel shears are developed. In this pattern the Sungurlu, Kızılırmak, and Yağbasan-Faraşlı Fault Zones constitute the y-shears. The Eldivan Fault Zone (EFZ), which defines the western margin of the Çankırı Basin (sub areas 1-3) is almost parallel to the orientation of the expected compressional structures (f in Figure 2.09b) in a Riedel system, although, it slightly deviates from it (approximately 15° anticlockwise).

2.4 Gravity

The gravity data over the Çankırı Basin and adjacent areas was obtained from MTA (General Directorate of Mineral Exploration and Research, Ankara-Tukey). The data set has a 2*2km average sample interval. It was gridded using the Krigging method. The resultant image of the processed gravity data is illustrated in Figure 2.10.

In the processed gravity image, the rim of the basin, the granitoids of the Kırşehir Block, and two buried (blind) thrust belts (discussed below; one in the central northern part and one in the eastern margin) are expressed respectively as a positive anomaly with respect to the basin in-fill (Figure 2.10). In addition, a NE-SW trending fault that dextrally displaces the northern margin of the Çankırı Basin is recognized. This fault is seen only in the pre-Neogene units (Figure 2.03b and 2.08) but can be traced, below the cover of Neogene units, for a considerable length (approximately 30 km) on the processed gravity image. In the southern
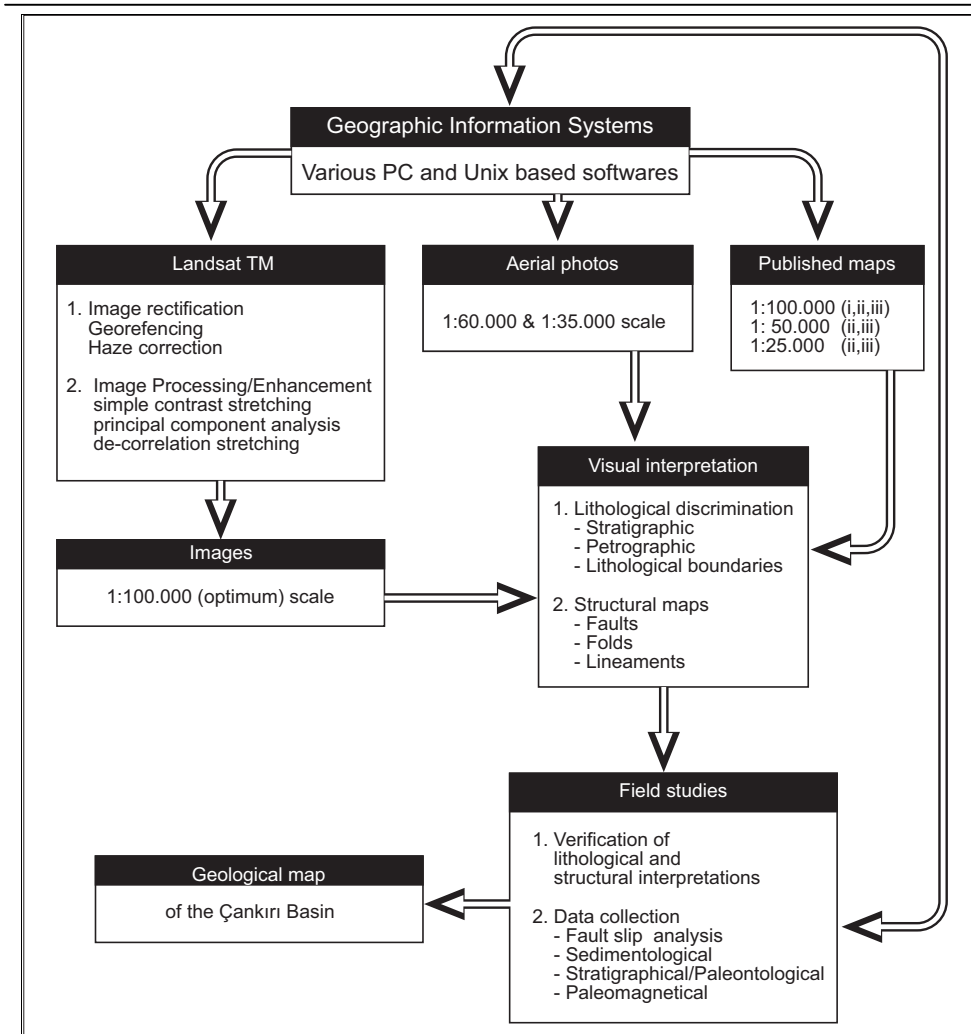
Figure 2.07 Flow chart illustrating the steps followed in the production of the geological map of the Çankırı Basin. The numbers i-iii indicate the references of the published maps. i. Dellaloğlu et al. (1992), ii. Akyürek et al. (1980), iii. Özçelik and Öztaş 2000).
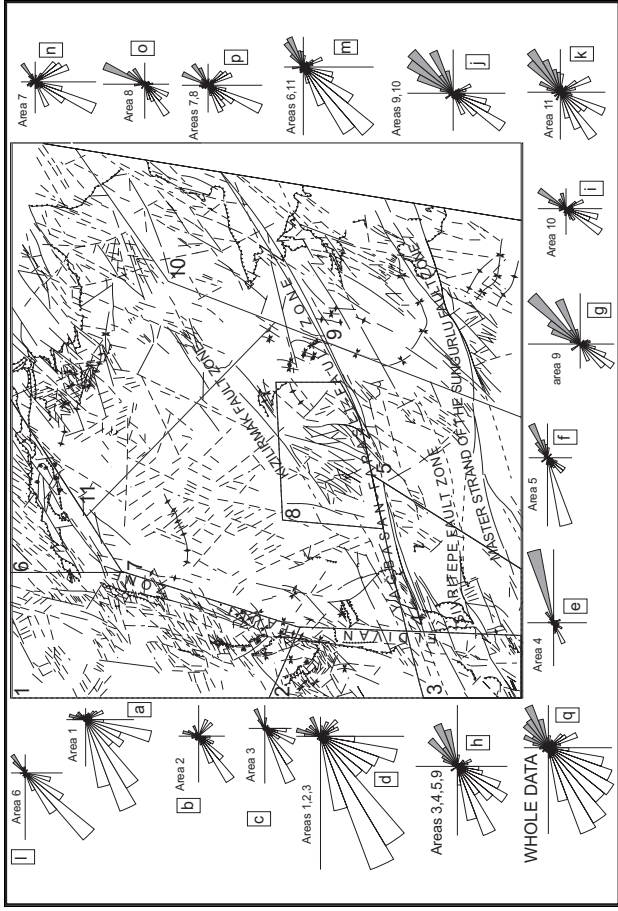
Figure 2.08 Lineament map of the Çankırı Basin. a-q) rose diagrams for each selected sub area and combinations of some sub areas. The upper quadrants of the rose diagrams display the fault classes and lower quadrants display the photo-lineament classes (see Tables 2.02 and 2.03 for the details of frequencies).

Table 2.02 Frequencies (percentages) of the faults in the study area.

PERCENTAGES OF THE FAULT LENGTHS IN THE SUB AREAS																				
west										east										
AREA	80-89 W								0-9W	1-10E								81-90E		TOTAL LENGHT
1	0	3	1	1	3	0	3	0	3	17	23	14	6	14	4	7	0	0	0	10
2	0	4	7	4	0	0	0	0	0	11	25	18	4	7	0	18	0	0	0	4
3	0	5	0	0	5	0	0	0	5	0	0	0	5	10	24	48	0	0	0	3
4	0	0	2	0	2	0	0	2	0	4	2	0	2	4	10	4	61	6		7
5	5	0	0	0	0	5	3	1	0	0	0	3	0	9	15	30	18	11		10
6	7	3	2	5	0	0	0	0	7	0	0	0	3	22	30	8	5	8		9
7	0	2	0	0	6	5	8	6	3	0	5	0	3	8	21	25	8	0		9
8	0	0	0	5	0	2	2	3	10	2	6	42	3	5	18	3	0	0		9
9	0	0	0	0	1	4	1	0	0	1	4	13	15	28	7	20	6	0		20
10	0	6	0	4	0	0	0	6	4	0	6	16	27	0	10	6	14	2		7
11	0	3	5	2	1	4	2	2	6	2	2	1	2	3	11	28	14	11		13
COMBINATION OF SOME OF THE SUB AREAS																				
1,2,3	0	3	3	2	3	0	2	0	3	13	19	13	5	12	7	17	0	0	0	17
3,4,5,9	1	0	0	0	1	3	1	1	0	1	2	7	8	18	11	22	18	4		40
9,10,	0	2	0	1	1	3	1	2	1	1	5	13	18	21	8	16	8	1		27
6,11	3	3	4	3	1	3	1	1	6	1	1	1	3	10	18	20	10	10		22
7,8	0	1	0	2	3	3	5	5	6	18	6	21	3	6	19	14	4	0		17
																		BULK=28,81		

part of the basin, the Yağbasan-Faraşlı and the main strand of the Sungurlu Fault Zones (YFFZ and MSFZ, respectively) are delineated on the gravity image (Figure 2.10). Pseudo-stereo shaded relief images facilitate reveal a variation of the in-fill thickness and help the identification of structures chiefly outline of the rim, Yağbasan-Faraşlı Fault Zone (YFFZ), Master Strand of the Sungurlu Fault Zone (MSFZ) and a basement step in the Eastern Margin of the Kırşehir Block (Figure 2.10b and c). The basin fill is found to be the thickest along a NE trending belt in the northeastern part of the basin (Figure 2.10, see also Özçelik and Öztaş 2000). In addition, it is observed that the eastern boundary of the Kırşehir Block is a steeply dipping discontinuity, which is interpreted as a normal fault on the seismic sections transverse to this structure.

2.5 Three Dimensional (3D) Volume Model

2.5.1 Introduction

3D Modeling characterizes the subsurface geology in three dimensions. The process consists of identification of geological entities (i.e. formation boundaries, unconformities, faults, etc.) and their interpolation. The flexibility and 3D visualization capabilities of the interface allow the interpreter to visually analyze data in any direction and decide on the

continuity and extrapolation of geological units and discontinuities in 3D. This in turn improves the interpretation of geological features in the volume of interest. In this study, the geometrical functionality of the LYNX software (Lynx Geosystems Inc. 1997) was used. The geometrical modeling can simply be defined as the definition and interpretation of the boundaries of geo-objects.
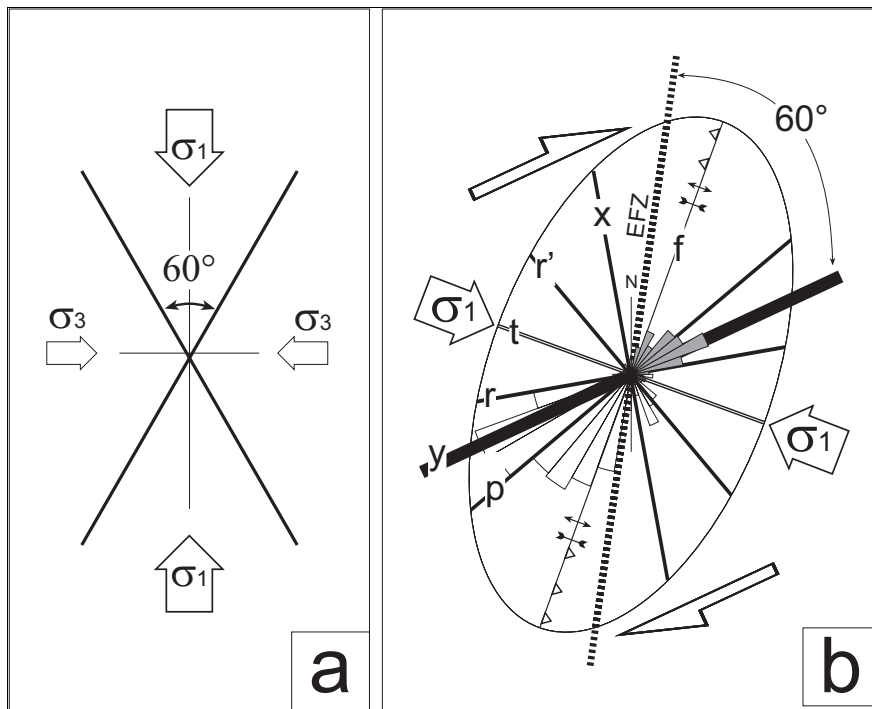
Figure 2.09 a) Figure illustrating Andersonian geometric relationship between principal stresses (σ_1-σ_2-σ_3) for brittle faults and the dihedral angle between the faults that would develop under the indicated stress orientations (σ_2 is perpendicular to the plane of the figure), b) Riedel pattern of deformation and respective stress orientations (adopted from Bartlett et al. 1981, Biddle and Chistie-Blick 1985 and Dresen 1991). Note the angle between the Eldivan Fault Zone (EFZ) and σ_1. N: north, y: principal displacement zone, r: synthetic shear, r': antithetic shear, p: secondary synthetic shear, f: folds and high angle thrust faults, t: extension fractures.

2.5.2 Methodology

The data available for 3D modeling consists of geological cross-sections based on the 2D seismic-sections and geological map (discussed above). The seismic sections were acquired in three time periods between 1988 and 1996 and were processed, stacked and migrated by the TPAO-Exploration Department (see Őzçelik and Őztaş 2000 for a full account). Unfortunately, no depth conversion was possible due to lack of sufficient borehole information. The orientations of the seismic lines are given in Figure 2.11a.

15

Table 2.03. Frenquencies (percentages) of the photo-lineaments in the study area

PERCENTAGES OF THE PHOTO-LINEAMENTS IN THE SUB AREAS																			
	west									east									
AREA	80-89 W								0-9W	1-10E								81-90E	TOTAL LENGHT
1	1	0	1	1	2	3	4	1	1	3	13	7	8	6	16	20	14	0	28
2	0	0	8	2	8	1	0	0	0	5	3	7	6	15	25	14	4	0	5
3	5	0	0	0	2	1	0	2	0	10	6	15	8	5	19	27	1	0	6
4	0	0	3	1	0	4	9	2	0	4	6	6	11	7	3	25	10	12	6
5	6	0	0	0	3	0	0	0	0	1	3	6	12	12	7	6	41	4	6
6	0	0	0	2	0	0	0	0	0	0	11	1	19	36	22	8	0	1	11
7	2	0	1	3	9	10	12	1	0	2	9	22	12	3	1	9	0	2	10
8	2	0	0	0	2	3	3	3	5	0	1	16	8	14	23	12	10	0	6
9	0	0	0	0	3	0	5	6	3	5	9	15	22	18	2	11	0	2	6
10	0	0	0	0	0	6	10	4	0	4	18	14	23	3	8	6	0	3	4
11	5	2	1	1	2	5	9	4	1	3	3	13	8	7	15	11	7	1	12
COMBINATION OF SOME OF THE SUB AREAS																			
1,2,3	2	0	2	1	3	2	3	1	1	5	10	8	8	7	17	20	10	0	39
3,4,5,9	3	0	1	0	2	1	3	2	1	5	6	10	13	10	8	17	13	4	23
9,10,	0	0	0	0	2	3	7	5	1	4	13	15	23	12	4	9	0	2	10
6,11	3	1	1	1	1	3	5	2	1	1	7	7	13	21	18	10	4	0	23
7,8	2	0	1	2	7	8	9	2	1	1	6	20	10	7	9	10	4	1	16
																		BULK=71,19	

Interpretations of the seismic sections was done manually, that is visual interpretation directly from the hard-copies, on the time sections. The interpreted sections were then correlated with the geological map to identify the litho-stratigrahic units. The boundaries of exposed units on the map were extrapolated in the seismic sections and these were subsequently re-interpreted. The final interpretations were digitized using a Calcomp ISO-A0-tablet digitizer. The digitized sections were subsequently introduced to the LYNX-software (Lynx Geosystems Inc. 1997) and georeferenced. In order to generate a 3D model of the area of interest, regularly spaced parallel sections are required (Figure 2.11). To do this, volume models with a finite lateral extent were generated for each of the seismic section independently (Figure 2.12). Then, these volume models were projected onto the plane of the intermediate section. For the construction of each intermediate section, the volume models of the closest seismic sections were used (Figure 2.11). In the next intermediate section, the volume model of the previous seismic sections, the first developed intermediate section and the next seismic sections were projected. After this, the next intermediate section was interpreted and used to improve the previous intermediate sections. Transverse sections were then generated and used to improve the interpretation of the previous intermediate sections. This procedure was repeated iteratively until the final fence diagram of the region was generated (Figure 2.13). Finally, a

number of depth maps were derived at 3.50s (second), 2.25s, and 0.50s time levels (Figure 2.14) for comparison with the surface geological map and the gravity anomaly map.
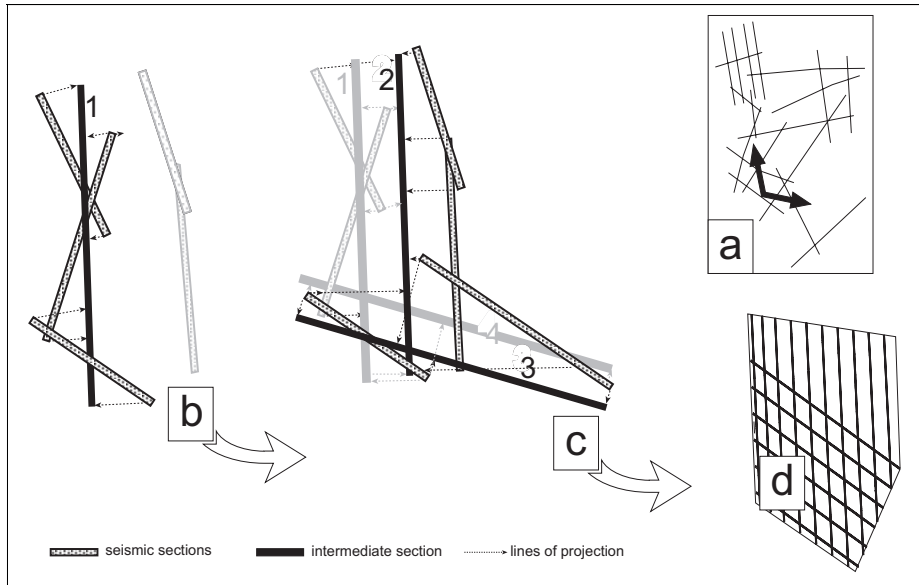
Figure 2.11 a) Orientations of the seismic sections. Arrows are the orientations of the intermediate sections that are used to generate the fence diagram of that part of the Çankırı Basin. b-c) Procedure followed in construction of intermediate sections. After the first intermediate section is produced using the closest seismic sections (b), then the next section is produced using another set closest to the second intermediate section. The previous seismic and intermediate sections including the transverse sections that are produced with the same procedure (3-4 in c) are also used to smooth-out the previous sections. d) final orientations of the intermediate sections.

2.5.3 Results

In the seismic sections, 9 different rock packages were identified (Figure 2.13a). These are, from older to younger; 1. Lithologies of the Kırşehir Block and the Late Cretaceous to Paleocene units (here referred to as "Late Cretaceous units"), 2. "Tertiary clastics", 3. an Early to Middle Eocene marker horizon (Kocaçay Formation) "nummulitic limestone", 4. "Salt domes" including adjacent deformed rocks. The very thick Middle Eocene to Oligocene "Incik Formation" is differentiated into two sub units namely a lower and upper unit (5 and 6), 7. Oligocene "Güvendik formation", 8. "Middle Miocene to Tortonian" units (Çandır-Tç and Tuğlu-Ttu formations), 9. "Late Miocene units" (Süleymanlı and Bozkır formations) together with Plio-Quaternary units including alluvium. In addition, in the lower parts of some of the seismic sections, a very distinct reflection horizon was observed (indicated with arrow in Figure 2.13a). However, this reflector could not be correlated with any of the exposed lithologies or bore-hole data of the Çankırı Basin. Also, the interface between the northern tip of the Kırşehir Block and the Late Cretaceous units was not distinguishable (indicated with "?" in the Figure 2.13a). This might indicate, that the

17

Kırşehir Block extends further to the north outside of the seismic coverage area or, due to seismic attenuation, the interface is obscured.

The most spectacular structures in the seismic sections are the northern and eastern fold and thrust belts, a step (normal fault) in the eastern margin of the Kırşehir Block, salt domes, and the normal faults mainly in the sediments on the Kırşehir Block and which could be continued into the block (Figure 2.15).

The Çankırı Basin is floored by the NAOM and associated Late Cretaceous units. Almost all Early Tertiary and Neogene units (Figure 2.02) display a wedge like geometry thinning from north to south and from east to west (Figures 2.13,2.14b and c) and they are on-lapping on the Kırşehir Block (Figure 2.16). The basin fill is found to be the thickest in the NE part of the basin (Figures 2,13 and 2.15a).

The youngest unit affected by the thrust faults is the Oligocene Güvendik formation (Figure 2.13b), which indicates that thrusting lasted at least until the Oligocene. These thrust faults were displaced by a number of normal faults oriented in various directions, namely NE-SW to NNE-SSW (Figures 2.13b and 2.15a and b). The eastern thrust belt is oriented parallel to a basement step of the Kırşehir block which may account for the accretion of these thrust sheets in this part of the basin (Figure 2.13b). The northern thrust faults have displaced the Middle Eocene to Oligocene İncik Formation and also have affected the Middle to Late Miocene units, resulting in folding at the tip lines of the faults (Çandır, Tuğlu, Süleymanlı, and Bozkır formations). The concentration of thrust faults and accretion of thrust sheets in the northern part of the basin may indicate indirectly that accretion is affected by a ramp formed at the northern tip of the Kırşehir Block. Unfortunately, it could not be identified in the seismic sections.

The salt domes concentrate along a NNE-SSW line in the east central part of the volume model. Most of the salt domes arise from the top of the Early to Middle Eocene Kocaçay Formation (Tko, Figures 2.13 and 2.15) and affected the Middle Miocene to Tortonian units (Figure 2.14b). This indicates that the salt domes were mobilized in post-Middle Eocene to Tortonian.

The normal faults observed within the Middle Miocene to Tortonian units (Tç and Ttu) have the characteristics of dominant growth faults with thicker sediments on the down-thrown side and thinner sediments on the up-thrown side. Some of these normal faults display typical inversion structures (McClay 1989) (Figures 2.15c and 2.16).

2.6 Discussion

The geological map, time section maps obtained from the 3D volume model and the images obtained from gravity data were integrated in a GIS and the results presented as different data layers (see Figure 2.17). Overlaying the geological map and the time sections allowed recognition of the vertical continuation and of the geometries of most of the faults recorded on the surface geological map. Even the least pronounced structures, such as the NNE-SSW oriented growth faults, developed mainly in the sediments on the Kırşehir Block, as well as the NE-SW oriented faults, which are the vertical continuation of the Kızılırmak and Yağbasan-Faraşlı Fault Zones, are clearly traceable from surface down to the 3.50s time section (Figure 2.17).

The wedge-like geometry of the Early Tertiary units indicates an asymmetry to the basin in-filling. On-lap patterns in the sediments on the Kırşehir Block indicate migration of

the depocenter towards the Kırşehir Block (Figures 2.13 and 2.15), which in combination with their regressive character, syn-deformational geometries and provenance (discussed in chapter 3) indicates that they were deposited during the development of the thrust belts.

In the overlay map produced from the processed gravity data and the 3.50s time section map, the in-fill of the basin and the positive gravity anomalies fit perfectly with each other (Figure 2.18a). In addition, the salt bodies, especially in the northeastern part of the volume area, correspond to a gravity low. The relatively high NE-SW trending gravity anomaly in the northern part of the Çankırı Basin corresponds to the northern thrust belt. The dextrally displaced gravity high in the southernmost part of the model area corresponds to the Yağbasan-Faraşlı Fault Zone (YFFZ in Figure 2.03), which is also recognized in the time sections (Figure 2.14).

The displacement of the thrust faults by normal faults and inversion of these normal faults indicates that the Çankırı Basin evolved during at least three different phases of deformation from Early Tertiary to recent. The earliest deformation phase is characterized by compressional deformation associated with thrusting from Late Paleocene to pre-Early to Middle Miocene (pre-Burdigalian). This phase corresponds to deformation phase-2 discussed in chapters 4 and 5. The displacement of these thrust faults by normal faults indicates that the compressional deformation phase was followed by an extensional deformation phase. Inversion of the normal faults indicates a possible phase of compressional deformation after the extensional phase. Each of these deformation phases are discussed in more detail in chapters 3,4,5 and 6.

2.7 Conclusions

I.   A geological database was established for the Çankırı Basin with input from satellite images, aerial photos, gravity data, seismic sections and field studies. This database was used as a basis for the research presented in the following chapters in this thesis.

   1.   Twenty-eight (28) lithostratigraphic units are recognized and their boundaries traced using GIS and advanced cartographic softwares. Six new units are introduced in this study. The resulting map is presented in Figure 2.03b.

   2.   A lineament map of the study area was prepared and the lineaments were classified according to their reliability. Their geometry is analysed with the help of rose diagrams. It is concluded that the lineaments display a Riedel geometry.

II.   Gravity images of the basin were obtained using gravity data with 2*2km sampling interval. From the gravity anomaly images, major structures were identified and the relative thickness of the basin in-fill were estimated.
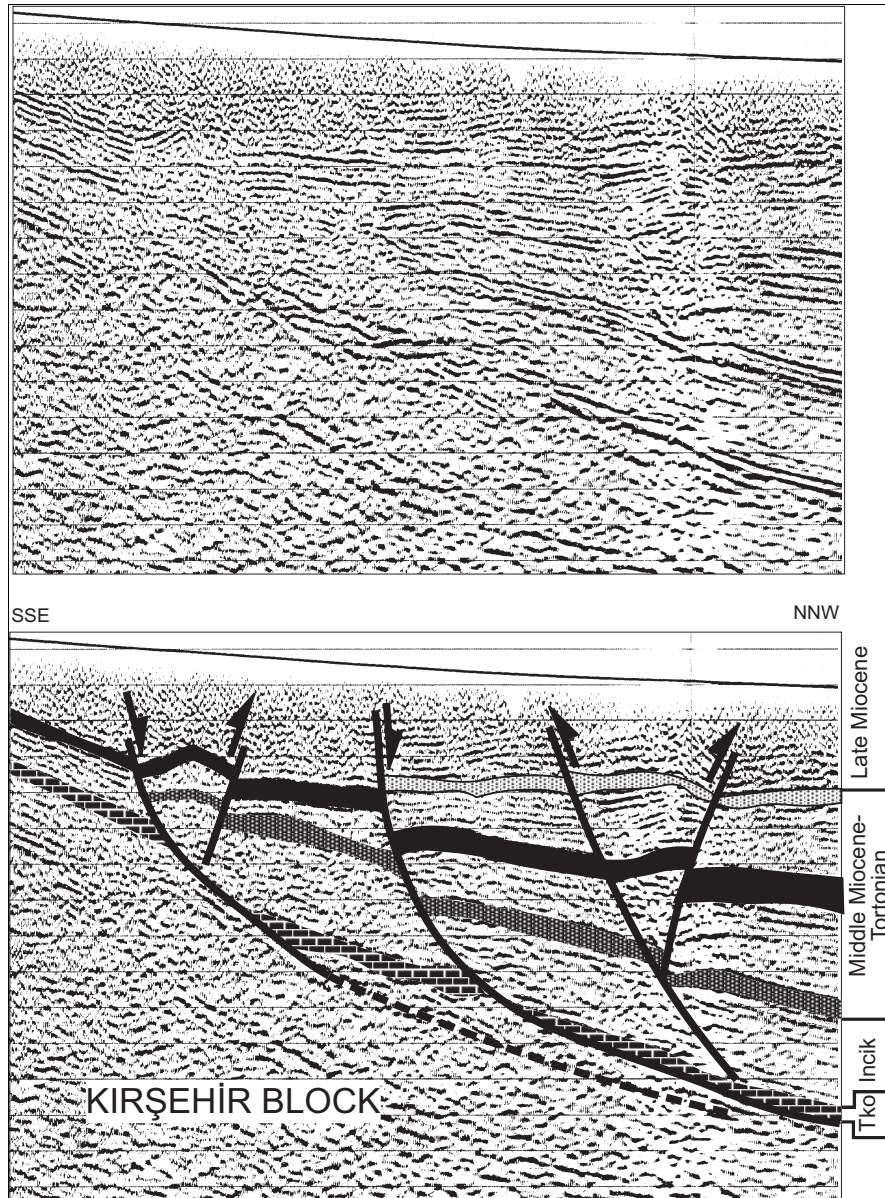
Figure 2.16 Original (a) and interpreted NNW-SSE oriented seismic section (b). Note that there is no thickening on the downthrown sides of the normal faults for the Incik Formation, while it is apparent for the Middle Miocene to Tortonian units. Note also inverted nature of some of these normal faults. Tko: Kocaçay Formation.

III. Gravity images of the basin were obtained using gravity data with 2*2km sampling interval. From the gravity anomaly images, major structures were identified and the relative thickness of the basin in-fill were estimated.

IV. A three dimensional (3D) model of the basin was generated from 24 interpreted seismic sections. Subsurface maps (time sections) from the 3D model at 3.5s 2.25s and 0.5s were obtained. The resulting geometrical constraints are outlined and used as a basis for further unravelling of the history of the Çankırı Basin as discussed in the next chapters. The following features were recognized:

1. Two buried thrust belts in the northern and eastern part of the volume model are recognized in the seismic sections. The youngest unit affected by these thrusts was found to be the Oligocene Gűvendik formation which indicated that thrusting took place at or continued past the Oligocene

2. The Early Tertiary units have a wedge-shaped geometry and display on-lap patterns onto the Kırşehir Block. Also considering the regressive nature of these units, it is concluded that these units were deposited coevally with activity of the above thrust faults.

3. A number of growth faults, some of which are inverted, are observed in the seismic sections and their 3D continuity was constrained.

4. Salt domes are recognized in the eastern part of the model area along a NNE-SSW zone. These salt domes originated at the top of the Early to Middle Eocene Kocaçay Formation and have affected the Middle Miocene to Tortonian units, which indicates post-Middle Eocene and pre-latest-Late Miocene (Messinian) mobilization of these salt bodies.

V. Overlaying of the gravity image and time sections demonstrated that the gravity lows correspond to areas of thick basin infill and to salt bodies, and highs correspond to the ophiolitic melange and to the granitoids. A perfect fit of the gravity highs with the Kırşehir Block and with the thrust belts confirms the reliability of the generated 3D model.

VI. Three distinct deformation phases have been recognized in the seismic sections and are visualized in the 3D model. The earliest phase (from Late Paleocene to pre-Middle Miocene) is characterized by compressional deformation associated with thrusting, the second phase (Middle Miocene) is characterized by extensional deformation associated with normal faulting, and the latest phase (from Late Miocene to recent) is characterized by a new phase of compressional deformation, which caused inversion of some of the normal faults.

21

3

PRE-NEOGENE TECTONOSTRATIGRAPHY AND EVOLUTION OF THE ÇANKIRI BASIN
(Central Anatolia, Turkey)

Abstract

The Çankırı Basin includes more than 3 kms of pre-Neogene in-fill. The litho-stratigraphical units of the Çankırı Basin are subdivided into two main groups, the northern and southern units. The northern units include the Late Cretaceous to Paleocene Bűrtű group, the Late Paleocene to Middle Eocene Iskilip group, and the post-Middle Eocene to Oligocene Kalınpelit group. The Bűrtű group includes, the NAOM, Yaylaçayı, Yapraklı, Malıbogazı, Kavak, Badiğin, and Dizilitaşlar formations which were deposited within fore-arc to inter-arc basins during the subduction of the northern Neotethys. The Iskilip group includes the Hacıhalil, Yoncalı, Karbalçik, Bayat, Osmankahya and Kocaçay formations. The Kalınpelit group includes the Incik and Gűvendik formations. The southern units include the Late Paleocene to Middle Eocene Sivritepe group, which includes the Karagűney and Mahmatlar formations. The Iskilip and Kalınpelit groups together with the Sivritepe group were deposited within a thrust regime during which the depocenters and thrust faults migrated southwards towards the basement and which indicate that the Çankırı Basin evolved as a series of piggy-back basins in the Late Paleocene to Oligocene. Thrusting and related sedimentation was continued until the Aquitanian (ca 20.5 Ma, Early Miocene).

3.1 Introduction

This chapter deals with the pre-Neogene stratigraphic and tectonic development of the Çankırı Basin. The next chapter deals with the Neogene development. This separation is made because of a marked change in the depositional styles and tectonic development of the Çankırı Basin at the beginning of the Neogene.

The Late Cretaceous to Early Tertiary stratigraphy of the Çankırı basin (Figure 3.01) has been studied by a number of researchers (chiefly; Norman 1972, Birgili 1974, Ayan 1969, Akyűrek *et al*. 1984, Tűysűz and Dellaloğlu 1992, Dellaloğlu *et al.* 1992, Özçelik 1994, Koçyiğit *et al*. 1995). In this contribution, the stratigraphy of the basin is updated as a result of newly gathered data. The data are presented and discussed. Each unit has been studied in detail in the field. They have been re-mapped and the result is shown in Figure 3.02. The units that are recognized for the first time are defined and are named according to the North American Stratigraphic Code (1983). The contact relations were examined in detail. The identification of marine fossils in appropriate units and the assigned ages of the units were carried out by the Turkish Petroleum Company (TPAO), Research Laboratories. The first letter of formal stratigraphical names is given in capital letter whereas plurals and informal names (those introduced in this thesis) are given in lower case letters. Before describing the stratigraphic units of the Çankırı Basin, first the basement will be described.

3.2 Basement to the Çankırı Basin

3.2.1 Basement: Introduction

The basement to the Çankırı Basin is constituted by the Kırşehir Block, which is composed of metamorphics, granitoids and patches of ophiolites distributed on the block. The granitoids intrude the ophiolites, causing thermal metamorphism, and the metamorphics (Erler *et al*. 1991, Yalınız 1995). In the study area, the metamorphics are not exposed but the Kırşehir Block is represented by the ophiolites and by the intruding Sulakyurt Granitoids (Figures 3.01 and 3.02) which has an age of Late Cretaceous to pre-Paleocene and thus predates the formation of the Çankırı Basin.

3.2.2 A Brief Outline of the Characteristics of Constituent Rocks of the Kırşehir Block

3.2.2.1 Ophiolites of the Kırşehir Block

The ophiolites on the Kırşehir Block are exposed within distributed patches (Figure 3.01). They are intruded by granitoids and are exposed as enclaves and roof pendants within these granitoids (Yalınız *et al*. 1996, Kuscu 1997, Gőncűoğlu *et al*. 1992,1993). They are composed of various ultramafics including mainly serpentinized peridotites and harzburgites, and locally wherlites, lherzolites, and plagio-granites, diabase dykes with dyke-in-dyke structure, pillow basalts, boninites and associated volcano sedimentary successions, which alternate with pelagic sediments including radiolarites with manganese nodules (Yalınız *et al*. 1996). According to Yalınız *et al*. (1996), the ophiolites in the south-western part of the Kırşehir Block (outside of the present study area) are generated from a supra-subduction setting.
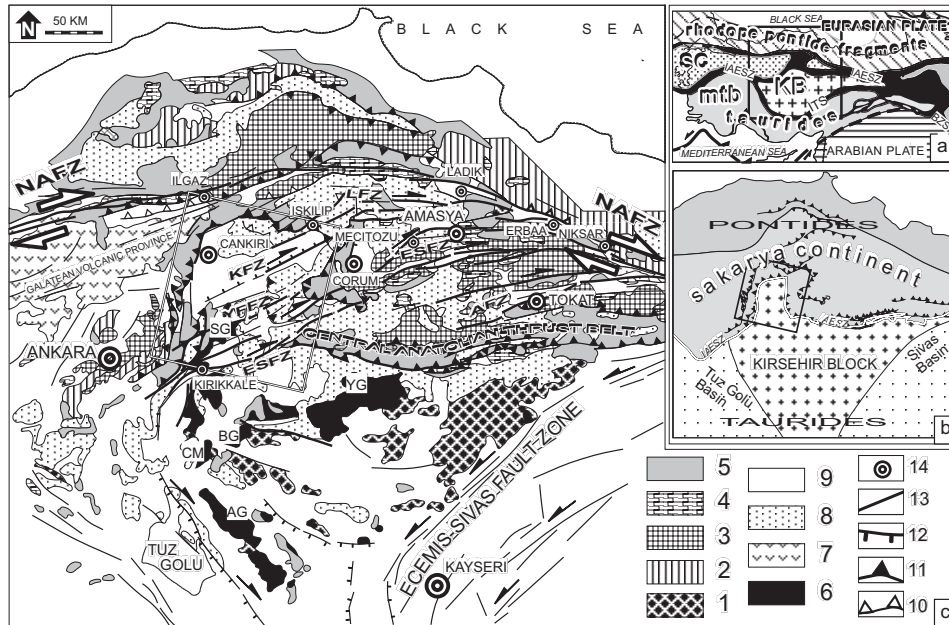
Figure 3.01 a) Inset map showing the geological outline of the Eastern Mediterranean area (Modified after Şengőr et al. 1984). BSZ: Bitlis-Zagros Suture, IAESZ: Izmir-Ankara-Erzincan Suture Zone, ITS: Intra-Tauride Suture, KB: Kırşehir Block, MTB: Menderes-Taurus Block, SC: Sakarya Continent. b) Tectonic setting of the Çankırı Basin. c) Tectono-stratigraphical map of Central Anatolia. Box shows the location of the Çankırı Basin. AFZ: Almus Fault Zone, ESFZ: Ezinepazari-Sungurlu Fault Zone, KFZ: Kızılırmak Fault Zone, LFZ: Laçin Fault Zone, NAFZ: North Anatolian Fault Zone, YFFZ: Yağbasan-Faraşlı Fault Zone. AG: Ağaçőren granitoids, BM: Baranadağ Monzonite, CM: Cefalıkdağ Quartz-Monzonite, SG: Sulakyurt Granitoids, YG: Yozgat Granitoids. 1. Pre-Late Cretaceous metamorphic basement of the Kırşehir Block, 2. Pre-Jurassic metamorphic basement of the Sakarya Continent, 3. Triassic Karakaya Complex, 4. Jurassic-Cretaceous platform carbonates on the Sakarya Continent, 5. Late Cretaceous (?) ophiolites and ophiolitic melanges, 6. Pre-Paleocene granitoids of the Kırşehir Block, 7. Galatean Volcanic Province (GVP, Toprak et al. 1996), 8. Paleogene units (mainly marine), 9. Neogene and Quaternary cover, 10. reverse faults, 11. thrust faults, 12. normal faults, 13. strike-slip faults and faults with unknown sense of movement, 14. major towns (modified after Barka and Hancock 1984, Gőrűr et al. 1984, Őzçelik 1994, Kaymakci and Koçyiğit 1995).

In the study area, mainly pillow basalts, various dykes and pelagic successions including radiolarites and radiolarite bearing cherty limestones are present. Based on trace element geochemistry (mainly REE) of the samples collected from the basalt units in the ophiolites, in the study area, Gőncűoğlu *et al.* (2000) proposed that these ophiolitic units are generated from a wide range of tectonic settings extending from subduction to ensimatic arc environments.

3.2.2.2 Granitoids of the Kırşehir Block

In the Kırşehir Block, the granitoids are divided into three groups: (1) a number of large plutons which form a north-west convex arcuate belt and extend from the northern tip of the Cankiri Basin (where they are represented by the Sulakyurt Granitoids) to its

39

16
kilometer
N

BADIĞIN
BÜRTÜ
HACIHALIL
8
7
6
11
12b
10c
KUNDUZLU
YAPRAKLI
13
17
15
ISKILIP
12c
18
BAYAT
ÇANKIRI

NORTH ANATOLIAN FAULT ZONE

14

HANCILI

ÇANDIR
9
Gözükızıllı
Güvendik
SULAKYURT
19
SUNGURLU

KALECİK

y
10b
y'
SIVRITEPE
10a
C
KIRIKKALE

Rodent sites

Syncline

Anticline

Overturned Syncline

Overturned Anticline

Oblique and Strike-slip faults

Reverse and Thrust faults

Probable faults

NEOGENE and QUATERNARY

SOUTHERN UNITS

SIVRITEPE GROUP

Eocene
- Mahmutlar Formation
- Karagüney Formation

pre-Paleocene
- Sulakyurt Granite
- Ophiolites intruded by the Granites

NORTHERN UNITS

BÜRTÜ GROUP

Paleocene
- Dizilitaşlar Formation
- Badiğin formation
- Kavak formation

Late Cretaceous
- Malıboğazı Formation
- Yapraklı Formation
- Yaylaçayı Formation
- North Anatolian Ophiolitic Melange (NAOM)

Triassic
- Karakaya Complex

KALINPELIT GROUP

mid-Oligocene
- Güvendik formation

post-Midd. Eocene pre-mid-Oligocene
- Incik Formation

ISKILIP GROUP

Late Paleocene to Middle Eocene
- Kocaçay Formation
- Osmankahya Formation
- Bayat Formation
- Karabalçık Formation
- Yoncali Formation
- Hacıhalil Formation

GALATEAN VOLCANIC PROVINCE

Figure 3.02 Geological map of the Çankırı Basin. The numbers in circles refer to the figure numbers of the measured sections. The blow up figures depict the Malıboğazı and Bayat formations.

southern tip along the western margin (Figure 3.01c), (2) a relatively narrow and smaller set of isolated plutons along the eastern margin, and (3) a very large batholith exposed around Yozgat (Erler *et al*. 1991; Akıman *et al*. 1993; Erler and Bayhan, 1995).

The granitoids were generated during and after the southward obduction of the ophiolites from the northern branch of the Neotethyan ocean, onto the Taurides during the Late Cretaceous period (Erler *et al.* 1991; Akıman *et al.* 1993) and before the Late Maastrichtian (Yalınız *et al.* 1996). They are the consequences of crustal thickening due to arc to arc or arc to continent collision (Göncüoğlu *et al*. 1992; 1993). In general, the Central Anatolian granitoids are members of two broad classes; granitoids with S-type characteristics and granitoids displaying both S-and I-type characteristics. In other words, they display distinctive features of H-type (hybrid) granites, and plot both in island arc and collision fields with within plate signatures on trace element discrimination diagrams (Bayhan, 1987; Erler *et al*. 1991; Akıman *et al*. 1993; Erler and Bayhan, 1995). Consequently they may be accepted as collision granitoids. The geological evidence indicates a two-fold obduction resulting in two phases of magmatism producing the above two different types of granitoids (Göncüoğlu *et al*. 1991). The earlier phase generated S-type syn-collisional granitoids due to crustal thickening due to the obduction of the MORB-type ophiolites of the northern branch of the Neotethys (Vardar Ocean) (Göncüoğlu *et al*. 1992; Yalınız *et al*. 1996) onto the protoliths of the Kırşehir Block. The second phase is due to obduction of supra-subduction zone ophiolites (SSZ) onto the metamorphics and previously obducted ophiolitic mélange due collision of the ensimatic arc with the Taurides. They are characterized by post-collisional granitoids and syenitoids, the granitoids displaying both S and I-type characteristics. These were generated by post-collisional extension after the second obduction event had ceased (Erler *et al*. 1991; Geven, 1992; Göncüoğlu *et al*. 1993, Erler and Göncüoğlu, 1996). Both the syn-collisional and post-collisional granitoids cut across the metamorphics of the Kırşehir Block (Kuscu 1997).

The radiometric data on the granitoids are rather scarce. The S-type granitoids have been dated at 95±11 Ma (Göncüoğlu 1986). Ayan (1963) reported an age of 54 Ma for the Baranadağ Monzonite (Figure 3.01c) in the western margin of the Kirsehir block using the total Pb method. Gündoğdu *et al*. (1988) dated the Cefalıkdağ quartz monzonite (Figure 3.01c) using the Rb-Sr whole rock-mineral isochron method at 71±1 Ma and 71.8±1.1, respectively. Güleç (1994) found that the age of the Ağaçören granitoids (Figure 3.01c) is 110±14 Ma based on whole rock Rb-Sr isotope (Figure 3.01c). Based on stratigraphic data, Erler *et al*. (1991) have reported the all the granitoids within the Kırşehir Block are older than Palocene and thus predate the Çankırı Basin.

The Sulakyurt granitoids lie within the northernmost part of the Kırşehir Block and directly underlies the southern part of the Çankırı Basin (Figure 3.01). It is composed of intensely altered micro-phanaritic to phanaritic hornblende granite, granodiorite, diorite, syenite, and monzonite (Erler *et al*. 1991, Norman 1972, Akıman *et al*. 1995, Kuşcu 1997). It also includes various felsic dykes ranging from aplite to vitric rhyolite. According to Norman (1972), the geochemical characteristic of the Sulakyurt Granitoids varies depending on the wall rock properties indicating assimilation of the wall rock. The grain size decreases outwards from the pluton interior and is associated with "chilled margins" and contact metamorphism (Norman 1972). It has not been isotopically dated. An indirect age is indicated by the presence of its pebbles in the various Early to Middle Eocene units (mainly in the Mahmatlar Formation and more sparsely in the Karagűney and Karabalçik

41

formations). It intrudes the NAOM and Campanian-Maastrichtian units indicating that it was emplaced some time within the Campanian to pre-Early to Middle Eocene interval. As outlined, in the previous section, the Sulakyurt granitoids intrude the ophiolites and it could have been emplaced prior to Paleocene as a part of post collisional granitoid suit to which it is chemiaclly related.

3.3 Stratigraphy

The main groups which cover all but the south-western corner of the basin will be described as the **northern units**, and the other but less extensive units limited to the south-western part of the basin will be described as **southern units**. First the northern units will be described.

3.3.1 Northern Units

The stratigraphy of the northern rim of the Çankırı Basin can be divided into three groups. The first group is represented by an ophiolitic melange (NAOM), associated volcano-sedimentary successions (Yaylaçayı and Yapraklı formations), and laterally grading and locally overlying shallow marine and partly continental units (Malıboğazı, Kavak, Badiğin and Dizilitaşlar formations. These units are informally named as the Bürtü Group (see Figure 3.03) The lower part of this group (NAOM, Yaylaçayi and Yapraklı formations) was previously interpreted to be associated with accretionary wedge (subduction complex) growth and development of a magmatic arc and arc related basins during the northwards subduction of the Tethys during the Late Cretaceous (Şengőr and Yılmaz 1981, Koçyiğit *et al*. 1988, Koçyiğit 1991, Tüysüz and Dellaloğlu 1992, Özçelik 1994, Tüysüz *et al*. 1995). The second group represents Paleocene (?) to Middle Eocene mainly marine flysch to molasse successions (Hacıhalil, Yoncalı, Karabalçık formations) and associated Middle Eocene volcanics and feeder dykes (Bayat Formation) covered by continental red clastics and a nummulitic condensed sequence of Middle Eocene age (Osmankahya and Kocaçay formations respectively). The third group comprises a very thick sequence of continental red clastics and evaporites of post-Middle Eocene to Oligocene age (Figure 3.03). The second and third groups were named the İskilip Group by Dellaloğlu *et al*. (1992). In this article the name "Iskilip Group" is restricted to the second group. The third group is informally named the Kalınpelit Group. All of these groups will be described in the following sections.

3.3.1.1 Bürtü Group

3.3.1.1.1 North Anatolian Ophiolitic Mélange (NAOM, Upper Cretaceous)

North central Anatolia is dominated by a number of ophiolitic belts with various rock constituents. Previous researchers named these ophiolitic units based on their present day geographic locations, the rock constituents and inferred oceanic domain of their origin. In this study, the nomenclature of Rojay (1993) is adopted for the NAOM. He proposed a generalised nomenclature for all of the ophiolite bearing units in north central Anatolia without consideration of local constituent lithologies, age and inferred tectonic setting.

The NAOM is exposed along the western, northern and eastern rim of the Çankırı Basin (see Figure 3.02). In the central part of the basin, the NOAM is intersected at a depth of 3200m (Öçelik and Öztaş 2000) and consequently considered to be underlying much of the Çankırı Basin. Boundary relationships of the NAOM with other units of the Çankırı Basin are summarized in Figure 3.04.

42
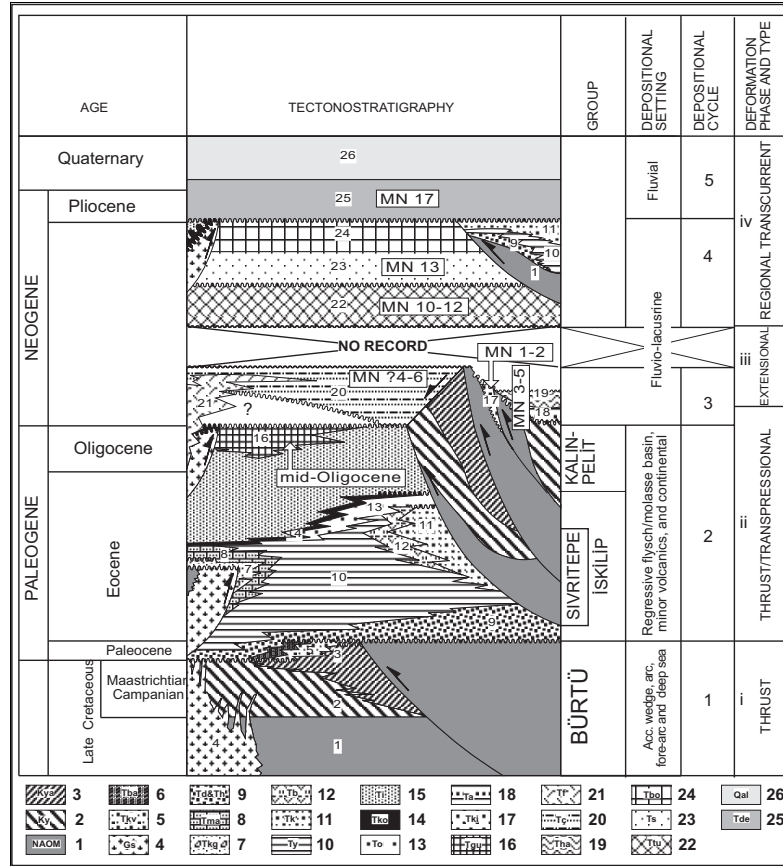
Figure 3.03 Generalized tectono-stratigraphic column of the units exposed in and around the Çankırı Basin. 1. North Anatolian Ophiolitic Melange-NAOM, 2. Yaylaçayı Formation (distal fore-arc sequence), 3. Yapraklı Formation (proximal fore-arc facies), 4. Sulakyurt Granitoids of the Kırşehir Block, 5. Kavak formation (red clastics and carbonates), 6. Badiğin formation (neritic limestones), 7. Karagűney Formation (clastics derived mainly from the Kırşehir Block) 8. Mahmatlar Formation (clastics derived from the Sulakyurt Granitoids), 9. Dizilitaşlar and Hacıhalil formations (mainly turbiditic clastics and intercalated limestones), 10. Yoncalı Formation (Eocene flysch), 11. Karabalçık Formation (distributary channel conglomerates and sandstones with coal seams), 12. Bayat Formation (Eocene volcanics and volcanoclastics), 13. Osmankahya Formation (mixed environment clastics and red beds), 14. Kocaçay Formation (Middle Eocene nummulitic limestone covering both basin in-fill and the granitoids), 15. İncik Formation (Late Eocene to Oligocene continental red clastics), 16. Gűvendik formation (Oligocene evaporites), 17. Kılçak Formation (fluvio-lacustrine clastics), 18. Altıntaş Formation (fluvial red clastics exposed only in the Hancılı Basin), 19. Hancılı Formation (Lacustrine deposits exposed only in the Hancılı Basin, 20. Çandır Formation (fluvio-lacustrine clastics), 21. Faraşlı Basalt, 22. Tuğlu formation (early-Late Miocene evaporites and lacustrine shale/marl), 23, Sűleymanlı formation (fluvio-lacustrine red clastics), 24. Bozkır Formation (evaporites), 25. Deyim Formation (fluvial clastics), 26. Alluvium. MN zones and a mid-Oligocene age were obtained at certain horizons within post-Middle Eocene units and discussed in chapter 4.

43

Lithologically, the NAOM is composed a tectonic mixture mainly of spilites, pillow lavas, diabase dykes, red to purple radiolarian chert, cherty limestone, reddish pelagic mudstone and various serpentinized ultramafic rocks such as peridotites, harzburgites and pyroxenites. The NAOM also includes layered gabbros, plagio-granites and blocks derived from basement metamorphics of the Sakarya Continent and various limestones derived from nearby platforms during accretion (Koçyiğit *et al.* 1988, Koçyiğit 1991, Rojay 1993, Őzçelik 1994). Although, the Yaylaçayı Formation is locally incorporated into the development of the NAOM and constitute its matrix. However, the matrix of the NAOM is missing in most areas (Koçyiğit *et al.* 1991, Rojay 1995). Dellaloğlu *et al.* (1992) concluded that NAOM represents a complete ophiolitic sequence, supposedly originated from the northern Neotethys Ocean (Vardar Ocean). Variations occur geographically. The most complete sequence occurs in the north.

The difference between the NAOM and the ophiolites intruded by the Sulakyurt Granitoids, in the central part of the basin, is that the southern ophiolites were intruded by the Sulakyurt granitoids lack a melange character and are characterized by a greater abundance of gabbros, various dykes displaying dyke-in-dyke characteristics and dykes with a singe chilled margins. They are also less deformed. These relationships indicate that the southern ophiolitic units were emplaced as an intact ophiolitic slab and later intruded by the Sulakyurt granitoids, while the northern ones were incorporated into the accretionary wedge of the subducting northern Neotethys. There has been no attempt to correlate these two ophiolitic units.

3.3.1.1.2 Yaylaçayı Formation (Ky, Campanian to Maastrichtian)

The Yaylaçayı Formation was first named by Yoldaş (1982). It consists mainly of a volcano-sedimentary sequence (Figure 3.06). and is exposed in the rim of the Çankırı Basin associated with the NAOM (Figure 3.01). It is regarded as a distinct formation because locally it has preserved its internal structure, although, locally it constitutes part of the matrix of the NAOM. Lithologically, the Yaylaçayı Formation exhibits very rapid lateral facies changes. The dominant character of the unit is the presence of various volcanogenic horizons in which basalts, tuffs and tuffites are intercalated with shales and pelagic marly limestones (Figure 3.06). In general it is composed of three distinct lithological associations. From bottom to top there are: 1) marl, marly pelagic limestone, volcanogenic sandstone, and tuff alternations, 2) pelagic fauna bearing micritic limestone and green shale alternation, intercalated with alternations of spilitic olistostromes and tuff, 3) turbiditic sandstone and shale alternations intercalated with tuff, agglomerate, beige colored silty argillaceous limestone, and marl grading upward into a benthic fossil bearing sandy limestone (Figures 3.06 and 3.07).

The age of the unit varies from Maastrichtian (Yoldaş, 1982), Cenomanian-Campanian (Akyürek *et al.* (1984), to Santonian-Campanian (Tüysüz 1985 and Dellaloğlu *et al.* 1992), and Senonian-Early Paleocene (Őzçelik 1994). The following foraminifera fauna have been identified at the base of the Yaylaçayı Formation: *Orbitoides* ex gr *medius*, *Heterocyclina* sp., *Textularidae* (Figure 3.06) and from the upper part of the formation following nanno fossils have been identified: *Quadran fribidus, Quadran gothicana, Microrhabdus. decarutus,* crib*. chreuvengi, Eif. furrseifeli* and which are of Late Campanian to Maastrichtian age (Figure 3.07). Considering these ages and that of the above fauna, it is concluded that the Yaylaçayı Formation was deposited in the Campanian to Maastrichtian interval.

44

	Tgu	Ti	Tko	To	Tb	Tk	Ty	Tm	Tkg	Th	Td	Tba	Tkv	Kya	Ky	NAOM	Gs
INCIK	LVT+U+T																
KOCAÇAY	N/A	U+T															
OSMANKAHYA	N/A	U+T	LVT+T														
BAYAT	N/A	U+T	LVT+T	LVT+T													
KARABALÇIK	N/A	U+T	LVT+T	LVT+T	LVT+T+I												
YONCALI	N/A	U+T	LVT+T	LVT+T	LVT+T+I	LVT+T											
MAHMUTLAR	N/A		LVT+T	LVT+T	N/A	LVT+T	LVT+T										
KARAGUNEY	N/A	U+T	LVT+T	LVT+T	N/A	LVT+T	LVT+T	LVT									
HACIHALIL	N/A	T	N/A	N/A	I+T	LVT+T	LVT+T	LVT?+T	LVT?+T								
DIZILITASLAR	N/A	U+T	N/A	N/A	N/A	LVT?+T	LVT?+T	LVT?+T	LVT?+T	N/A							
BADIGIN	N/A	U+T	N/A	N/A	N/A	N/A	N/A	N/A	N/A	LVT?	LVT?						
KAVAK	N/A	U+T	N/A	N/A	N/A	N/A	N/A	N/A	N/A	LVT?	LVT?	LVT					
YAPRAKLI	N/A	U+T	N/A	U	T+I	T	T	N/A	N/A	U+T	U+T	U+T	U+T				
YAYLACAYI	N/A	U+T	N/A	U+T	T+I	T	T	U	U	U+T	U+T	U+T	U+T	LVT+T			
NAOM	U+T	U+T	U+T	U+T	T+I	U+T	T	U+T	U+T	U+T	U+T	U+T	U+T	LVT+T	I		
SULAKYURT GRANITE	N/A	U+T	U	U+T	N/A	N/A	N/A	U+T	U+T	N/A	N/A	N/A	N/A	N/A	T	I	
KARAKAYA COMPLEX	N/A	N/A	N/A	N/A	N/A	N/A	N/A	N/A	N/A	N/A	N/A	N/A	N/A	N/A	T	T	N/A

LVT: LATERAL AND VERTICAL TRANSITION
U: UNCONFORMABLE
T: TECTONIC
I: INTRUSIVE
N/A: NO CONTACT RELATIONSHIP AVAILABLE
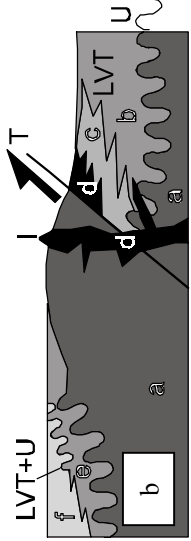
Figure 3.04 a) Contact relationships between the pre-Neogene units. b) A conceptual cross-section to explain various contact relationships observed in the Çankırı Basin.

Figure 3.05 Summary correlation chart based on previous studies carried out in and around the Çankırı Basin. MBOGZI: Malıboğazı, YPRL: Yapraklı, K.Cay: Kocaçay, O.KAH: Osmankahya, Y.CAYI: Yaylaçayı, KRZBS: Kirazbaşı. All of the names indicate formations otherwise indicated.

3.3.1.1.3 Yapraklı Formation (Kya, Campanian-Paleocene)

The Yapraklı Formation was first named by Birgili *et al*. (1974). It is characterized by limestones with macrofossils and fine grained clastics.

The Yapraklı Formation (see Figure 3.07, 3.08, and 3.09) displays local coarsening upwards sequences and evidence for the progressively shallowing of the depositional environment as indicated by the transition from fine clastics to neritic limestones. The bottom of the formation is composed of explosive volcanics such as white tuff and agglomerate intercalations. In the middle it is characterized by turbiditic yellow to buff colored, macrofossil bearing, volcanogenic conglomerate, sandstone, grey, green, reddish shale. Towards the top, limy units and fossiliferous limestones are present. Locally, the unit includes olistostromal horizons. In addition, the unit also includes thick-shelled pelecypoda, wood and plant remains especially in its upper parts, which indicates close proximity to the margin of the basin.

Dellaloğlu *et al*. (1992) have proposed a Senonian to Maastrichtian age for this formation based on planktonic foraminifera, gastropoda and pelecypoda fossils. However, the fossils identified in the sections studied in the course of this research yielded Maastrichtian to Paleocene age in the Malıboğazı section (Figure 3.09) and Maastrichtian in the Kağnıkonağı section (Figure 3.07), and Campanian to Maastrichtian in the Badiğin section (Figure 3.08). This age range indicates that the Yapraklı Formation was deposited diachronously in the Campanian(?) to Paleocene interval.

3.3.1.1.4 Malıboğazı (Km), Kavak (Tka) and Badiğin (Tbd) Formations (Late Cretaceous-Paleocene)

These three formations are only exposed in limited outcrops in the Çankırı Basin. The boundary relationships for these units are summarized in Figure 3.04.

The Malıboğazı Formation was previously named by Ayan (1969). It is exposed only in the south-western part of the Çankırı Basin (Figure 3.02). It comprises approximately 200m thick condensed neritic reefal limestone with rich *Rudist*, *Exogyra*, and *Orbitoides* (Figures 3.08 and 3.09).

The Kavak and Badiğin formations are informally named in this study. They are exposed only in the north-western part of the basin (Figure 3.02). The Kavak formation comprises approximately 100m thick polygenic conglomerates with a limy matrix overlain by a very thickly bedded red to purple conglomerate and sandstone alternation. It includes reworked Late Cretaceous fauna and detritus derived mainly from the NAOM, Yaylaçayı and Yapraklı formations (Figure 3.08).

The Badiğin formation is exposed in the north-western corner of the Çankırı Basin (Figure 3.02). It is composed of 100 to 200m thick buff to yellow marl containing gastropoda, exeogyra, worm tracks and pelecypoda fragments and a very thick fossilifereous sandy limestone with intercalations of red sandstone containing fossil fragments and limestone concretions and of calcite cemented conglomerate (Figures 3.08 and 3.09). It was deposited within a continental to neritic environment in the latest Maastrichtian to Paleocene.

Figure 3.06 Measured stratigraphical section for the Yaylaçayı and Dizilitaşlar formations. The coordinates at the top of the figure are the beginning and ending northing (N) and easting (E) for the stratigraphic section (UTM based Turkish Grid).

N:21000-20250 E:97950-96500 G32-a3

FORMAT. | AGE | LITHOLOGY

Covered by Neogene

YAYLAÇAYI — LATE CAMPANIAN-MAASTRICHTIAN

Conglomerate with red to purple sandy and muddy matrix. Pebbles are derived mainly from volcanics

Creamy white to buff marl and greenish gray shale alternationl

Creamy white to buff clayey and tuffaceous limestone

Cross-bedded greenish gray to buff sandstone lenses

Polygenic dark green to gray conglomerate. Pebbles are mainly derived from ophiolites

Thin coal seams and organic rich mudstone

*84

84: *Quadran Fribidus*
Quadran gothicana
Microorhabdus decarutus
Crib. chreuvengi
Eif. furrseifeli

KARABALÇIK — E.-MIDD. EOCENE

TECTONIC CONTACT

Dark brown to greenish gray shale rich in organic matter and plant remains

83
82
81
80

79
78

Floating grais and pebbles in sandstone

ANGULAR UNCONFORMITY

NAOM — LATE CRET

Serpentinite and ultramafics

Massive basalt, various volcanics and volcaniclatics

TECTONIC CONTACT

Spilitic and pillow basalt

Matrix of the melange. Red to purple jasper and radiolarite, various volcaniclastics and vario-colored mudstone

KARABALÇIK — EARLY TO MIDDLE EOCENE

YONCALI

Plant remains

Shell fragments

Scoured base

20 metre

Figure 3.07 Measured stratigraphical section for the Yaylaçayı and Karabalçık formations. The coordinates at the top of the figure are the beginning and ending northing (N) and easting (E) for the stratigraphic section (UTM based Turkish Grid).
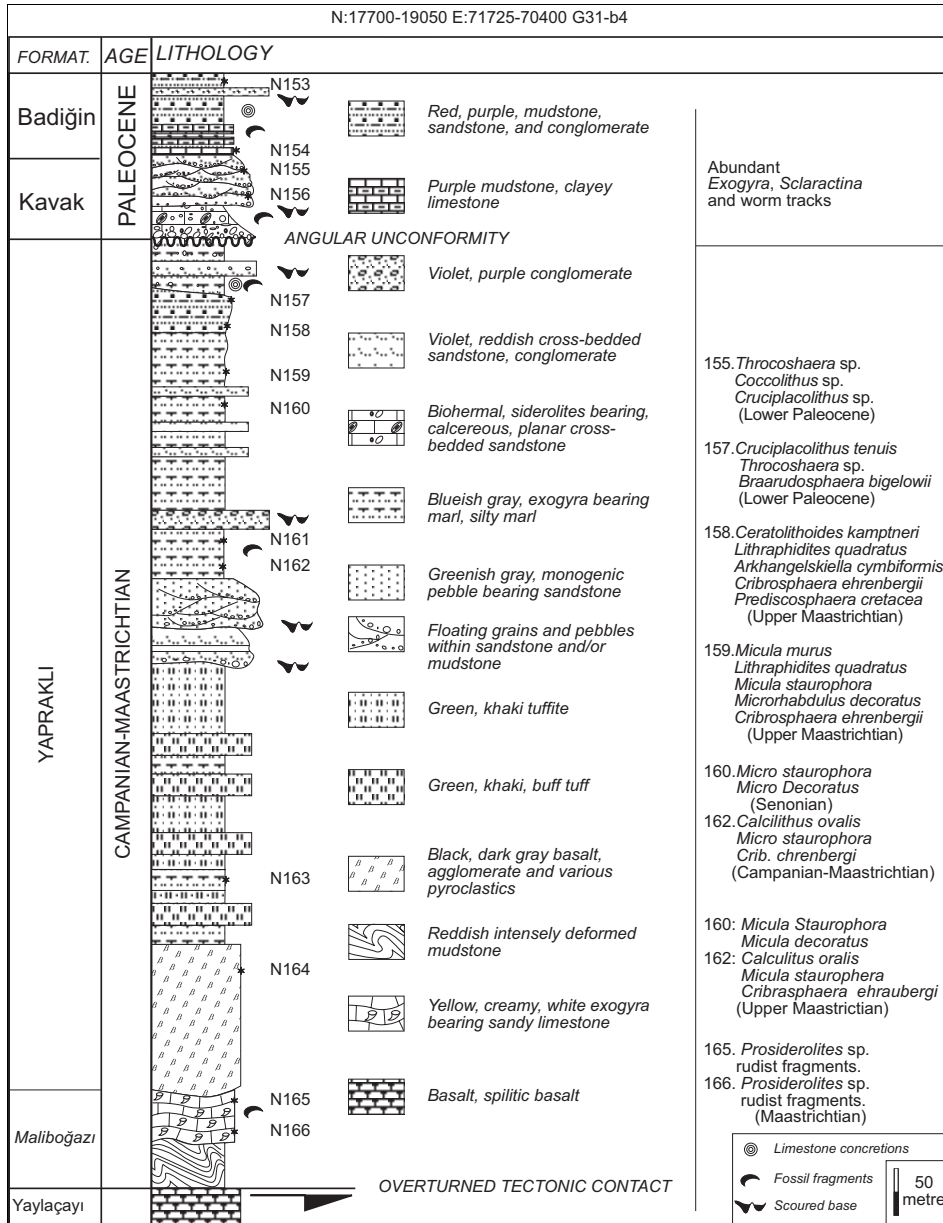
Figure 3.08 Measured stratigraphical section for the Yaprakli Formation. The coordinates at the top of the figure are the beginning and ending northing (N) and easting (E) for the stratigraphic section (UTM based Turkish Grid).

50

3.3.1.1.5 Dizilitaşlar Formation (Td, Maastrcihtian-Paleocene)

The name Dizilitaşlar Formation was first used by Norman (1972) for the Paleocene flyschoidal conglomerates and sandstones intercalated with neritic limestones (Figure 3.10). In the southwestern part of the Çankırı Basin, it is composed of an approximately 60 m thick green, greenish grey medium to thick (10-50 cm) bedded shale and thin (2-5 cm) bedded sandstone alternation at the bottom. This is succeeded conglomerates, thickly bedded (1-2 m locally) sandstone and shale alternation. The conglomerate pebbles are derived from the NAOM, Yaylaçayı, Yapraklı and Malıboğazı formations and felsic magmatic rocks (quartz-latite member of the NAOM). The sandstones are locally cross-bedded and graded. It is overlain by an approximately 50 m thick shale sequence alternating with thin-bedded sandstones (Figure 3.10).

The central part of the formation (Figure 3.10) is constituted by an approximately 100 m thick buff to dark grey neritic limestone (D3 member of Norman 1972), calcarenite and intercalated pebbly sandstone, boulder-conglomerates and shale. It also includes olistostromal horizons in which limestone blocks are set in a shaly matrix. The limy horizon is followed upwards by an alternation of medium to thick bedded shale and thin bedded sandstone with a cumulative thickness of approximately 200m. At the western margin of the basin, the Dizilitaşlar Formation is intensely deformed and folded. At the bottom, the Dizilitaşlar Formation is characterized by conglomerates and followed upwards with the neritic limestones. At the top part, it is constituted by an approximately 150m thick lime-cemented sandstone and conglomerates followed upwards with, approximately 150m thick, graded sandstone and thin beds of shale alternation of. In the northern margin of the basin, the Dizilitaşlar Formation is represented by a thin sandstone, shale alternation at the bottom and a very thick massive neritic limestone followed by a thin alternation of sandstone and shale (Figure 3.10).

The age of the Dizilitaşlar Formation is Paleocene (Norman 1972, Dellaloğlu *et al*. 1992).

According to Kazancı and Varol (1990), the Dizilitaşlar Formation, in the western margin of the Çankırı Basin, comprises a mass flow-dominated fan-delta (terminology after Nemec 1990; Postma 1983) complex at the bottom and sand dominated turbidites at the top. The limestones within the Dizilitaşlar Formation (D3 member) were deposited in fringing patch reefs in a regressive setting.

3.3.1.2 İskilip Group

3.3.1.2.1 Hacıhalil Formation (Th, Late Paleocene to Middle Eocene)

This formation was first named by Birgili *et al*. (1974). It is composed of alternations of conglomerates, sandstones and shale (Figure 3.11). Its correlation with the previous studies is illustrated in Figure 3.03 and the contact relations are indicated in Figure 3.04. It is exposed mainly in the northern and north-eastern margin of the basin (Figure 3.02). Its thickness ranges between 300 to 1360m.

In the northern part of the basin near Hacıhalil village (Figure 3.02), approximately 30m thick conglomerates rest on the NAOM (Figure 3.12b). The beds are up to 3m thick, poorly sorted and locally loosely packed. The matrix consists of sandstones. The largest pebbles are up to 20cm in diameter and are derived from the NAOM, Yaylaçayı, and Yapraklı formations. They are sub rounded to ellipsoidal, frequently displaying imbrication. The sandstones are up to 2m thick and locally graded. The shales include widespread

bioturbation, floating pebbles, mud-balls, plant and macro fossil fragments and widespread nummulite fossils (Figure 3.11). In this area, according to the sedimentological study of Ocakoğlu and Çiner (1997), the Hacıhalil Formation comprises 6 different facies. They are, from north to south: proximal alluvial fan, braided river, meandering river, fan delta, near shore to prodelta/open marine facies. The main sources of sediments are located to the north-west although sediments were also supplied from the south-east (Ocakoğlu and Çiner 1997).
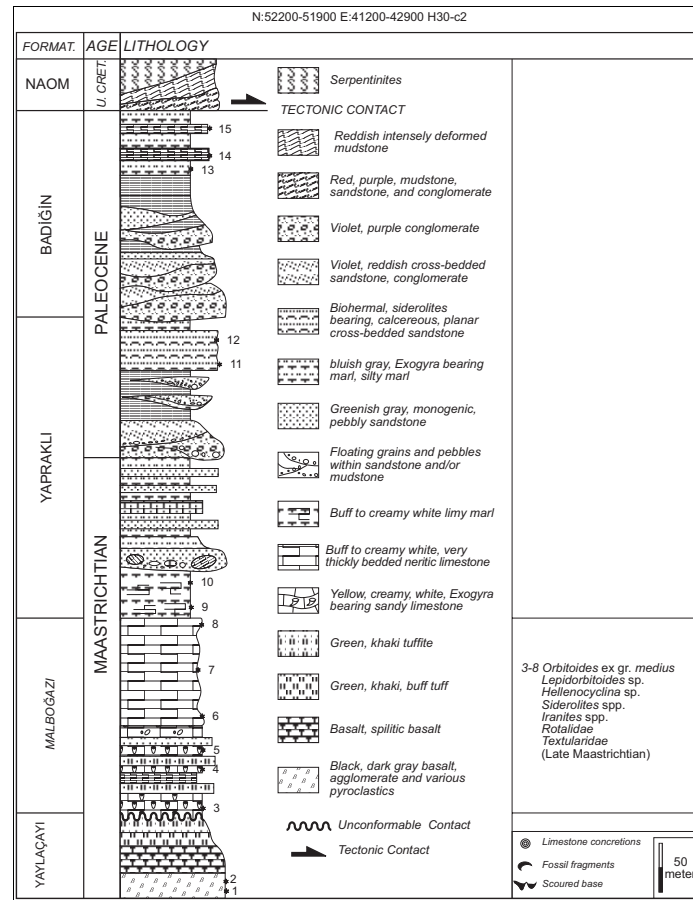
Figure 3.09 Measured stratigraphical section for the Malıboğazı, Yapraklı and Badiğin formations. The coordinates at the top of the figure are the beginning and ending northing (N) and easting (E) for the stratigraphic section (UTM based Turkish Grid).

The age of the Hacıhalil Formation, as indicated by its fossil contents (see Figure 3.11), is Late Paleocene to Middle Eocene, which has also been reported by Aziz (1974), Yoldaş (1982), Tüysüz (1985), Dellaloğlu *et al*. (1992), Õzçelik (1994).

3.3.1.2.2 Yoncalı Formation (Ty, Late Paleocene to Middle Eocene)

The Yoncalı Formation was first named by Birgili *et al*. (1974). It consists mainly of shale and sandstone alternations (Figures 3.13 and 3.14). It is always transitional at the bottom with the Hacıhalil Formation and has lateral and vertical gradations to the Karabalçık, Bayat, Osmankahya and Kocaçay formations. It is unconformably overlain by the Incik and younger formations. It has tectonic boundary relationships with the NAOM and is intruded by, generally, WNW-ESE orientated feeder dikes to the Bayat Formation (Őzçelik 1994, Demirer *et al*. 1992).. For example, in the north-eastern part of the area, the thrust contact between underlying Yoncalı Formation and overlying NAOM is intruded (Figure 3.12b, see also Őzçelik 1994). This relationship is very important as it constrains the tectonic emplacement of the NAOM that took place during or after the Late Paleocene to Middle Eocene.

In the northern part of the basin, the Yoncalı Formation is composed mainly of alternations of shale, sandstone and thin beds of conglomerate. The shales are dark green to dark grey, thin to thickly (10-100cm) bedded. The sandstones are dark green to buff, fine to medium grained. They are graded, planar cross-bedded and current ripple laminated at various levels. The conglomerates are made up of pebbles derived mainly from ophiolitic rocks including radiolarian chert, serpentinite, micritic limestones, basalt, and tuffs. They are subrounded to rounded, the largest clast size is around 5cm in diameter. Graded bedding is evident in places. The Yoncalı Formation also comprises olistostromes containing pelagic limestone, spilitic basalt and serpentinite blocks of various sizes (up to few tens of meters) embedded in the dark grey shales (Figures 3.13 and 3.14).

In the eastern margin, the Yoncalı Formation is characterized by regular alternations of sandstone, siltstone, shale, and pelagic limestone (Figure 3.14). The thickness of the beds ranges between 2-10 cm. In this part of the basin, the base of the Yoncalı Formation is also not exposed, as it is thrusted the NAOM.

The age of the unit is Late Paleocene to Middle Eocene as indicated by its fossil content (Figure 3.13 and 3.14).

3.3.1.2.3 Karabalçık Formation (Tk, Late Paleocene to Middle Eocene)

The Karabalçık Formation is represented mainly by conglomerates with alternating sandstones and shales and tuff/tuffite intercalations (Figures 3.13 and 3.15). It is well developed in the western and northern parts of the basin. In the east it is either not developed or represented by the channel-like patches of conglomerates within the Yoncalı Formation and channel-like conglomerates unconformably resting on the NAOM. In the northern part of the basin, the Karabalçık Formation laterally grades into the Yoncalı, Bayat and Osmankahya formations (Figures 3.03 and 3.04).

In the northern part of the Çankırı Basin, the Karabalçık Formation is characterized at the bottom by green, greenish grey, yellow to buff, thick bedded sub-rounded to well rounded pebbles of quartzite, mafic volcanics, vitric tuff, marble, granodiorite, white fossilifereous limestone, various green-schists, sandstones, radiolarian chert, and micritic limestones. Some parts of the conglomerates are intensely oxidised and have a clayey and sandy matrix cemented by secondary calcite. Towards the top, the conglomerates are succeeded by an alternation of yellowish grey, medium to thickly bedded sandstone, greenish grey medium to thickly bedded shale, and orange to buff thickly bedded

conglomerates. Higher up in the section the Karabalçık Formation is composed of sandstone, siltstone and marl alternations and at least four levels of economical coal horizons (up to 2m thick). Towards the top, a number of olistostromal levels and very thick (>5m) cross-bedded conglomeratic sandstones dominate (Figure 3.16). The top part includes intercalations of conglomerate and sandstones with fossiliferous horizons characterized by imbrication of transported and reworked nummulite fossils (Figure 3.15). The orientation of cross beds indicates sediment transport in NW to SE direction .
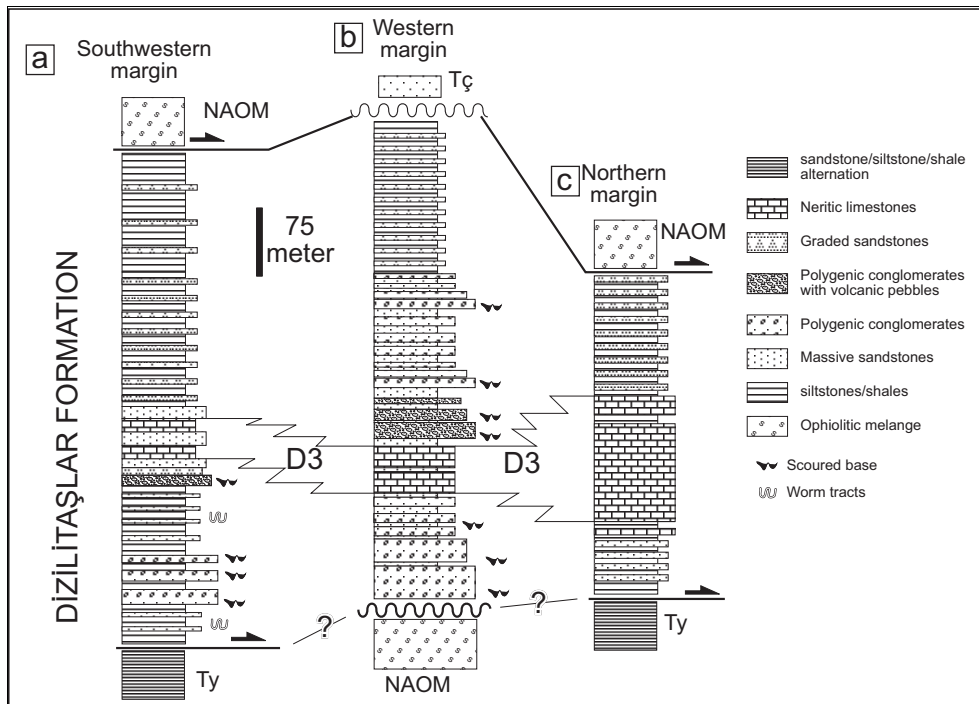
Figure 3.10 Generalized columnar sections for the Dizilitaşlar Formation in the southwestern, western and northern margins of the Çankırı Basin (partly modified after Norman 1972, Dellaloğlu et al.1992).

In the western parts of the basin, the Karabalçık Formation displays a very well developed coarsening upwards sequence starting from the Yoncalı Formation at the bottom and grading into the Osmankahya Formation, which in turn grades into Kocaçay Formation that marks the youngest marine unit in the basin. The beds of conglomerates may locally reach up to 5m thicknesses. Generally, they are loosely packed, unsorted and lack any internal sedimentary structure. But locally planar cross-bedded and graded horizons are present. The sandstones are medium to thickly bedded. Age of the formation is Late Paleocene to Middle Eocene as indicated by its fossil content (Figure 3.13 and 3.14).

3.3.1.2.4 Bayat Formation (Tb, Late Paleocene to Middle Eocene)

This unit was first named by Ayan (1969). It is a widespread unit in the northern and north-eastern parts of the study area. It is characterized by a volcano-sedimentary sequence. In the east, it is exposed along a narrow north-south strip (Figure 3.02).
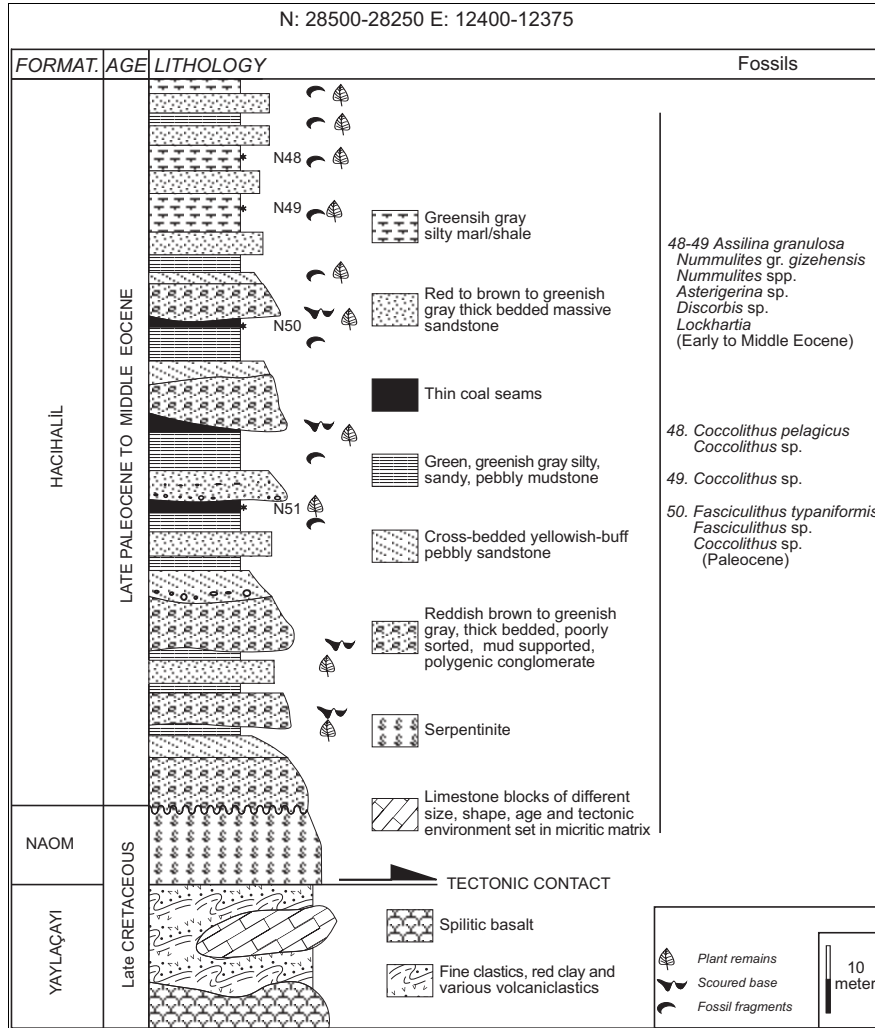
Figure 3.11 Measured stratigraphical section for the Hacıhalil Formation. The coordinates at the top of the figure are the beginning and ending northing (N) and easting (E) for the stratigraphic section (UTM based Turkish Grid).

55

a

SSW — X

Neogene

Incik

Osmankahya

Kocaçay

Karabalçık

Bayat

Yoncalı

Yaprakli

NAOM & Taylaçayı

Hacıhalil

X' — NNE

?

b

Hacıhalil

Yoncalı

NAOM

Coal seam

Green shale

Cross-bedded sanstone

Red polygenic conglomerate

30 meter

c

SW

NE

NAOM

Dykes

YONCALI

Locally intensely folded and sheared sandstone/siltstone/shale alternation

100 meter

56

Figure 3.12 a) Schematic cross-section along the line x-x' (for location see Figure 3.02c). b) schematic cross-section illustrating the thrust contact between the North Anatolian Ophiolitic Melange (NAOM) and the Yoncalı Formation is cut by the dykes of Bayat Formation. c) Blow-up figure depicting the relation between NAOM, Hacıhalil and Yoncalı formations.

Figure 3.13 Measured stratigraphical section for the Yoncalı and Karabalçık formations. The coordinates at the top of the figure are the beginning and ending northing (N) and easting (E) for the stratigraphic section (UTM based Turkish Grid).

N:78175-70900 E:22850-22250 H32-b2

FORMAT.	AGE	LITHOLOGY	DESCRIPTION	FOSSILS

İNCİK — U. EO. M. OLI.

BAYAT

YONCALI — LATE PALEOCENE TO MIDDLE EOCENE

YAYLAÇAYI

N212
N213
N214
N215
N216
N217
N218
N219
N220
N221
N222
N223
N224
N225

Descriptions:

Fluvial red, polygenic, poorly sorted locally inversely graded conglomerates

Volcanic breccia, agglomerate

Various pyroclastics, tuff, tuffite

Basalt, basaltic andesite

Greenish grey, shale, siltstone, sandstone alternation

Cross-bedded and locally graded sanstones

Poor to moderately sorted, pebble imbricated conglomerate

Red to purple, greenish grey mudstone

Olistostromal spilites

Serpentinites

Limestone blocks and olitostrommes

Sheared shale, siltstone, sandstone and thin limestone alternation

OVERTURNED TECTONIC CONTACT

Fossils:

213: *Discoaster binodosus*
Coccolithus pelacigus

217: *Ceratolithus aculeus*
Micula decoratus
Eiffellithuseximus
Micula staurophora

224. *Globigerina* sp.

224. *Sphenolithus radius*
Coculithus sp.
Tribroliyhus Orthostylus
Cycloccolithus fau.

225. *Discostea ladocunis*
Tribroliyhus orthostylus
Cycloccolithus fau.

50 metre

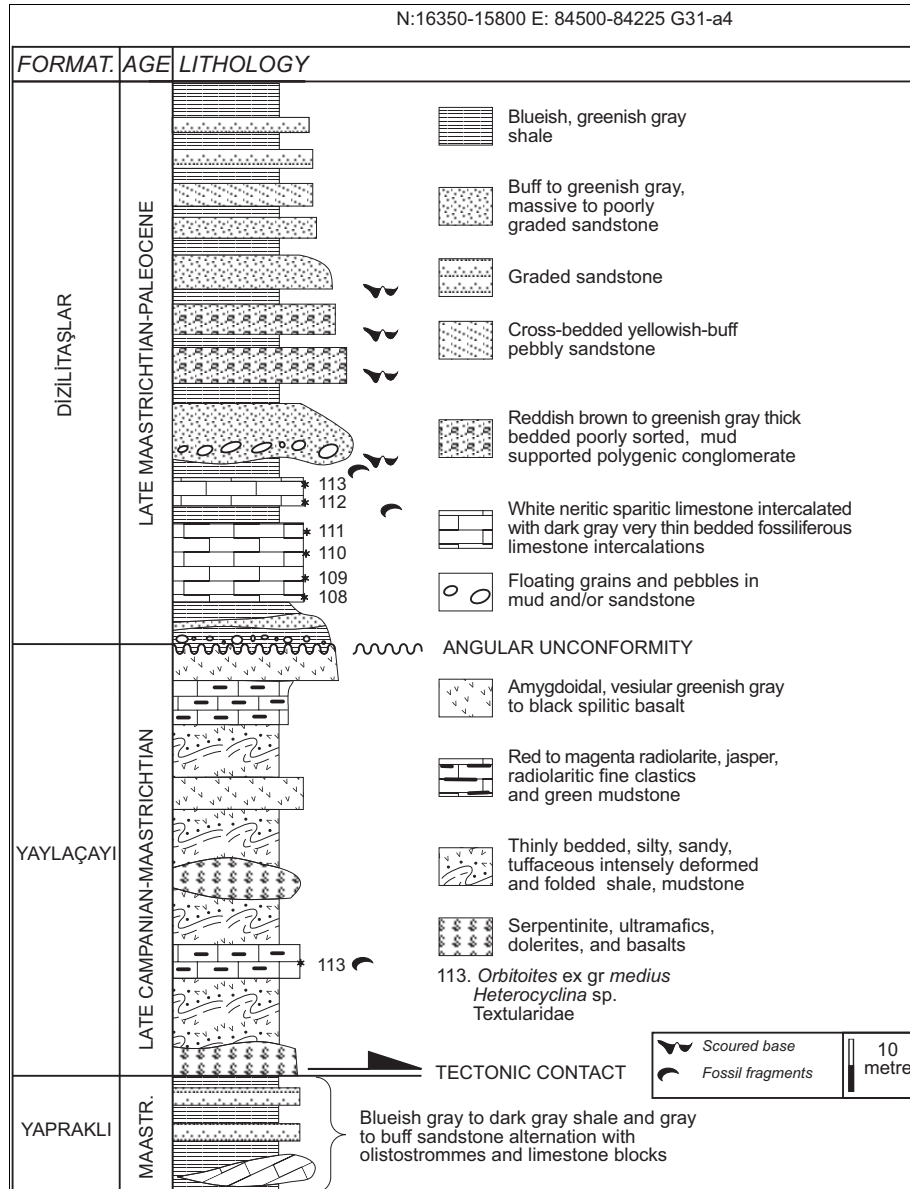*Figure 3.14 Measured stratigraphical section for the Yoncalı and the Bayat formations. The coordinates at the top of the figure are the beginning and ending northing (N) and easting (E) for the stratigraphic section (UTM based Turkish Grid).*
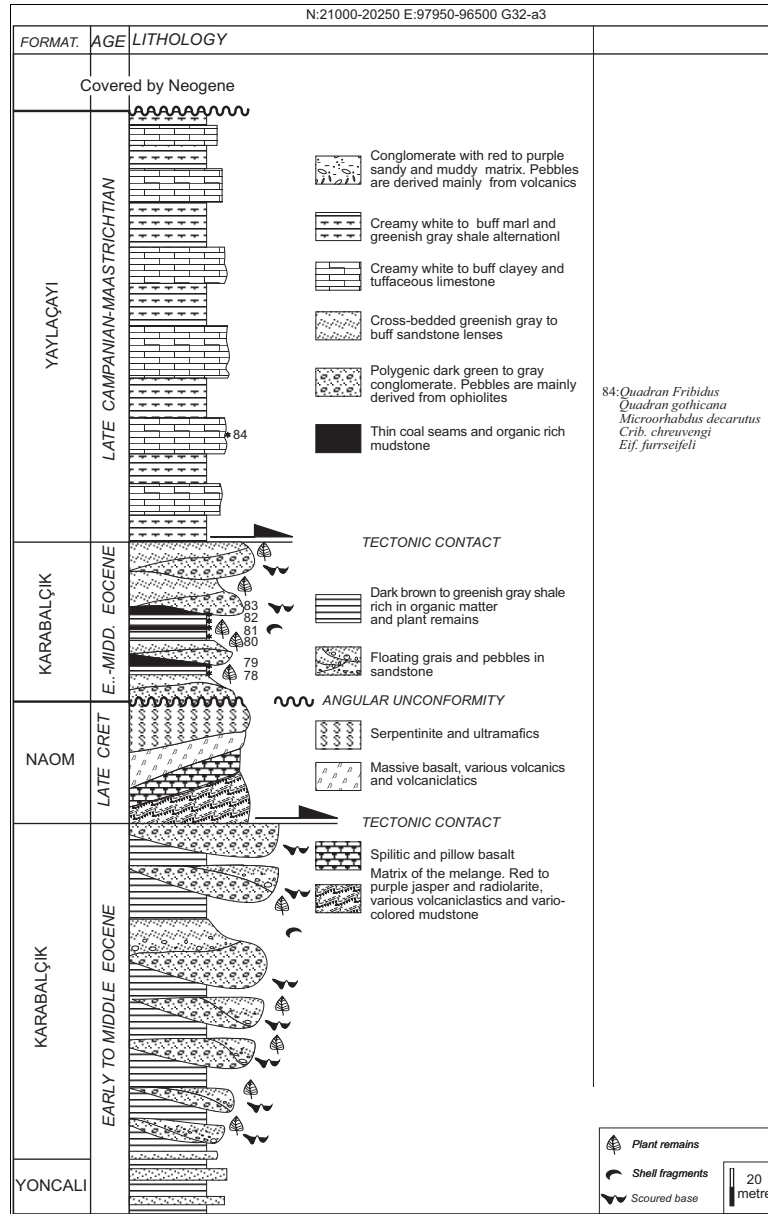
58

Locally, the Kocaçay Formation has an inter-fingering relationship with the Bayat Formation (Figure 3.18).

Lithologically, the Bayat Formation comprises two distinct parts (Figures 3.15,3.17 and 3.18). The lower part is composed of marl, sandstone, conglomerate, and tuff intercalations. The marls are green to dark green, medium to thickly bedded, generally tuffaceous, and locally contain conglomerate lenses of volcanogenic material. Sandstones are yellowish green, dark grey, generally medium bedded. The grains are medium to coarse in size, sub-angular to sub-rounded, derived from mafic to intermediate volcanics. They also contain wood and plant remains. The conglomerate lenses within the marls and tuffs are green to grey, medium to thick bedded. Pebbles are up to 10cm in diameter, sub-rounded. Tuffs are green, yellowish green, thin to medium bedded.

The upper part of the Bayat Formation is composed mostly of various volcanics intercalated with tuffaceous marls. Based on their origin and composition, the volcanics of the Bayat Formation are divided into four categories (Demirer *et al*. 1992): 1) tholeiitic-basalts and tholeiitic-olivine basalt of mantle origin, 2) hornblende-biotite-andesite, biotite-andesite, pumicic biotite-andesite, and hornblende-andesite lavas; 3) basaltic and andesitic lavas derived from continental crustal setting and 4) tuffs and agglomerates. In the north-east, just outside the studied portion of the Çankırı Basin, a number of NW-SE to WNW-ESE oriented dykes, which may range up to 10 km in length, have intruded the NAOM, Yoncalı and Karabalçik formations. Based on the similarity of their geochemical characteristics and emplacement ages, these dykes were interpreted to be the feeders of the volcanics of the Bayat Formation (see Özçelik 1994).

In this part of the Çankırı Basin, the Bayat Formation starts with medium bedded, poligenic conglomerates at the bottom and continues upward with an alternation of green, greenish grey tuffaceous sandstone and marl intercalated with tuff and agglomerates (Figures 3.15,3.17 and 3.18). The age of the Bayat Formation is Late Paleocene to Middle Eocene as indicated by its fossil content (Figure 3.15 and 3.18).

3.3.1.2.5 Osmankahya Formation (To, Early to Middle Eocene)

The Osmankahya Formation was first named by Birgili *et al*. (1974). It is characterized mainly by continental red clastics. Together with the Kocaçay Formation, it covers both the basin in-fill and the basement (Figures 3.15 and 3.19).

Lithologically, the Osmankahya Formation is composed of conglomerate, sandstone and mudstone alternations. In the northern part of the basin, it is characterized by very thick polygenic conglomerates, cross-bedded sandstones and red mudstones intercalated with thin tuffaceous beds. The pebbles of the conglomerates are locally imbricated and sandstones are characterized in some levels by ripple laminations (climbing and symmetrical ripples in places), trough and planar cross bedding and locally by epsilon cross-bedding indicating river channels. The cross-bedded conglomerates may reach up to 20m in thickness. In the northern part of the basin, west of Bayat, the cross-beds, pebble imbrications and very large-scale cross-bedding indicate an approximate NW to SE transport direction. In the west of Bayat town, the Osmankahya Formation includes inter-fingering of sandstones containing possibly intraformationally reworked and imbricated nummulite fossils.
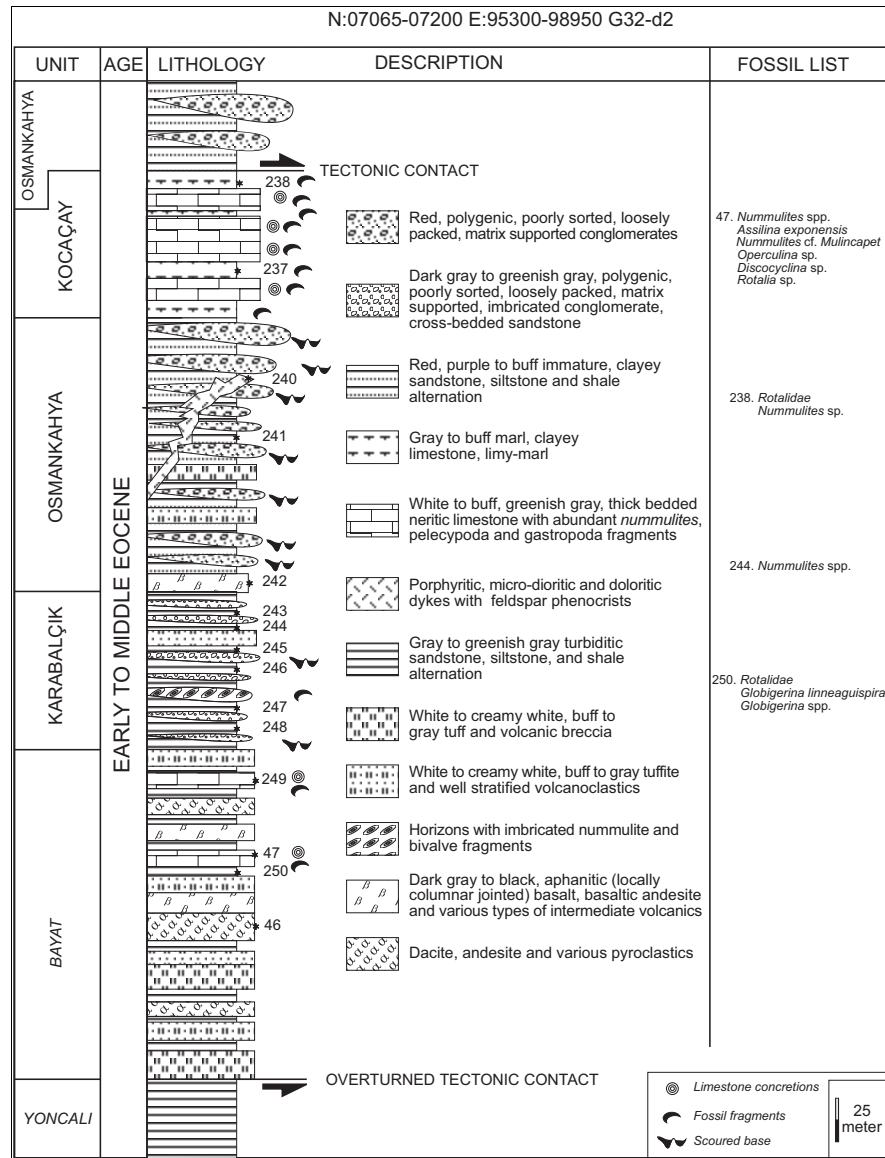
Figure 3.15 Measured stratigraphical section for the Bayat, Yoncalı, Karabalçık, and Kocaçay formations. Note that the Bayat Formation underlies the Yoncalı Formation that is generally higher in the stratigraphical position then the Yoncalı and Karabalçık formations. The coordinates at the top of the figure are the beginning and ending northing (N) and easting (E) for the stratigraphic section (UTM based Turkish Grid).

60
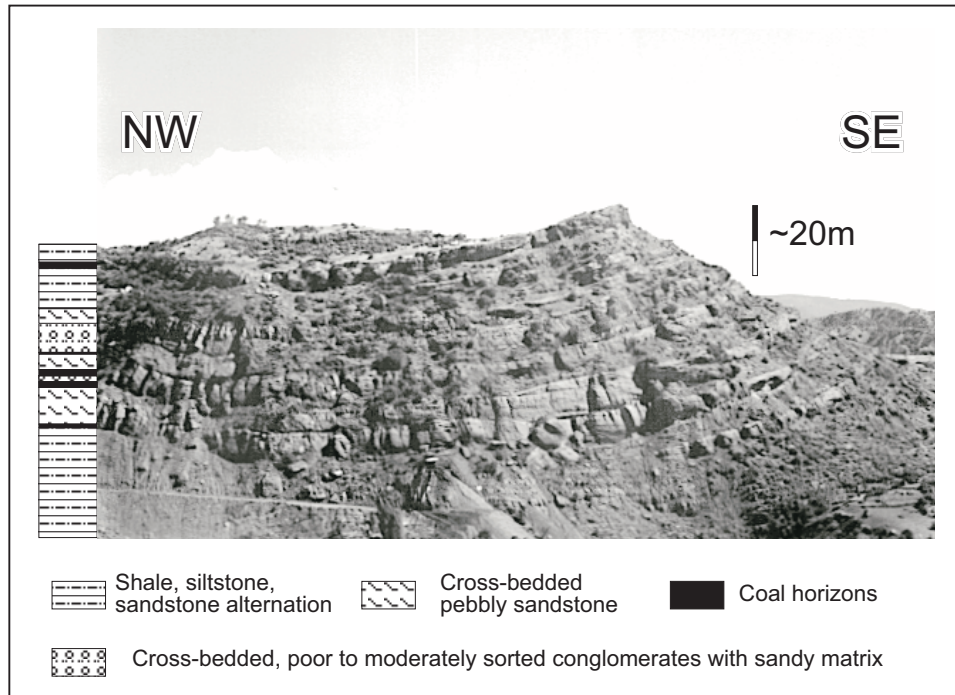
Figure 3.16 Photograph of upper coal bearing parts of the Karabalçik Formation in the northern part of the Çankırı Basin (Location is around N:07065, E:95300 G32-d2 quadrangle, view to NE).

In the south-western part of the study area, the Osmankahya Formation is characterized by an approximately 100 m thick alternation of red and greenish grey sandy mudstones, sandstones and lensoid conglomerates. At the top, the unit is characterized by an approximately 10m thick purple to brick red mudstone that grades into the Kocaçay Formation.

In the central parts of the basin, the Osmankahya Formation always separates granitoids of the Kırşehir Block from the Kocaçay Formation (Figures 3.02 and 3.19). and is characterized by red to brick red mudstones and sandstones.

The age of the unit, based on its stratigraphical position and pollen analysis, is Early to Middle Eocene (Ünalan, 1982; Yoldaş, 1982; Dellaloğlu *et al*. 1992).

3.3.1.2.6 Kocaçay Formation (Tko, Early to Middle Eocene)

This unit was first named by Birgili *et al*. (1974). It is characterized by a few meters to 100 m thick nummulitic and macrofossil dominated fossilifereous limestone and locally conglomeratic limestone with intraformationally reworked nummulites. It is one of the key horizons of the basin as it covers both the basin in-fill and the basement. It is a condensed sequence.

The Kocaçay Formation is divided into two distinct lithological levels (Figure 3.18). The lower most level is composed of thick-bedded nummulitic limestone with thin bedded marl intercalations. The topmost level is composed of brown to dark green, medium bedded, medium to fine-grained tuffaceous sandstone and shale alternation and marl intercalation. In south-eastern part of the study area it grades into an evaporitic horizon belonging to the Incik Formation. In the south-western part of the basin, the Kocaçay Formation is exposed in a narrow N-S oriented belt where it is characterized by nummulites, gastropods, and pelecypoda, laterally grading into conglomeratic, nodular limestone levels.

The age of the unit is Early to Middle Eocene as indicated by its fossil content (Figure 3.19).

3.3.1.3 Kalınpelit Group

The Kalınpelit group comprises the İncik and Gűvendik formations.

3.3.1.3.1 İncik Formation (Ti, post-Middle Eocene to Oligocene)

The İncik Formation was first named by Aziz (1975) and Birgili *et al* (1974). It is characterized by continental red clastics and it is the most widespread and voluminous units in the basin with thickness of more than 2000m.

In the northern areas of the basin, the Incik Formation is monotonous with the alternation of very thickly bedded (~2m) red conglomerates alternating with very thickly bedded, poorly sorted, immature red sandstones and purple to brick red, thick to very thickly bedded mudstones (Figure 3.20). The conglomerates and sandstones display lensoid patterns which, from north to south, laterally become thinner and finer and may pinch-out. From north to south, a number of internal angular unconformities (Figure 3.25) coinciding with a number of coarsening upwards sequences are observed in the northern part of the basin. The angular discrepancy between the underlying and overlying sequences of the İncik Formation decreases from north to south. The pebbles are derived mainly from the NAOM and Yaylaçayı Formation, including serpentinites, ultramafics, radiolarites and various volcanics.

In the south-west of the basin, the İncik Formation has similar characteristics similar to its northern counterparts. The grain size, the dips of the bedding, bed thickness and the overall thickness of the unit decrease from west to east and the formation on-laps on to the basement (Figure 3.25d).

In the east, the İncik Formation conformably rests on the Kocaçay Formation. At the bottom it is characterized by creamy white gypsum, which laterally and vertically grades into green shale and is the oldest gypsum observed in the field. The color of the shale gradually changes from green to red and finally into purple. It is approximately 50m thick. The sequence is followed upwards by thin to medium bedded (10-50 cm), brick red to purple, ripple laminated, tabular cross-bedded sandstones alternating with red to purple, siltstone and silty-mudstones. Higher up in the section, the sequence is characterized by an alternation of brick red to purple sandstones, siltstones, shale and greenish gray to bluish gray shale and very thick bedded (1-2m) red to orange gypsum horizons. The sequence gradually becomes coarser grained and the beds thicker. In the upper parts, the unit is characterized by circa 500m of monotonously alternating thick to very thick-bedded polygenic conglomerates, and red sandy to silty shales. The overall sequence coarsens upwards and only in the top most 100m of the unit is a fining upwards sequence

62

present. As in the other parts of the basin, internal angular unconformities are frequently encountered (Figure 3.25).

Figure 3.17 Measured stratigraphical section for the Bayat and Kocaçay formations. Note the inter-tonguing of the Kocaçay Formation. The coordinates at the top of the figure are the beginning and ending northing (N) and easting (E) for the stratigraphic section (UTM based Turkish Grid).

63

N:00800-00700 E:05550-01900 G32-d2

FORMAT.	AGE	LITHOLOGY	EXPLANATIONS	FOSSILS

İNCİK — U. EOC OLIGO

LOCAL UNCONFORMITY

KOCAÇAY — MIDDLE EOCENE

N101
N100
N99
N98
N97
N96

Alveolina and nummulites bearing pebbly limestone.

Cross-bedded sandstone

101. *Orbitolites* sp.
Gypsina sp.
Asterigerina sp.
Alveolina sp.

100. *Discocyclina discus*
Operculina spp.
Discocyclina spp.
Hasterigerina sp.
Nummulites milnecaput
Alveolina spp.
Nummulites spp.

BAYAT — EARLY-MIDDLE EOCENE

Conglomerate and pebbly limestone with bivalve fragments

Lenses of nummulite, alveolina, assilina, and shell fragments bearing reefal limestone

Poligenic conglomerate with pebbles of radiolarite, chert, spilite and various volcanics

N94

Marl, shale

Tuff

Tuffite

99. *Sphaerogypsina* sp.
Alveolina sp.
Operculina sp.
Rotalidae

98. *Discocyclina* spp.
Nummulites spp.
Sphaerogypsina sp.
Operculina sp.
Rotalidae

N93
N92
N64
N65
N66

Andesite and basaltic andesite

Tuff, tuffite, agglomerate, and volcanic breccia

N67

Shale, siltstone, sandstone alternation (sandstone/shale=1/10)

N68

N69

97. *Rotalidae*
Anomalinidae
Acarina bullbroski
Globigerina lineaperta
Globigerina eocenae
Globigerina lineapurspina
Turborotalia cerr. frontosa
Turborotaila cerr. pasagonensis
Pemma Popilotus
Sphenolithus abtusus ch. Expasus
Zygr. Biyugatus
Braarudosphaera bigelowii
Chiastmolithus grandus
Discoaster barbadiensis
Helicosphaera sensinulum

96. *Discoaster binodosus*
Cyclocea famusus

94. *Operculina* sp.
Miliolidea

KARABALCIK

Alternation of green, purple, grey tuff and various volcaniclastics

N70
N71

70. *Acarina bullbroski*
Globigerina eocena
Globigerina lineoperta

N72
N73

YONCALI

Concretions
scoured base
plant remains
shell fragments

60 meter

Figure 3.18 Measured stratigraphical section for the Karbalçık, Bayat and the Kocaçay formations (compare the stratigraphical positions of Bayat and other units with the Figures 3.13 and 3.14). The coordinates at the top of the figure are the beginning and ending northing (N) and easting (E) for the stratigraphic section (UTM based Turkish Grid).
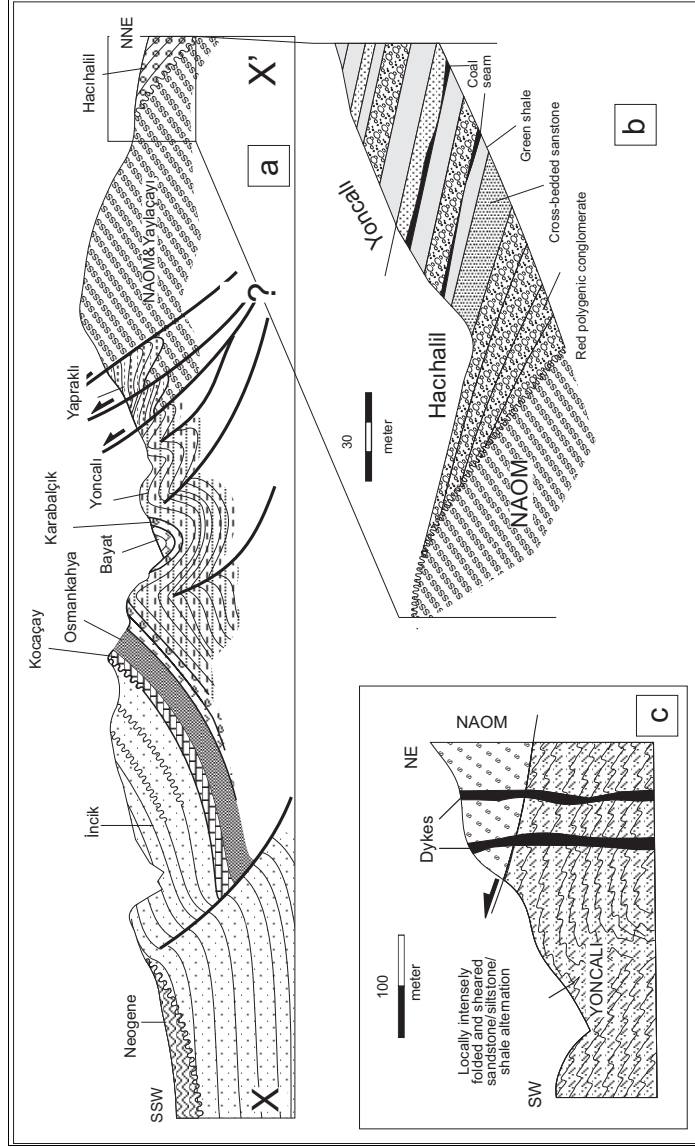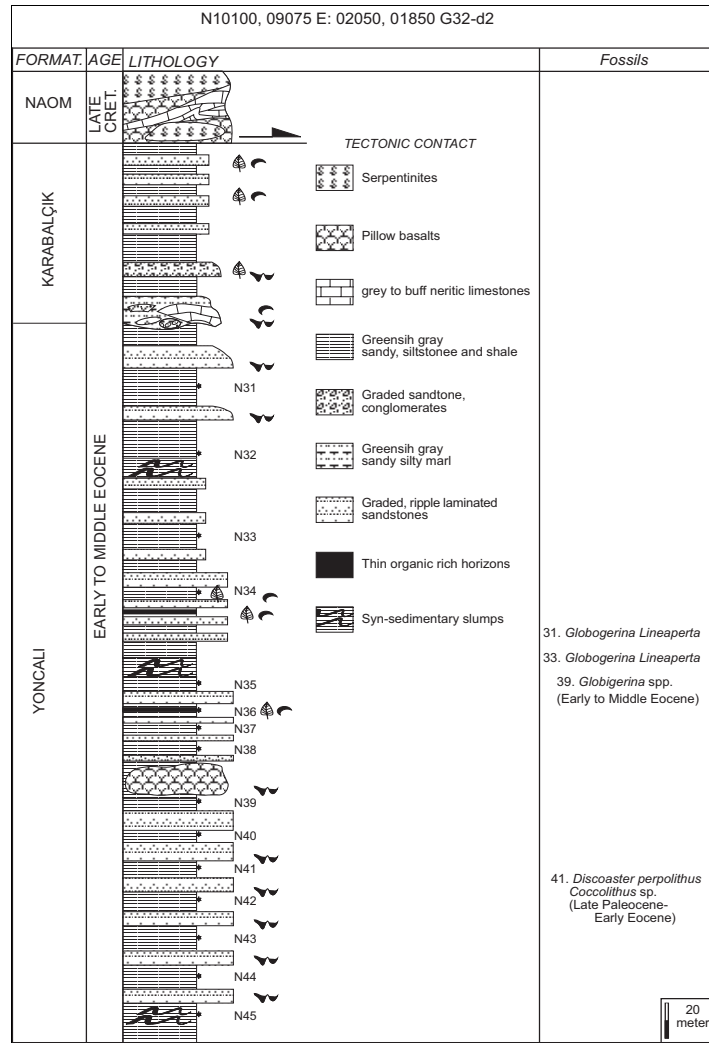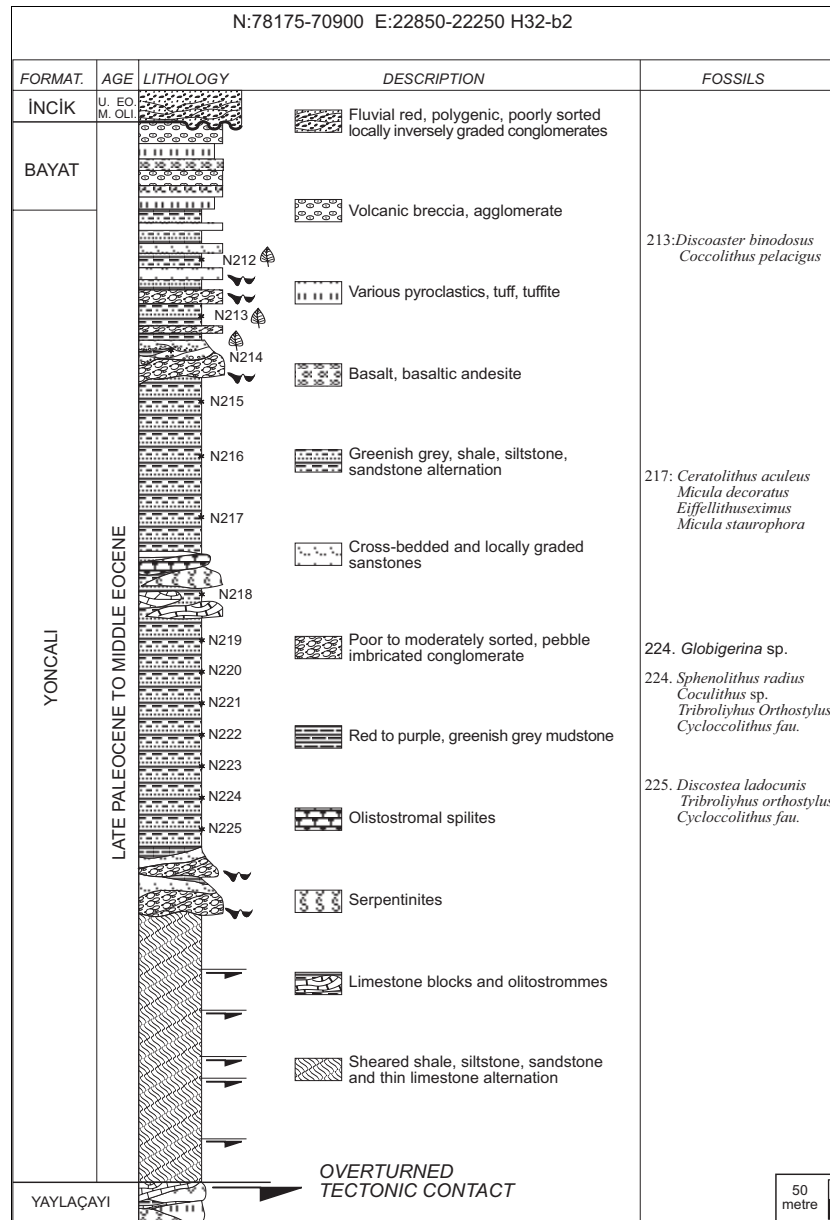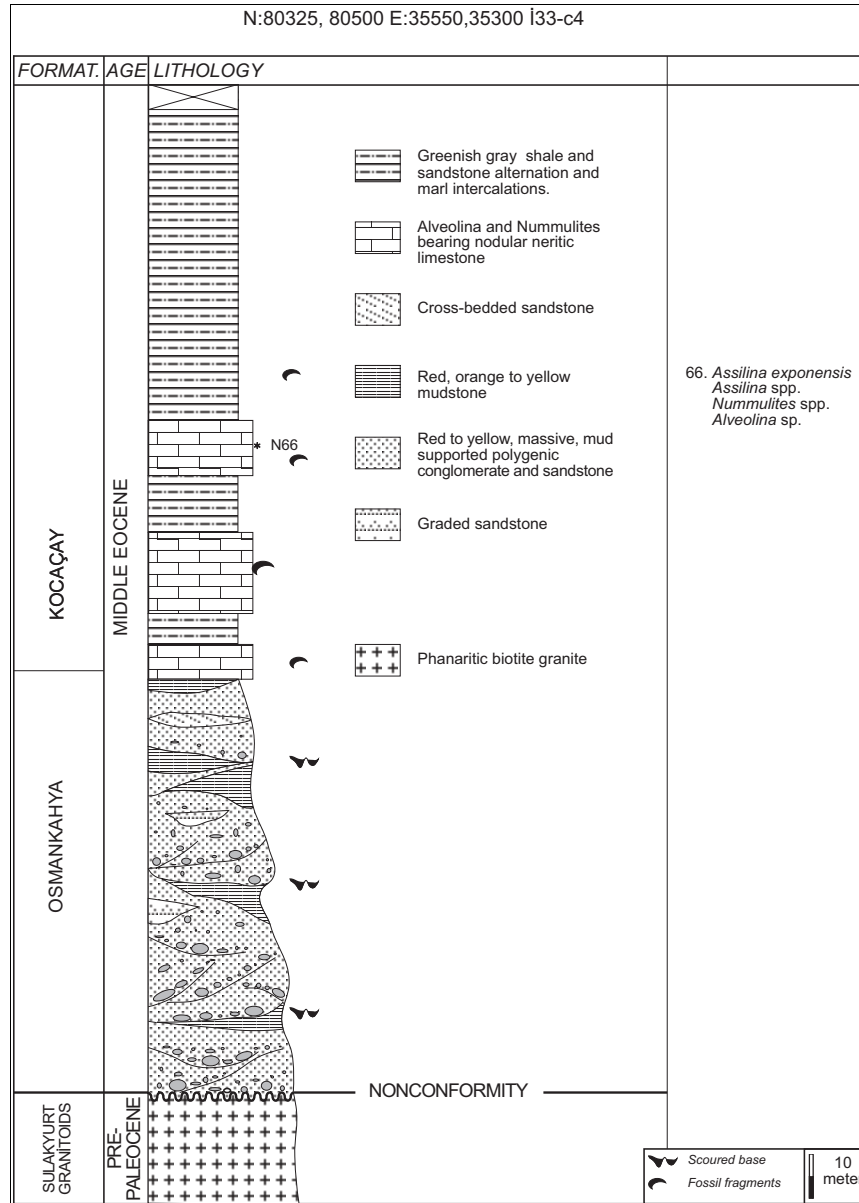
Figure 3.19 Measured stratigraphical section for the Osmankahya and the Kocaçay formations. The coordinates at the top of the figure are the beginning and ending northing (N) and easting (E) for the stratigraphic section (UTM based Turkish Grid).

65

In the Sağpazar-1 well drilled by the Turkish Petroleum Co. near 20 km south of Bayat (Figure 3.02), the İncik and Kocaçay formations inter-finger and the İncik Formation is characterized by a very thick sequence of (>2000m) evaporites, conglomerates, sandstones and shale alternations. The evaporites include gypsum, anhydrite, and rock-salt which were not encountered during the field studies. The evaporites are also known from rock-salt mines in the basin.

The age of the Incik Formation is not known precisely, because of a lack of fossils. Based on its relation with the Early to Middle Eocene Kocaçay Formation and the overlying Oligocene Güvendik formation, the age of the formation is bracketed between post-Middle Eocene and pre-Oligocene.

3.3.1.3.2 Güvendik Formation (Tg, Oligocene)

The Güvendik formation is named for the first time in this study. In previous studies (see Figure 3.03) it was erroneously mapped together with the Upper Miocene Tuğlu formation (discussed in chapter 4). In this study they are recognized and mapped separately (Figure 3.02) for the reasons outlined below.

Although, the Güvendik formation is intensely deformed at the bottom and the top, three distinct levels can still be recognized (Figure 3.20). At the bottom and the top, it is composed of very thickly bedded, finely laminated and intensely deformed gypsum alternating with thin to medium bedded buff to creamy white gypsifereous marls. In the middle, it is composed of greenish grey shales frequently scoured by lenses of micro-conglomerates. Five km west of Güvendik village (Figure 3.02), the shales include very thin organic horizons with fresh water gastropoda and pelecypoda fragments. From samples collected at this site *Eucricetodon sp.* and from the Gözükızıllı sites (for the location of these sites see Figure 3.02) *Eucricetodon* sp. (only incisors), *Ctenodactylidae*, and *Tataronyinen* n.gen. n.sp. rodents were found. Based on these rodents, an Oligocene age is deduced for the Güvendik formation (Figure 3.20).

3.3.2 Southern Units

The southern units include the Sivritepe group, which consists of the Karagüney, and Mahmatlar formations.

3.3.2.1 Sivritepe Group

The Sivritepe group comprises the Late Paleocene to Middle Eocene Karagüney and Mahmatlar formations.

3.3.2.1.1 Karagüney (Tkg) and Mahmatlar (Tm) Formations (Late Paleocene to Middle Eocene)

The Karagüney and Mahmatlar formations are exposed only in the south-western part of the Çankırı Basin. The stratigraphical position of these two formations is very different from any other of the basin filling units of the Çankırı Basin because they are the oldest units which are resting directly on the Kırşehir Block (Figures 3.02,3.22a, and 3.23) and include detritus derived mainly from the Sulakyurt granitoids and the intruded ophiolites. The Karagüney and Mahmatlar formations were first named and described by Norman (1972).
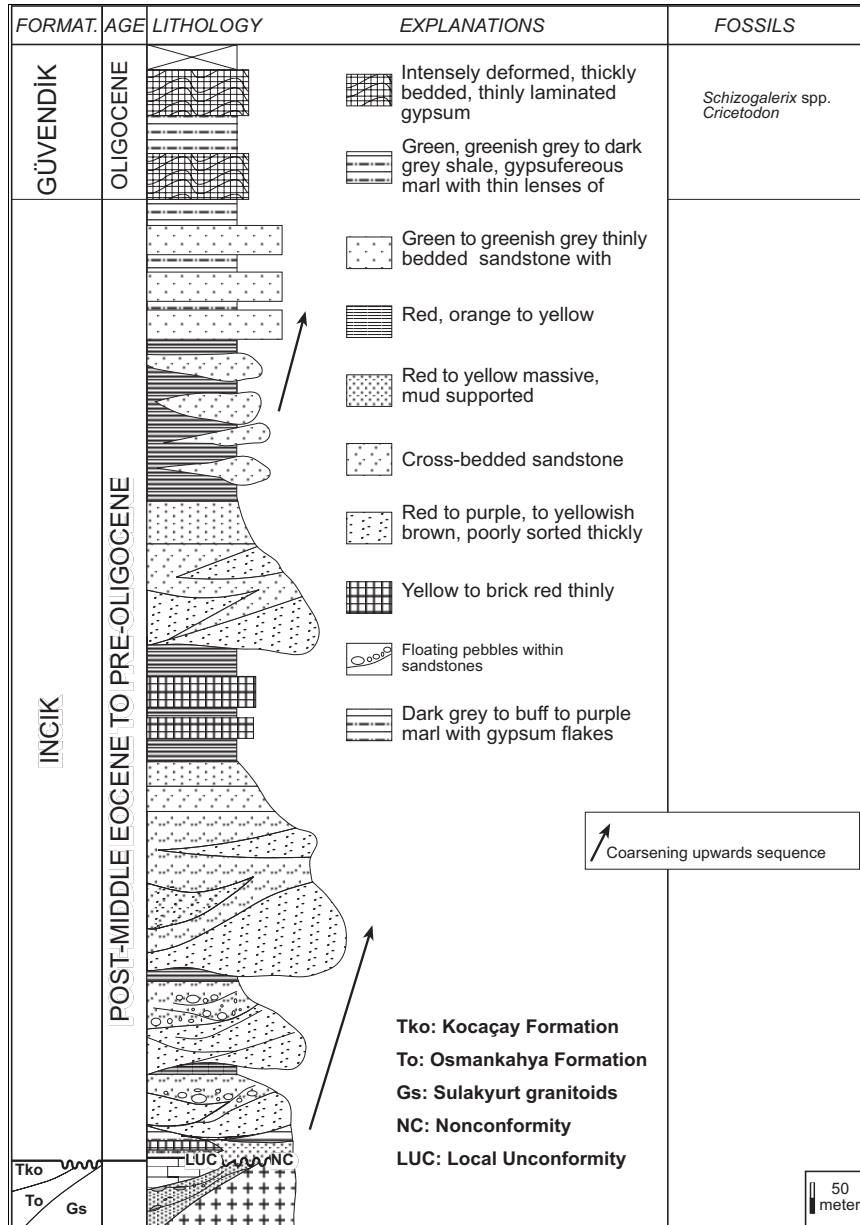
Figure 3.20 Generalized stratigraphical section for the İncik and Gűvendik formations (İncik formation is partly modified after Dellaloğlu et al. 1992)

67

The Karagüney Formation (Figure 3.21) is composed of reddish conglomerates characterized by sub-angular blocks and boulders derived from ophiolites in a fining upwards sequence. The granite clasts are only observed in the upper parts of the unit and they reach up to 50cm in diameter. The boundary relations of the Karagüney Formation with other units are indicated in Figure 3.04. The thickness of the unit is about 100 m.

The Mahmatlar Formation (Figure 3.21) is characterized mainly by detritus derived from the granitoids. It includes sub angular to ellipsoidal granite and ophiolite related boulders and blocks at the bottom. The grain size rapidly decreases and the matrix becomes more limey and nummilite fossils become dominant from bottom to top and from north to south. In the upper parts of the formation, arkosic sandstones dominate (Figure 3.21). The thickness of the unit is variable and reaches a maximum of about 200 m near Sivritepe Hill (Figure 3.02).

The sub-angular blocks and boulders indicate that they have not been transported long distances and hence are more likely to be derived from the ophiolites that are intruded by the granitoids in the center of the basin (Sulakyurt granitoids) rather than the ophiolites at the rim of the basin. Having mainly ophiolite pebbles in the Karagüney Formation and granitic pebbles in the overlying Mahmatlar Formation indicate an inverse stratigraphical relationship during the erosion and transportation processes; such that, first the ophiolitic cover was eroded away then the underlying granitoids were eroded (i.e. progressive un-roofing) (Figure 3.22b).

In the study area, no fossils have been recovered from the Karagüney and Mahmatlar formations. However, these two units laterally grade into the Late Paleocene to Middle Eocene Yoncalı Formation of the northern part of the basin and allows correlation between the two areas. Based on this relationship, the Karagüney and Mahmatlar formations are interpreted to have been deposited in the Late Paleocene to Middle Eocene.

3.4 Temporal Relationships

A correlation chart for pre-Neogene of the Çankırı Basin is presented in Figure 3.24. Due to repeated tectonic activity, which is characterized by two distinct thrusting events and later by extensional and, finally, by regional transcurrent tectonics (discussed in the chapters 4 and 5), the boundary relationships and lateral continuity between individual formations are partly obliterated. The most noticeable boundary relationships observed, in relation to the evolution of the Çankırı Basin, are the syn-depositional unconformities between different formations and frequently within the same formation (e.g. İncik Formation). The types of unconformities encountered in the field are depicted in Figure 3.25 and are thought to reflect tectonic activity.

The oldest syn-depositional unconformities are observed between the NAOM and the Malıboğazı Formation (indicated by 3 in Figure 3.24) and between the Yapraklı and Kavak formations in the NW part of the Çankırı Basin (Figures 3.25a and 3.24). This unconformity in turn is unconformably overlain by the İncik Formation (Figure 3.25a). The Kavak formation unconformably overlies the thrust contact between Yapraklı and Yaylaçayı formations (indicated by 2 in Figure 3.24). These relationships are interpreted as indicating syn-depositional thrusting during the deposition of the Yapraklı and Kavak formations in which thrusting occurred from NW to SE (present day orientations) (Figures 3.02 and 3.24).

FORMAT.	AGE	LITHOLOGY	EXPLANATIONS

Pebbly-, Sandy-, silty-, clayey-limestone with nummulites

Yellow, buff to creamy white arkosic silty-, limy-shale/marl with nummulits

Yellow to buff, creamy white to pinkish arkosic, cross-bedded sandstone

Conglomerates mainly with granitic and minor ophiolitic pebbles, cobbles and boulders

Poorly sorted pebbly sanstones with sub-angular to sub-rounded pebbles derived from ophiolites and granitoids

Poorly sorted boulder to cobble conglomerates with sub-angular grains derived from the ophiolites and the granitoids

Red to purple, to yellowish brown, pebbly sandstones with pebbles derived only from the ophiolites

Green to red to yellow to brick red conglomerates with angular pebbles derived only from the ophiolites

ophiolites intruded by the Sulakyurt granitoids

Sulakyurt granitoids

NONCONFORMITY

20 meter

Figure 3.21 Generalized stratigraphical section for the Karagűney and Mahmatlar formations around the Sivritepe Hill (partly based on Norman 1972).

69

The same relations are also observed between İncik Formation and underlying Kocaçay Formation and within the İncik Formation itself (Figure 3.21b and c) which is indicative of contemporaneous differential uplift due to tectonic activity and sedimentation during the deposition of the İncik Formation in post-Middle Eocene to pre-Oligocene times.

Another type of contact relationship is the progressive on-lap of the Osmankahya, Kocaçay, and İncik formations on the granitic basement (Figure 3.22, 3.23 and 3.25e). This, together with the syn-depositional unconformities in the outer (away from the basement) parts and on-lap patterns on the basement, indicate progressive migration of the depocenter towards the basement (see also chapter 2).

The most evident boundary relationship with respect to timing of thrusting is observed in the NE just outside of the study area but within the Çankırı Basin (see Özçelik 1994). Here a number of NNW-SSE oriented feeder dykes for the volcanics of the Bayat Formation cut the thrust contact between the Yoncalı Formation and the NAOM (Figure 3.12c) indicating that thrusting occurred before the deposition of the Bayat Formation in the Early to Middle Eocene.

According to Norman (1972) and Görür *et al*. (1984) the contacts between the Paleocene and Eocene units are transitional in the south-western part of the Çankırı Basin and further to the SW, in the Tuz Gölü (Salt Lake) Basin (Figure 3.01). However, it is tectonic in the studied portion of the Çankırı Basin. The relationship between these units is very important with respect to the tectonic evolution of the basin. It infers that the tectonism and accompanying sedimentation is continuous from the Late Cretaceous to Eocene. However, the reworked Paleocene fauna in the Yoncalı and Karabalçık formations in the SW margin of the basin implies that the boundary between the Late Cretaceous to Paleocene formations and the Late Paleocene to Middle Eocene formations must at least be a local unconformity. This relation implies two possibilities. The first one is that the local unconformable relationship between the Dizilitaşlar and Eocene units is a syn-depositional unconformity and, consequently thrusting and sedimentation were coeval. The second possibility is that it is a regional unconformity and that after the deposition of the Dizilitaşlar Formation the tectonic regime completely changed; that is in the Late Paleocene to Early Eocene, a new tectonic phase commenced. We prefer the second option because the tectonic events in the Late Cretaceous to Paleocene and in the Early Tertiary (as explained in the next section) and the paleomagnetic results (see chapter 7) support this view.

3.5 Discussion

3.5.1 Importance of the Lateral Gradation Between Northern and Southern Units

In the southwestern part of the basin, the Karagűney and Mahmatlar formations which are the southern, laterally grade into the northern units chiefly Yoncalı, Karabalçık and Osmankahya formations (Figure 3.22 and 3.23). As discussed previously, the southern units are derived mainly form the ophiolites and the granitoids of the Kırşehir block. The inverse stratigraphic relationship between the stratigraphic position of the source and the sediments indicates progressive unroofing of the Kırşehir Block (Figure 3.22b). The lateral gradation of these units with the northern units indicate that in Early to Middle Eocene times the Çankırı Basin was supplied with detritus both from the rim areas and from the

basement (Figure 3.26). The on-lap pattern of the northern and southern units on to the basement (see also chapter 2) indicates that the depocenter migrated towards the basement, which contemporaneously shed detritus to the southern units (Figure 3.26).

3.5.2 Lateral Gradations within the Northern Units

The Yaylaçayı Formation locally constitutes the matrix for the NAOM, which indicates that deposition of the Yaylaçayı Formation and generation of mélange (NAOM) were contemporaneous. The Yaylaçayı Formation was deposited within fore-arc to inter-arc environments and includes volcanics and volcanoclastics, which originated from a seamount setting (Tűysűz *et al*. 1995). The Yapraklı Formation is time equivalent of the Yaylaçayı Formation but was deposited in shallower and proximal depositional settings. Lateral gradation of the Malıboğazı Formation with the Yapraklı Formation and the presence of rudist fossils indicate that the Malıboğazı Formation was deposited in areas where the water depth was shallow enough for rudists and other benthic fauna to survive and which indicates shallowing of depositional environments due to differential uplift. Koçyiğit *et al*. (1988) and Koçyiğit (1991) argued that the rudist bearing units, in the Ankara region (Figure 1), were deposited at the crest of an accretionary wedge, which was locally uplifted and eroded to supply detritus from the NAOM to a unit, which is the time equivalent to the Kavak formation in the Çankırı Basin.

The Kavak formation was deposited in a transitional continental to marine (mixed) environment in which in the neritic parts the Badiğin formation was deposited (Figure 3.24b). The Presence of sub-angular blocks and boulders derived from the NAOM and from the other Late Cretaceous units indicate that this formation was deposited close to its source. During the deposition of this unit, the NAOM, Yaylaçayı and Yapraklı formations must have been sub-aerially exposed locally, in order to supply detritus to this unit. A local unconformable relationship between the Kavak and Yapraklı formations indicates ongoing sedimentation and tectonism that resulted in contemporaneous local uplift due to thrusting and accompanied by sedimentation, which accommodated the space, created in the front of the thrusts. A similar relationship is also observed between the Yaylaçayı and Dizilitaşlar formations (Figure 3.06, 5 in Figure 3.24). As seen in the Figure 3.24a, the Malıboğazı Formation has similar tectono-stratigraphical characteristics to the Kavak and Badiğin formations. Considering its relation with the Yaylaçayı and Yapraklı formations, the depositional environments of the Malıboğazı Formation must have been similar to the Kavak and Badiğin formations (3 in Figure 3.24). These observations indicate that during the Late Cretaceous to Paleocene thrusting occurred along with thrust related sedimentation (Figure 3.24b). The presence of plant remains and dominance of terrigeneous material in the Yapraklı Formation and the other Paleocene units and the dominance of continental settings in many areas of Turkey (Şengőr and Yılmaz 1981, Gőkten 1983, Gőrűr *et al*. 1984, Gőncűoğlu *et al*. 1993, Okay *et al*. 1996) indicates that the depositional environments were close to the land and the marine areas were restricted.

The Hacıhalil, Yoncalı, Karabalçık, parts of the Bayat, the Osmankahya, and Kocaçay formations are mainly marine formations and have lateral gradations with each other. Among these the Hacıhalil Formation is continental in its lower part and gradually becomes marine as it grades into the Yoncalı Formation. The Yoncalı Formation represents the more basinal facies of these formations and is characterized by a flyshoid sequence. The Karabalçık Formation is represented by conglomerates with local coarsening upwards sequences. The Osmankahya Formation overlies the Karabalçık

Formation and was deposited mainly in continental settings intercalated with marine settings. The Kocaçay Formation covers all of these units and is characterized by a condensed sequence of nummulitic limestones. The Bayat Formation is represented mainly by volcanic and volcanogenic units embedded within the Early to Middle Eocene sequence. The Incik Formation is characterized mainly by continental deposits and overlies all the above units (Figure 3.24a) and is characterized by local unconformities developed progressively during the activity on the thrust faults (syn-depositional unconformities, Figure 3.25) and is associated with coarsening upwards sequences. The Güvendik formation was deposited within lacustrine settings as evidenced by the presence of lacustrine fauna (Figure 3.20).

The Early Tertiary formations of the Çankırı Basin are organized in a way that the oldest units (e.g. Dizlitaşlar and Hacıhalil formations) crop out parallel to and close to the basin rim while the other formations (Yoncalı to Güvendik formations) become younger towards the center of the basin (Figure 3.02). The on-lap patterns of these formations onto the Kırşehir Block (discussed previously and in chapter 2) indicates that the depocenter migrated basement-ward (Figure 3.24a) i.e. south-wards. The depositional environments became shallower and finally continental, from the base towards the top (see Figure 3.24a). In addition, the Early Tertiary units have a wedge shaped geometry thinning towards the basement (see Figures 3.12,3.22,3.23 and chapter 2), which indicates that the depocenter migrated towards the basement and together with associated syn-depositional unconformities indicate a coupling between sedimentation and deformation in the Early Tertiary.

The organization of facies, which become relatively younger from the basin rim towards the center (Figure 3.24a), wedge-like in-fill patterns and progressive, syn-depositional unconformities can be produced in various tectonic regimes extending from extensional, transcurrent to thrust regimes. However, cross-cutting of thrust faults by dykes that fed the volcanics of the Bayat Formation (Figure 3.12c), basement-wards migration of thrust faults (see chapters 2,5 and 6) indicate presence of thrust regime in Early Tertiary.

Based on the information discussed above, in association with data discussed in chapter 2, and the cross-sections shown in Figures 3.12,3.22 and 3.23, the depositional environments of the Early Tertiary in-fill of the Çankırı Basin has been reconstructed (Figure 3.26). It has already been discussed that the paleo-currents in the Hacıhalil sector of the Çankırı Basin indicates manly south-eastward, with minor northwards, sediment transport which indicates that the basin rim (Bürtü group) was exposed locally in the are south of Hacıhalil village (Figure 3.02) during the deposition of the Hacıhalil Formation. The local unconformities, at the crest of a thrust wedge (discussed in chapter 2) during the deposition of the Incik Formation indicates south-wards transport of the thrusts which was accompanied by deposition both in the front and the rear of the thrust faults. This relationship indicates that the Çankırı Basin was evolved within a thrust regime with associated piggy-back basins (terminology after Ori and Friend 1984), in the Late Paleocene to Oligocene (Figure 3.26).

3.5.3 Evolutionary Scenarios of the Çankırı Basin

The facies characteristics, stratigraphic relationships and depositional environments discussed above indicate that the Çankırı Basin evolved into two distinct episodes. The first took place in the Late Cretaceous to Paleocene and the second in the Late Paleocene to Oligocene.
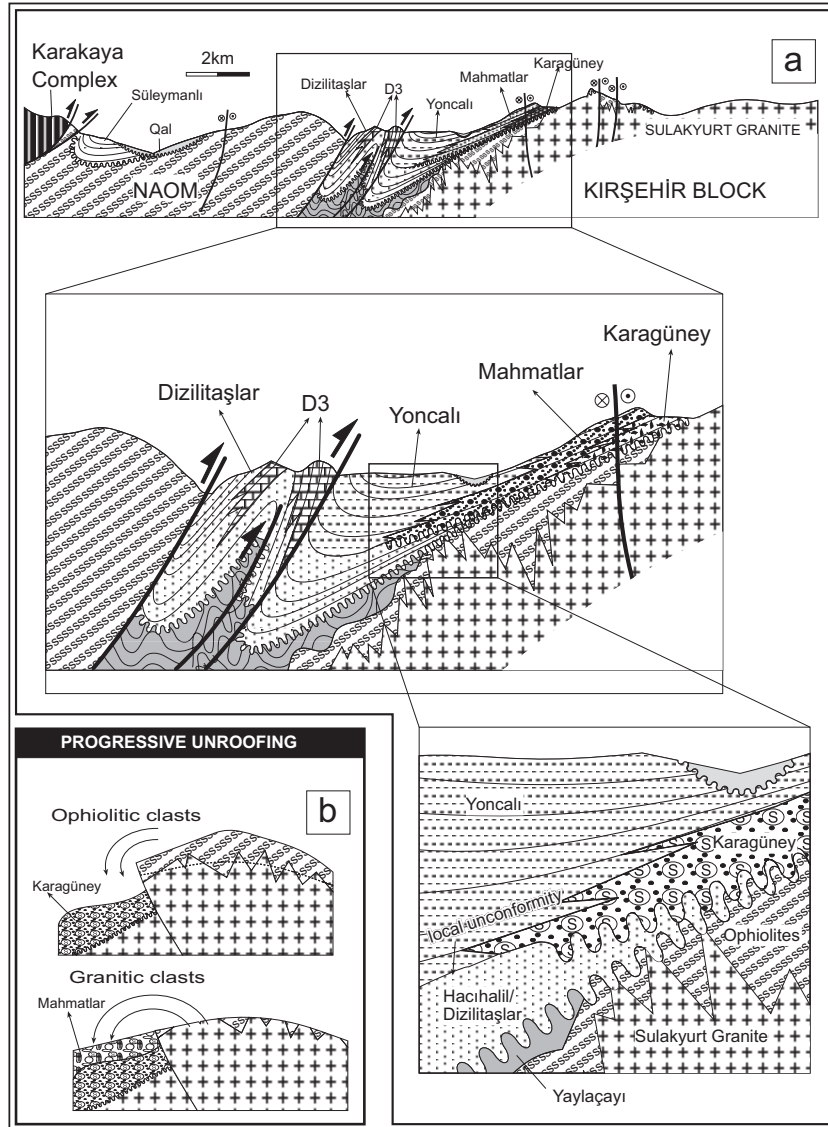
Figure 3.22 a) Sketch cross-section along the line z-z' (see its location in Figure 3.02). b) conceptual cross-sections illustrating the progressive un-roofing of the granites of the Kırşehir Block and its reflection in the Karagűney and Mahmatlar formations.

73
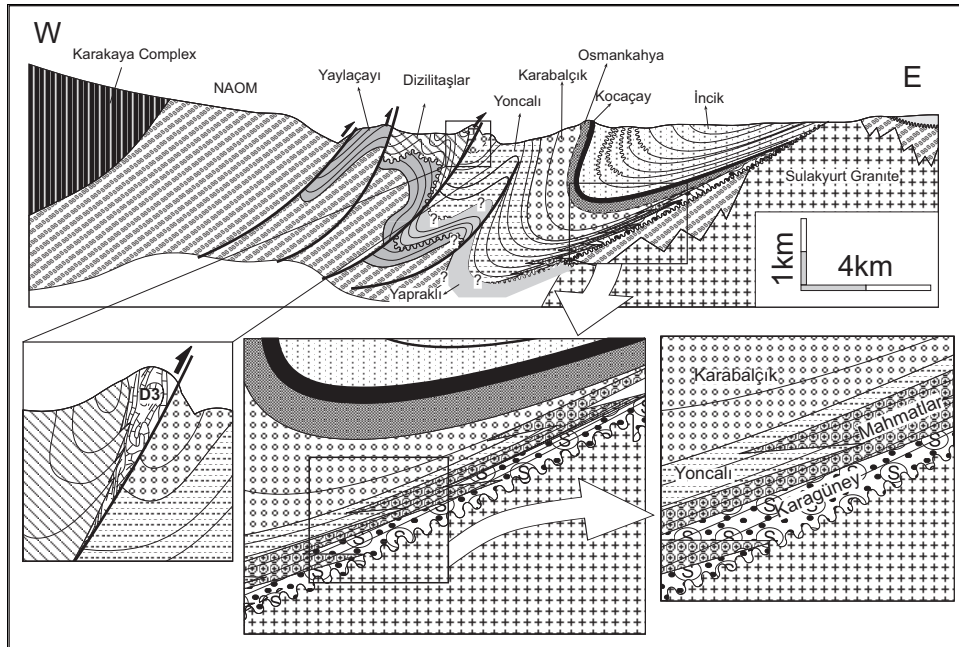
Figure 3.23 a) Sketch cross-section along the line y-y' (see its location in Figure 3.02). Note the lateral transition between Yoncalı Formation and Karagűney and Mahmatlar formations.

3.5.3.1 Late Cretaceous to Paleocene

The NAOM has been interpreted as the subduction complex related to the Neotethys ocean (Koçyiğit *et al*. 1988, Koçyiğit 1991). Subduction commenced in the Cenomanian to Maastrichtian interval northwards under the Pontides (Şengör and Yılmaz 1981, Saner 1980, Koçyiğit *et al*. 1988, Koçyiğit 1991, Okay 1984, Dellaloğlu *et al*. 1992, Göncüoğlu *et al*. 1991, 1992, 1993, 1994, Tüysüz and Dellaloğlu 1992, Özçelik 1994, Tüysüz *et al*. 1995, Okay *et al*. 1994, Okay *et al*. 1996).

According to Dellaloğlu *et al*. (1992), the subduction of Neotethys in this area occurred along two trenches (Figure 3.27). The southern one is an intra-oceanic subduction zone associated with an ensimatic-island arc (Tüysüz *et al*. 1995), which generated, in its early phase, a coeval supra-subduction zone ophiolites that are now exposed as patches of outcrops on the Kırşehir Block (Yaliniz *et al*. 1996). Coeval subduction took place to the north beneath the Sakarya Continent and gave rise to the Late Cretaceous part of the Galetean Volcanic Province (Toprak *et al*. 1996) (Figure 3.27a). The Yaylaçayı and Yapraklı formations were supposedly developed in the area between these two arcs (Tüysüz and Dellaloğlu 1992) that are the sources of volcanics and detritus to these units. In such a model, the Yapraklı Formation represents the proximal facies of this inter-arc to for-arc basin as implied by neritic carbonates and terrestrial clastics, while the Yaylaçayı Formation represents the more basinal facies (Figure 3.27).

In the Maastrichtian, the ophiolites obducted onto the Kırşehir Block (Yalınız *et al*. 1996) and gave rise to the delamination and thickening of the Kırşehir Block crust that generated collision granites (Akiman *et al*. 1993), while in the north, in the Çankırı Basin, the basin narrowed and deep sea conditions were progressively replaced by shallower conditions. The ophiolitic units were uplifted and sub-aerially exposed and supplied detritus to the Kavak and Badiğin formations. Uplift of these units might have been accelerated due to subduction of the ensimatic arc, which is now embedded within the Yaylaçayı Formation (Tűysűz *et al*. 1995). In the shallower settings, the Malıboğazı Formation might have been deposited as fringing reefs (as proposed by Koçyiğit 1991 for the similar units in Ankara region).
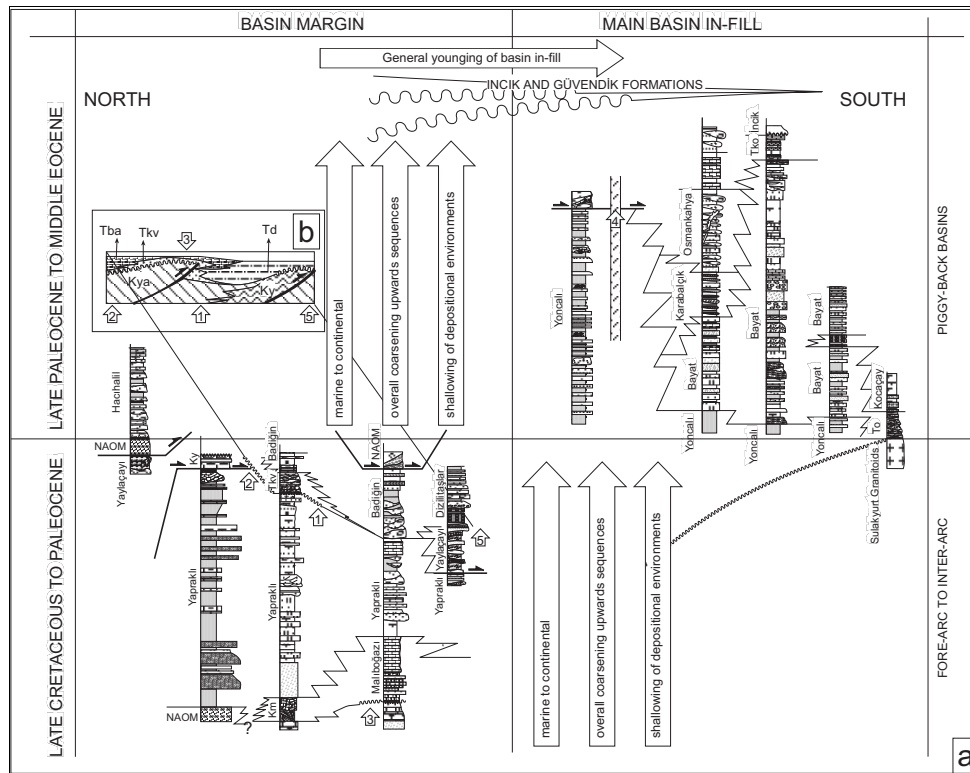
Figure 3.24 a) Correlation chart for pre-Neogene formations of the Çakırı Basin. Note that unconformable contact cover the thrust fault between the Yapraklı and Yaylaçayı formations (indicated with an arrow and 2). Note also local unconformable relationships between Yapraklı-Kavak (indicated with an arrow and 1), Malıboğazı-Yaylaçayı (indicated with an arrow and 3), Yaylaçayı-Dizilitaşlar (indicated with an arrow and 5) formations. Note also lateral transitions between Yoncalı, Karabalçık, Bayat, Osmankahya, and Kocaçay formations and the intrusion of the thrust contact between NAOM and the Yoncalı Formation (indicated with an arrow and 4) by the feeder dykes of the volcanics of the Bayat Formation. b) Conceptual cross-section illustrating tectono-stratigraphical positions of the Yaylaçayı (Ky), Yapraklı (Kya), Dizilitaşlar (Td), Kavak (Tka), and Badiğin (Tba) formations deposition of which were coupled with thrusting.

75
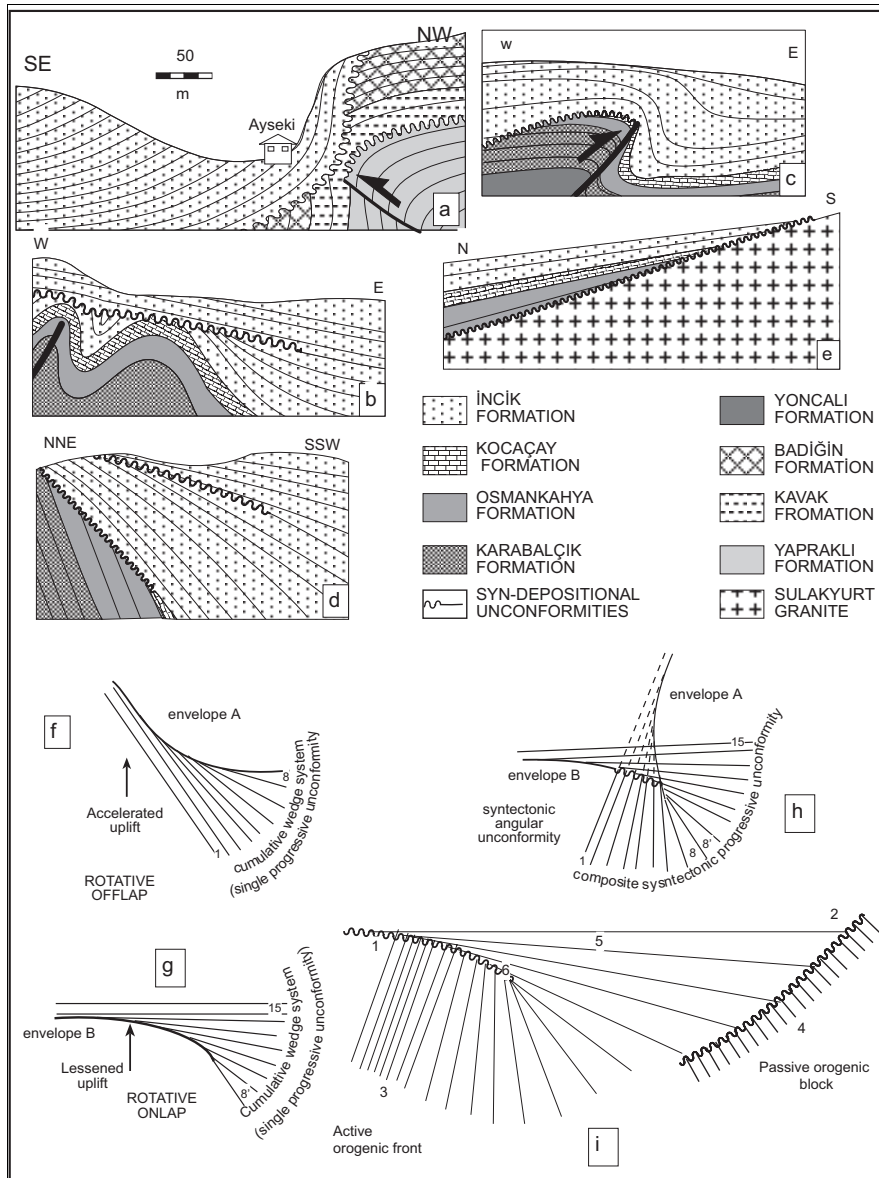
Figure 3.25 a-e) Sketch cross-sections illustrating the various types of syn-depositional (=syn-tectonic) unconformities observed during the field studies. f-l) Conceptual development of syn-depositional unconformities in areas where deformation and deposition are coupled. The numbers 1-5 are the time lines (adopted from Riba 1976 and Anadón (1986). See text for the discussion.

76
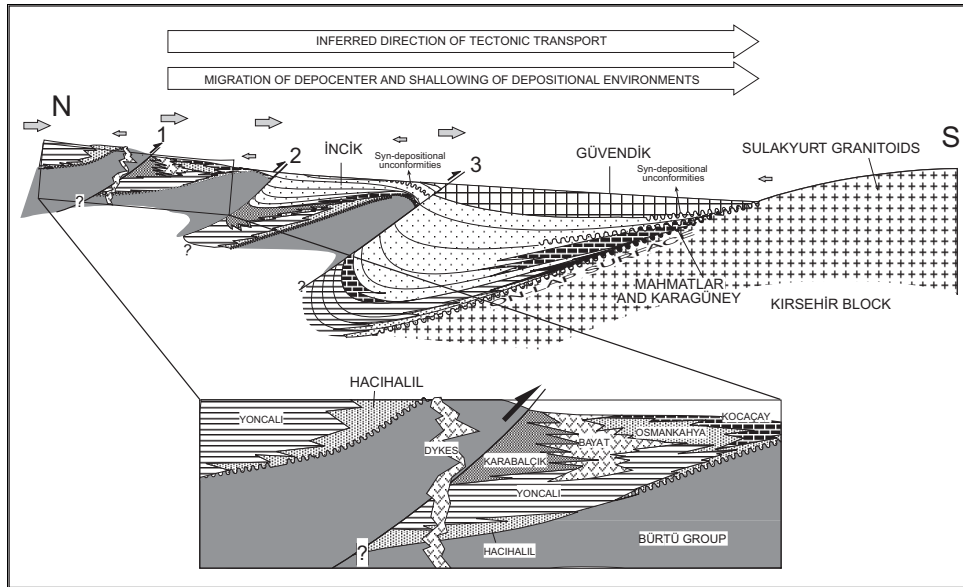
Figure 3.26 A conceptual cross-section illustrating Early to Middle Eocene to Oligocene coupling between thrusting and coeval deposition. Numbers 1-3 are the sequences of thrusts, which are thought to have developed in the Late Paleocene to Oligocene. Note that the dykes of the Bayat Formation cross-cut the thrust contact between the NAOM and the Yoncalı Formation. The arrows indicate the direction of sediment transport size of which is proportional with the amount of transported sediment.

In Late Maastrictian to Paleocene, the oceanic domains were completely consumed, ophiolitic mélange generation and volcanism ceased due to collision of Kırşehir Block and Sakarya continent (continent-continent collision) (Şengőr and Yılmaz, 1981, Gőrűr *et al*. 1984, Tűysuz 1989, Koçyigit 1991, Dellaloğlu *et al*. 1992, Rojay 1993, Okay *et al*. 1996,). This gave way to rapid uplift and influx of clastics transported by turbidity currents (Norman 1972) into the deeper parts of the basin that resulted the Dizilitaşlar Formation.

3.5.3.2 Late Paleocene to Oligocene Evolution of the Çankırı Basin

The reconstruction of the depositional environments for the Late Paleocene to Oligocene in-fill of the Çankırı Basin is illustrated in Figure 3.28. The Late Paleocene and Eocene are characterized by very rapid lateral and vertical facies changes, a consistent relative younging of units from the rim towards the basin center and an on-lapping onto the granitoids of the Kırşehir Block (Figures 3.22, 3.23, 3.24a and 3.25d).

The Hacıhalil Formation was deposited in facies conditions ranging from proximal alluvial fan, to braided river, to meandering river, to fan Delta, to near shore and to prodelta/open marine facies (Ocakoğlu and Çiner, 1997). The Hacıhalil Formation is laterally transitional and always underlies the Yoncalı Formation. This relationship may indicate a gradual rise of the sea level that caused fining upwards sequences and a relative deepening of depositional environments from continental to a deep marine facies (Yoncalı Formation) (Postma and Roep 1985, Nemec1990, Walker and James 1992, Reading 1996).

77
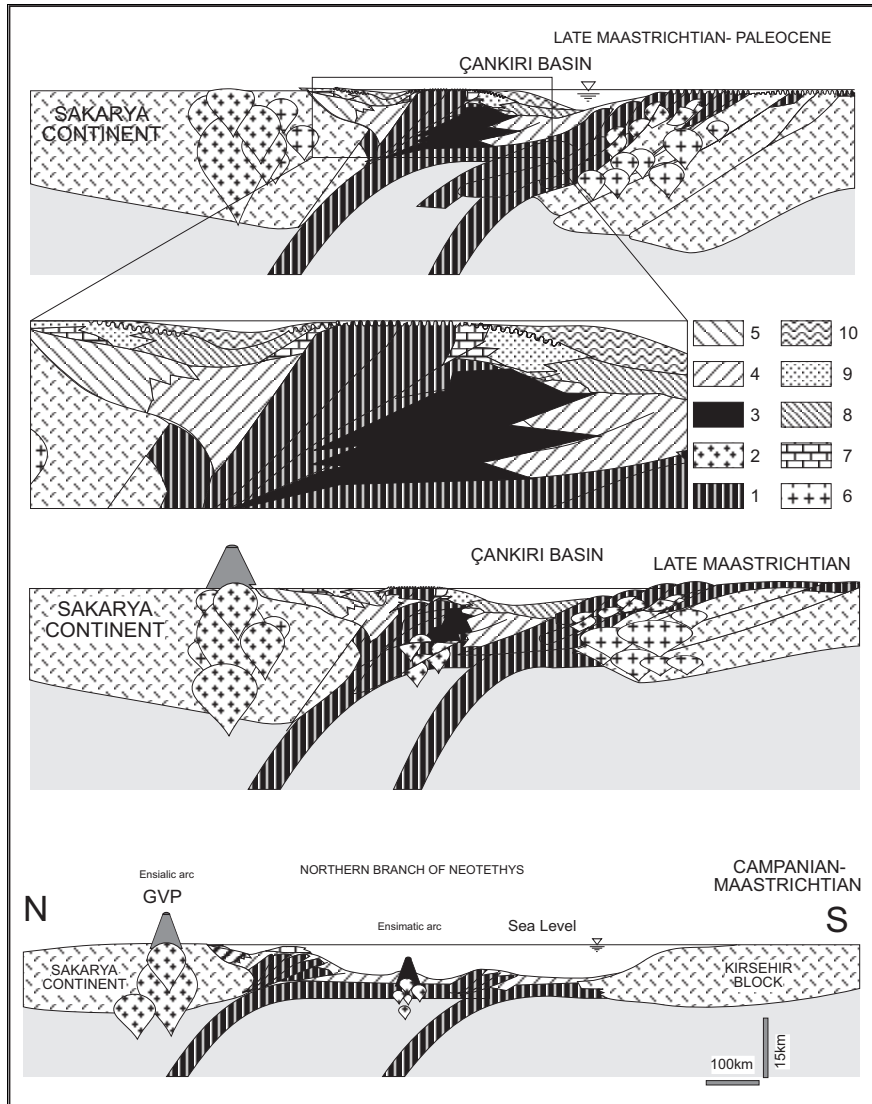
Figure 3.27 Conceptual, scenarios for the Late Cretaceous to Paleocene evolution of the northern branch of the Neotethys. 1. oceanic crust and ophiolites, 2: arc granites, 3: Island arc, 4. Yaylaçayı Formation, 5. Yapraklı Formation, 6. Collision granites, 7. Malıboğazı Formation, 8. Badiğin formation, 9: Kavak formation, 10. Dizilitaşlar Formation (modified after references cited in the text).

The alternation of graded sandstone, siltstone, shale and the presence of current ripples indicate that the Yoncalı Formation was deposited by turbidity currents (Bauma 1962, Walker and James 1992). Considering its position relative to the Karabalçık and

78

Osmankahya formations, it may represent prodelta clays, near shore clastic settings to deep marine settings (Reading and Collinson 1996, Johnson and Baldwin 1996, Walker and James 1992).

The presence of benthic fauna, plant remains and coal seams indicate that the Karabalçık Formation was deposited in relatively shallow marine conditions, which laterally and/or temporally changed into marshy conditions. The large scale cross-bedding and the presence of boulders and blocks within the conglomerates and the presence of channels of conglomerates of the Karabalçık Formation within the Yoncalı Formation indicates that the Karabalçık Formation constitutes the fore-set beds of a south facing delta. The channels in the Yoncalı Formation might indicate a distributary channel system of this delta (see Postma and Roep 1985, Postma *et al.* 1988, Nemec 1990, Walker and James 1992, Johnson and Baldwin 1996, Reading and Collinson 1996).

The Osmankahya Formation was deposited in a prograding near shore setting where fluvial deposition was the dominating agent (Colinson 1996, Walker and James 1992).

The Kocaçay Formation laterally grades and covers all the Eocene units. The presence of nummulites and bivalves and the local presence of conglomerates and sandstones indicates that the Kocaçay Formation was deposited in very shallow water conditions (Walker and James 1992, Kendall and Harwood 1996, Wright and Burchette 1996).

The İncik Formation is deposited in continental settings. Its lateral gradation to the Kocaçay Formation and the presence of greenish grey shale indicate a continental to marine transition (mixed environment). The presence of evaporates indicates arid climate conditions (Walker and James 1992, Reading and Collinson 1996, Kocurek 1996).

The presence of thick evaporites and fresh water fauna in the Güvendik formation indicates that it is deposited under saline conditions, possibly in playa lakes in an arid environment (Walker and James 1992, Kocurek 1996).

3.5.4 Tectonostratigraphical Evolution of the Çankırı Basin during the Late Cretaceous to Oligocene

As discussed in the previous sections, the tectono-stratigraphical evolution of the Çankırı basin occurred mainly in two main episodes. The first one took place in the Late Cretaceous to Paleocene and the second in the Late Paleocene to Oligocene.

The Late Cretaceous to Paleocene evolution of the basin was associated with the northwards subduction of the northern Neotethys under the Sakarya Continent (Şengör and Yılmaz 1981, Gőrűr *et al*. 1984, Koçyiğit 1991, Dellaloğlu *et al*. 1992, Tűysűz *et al*. 1995). The first sub-aerially emergence of the rim lithologies occurred in the Maastrictian. It is proposed that the emergence of the rim lithologies was associated with the collision of the sea mount (see Tűysűz et al. 1995) with the Sakarya Continent. In the south of the sea mount, the Çankırı Basin continued to its evolution as a remnant basin which was relatively narrowed due to subduction along the southern trench that was associated with ensimatic arc (Figure 3.27). As discussed previously, in the periphery of the emergent areas, the Malıboğazı, Kavak and Badiğin formations were deposited while in the relatively deeper parts deposition of Yaylaçayı and Yapraklı formations were continued.

79
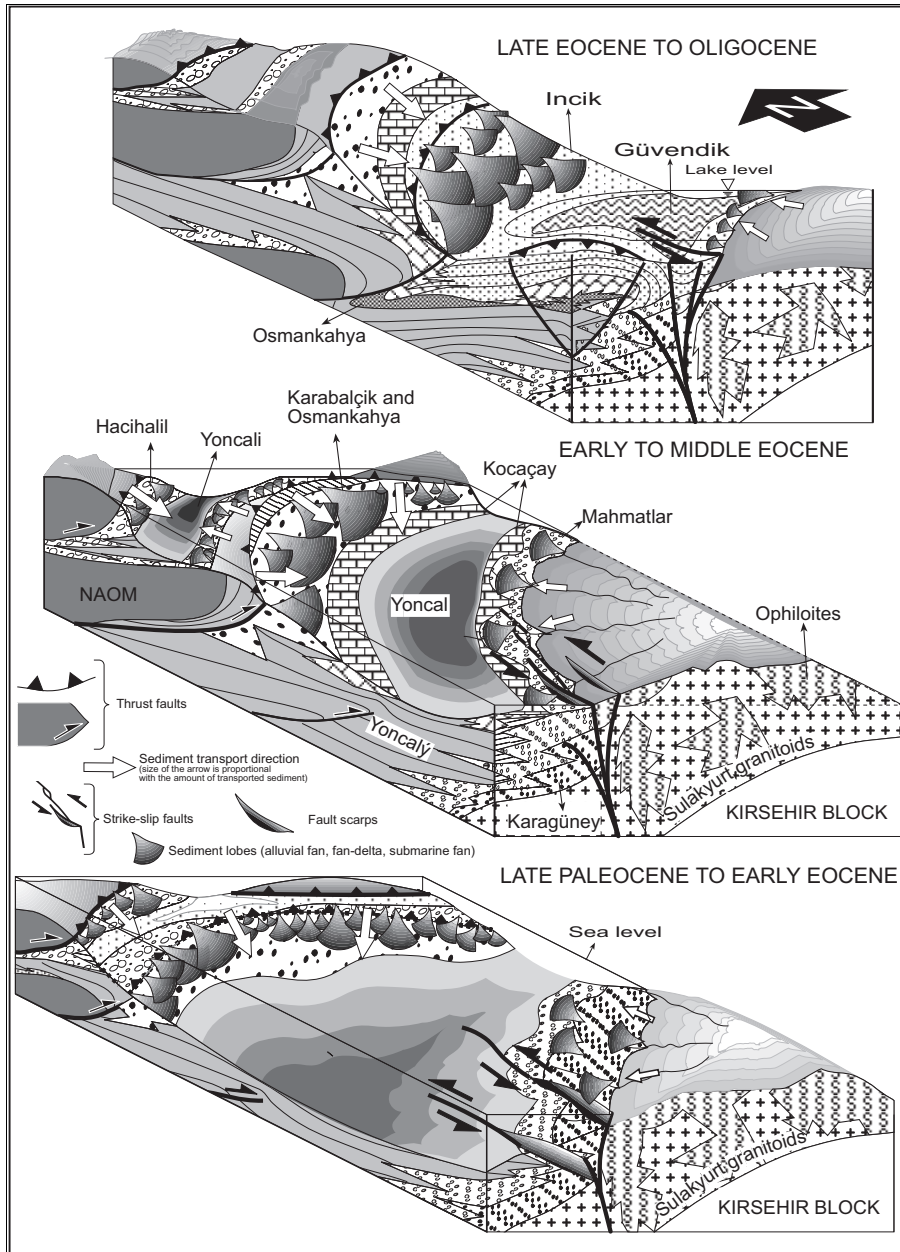
Figure 3.28 Block diagrams illustrating the Late Paleocene to Oligocene evolution of the Çankırı Basin. See text for the explanations.

80

At the same time, obduction of the ophiolites onto the Kırşehir Block was taking place in the south (Yalınız *et al.* 1996). At the end of the Late Cretaceous, the obduction processes and the intrusion of granitoids into the Kırşehir Block terminated (Erler *et al.* 1991, Akiman *et al.* 1993, Gőncuoğlu *et al.* 1991, 1992, 1993, 1994). The presence of granite pebbles in the Late Paleocene to Middle Eocene southern units and also in the Karabalçik Formation indicates that the granitoids were un-roofed by Late Paleocene and supplied detritus mainly to the Karagűney Formation. This relationship indicates that the Kırşehir Block was sub aerially exposed and supplied detritus to the Çankırı Basin from the Late Paleocene.

As discussed earlier, due to the southwards migration of the thrust faults and associated migration of the depocenters, the depositional environments become shallower and finally passed into the continental settings (Figure 3.24a). This relation indicates that the basin had been closing since the Late Paleocene. In the post- Middle Eocene to Oligocene the basin became completely restricted, the sea withdraw and continental conditions prevailed during the deposition of the İncik and Gűvendik formations (Figure 3.28c).

As will be discussed in chapters 4 and 6, the thrusting and associated closure of the basin ended in Early Miocene (end of Aquitanian, ca. 20.5 Ma). In Burdigalian, a new tectonic regime was established in the Çankırı Basin that will be discussed in the next chapter.

3.6 Conclusions

I.	An updated stratigraphic framework for the Çankırı basin is presented. The stratigraphical units are subdivided into two main groups based on their provenance. These are further subdivided based on their tectono-stratigraphic characteristics and their lateral and vertical relationships. These are:

1. Northern units; divided into three groups:

- The Bűrtű group includes the NAOM, Yoncalı, Yapraklı, Malıboğazı, Kavak, Badiğin and the Dizilitaşlar formations. These units were developed during the closing of the northern branch of the Neotethys in the Campanian to Paleocene.

- The Iskilip group is of Late Paleocene to Middle Eocene age and includes the Hacıhalil, Yoncalı, Karabalçık, Bayat, Osmankahya, and Kocaçay formations. Their depositional environments become shallower from the rim towards the basin center, and from bottom to top, indicating closing of the basin.

- The Kalınpelit group is of post-Middle Eocene to Oligocene age and includes the İncik and the Gűvendik formations, which were deposited within continental settings and represent the terminal phase of thrust related sedimentation in the Çankırı Basin.

2. Southern units consist of the Sivritepe group, which includes the Karagűney and Mahmatlar formations of Late Paleocene to Middle Eocene age. They

received their detritus from the Kırşehir Block, indicating that the Kırşehir Block was sub aerially exposed in the Late Paleocene.

II.   Thrusting and progressive closure of the Çankırı Basin continued at least until Oligocene.

III.   Sequential basement-wards (overall southwards) migration of the thrust faults and of the depocenters indicates that the Çankırı Basin evolved as a series of southwards migrating piggy-back basins in the Late Paleocene to Oligocene time interval.

4

TECTONIC IMPLICATIONS OF THE NEOGENE STRATIGRAPHY OF THE ÇANKIRI BASIN
(Central Anatolia, Turkey)

Abstract

The Çankırı Basin is straddled between the Sakarya Continent of the Pontides in the north and the Kırşehir Block of Taurides in the south. It includes Neogene units that have a total thickness of more than 1 km. There is great variation in their spatial distribution, age, geometry and tectonic settings. Eight different Neogene formations and two distinct tectonic regimes were identified in the Neogene. They were mapped by means of remote-sensing techniques while their depositional environments and tectonic settings were established in the field. The formations were dated using rodent fossils.

The Kılçak Formation of Aquitanian age is the oldest Neogene unit in the study area. It was deposited during a phase of compressive deformation which terminated synchronous with the end of Kılçak deposition. The younger Neogene units are the Altıntaş Formation of Burdigalian age, the Hancılı Formation of Burdigalian to Langhian age, the Çandır Formation of Burdigalian? to Serravalian age. These formations were deposited in an extensional tectonic regime, which replaced the pre-Burdigalian thrust regime. The upper part of the Neogene is represented by the Tuğlu formation of Tortonian age, the Sűleymanlı and the Bozkır formations of Messinian to Pliocene age, and finally the Gelasian Deyim Formation. The Tuğlu, Sűleymanlı and Bozkır formations were deposited in a compressional tectonic regime, which gradually changed in character to a transcurrent setting.

4.1 Introduction

The pre-Neogene tectonics of the Çankırı Basin were outlined in the previous chapter. This chapter deals with the Neogene. The separation of the two is made because of a marked change in depositional styles and tectonic settings. The Neogene tectonics of the Çankırı Basin (Figure 4.01 and 4.02) are characterized by a complex deformational history that is distinguished by lateral changes in the type, style and trends of the structures which were developed within the Neogene units (Figure 4.03). Therefore, the establishment of an accurate stratigraphy for the Neogene units is important if these tectonic events are to be temporarily constrained.

After termination of marine conditions in the Middle Eocene (see chapter 3), the evolution of the Çankırı Basin continued under continental settings and resulted in red clastics characterized by conglomerates, sandstones, siltstones and widespread evaporites. Depositional conditions varied both, temporarily and spatially, throughout the basin. Continental deposits are difficult to date because of a poorly developed fossil record. Unlike marine sediments, the rate of continental sedimentation is higher and more diverse (Mial 1978, 1996). Except in lacustrine settings, the preservation potential of the fossils is less due to sub-aerial conditions and rapid sedimentation, and, because of which, they become diluted so that finding them is very difficult. In addition, the reworking of preserved fossils is also very common as indicated by syn-depositional unconformities that further exaggerate the problem. Moreover, in continental settings lateral and vertical variations in facies are high and finding fossils in each horizon and facies is almost impossible for the above reasons. Fortunately, some fossil groups (pelecypoda, gastropoda, ostracoda, etc) help to date the continental units. However, they have very broad age ranges (Rőgl and Steininger, 1984, de Bruijn *et al*. 1992, Steininger *et al*. 1996, 1999) that often exceeds the frequency and extent of changes in sedimentation that occur during an evolving tectonic event. This means that, they are not sufficiently precise to date and resolve successive tectonically induced geological events that occur over short time spans. With respect to the Çankırı Basin, an additional difficulty arises because of the few studies that have attempted to establish a continental stratigraphy within Turkey; exceptions are Benda (1971), Irrlitz (1971), Rőgl and Steininger (1984) using mainly pollenomorphs, Ozansoy (1957), Şenyűrek (1960), Tekkaya *et al*. (1975), de Bruijn and Saraç (1992), de Bruijn *et al*. (1993), de Bruijn and Koenigswald (1994), Űnay (1994), Şen *et al*. (1998) who have used mammals. Of these, micro-mammals (e.g. rodents) are a highly specialized group that can yield very precise and narrow age ranges especially in the Neogene (de Bruijn *et al* 1992, Falbush *et al*. 1995, Steininger *et al*. 1996,1999) and consequently may provide a constrained Neogene stratigraphy for the Çankırı Basin.

Current studies of Neogene rodents in Turkey, in general, and Çankırı region, in particular, in combination with radiometric and paleomagnetic studies have contributed to the establishment of a Neogene stratigraphy in Turkey (de Bruijn and Saraç 1992, de Bruijn *et al*. 1993, de Bruijn and Koenigswald 1994, Űnay 1994, Krijgsman 1996, Krijgsman *et al*., 1996, Krjigsman 2000). In this context, we aim at establishing and describing the Neogene stratigraphy of the Çankırı Basin (Figures 4.01,4.02 and 4.03) and to use it to chronogically constrain the tectonic development of the Çankırı Basin during the Neogene.
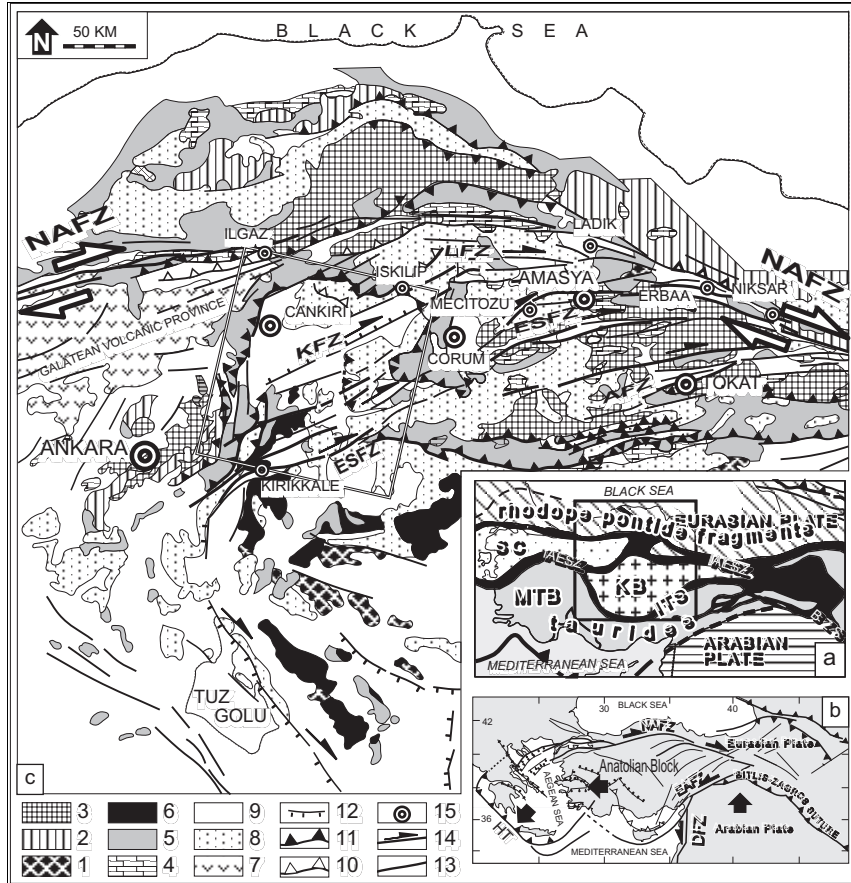
Figure 4.01 a) Inset map showing the geological outline of the Eastern Mediterranean area (Modified after Şengőr et al. 1984). BSZ: Bitlis-Zagros Suture, IAESZ: Izmir-Ankara-Erzincan Suture Zone, ITS: Intra-Tauride Suture, KB: Kırşehir Block, MTB: Menderes-Taurus Block, SC: Sakarya Continent. b) Active tectonic outline of Turkey and surrounding regions. DFZ: Dead Sea Fault Zone, EAFZ: East Anatolian Fault Zone, HT: Hellenic Trench, NAFZ: North Anatolian Fault Zone. Large black arrows are the movement directions of Arabian plate and Aegean-Anatolian Block (modified after Barka and Hancock 1984, Gőrűr et al. 1984, Őzçelik 1994, Kaymakci and Koçyiğit 1995). c) Detailed tectono-stratigraphical map of the central Anatolia. Box shows the location of the study area. AFZ: Almus Fault Zone, ESFZ: Ezinepazari-Sungurlu Fault Zone, KFZ: Kızılırmak Fault Zone, LFZ: Laçin Fault Zone, NAFZ: North Anatolian Fault Zone, YFFZ: Yağbasan-Faraşlı Fault Zone. 1. Pre-Late Cretaceous metamorphic basement of the Kırşehir Block, 2. Pre-Jurassic metamorphic basement of the Sakarya Continent, 3. Triassic Karakaya Complex, 4. Jurassic-Cretaceous platform carbonates on the Sakarya Continent, 5. Late Cretaceous (?) ophiolites and ophiolitic melanges, 6. Pre-Paleocene Granitoids of the Kırşehir Block, 7. Galatean Volcanic Province (GVP, Toprak et al. 1996), 8. Early Tertiary units (mainly marine), 9. Neogene and Quaternary Cover, 10. reverse faults, 11. thrust faults, 12. normal faults, 13. faults with unknown sense of movement,, 14. active strike-slip faults. 15. major towns.

85

Figure 4.02 Geological map of the Çankırı Basin. EFZ: Eldivan Fault Zone, KFS: Kırıkkale Fault Set, SFMS: Master Strand of the Sungurlu fault Zone, STFZ: Sivritepe Fault Zone, YFFZ: Yağbasan-Faraşlı Fault Zone.
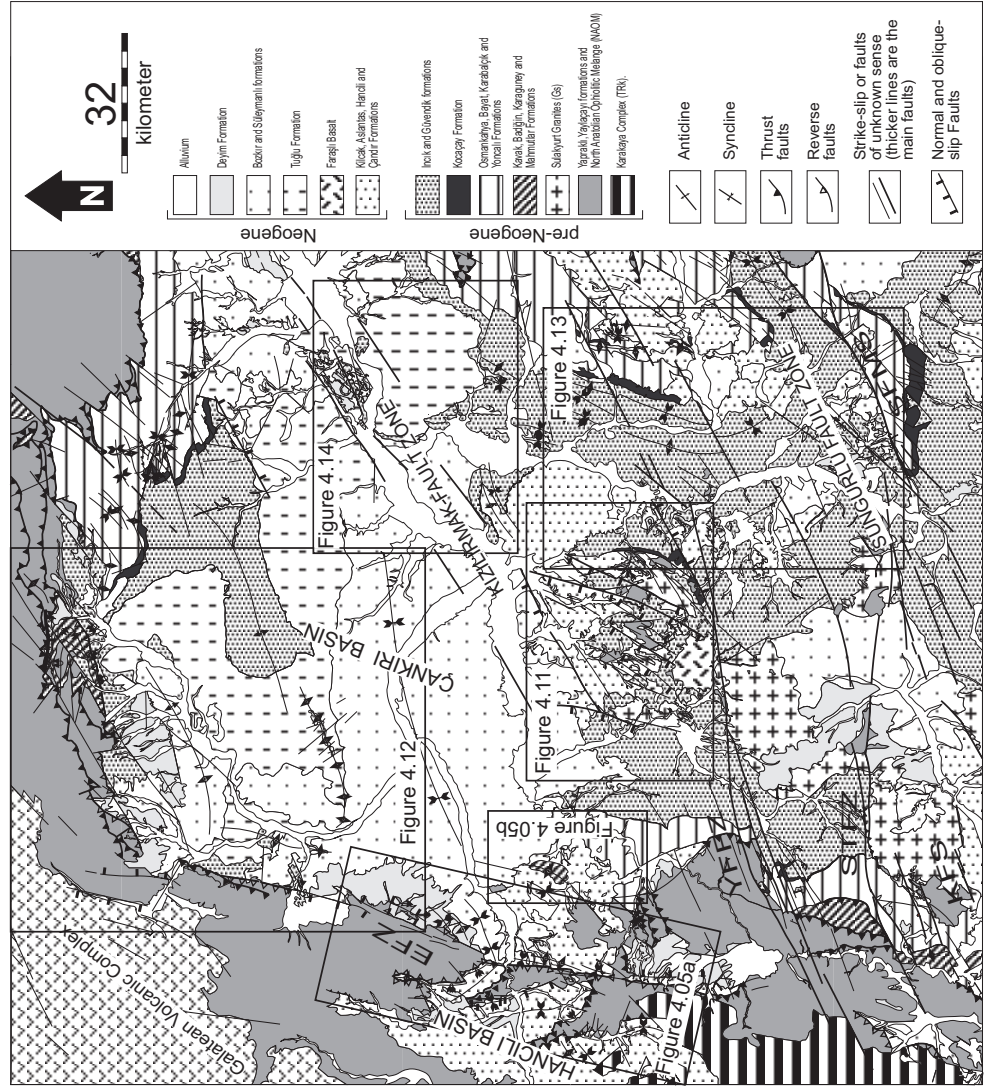
4.2 Neogene Stratigraphy

Although, the region was previously mapped and a number of lithostratigraphic units were established, the ages of those units were based on superposition and most of the units were intermixed with each other (see Figure 4.04). This study has re-mapped and established a higher resolution stratigraphy of the Çankırı Basin and the adjacent Hancılı Basin using mammal fauna.

The ages suggested for the various formations are based on the biostratigraphical correlations of the succession of rodent faunas of Anatolia with the European MN schemes. Although, the local Miocene succession is well established and allows dependable correlations within Anatolia based on the evolution of the dentition in a number of *murid* genera (i.e. *Cricetedon*, *Spanocricetedon*, *Democricetedon*, and *Mirebella*, Hans de Bruijn personal communication, 1999). The correlation of the Early Miocene part of the local zonation with the MN zones remains uncertain due to fauna dissimilarity and the limited number of magnetostratigraphic and radiometric ages of mammal bearing deposits available (Krijgsman *et al*. 1996).

The oldest Neogene unit in the study area is the Kılçak Formation of Aquitanian age, it is followed in order of younging, by the Altıntaş Formation of Burdigalian age, the Hancılı Formation of Burdigalian to Langhian age, the Çandır Formation of Burdigalian? to Serravalian age, the Tuğlu Formation of Tortonian age, the Süleymanlı and Bozkır formations of Messinian to Pliocene age, Deyim Formation of Late Pliocene (Gelasian) to Early Quaternary age and finally there is the Recent alluvium (Figure 4.03).

Figure 4.03 Generalized tectono-stratigraphic column of the units exposed in and around the Çankırı Basin. 1. North Anatolian Ophiolitic Melange-NAOM, 2. Yaylaçayı Formation (distal fore-arc sequence), 3. Yapraklı Formation (proximal fore-arc facies), 4. Sulakyurt Granitoids of the Kırşehir Block that intruded in pre-Paleocene, 5. Kavak formation (red clastics and carbonates), 6. Badiğin formation (neritic limestones), 7. Karagüney Formation (clastics derived mainly from the Kırşehir Block) 8. Mahmatlar Formation (clastics derived from Sulakyurt Granitoids), 9. Dizilitaşlar and Hacıhalil formations (mainly turbiditic clastics and intercalated limestones), 10. Yoncalı Formation (Eocene flysch), 11. Karabalçık Formation (distributary channel conglomerates and sandstones with coal seams), 12. Bayat Formation (Eocene volcanics and volcanoclastics), 13. Osmankahya Formation (mixed environment clastics and red beds), 14. Kocaçay Formation (Middle Eocene nummulitic limestone covering both basin in-fill and the granitoids). 15. İncik Formation (Late Eocene to Oligocene continental red clastics), 16. Güvendik formation (Oligocene evaporites), 17. Kılçak Formation (fluvio-lacustrine clastics), 18. Altıntaş Formation (fluvial red clastics exposed only in the Hancılı Basin), 19. Hancılı Formation (lacustrine deposits exposed only in the Hancılı Basin, 20. Çandır Formation (fluvio-lacustrine clastics), 21. Faraşlı Basalt, 22. Tuğlu formation (early-Late Miocene evaporites and lacustrine shale/marl), 23, Süleymanlı formation (fluvio-lacustrine red clastics), 24. Bozkır Formation (evaporites), 25. Deyim Formation (fluvial clastics), 26. Alluvium. MN zones and a mid-Oligocene age were obtained at certain horizons within the post-Middle Eocene units. See chapter 3 for the description of the pre-Neogene units.

AGE			TECTONOSTRATIGRAPHY	DEPOSITIONAL SETTING	DEPOSITIONAL CYCLE	DEFORMATION PHASE AND TYPE
Quaternary			26	Fluvial	5	REGIONAL TRANSCURRENT
NEOGENE	Pliocene		25 MN 17	Fluvio-lacusrine	iv	
			24 11 9 10 23 MN 13 1 22 MN 10-12		4	
			NO RECORD MN 1-2		iii	EXTENSIONAL
			MN ?4-6 20 21 ? 17 MN 3-5 19 18	Regressive flysch/molasse basin, minor volcanics, and continental	3	
PALEOGENE	Oligocene		16 mid-Oligocene		2	THRUST/TRANSPRESSIONAL
	Eocene		13 11 14 12 8 7 10 9			
	Paleocene		6 5 3	Acc. wedge, arc, fore-arc and deep sea	1	i THRUST
	Late Cretaceous	Maastrichtian Campanian	2 4 1			

Legend:

Kya **3**	Tba **6**	Td&Th **9**	Tb **12**	Ti **15**	Ta **18**	Tf **21**	Tbo **24**	Qal **26**
Ky **2**	Tkv **5**	Tma **8**	Tk **11**	Tko **14**	Tki **17**	Tc **20**	Ts **23**	Tde **25**
NAOM **1**	Gs **4**	Tkg **7**	Tv **10**	To **13**	Tqu **16**	Tha **19**	Ttu **22**	

4.2.1 Kılçak Formation (Tki, Aquitanian)

The Kılçak Formation is exposed around and south of Kılçak village only (Figure 4.05). The Kılçak Formation unconformably overlies the pre-Neogene units and is tectonically overlain by the North Anatolian Ophiolitic Melange (NAOM) (Figure 4.05). It does not have any physical contact with the other Neogene units except the overlying

Deyim Formation. The detailed description of the unit was first given by Koçyiğit *et al.* (1995). However, they misinterpreted it as the part of the Altıntaş Formation (Figure 4.04). In this study, these two units are separated (Figure 4.05a).

The section where fossils were collected is completely disturbed and covered by the landslides. Therefore, a reference section of the unit was measured 1 km east of the Kılçak village and sample locations are extrapolated to this section (1 in Figure 4.05, see appendix-A, for the geographic co-ordinates of the section). In the reference section, the Kılçak Formation is composed of moderately sorted conglomerates and sandstones (Figure 4.06). It continues upwards with laminated shale, marl with gypsum flakes, white to buff limy-marl and thin clayey limestone and intercalations of thin coal seams and organically rich levels. Towards the top of the section, to the east of Kılçak village, the unit is coarser and composed of conglomerate, sandstone and greenish gray mudstone/shale alternations (Figure 4.06).

The samples, collected from the Kılçak localities (indicated with rodent sign in Figure 4.05), were found to contain the following rodents by Hans de Bruijn (Utrecht University, The Netherlands); *Meteamys alpani*, *Muhsinia* sp., *Cricetodon versteegi*, *Cricetodon* sp., *Spanocricetodon* sp., *Democricetodon* sp., *Deperetomys* sp., *Deperetomys anatolicus*, *Enginia beckerplateni*, *Enginia* cf. *djanpolati*, *Mirabella* sp., *Eumyarion* sp., *Parasminthus* sp., *Heterosminthus* cf. *orientalis*, *Palaeosciurus* sp., *Steneofiber* cf. *eseri*, *Grlirudinus engesseri*, *Vasseuromys* aff. *duplex*, *Bransatoglis complicatus*. This assemblage clearly fits between the *Meteamys* and *Muhsinia* dominated Late Oligocene fauna of İnkonak (Turkey) and the *Eumyarion* and *Spane/Democricetodon* faunas from Harami (Krijgsman *et al.* 1996). The faunas show minor differences suggesting a slow sedimentation rate. The relative position of many of the localities cannot be reconstructed in the field because of landslides, folding and poor exposure in the sampling site. The Kılçak locality is one of the well-known rodent type sections for the Early Miocene in the Eastern Mediterranean and the age of the unit is tightly constrained by rodent fauna. The fauna listed above best fit MN-1 and the lower part of MN-2 zones that corresponds to the lower part of the Early Miocene (Aquitanian, Figure 4.04) (see also de Bruijn and Saraç 1992, de Bruijn *et al.* 1993, de Bruijn and Koenigswald 1994, Űnay 1994, Şen *et al.* 1998).

4.2.2 Altıntaş Formation (Ta, Burdigalian)

The Altıntaş Formation was named and described by Koçyiğit *et al.* (1995), however, it was not differentiated from the Kılçak and the Çandır formations (Figure 4.04), and therefore, was incorrectly dated (see Figure 4.04). It unconformably overlies the North Anatolian Ophiolitic Melange (NAOM), but is also tectonically overlain by it (see Figure 4.05). It grades laterally and vertically in to the overlying Hancılı Formation. It is exposed only in the Hancılı basin (Figure 4.05) and composed of fining and thinning upwards sequence of alternating red, poorly to moderately sorted polygenic conglomerates, sandstones and locally intensely foliated and deformed red to dark greenish brown mudstone (Figure 4.07). The pebbles of the conglomerates are sub-rounded, ellipsoidal and derived from the nearby exposed blocks constituted by the NAOM. Other pebbles were derived from various igneous units, radiolarian chert, neritic limestone and low-grade metamorphic rocks of the Karakaya Complex (Figure 4.05). In the westernmost part of the Hancılı basin, andesitic and basaltic pebbles dominate. These pebbles are derived from the volcanic units that belong to Galatean Volcanic Province (GVP, Figure 4.02).

The present geometry of the Hancılı Basin is subdivided into 3 depressions, namely Hasayaz. Şemsettin, and Demirtaş depressions (Figure 4.05). Each depression is

separated from each other by two NW trending fault bounded horst-like structures along which the NAOM and the other Late Cretaceous units (Figure 4.03) are exposed and on top of which Altıntaş and Hancılı formation are preserved locally. In each depression, the size of the constituent grains of the Altıntaş Formation gradually decreases upwards and laterally from the adjacent horst-like block in the south-west to the north-east (Figure 4.07). The paleo-current patterns also indicate an overall northward direction of sediment transport (Figure 4.05c-f)). In the north-eastern part of each depression, the Altıntaş Formation is either not developed or it is represented by a very thin, alternation of red sandstone, red to purple mudstone and thin beds of white shale of playa lake origin. This pattern is repeated three times in each depression of the Hancılı basin (Figure 4.08).

Based on the rodents collected by Şen *et al*. (1998) near Şemsettin village (Figure 4.04) and its lateral gradation to the Hancılı Formation, a Burdigalian age is assigned to the Altıntaş Formation (Figure 4.07).

4.2.3 Hancılı Formation (Tha, Burdigalian to Langhian)

Hancılı Formation was first named by Akyűrek *et al*. (1980) and was later modified by Koçyiğit *et al*. (1995). However, the type section and the age given by Koçyiğit *et al* (1995) are incorrect (A. Koçyiğit and G. Saraç 1997, personal communication). It is exposed only in the Hancılı Basin (Figures 4.01 and 4.05). The Hancılı Formation laterally and vertically grades into the underlying Altıntaş Formation and is unconformably overlain by the Deyim Formation. It is tectonically overlain by the NAOM.

The type section of the unit is to the south of the Hancılı village (Figure 4.05). At the bottom, it is characterized by thinly bedded limy-marl/marly-limestone and grades upwards in to green to bluish green bentonitic clay, white to beige marl, nodular limestone, greenish gray shale and marls intercalated with tuffs and tuffaceous marls (Figure 4.07).

Six sections of the Hancılı Formation were measured and are illustrated in Figure 4.08. There is a marked decrease in the thickness of the unit in the north-eastern parts of each depression of the Hancılı Basin (Figure 4.05). In the south-western parts of each depression, tuffaceous units and cherty limestone horizons dominate while in the eastern parts organic rich horizons and bluish green marls and bentonites dominate (Figure 4.08).

The samples collected from 1 km south of the Hancılı village yielded the following fauna; *Megacricetodon* cf. *collongensis*, *Democricetodon sp*., *Cricetodon sp*., *Anomalomys sp*. (minor group), *Eumyarion sp*., *Spalacid indet*. (two species), *Peridyromys sp*. One of the spalacids is similar to, but slightly more primitive than, the one reported from Karydia (MN-4, Theodoropoulos, in prep) in the Greek part of Thrace. The Hancılı and Karydia associations share the same Anomalomys, but are otherwise quite different. It is not known yet, whether this is due to geographic position or biotope difference. There seems no reason to suppose a great deal of difference in age between these faunas, so MN-4- early MN-5 zones and Burdigalian to Langhian age is assigned to the Hancılı Formation.

TIME (Ma)	EPOCH		AGE	EUROPEAN FAUNAL ZONES	Ayan, 1969 Çankırı-Yerköy	Birgili, 1974 Çankırı-Çorum	Dellaloğlu et al., 1992 Çankırı	Özçelik, 1994 Çorum-NE-Çankırı	Koçyiğit et al., 1995 Hancılı-W Çankırı	THIS STUDY	Basins
	PLEIST.	LATE		?				ALLUVIUM		Alluvium	
1		EARLY	CALABR.	0.7	Alluvium	Alluvium	Alluvium	TERRACE DEPOSITS	BÜYÜK HACIBEY	Deyim	
2				? — 1.95				DODURGA Fm.			
	PLIOCENE	L.	GELAS.	MN-17 — 2.6	NEOGENE CONTINENTAL		DEYIM	DEYIM		? (ND)	
3		M.	PIACE.	MN-16 — 3.4		DEYIM					
4		E.	ZANCLIAN	MN-15 — 4.2	UPPER-RED Fm.		DEVREZ VOLCANICS		HANCILI	?	ÇANKIRI
5				MN-14 — 5.3						Bozkır	
6			MESSINIAN	MN-13 — 6.6		BOZKIR	BOZKIR	BOZKIR	?	Süleymanlı	
7				MN-12	UPPER-WHITE Fm.						
8	MIOCENE	LATE	TORTONIAN	MN-11 — 8.0 / 8.7		KIZILIRMAK	HANCILI	ALPAGUT		Tuğlu	
9				MN-10 — 9.7			KIZILIRMAK				
10				MN-9						(ND)	
11				— 11.1					ALTINTAŞ		
12			SERRAVALLIAN	MN-7-8	MIDDLE RED Fm.			KIZILIRMAK			
13		MIDDLE		— 13.5							
14				MN-6						Çandır / no contact relationship	
15			LANGHIAN	— 15.0						Hancılı	
16				MN-5							HANCILI BASIN
17			BURDIGALIAN	— 17.0 / MN-4	LOWER WHITE Fm.						
18				MN-3 — 18.0			NO DEPOSITION (ND)			Altıntaş	
19		EARLY									
20				— 20.5							
21			AQUITANIAN	MN-2						no contact relationship	
22				— 22.5						Kılçak	KILÇAK
23				MN-1 — 23.8	SALT MEMBER	BAYINDIR	BAYINDIR	BAYINDIR	BAYINDIR	(ND)	
	OLIGOCENE										

91

Figure 4.04 Correlation chart illustrating the relative ages of the units in the Çankırı and Hancılı basins and comparison of previous studies with this study. Correlation of the standard time units and faunal (Mammal Neogene-MN) zones is after Steininger (1999).
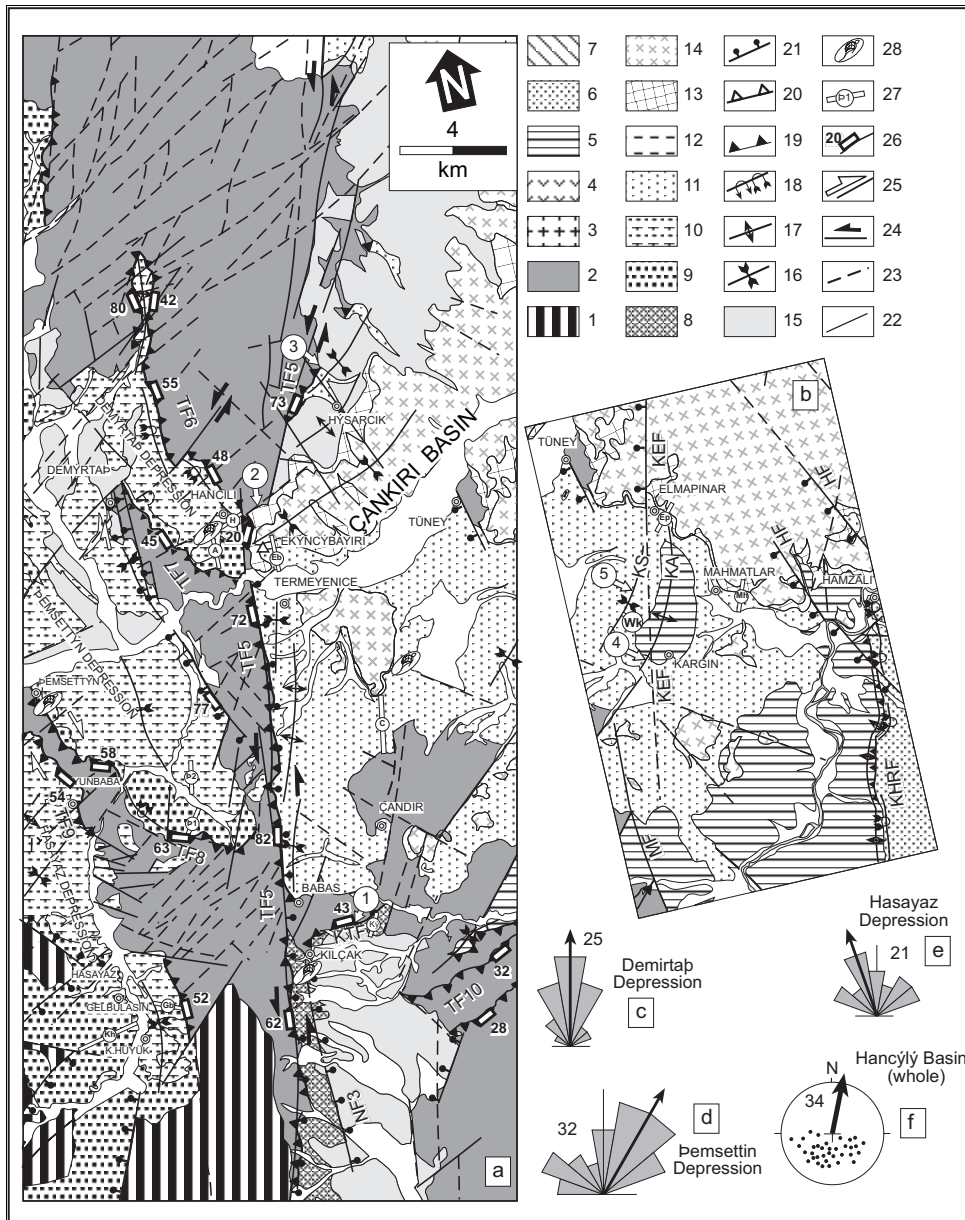
Figure 4.05 a-b) Geological maps of the western part of the Çankırı Basin around Hancılı and Çandır. Rose diagrams of paleocurrent data obtained from pebble imbrication (c-e) and cross bedding (f) within three depressions of the Hancılı Basin. The numbers next to the diagrams indicate the number of data. 1. Karakaya Complex, 2. Late Cretaceous units, 3. Sulakyurt Granite, 4. Galatean Volcanic Province, 5. Early Tertiary units, 6. İncik Formation, 7. Güvendik formation, 8. Kılçak Formation, 9. Altıntaş Formation, 10. Hancılı Formation, 11. Çandır Formation, 12. Tuğlu formation, 13. Süleymanlı formation, 14. Bozkır Formation, 15. Deyim Formation, 16. syncline, 17. anticline, 18. overturned fold, 19. thrust fault, 20. reverse fault, 21. normal fault, 22. strike-slip faults and faults with unknown sense of movement, 23. photo lineaments, 24. sinistral sense of movement, 25. dextral sense of movement, 26. dip of the fault scarps where they are best exposed, 27. line of measured section, 28. rodent fossil locality.

AGE	FORM.	LITHOLOGY	DESCRIPTION	FOSSILS
	Deyim		Alternation of yellow/buff poorly sorted conglomerate, sandstone and red to yellow sandy mudstone	
AQUITANIAN (MN-1 TO MN-2)	KILÇAK		1:Yellow, buff, greenish gray fissile siltstone. shale, mudstone	*Meteamys alpani* *Muhsinia* sp. *Cricetodon versteegi* *Cricetodon* sp. *Spanocricetodon* sp. *Democricetodon* sp. *Deperetomys* sp. *Deperetomys anatolicus,* *Enginia beckerplateni* *Enginia* cf. *djanpolati* *Mirabella* sp., *Eumyarion* sp. *Parasminthus* sp. *Heterosminthus* cf. *orientalis* *Palaeosciurus* sp. *Steneofiber* cf. *eseri* *Grlirudinus engesseri* *Vasseuromys* aff. *duplex* *Bransatoglis complicatus*.
			2: Horizons rich in organic matter/coal seams	
			3: sandy/silty clayey limestone, limy marl horizons	
			4. Creamy white limy marl with limy concretions and limestone nodules	
			5: Buff to creamy white to greenish gray marl with gypsum flakes	
			6: Alternation of greenish gray thin bedded siltstone, shale and sandstione	
			7. Lenses of fine grained conglomerate.	
			8. Fining and thinning upwards sequence of thin bedded fine grained conglomerate and thin bedded sandstone. Pebbles are subrounded to rounded, immature to moderately mature, rich in quartzite. They are derived from NAOM, Karakaya Complex and the Yaylaçayı Formation	
			—TECTONIC CONTACT—	10m
L. CRET.	NAOM		Mafic volcanoclastics, spilitic basalt, serpentinite.	

Figure 4.06 Generalized section of the Kılçak Formation (partly modified from Koçyiğit et al. 1995)

4.2.4 Çandır Formation (Tç, Burdigalian? to Serravallian)

Çandır Formation (Figure 4.09) was informally named by Tekkaya. (1975), who suggested a Late Miocene age for the unit. It was later modified by Koçyiğit *et al*. (1995). However, their age interpretation is not correct (A. Koçyiğit and G. Saraç 1997, personal communication). In the map and the type sections of Koçyiğit *et al*. (1995) the Çandır, Altıntaş, and Hancılı formations represent different facies of the same unit namely the Çandır Group (Koçyiğit *et al*. 1995). However, each of these units has different physical characteristics, age, tectonic and depositional settings. In this study, we have separated and re-mapped these units (Figure 4.02 and 4.05). The Çandır unit is one of the best known, and richest, fossil localities in Turkey (Şen *et al*. 1998). Therefore, we maintain the

name "Çandır Formation" as suggested by Tekkaya *et al*. (1975) although the Late Miocene age they suggested was wrong. It unconformably overlies the pre-Neogene units and is unconformably overlain by the Süleymanlı and Bozkır formations. In places, is also tectonically overlain by the NAOM. In the south-eastern part of the central part of the Çankırı Basin it is intercalated with the Faraşlı Basalt (Figures 4.10 and 4.11).

AGE	UNIT	THICK. (m)	LITHOLOGY	DESCRIPTION	FOSSILS	FACIES
GELASIAN MN-17	DEYIM.	20	1	1. Poorly to unsorted, polygenetic loosly packed conglomerates		FLUVIAL
BURDIGALIAN TO LANGHIAN (MN-4 to MN-5)	HANCILI FORMATION	190	2 3 4 5 4 3 6 7	2.Grey, Greenish blue shale with bentonite occurrences 3. Mudstone/shale RODENT FAUNA 4. Thin bedded clayey limestone with chert nodules 5. Dark grey mudstone with bentonitic and organic rich levels 6. Alternation of yellow to buff clayey lacustrine limestone shale and marl. 7. Thin coal seams	*Megacricetodon* cf. *collongensis*, *Democricetodon sp.* *Cricetodon sp.* *Anomalomys sp.* (minor group) *Eumyarion sp.* *Spalacid indet.* (two species) *Peridyromys sp.*	LACUSTRINE
BURDIGALIAN (MN-3 to MN-4)	ALTINTAS FORMATION	150	8 9	8. Red sandstone and siltstone RODENT FAUNA 9. Fining and thinnig upwards sequence of poorly sorted, loosly packed polygenetic red conglomerate	*age of the unit is based on Şen et al. (1998)*	FLUVIAL
UPPER CRET.	NAOM		10 UNCONFORMITY	10. Ophiolitic melange		

Figure 4.07 Generalized section of the Altıntaş and the Hancılı formations (partly modified after Koçyiğit et al. 1995).
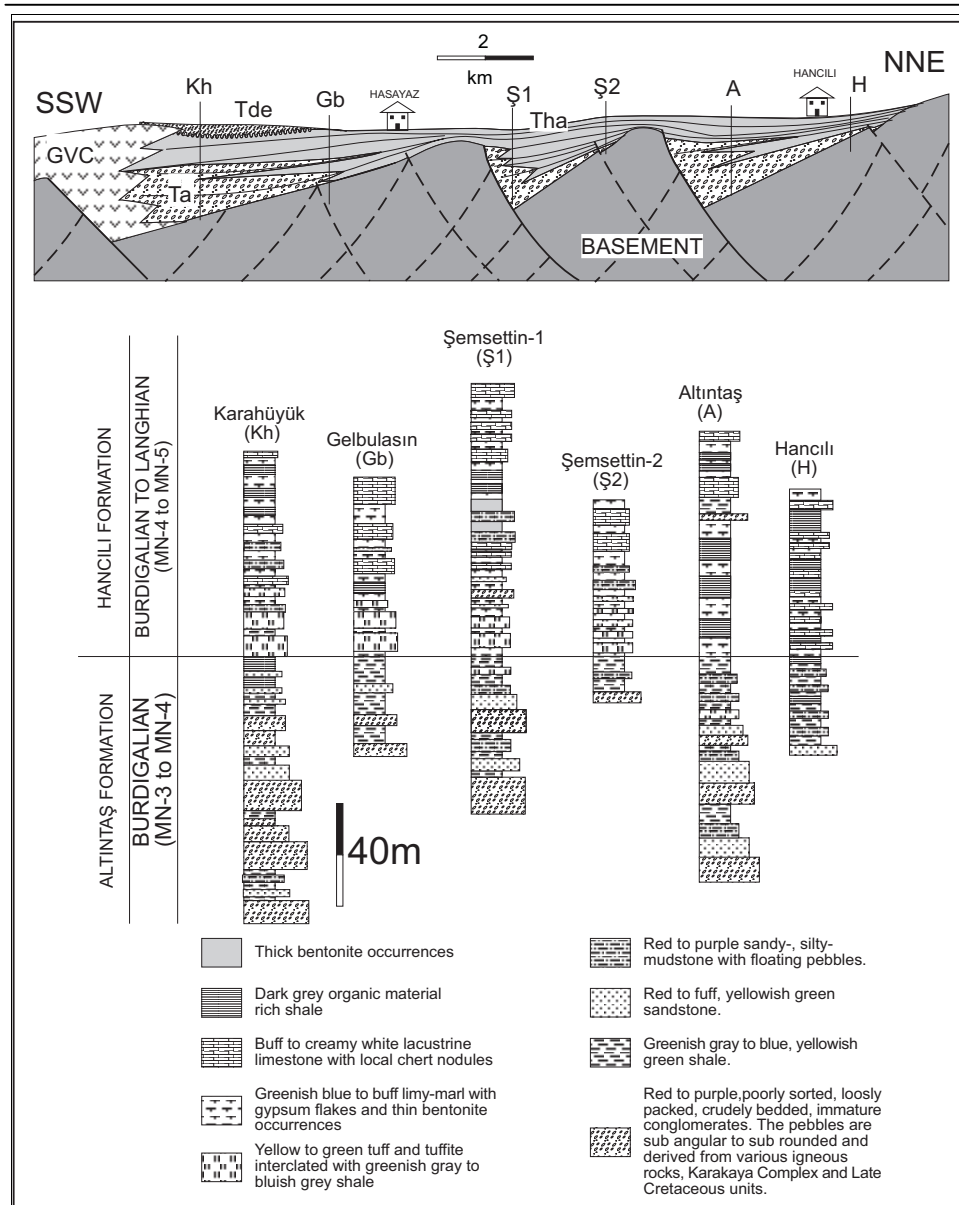
94

Figure 4.08 Correlation chart of the measured sections of the Altıntaş and the Hancılı formations and an interpreted sketch cross-section along an imaginary NNE-SSW line illustrating the relative positions of the measured sections (see Figure 4.05 for the locations of the measured sections). Vertical scale is 2 times exaggerated.

The type section of the Çandır Formation is 1km north of the Çandır village (Figure 4.05). In the lower part of the type section, the Çandır Formation is composed of an alternation of red to pink, buff to creamy white pebbly mudstone, clayey limestone, siltstone, matrix supported conglomerate intercalated with white, limy-marl, thin silty-limestone, oolite bearing limestone, clayey limestone, and very thin organic rich layers (Figure 4.09). Above this level is the alternation of red to pink sandy-silty mudstone, loose matrix supported conglomerate, clayey sandstone, siltstone intercalated with caliche limestone, paleosol horizons with carbonate concretions and cross bedded sandstone and conglomerates locally discordant with these horizons. At the top are the pink sandy, limy-concretion bearing mudstone, clayey porous limestone, siltstone, silty-limestone, white to creamy white marl, greenish shale alternations and clayey- pebbly-sandstone intercalation. The sequence becomes finer and thinner towards the top and to the north-east.

The upper levels of the Çandır Formation are characterized by an inter-fingering of fluvial and lacustrine sequences. Lateral variation of the Çandır Formation, indicated by various reference sections, is illustrated in Figure 4.10.

In the Mahmatlar section (Mh in Figure 4.05), the Çandır Formation is composed of an alternation of red clastics, including mainly red sandstone and shale intercalated with matrix and grain supported conglomerates, and creamy white to buff, pale brown to pinkish sandstone, shale/marl, sandy limestone, marly limestone, and very thick varve-like sandy-mudstones (Figure 4.10).

In the area between Dağhalilince to İnelgazili villages (Figure 4.10 and 4.11a), the Çandır Formation is composed dominantly of red to dark greenish brown conglomerate, planar and trough cross-bedded sandstones (Figure 4.10); grains of which were derived from the underlying pre-Neogene units including NAOM and the Sulakyurt Granite. The section displays a fining and thinning upwards sequence. The Çandır Formation, in this part of the basin (Figure 4.10) is also characterized by a very well developed cyclicity and a decimetre scale colour banding. Overall colour of the unit changes gradually towards the top. At the bottom it is brick-red to magenta to purple and dominated by conglomerates (x in Figure 4.11b), in the middle parts it is dark greenish purple to gray and dominated by cross-bedded sandstones (y in Figure 4. 4.11b and c), towards the top, it is buff to yellowish colors and dominated by sandstone, siltstone and shale alternations. (z in Figure 4.11b and c).

In the Akçavakıf reference section (Av in Figure 4.12a), the Çandır Formation is composed of alternation of matrix supported red to pinkish to buff conglomerate, clayey sandstone and sandy mudstones Figure 4.10). In the Derekutuğun section (Dk in Figure 4.12a), the Çandır Formation is exposed within an asymmetric anticline. In this section, it is composed of an alternation of brick red to pinkish conglomerates, pebbly sandstones and red mudstone. The pebbles of conglomerates are ellipsoidal and sub angular; largest clast size is around 20 cm. The pebbles are derived mainly from igneous and limestone blocks within the NAOM. The facies distribution, in this section, displays a very large-scale lensoid pattern. This relation, plus consideration of the sub-angular pebbles, indicate a very close proximity to the source. To the west of Derekutuğun village (Figure 4.12), limestone bearing facies dominate and the matrix of the conglomerates and the sandstones are constituted by limestone.

96

AGE	FORMATION	THICKNESS (m)	LITHOLOGY	EXPLANATIONS	DOMINANT FACIES

The stratigraphic column contains the following text entries:

Age column (left): MESSINIAN-PLIOCENE (MN-13); BURDIGALIAN? TO SERRAVALIAN (MN ?4 TO MN-6); U. CRT

Formation column: SÜLEYMANLI; ÇANDIR; NAOM

Thickness: 350

Explanations (top to bottom):

Brick red to purple conglomerate and thin bedded to laminated purple to dark brown mudstone alternation, intercalated with cross-bedded sandstones, and creamy white to buff marl at the the top

Pink sandy, limy concretions bearing mudstone, clayey limestone, siltstone, silty limestone white to creamy white marl, greenish shale alternations and clayey pebbly sandstone intercaltions.

RODENTS

Çandır

Cricetodon candirensis
Democricetodon aff. *gaillardi*
Megacricetodon collongensis
Pliospalax cf. *marmarensis*
Spermophilinus bredai
Tamlas sp.
Forsythia gaudryi
Albanensia sansaniensis
Myomimus n. sp.
Gliriulus daamsi
Muscardinus aff. *thaleri*
Eomyops cf. *catalaunicus*
Keramidomys thaleri

Alternation of red to pink sandy-silty mudstone, loose matrix supported conlomerate, clayey sandstone, siltstone intercalated with red calichy-limestone,limestone concretions bearing paleosols, and cross-bedded sandstone

Alternation of red to pink, buff to creamy white pebbly mudstone, clayey sandstone, siltstone matrix supported conglomerate intercalated with lacustrine white limy marl, silty limestone, oolite bearing limestone, clayey limestone, with very thin organic rich layers

RODENTS

Sarıyaka

Cricetodon sp.
Megacricetodon sp.
Schizogalerix sp.

Ophiolitic melange, volcanics and volcanoclastics, pillow basalts and diabase dykes

Dominant facies (right, top to bottom): FLUVIAL TO LAC.; LACUTRINE TO FLUVIAL; FLUVIAL; FLUVIAL TO LACUSTRINE
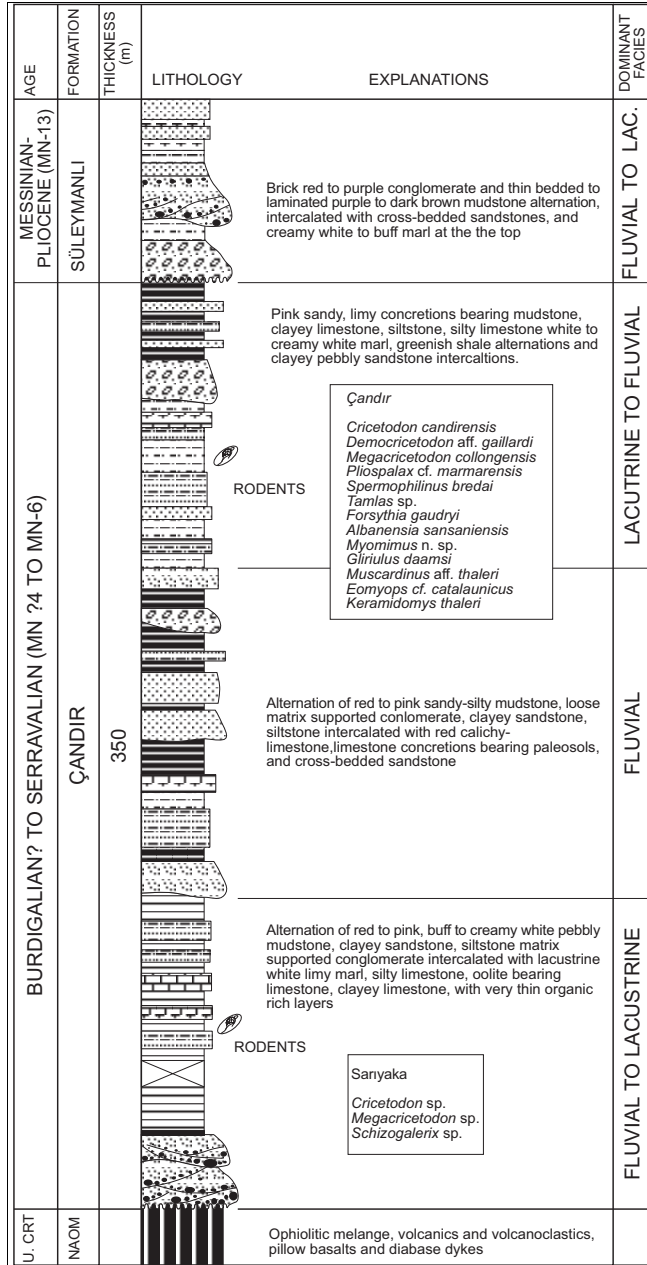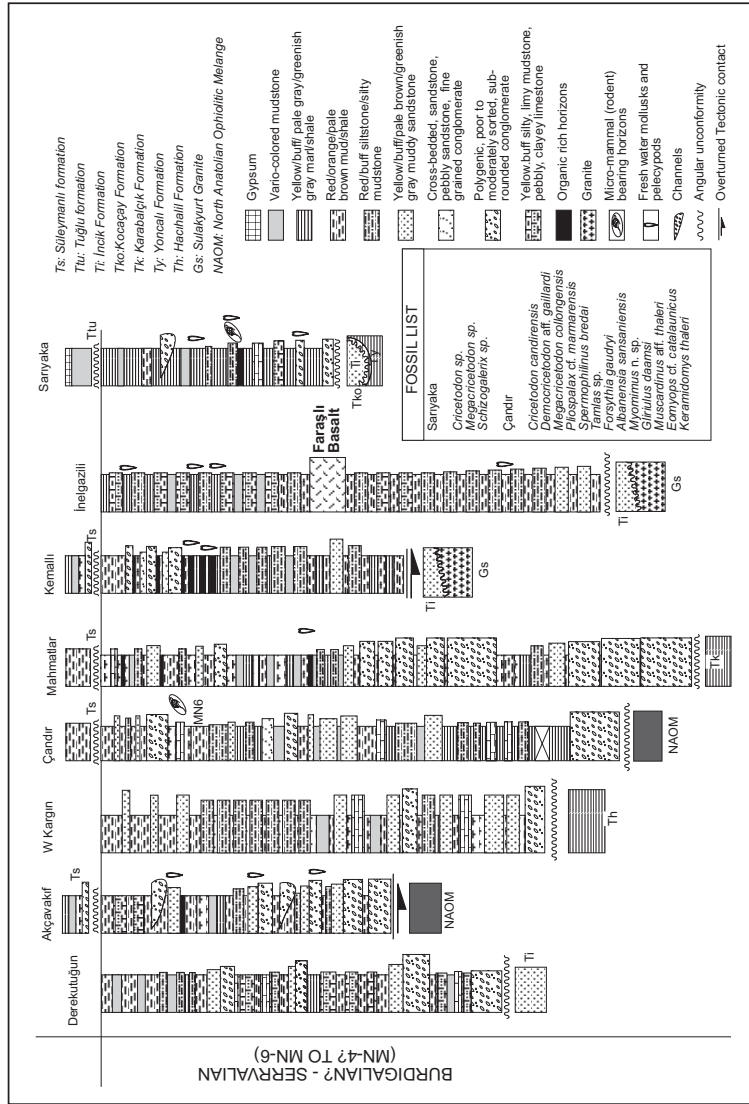
Figure 4.09 Generalized section of the Çandır Formation (fossil lists are from Çandır and Sarıyaka locations, see Figures 4.05 and 4.13 for the sample locations).

97

Figure 4.10 Correlation chart for the measured sections of the Çandır Formation. The relative position of the Faraşlı Basalt is extrapolated in the İnelgazili section (see Figures 4.04, 4.11, 4.12, and 4.13 for the locations of the sections).

In the Sarıyaka section (Sy in Figure 4.13a), in the south-east of the Çankırı Basin, it is locally dominated by an alternation of gray, green, greenish-gray shale, mudstone, beige to white marl, limy-marl, marly limestone alternation and intercalation of organic material rich horizons and lenses of immature to moderately mature lenses of conglomerate and cross-bedded sandstones (Figure 4.10).

In the Çandır fossil locality (indicated with rodent sign in Figure 4.05) the following rodents have been recognised; *Cricetodon candirensis*, *Democricetodon* aff. *gaillardi*, *Megacricetodon collongensis, Pliospalax* cf. *marmarensis, Spermophilinus bredai, Tamlas* sp., *Forsythia gaudryi, Albanensia sansaniensis, Myomimus* n. sp., *Glirulus daamsi, Muscardinus* aff. *thaleri, Eomyops* cf. *catalaunicus Keramidomys thaleri*. In the samples collected from the Sarıyaka locality *Cricetodon* sp., *Megacricetodon* sp., and *Schizogalerix* sp. are present. The unambiguous correlation of the Çandır assemblage to the MN scheme is impossible because it contains a number of species for which the ranges do not overlap in the European record (see de Bruijn *et al.* 2000), but occur from MN-4 to MN-7/8. Magnetostratigraphical results (Krigsman 1999) suggest a best fit for the fossiliferous level at about 14.1Ma (top MN-5), and an age interval between ±14.6-13.2 Ma (upper part of MN-5-MN-6) for Çandır section. These results do not conflict with the biostratigraphical correlations, but help to constrain the Middle Miocene age of the Çandır Formation. Besides, the Cricetodon specimens from Sarıyaka locality seem to represent the same species as the one in the assemblage from the Hancılı Formation, suggesting a correlation with MN-4. Therefore, the Çandır Formation apparently encompasses MN-4 to MN-6 (Burdigalian? to Serravalian).

4.2.5 Faraşlı Basalt

The Faraşli Basalt was first named by Aziz (1975). It is approximately 10 m thick, and is exposed mainly in the south central part of the Çankırı Basin. It was emplaced on the Kırşehir Block and Gűvendik Formation. In the south-eastern part of the Çankırı Basin it is intercalated with the Çandır Formation.

The Farşlı Basalt is composed of olivine and orthopyroxene bearing micro-granular (aphanitic) basalt, scoria with 2cm diameters of vesiculation filled with calcite, and columnar basalt.

Based on its relation with the Çandır Formation, it is assumed that the Faraşlı Basalt was extruded in Middle Miocene.

4.2.6 Tuğlu Formation (Ttu, Tortonian)

Tuğlu Formation is identified as a separate stratigraphic entity for first time in this study. In previous studies, (Ayan, 1969; Birgili *et al.* 1974, Dellaloğlu, 1992, Őzçelik, 1994) it has been regarded as a part of the mid-Oligocene Gűvendik formation and mapped together as Bayındır Formation (see Figure 4.04). The Tuğlu Formation is characterized by an alternation of intensely deformed yellowish evaporates and clastics. It unconformably overlies the Burdigalian? to Serravalian Çandır Formation, mid-Oligocene Gűvendik formation and other pre-Neoegen units. It is overlain unconformably by the Sűleymanlı formation of Messinian to Pliocene age (see later).

In the type section (Tu in Figure 4.14), the base of the Tuğlu formation is composed of dark gray shale, mudstone, siltstone, and sandstone alternations (Figure 4.15). In the middle parts, it is composed of an alternation of green, pelecypoda bearing stiff bentonitic

99

claystone and dark green to gray coloured organic rich mudstone, intercalated with 3-10 cm thick cherty limestone beds and lenses of conglomerate, and very thin (1-5 cm) coal seams (Figure 4.15). It gradually becomes marl dominated towards the top and grades laterally into an alternation of thick-bedded white gypsum and thick-bedded yellow to pinkish silty mudstone. Near Toyhane (Figure 4.14), the Tuğlu formation is exposed in outliers within the alluvial plain of the Kızılırmak river (5 and 6 in Figure 4.14). In these hills the Tuğlu Formation is intensely folded and has lost its internal structure which may be attributed to diapiric effects of nearby exposed salt domes. In the areas where internal structures are preserved. The Tuğlu formation is composed of an alternation of dark greenish gray silty mudstone, red to pink mudstone, dark gray laminated gypsum and marl. In the Karaçay section (Kç in Figure 4.13), the top gypsum bearing part of the unit is missing and only lower parts of the unit are preserved (Figure 4.15). In this section, the Tuğlu formation is composed of an alternation of green mudstone and dark green to dark gray mudstone, shale and lenses of conglomerate and sandstone. In the Sungurlu section (Su in Figure 4.13), the Tuğlu formation is composed of greenish gray mudstone, siltstone, sandstone and white marl alternations. In the NE of Sungurlu, the Tuğlu Formation is characterized by circa 50 m thick, thickly bedded (may reach up to 1m) partly loose clean sandstone alternating with thin beds of siltstone and gray mudstone.

In the north and the north-west of the Çankırı basin, the Tuğlu Formation gradually changes from dominantly gray to greenish gray colors to buff to pinkish, yellowish colors. In the area from Ovacık to Çankırı and Sűleymanlı villages (Figure 4.12a), it is intensely folded and deformed, and the internal structures and primary relationships are partly obliterated. In this area, wherever the internal structure is preserved, the formation is characterized by alternation of thick-bedded re-crystallized thick-bedded gypsum, pinkish to yellowish and buff mudstone and purple to dark greenish gray shale, siltstone and sandy mudstone. In the NW of Çankırı (Figure 4.12), it is characterized by very thick (5-10 m) red mudstone/shale alternating with buff to yellow re-crystallized intensely deformed gypsum. In the Kıvçak section, (Kç in Figure 4.12), it is almost undeformed and very well exposed. In this section, at the bottom it is composed of pinkish to yellowish sandy mud and siltstones. In the middle parts, the color gradually changes into gray tones and the strata is characterized by greenish gray mudstone/marl intercalated with gray gypsum levels. Towards the top, it is characterized by an alternation of thinly bedded greenish gray to white marl and white to gray gypsum. At the top, thick-bedded massive gypsum is exposed. In the NE of Çankırı, and in the area between Sarıyaka and Sungurlu, a number of rock-salt mines exploit dissolved salt that is supposed to have originated from the Tuğlu Formation.

In the samples collected from the Karaçay section (rodent sign near Kç in Figure 4.13) the following fauna has been determined; *Dipoides problematicus*, 3 species of murinae, *spalacid* indet, *Byzantinia* sp., *Myomimus* sp., *Keramidomys* sp*., Schizogalerix*, *Hipparion* sp. *Dipoides* is a Middle Turolian immigrant into Europe, from west Asia and north America. In association with *Byzantinia* and a diverse *murid* assemblage, it characterizes MN 12 zone.

The Tuğlu samples yielded the following fauna; *Parapodemus* (t6-t9 not connected and t1-t3 developed as a ridge in the M2), Cricetinae gen. Indet. *Byzantinia* sp., Zapodidea gen. Indet, *Myomimus* sp., *Schizogalerix* sp., *Erinaceid* indet., This association is not known from elsewhere, but seems to belong to the MN 10 zone. Based on fauna, the Tuğlu formation is assigned to Tortonian.

100

The presence of fresh water molluscs, and pelecypoda, together with an alternation of gypsum, marls, laminated claystones, and shales indicate a lacustrine origin for these facies in which the lake level fluctuated temporarily. The organic rich levels may indicate swampy areas in the periphery of the lake (Walker and James 1992, Talbot and Allen 1996). The lenses of sandstones with conglomerates indicate fluvial settings, which probably drained the lake.

4.2.7 Süleymanlı Formation (Ts, Messinian to Pliocene)

The Süleymanlı formation is defined in this study. The type locality is near Süleymanlı village in the south of Çankırı (Figure 4.12a). In previous studies it was regarded as a part of the Çandır Formation (see Figure 4.04). This unit was mapped and dated. The Süleymanlı formation unconformably overlies the Tuğlu and older formations including the Çandır Formation. It has lateral and vertical gradations into the Bozkır Formation (Figure 4.16).

In the type section near Süleymanlı village (Su in Figure 4.12), the Süleymanlı formation is characterized by an alternation of thin bedded red to buff, brick red mudstone, gray marl with rich small gastropod fragments, buff laminated mudstone, thin bedded siltstone, silty- and sandy-mudstone alternation. At the top, it grades into cream, yellowish gray marls and gypsum of the Bozkır Formation. Including the type section, 11 sections were measured in the field and illustrated in Figure 4.16. At the bottom, along the western margin of the Çankırı Basin, the Süleymanlı formation is dominated by conglomerates, towards the top and into the basin center it becomes finer and more shale/mud dominated (compare the sections close to rim with the others in Figure 4.16).

In the samples collected from Ayseki and from two localities near Çakıllı (Çakıllı-1 and-2), the following fauna have been determined; *Cricetinae* sp., *Occitanomys debruijni*, ?*Apodemus* sp.*, Myomimus* sp., *Prolagus* sp., This small collection lacks real markers. The presence of an evolved hamster and a *Occitamomys* type of *murid* excludes a mid-Tortonian (9.0 ma) age for this assemblage.

The Süleymanlı samples yielded the following mammals; Apodemus sp. (large), Apodemus sp. (small), Occitanomys (Hansdebruynia) sp., Cricetulus sp., Pseudomeriones sp., Calomyscus sp., Pliospalax sp., Tamias sp., Myomimus sp., Hipparion sp. This assemblage is assigned to MN-13. Based on this information, a Messinian to Pliocene age is assigned to the Süleymanlı Formation.

The thick conglomerate and sandstone-dominated levels of the Süleymanlı formation, which are exposed mainly along the marginal parts of the basin, indicate a fluvial origin (Walker and James 1992, Collinson 1996) for the facies with these assemblages. Fresh water molluscs and marl horizons indicate lacustrine origin (Walker and James 1992, Talbot and Allen 1996). The organic rich horizons indicate marsh and marsh settings (Walker and James 1992, Collinson 1996, Talbot and Allen 1996). Therefore, it is concluded that the Süleymanlı formation was deposited in alluvial fan to meandering river to lacustrine associations.
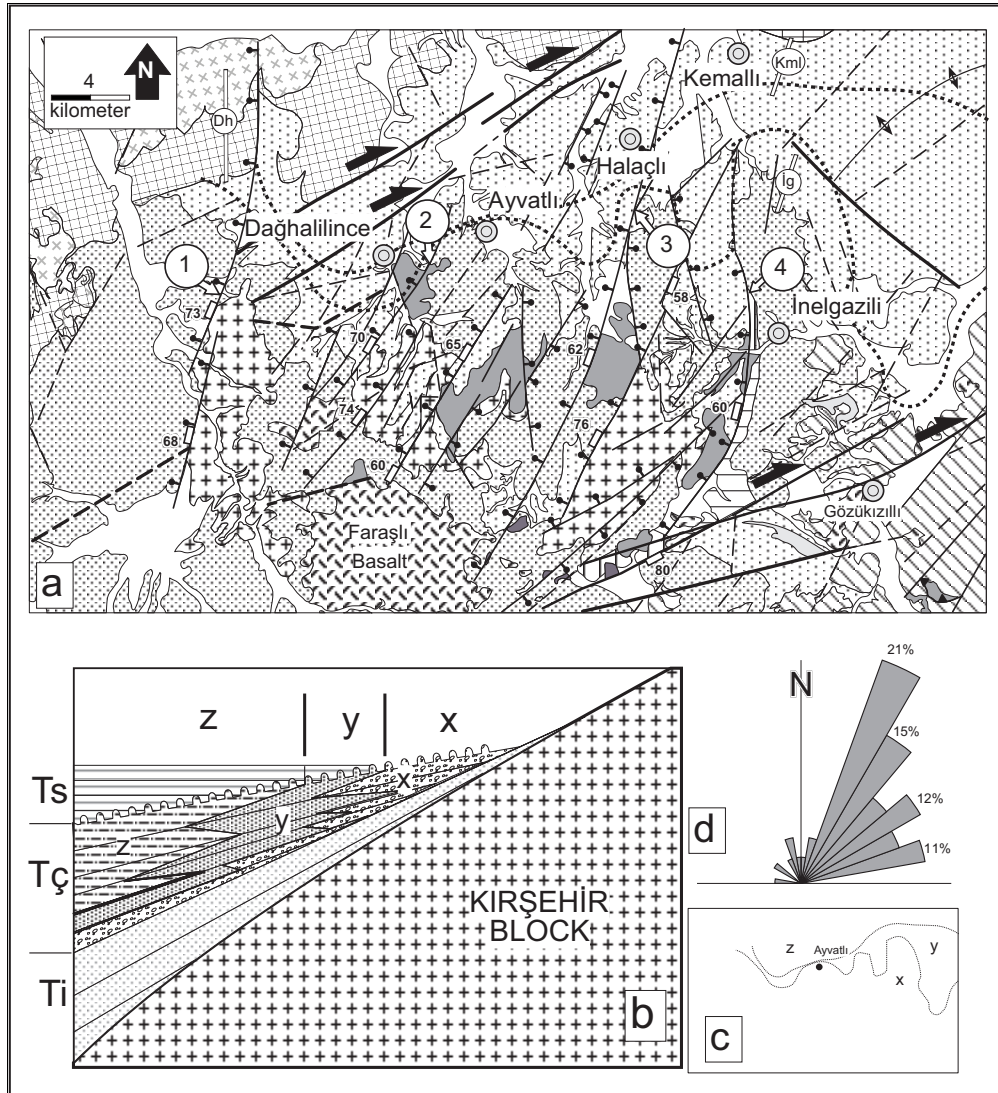
Figure 4.11 a) Geological map of the central part of the Çankırı Basin (see Figure 4.02 for its location). b) Schematic illustration of the interpreted cross-section of the facies (x,yz) of the Çandır Formation, in which grain size decreases from x to z (x: conglomerate dominated, y: sand dominated and z: shale dominated), c) Simplified map of facies (x,y,z) distribution of the Çandır Formation. d) Length weighted rose diagram of the faults that displace the granitic basement and the Çandır Formation, percentages indicate the length frequency of the faults (see Figure 4.05 for the explanation of the symbols).
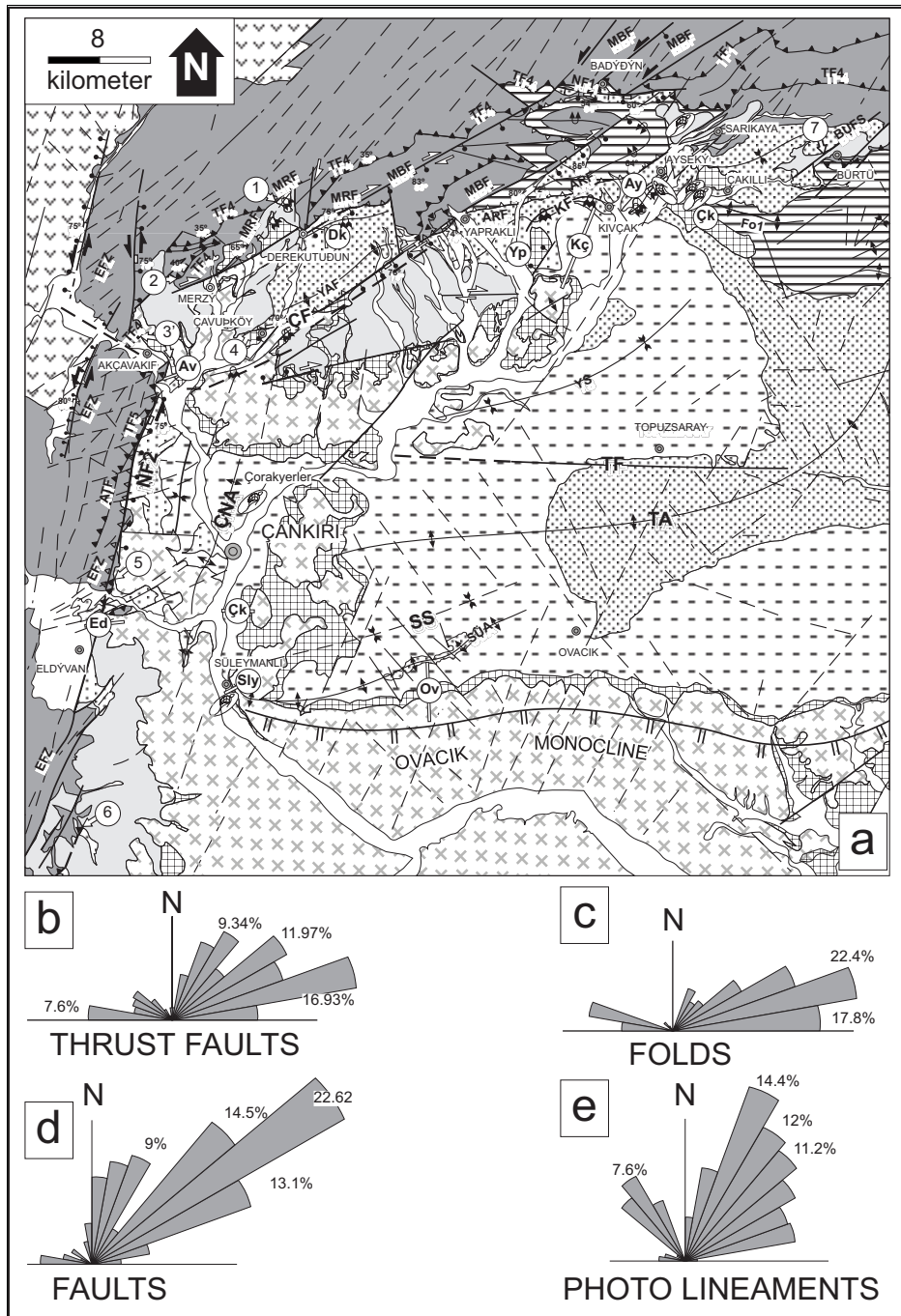
Figure 4.12 a) Geological map of the north-western part of the Çankırı Basin (see Figure 4.05 for the explanation of the symbols). b-e) Length weighted rose diagrams of the structures indicated.
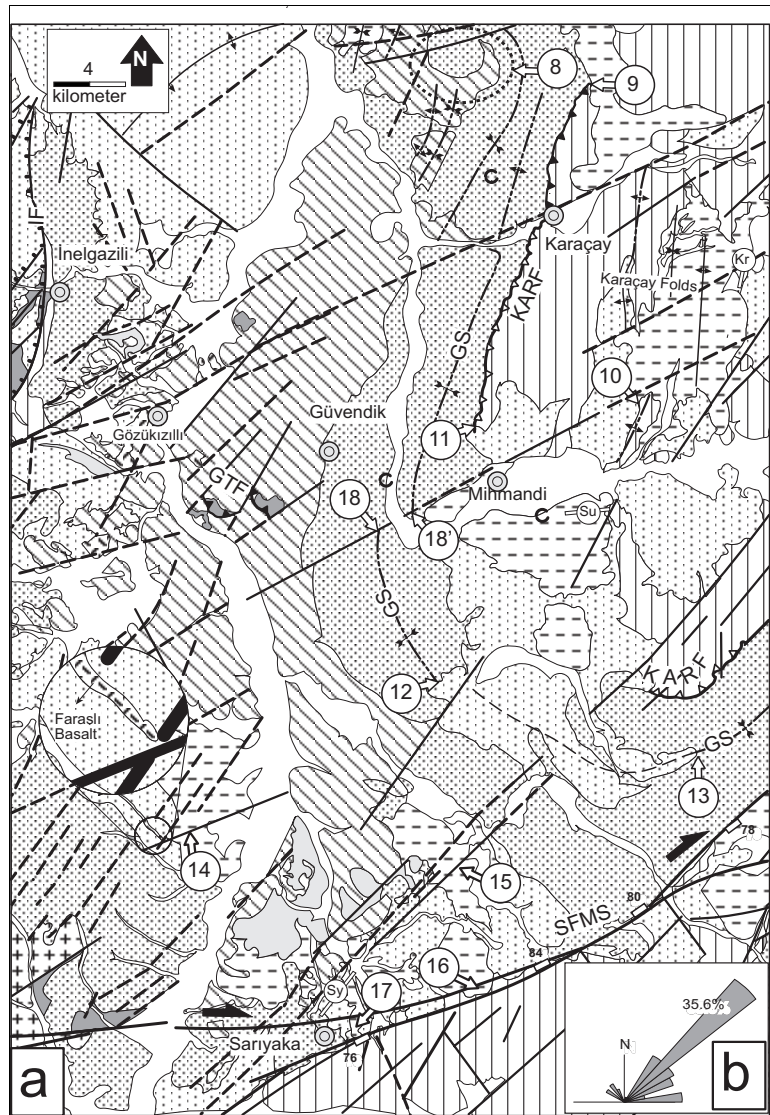

Figure 4.13 Geological map of the eastern margin of the Çankırı Basin (see Figure 4.05 for the explanation of the symbols). Note blow up figure illustrating the interlayering of the Faraşlı Basalt and the Çandır Formation.

Figure 4.14 Geological map of the north-eastern margin of the Çankırı Basin (see Figure 4.05 for the explanation of the symbols).

4.2.8 Bozkır Formation (Tbo, Messinian to Pliocene)

This unit was named by Aziz (1975) and later modified by others (see Figure 4.04). It grades vertically and laterally into the Sűleymanlı Formation. The Plio-Quaternary Deyim Formation unconformably overlies it. South of Mahmatlar, Kargın and Çandır villages (Figure 4.05) the Bozkır Formation directly rests on the Çandır Formation.

The dominant lithology of the Bozkır Formation is white to pale gray gypsum. It is composed mainly of an alternation of gypsum with marls and thin-bedded sandstones (Figure 4.16). Around the Ekincibayırı Hill (Eb in Figure 4.05), the base of the Bozkır Formation is composed of green, bluish gray marls intercalated with yellow, thinly bedded sandstone. Towards the top, it passes into white, beige, medium to thickly bedded gypsum (Figure 4.16). In the central parts of the Çankırı Basin, it is dominated by thickly bedded re-crystallised gypsum and thinly bedded yellow to buff gypsum flakes bearing marl. In the field, especially around the Bayat-Toyhane-Sağpazar-Tuğlu area (Figure 4.14), the Bozkır Formation very much resembles the Tuğlu Formation. The main difference between these two units is in the degree of deformation (Tuğlu formation is more deformed). Also the Tuğlu formation is more yellowish than the Bozkır Formation.
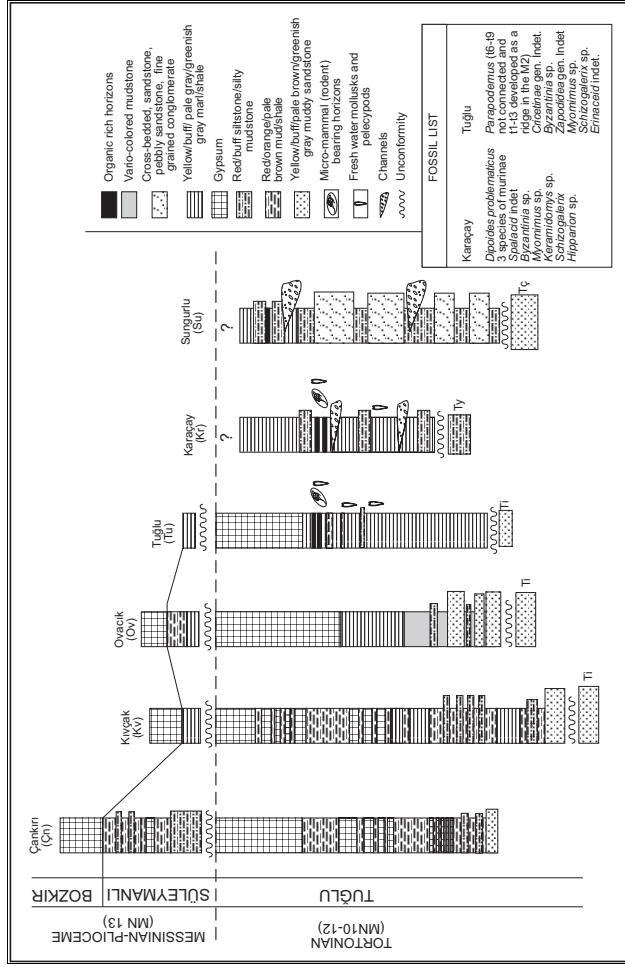
105

Figure 4.15 Correlation chart for the measured sections of the Tuğlu formation (see Figures 4.12, 4.13 and 4.14 for the location of the sections).
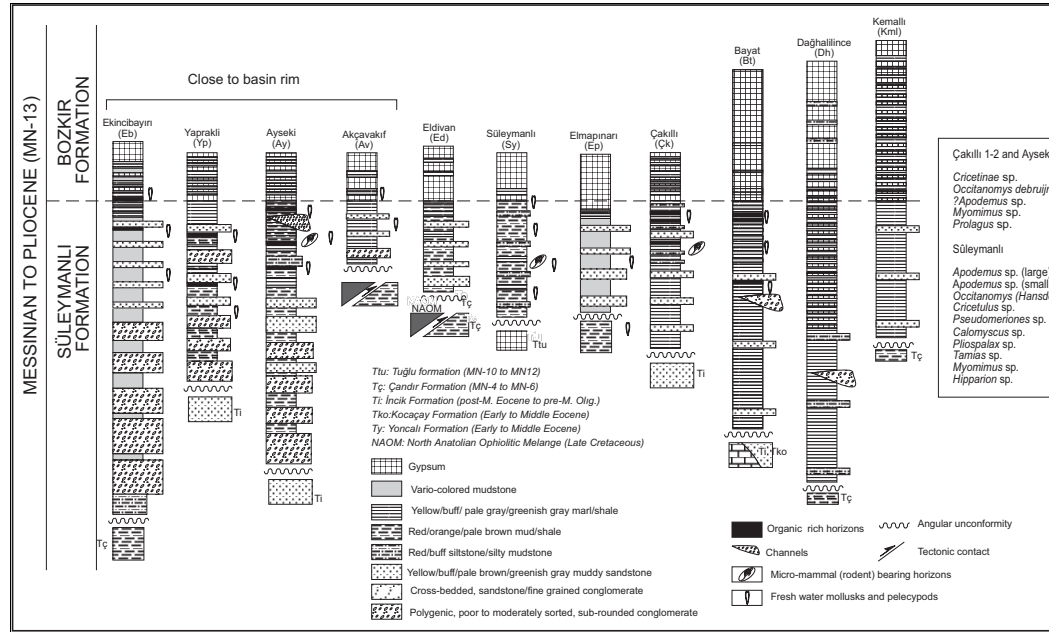
Figure 4.16 Correlation chart of the measured sections of the Sûleymanlı and Bozkır formations (see Figures 4.05,4.12 location of the sections).

Another distinguishing feature is the basal contacts.The Bozkır Formation is generally associated with the Sűleymanlı Formation that is red to purple in general.

In the area to west of Bayat, north of Toyhane (Figure 4.14), East of Ovacık (Figure 4.12), the Bozkır Formation is characterized by an alternation of white and pinkish beds. The white layers include an alternation of thin bedded to laminated gypsum with thinly bedded shale/marl. In the central western parts of the basin, the Bozkır Formation has thicker bedding than other parts of the basin. This relation may indicate that this area constituted the deeper parts of the depocenter during which the Bozkır Formation was deposited.

No fossil could be found to date the unit, however, its lateral and vertical gradation into the Sűleymanlı formation and unconformable relationship with the overlying Deyim Formation suggests Messinian to Pliocene age for the Bozkır Formation.

4.2.9 Deyim Formation (Tde, Gelasian to Early Quaternary)

The Deyim Formation was named by Aziz (1975). It is characterized by loosely compacted coarse clastics with intercalation of minor fine clastics. It is exposed mainly in the western, north-western, and central parts of the Çankırı Basin and in the adjacent Hancılı Basin (Figure 4.02). It unconformably overlies the older units and is unconformably overlain by the Quaternary alluvium.

The Deyim Formation is composed dominantly of variable sized, poorly sorted, polygenic loose conglomerate/gravel and sandstone, siltstone and mudstone. The colour of the unit is mainly controlled by the nearby source units. For instance, it is red coloured in the NW corner of the Çankırı Basin, near Yapraklı (Figure 4.12) where source rocks are the Oligocene red clastics. It is greenish gray near Sarıkaya village (Figure 4.12) where it has received detritus from Late Cretaceous volcano-clastics and pre-Neogene flyschoid basin in-fill. Near Hisarcık village (Figure 4.05) it is gray to greenish gray reflecting detritus from the NAOM.

The only locality where rodent fossils were collected was near Sarıkaya village on the NW margin of the Çankırı Basin (indicated with rodent sign near the Sarıkaya village in Figure 4.12). These samples yielded only *Microtus sp*. which indicates MN-17 zone or younger. Based on this information a Late Pliocene (Gelasian) to Early Quaternary age is assigned to the Deyim Formation.

4.3 Neogene Tectonics of the Çankırı Basin

In this section, the deformation style within, and tectonic relationships between, the Neogene units are given, along with the structures that developed in the Çankırı Basin and adjacent Hancılı Basin.

4.3.1 Temporal Relationships of Structures Developed in the Neogene

4.3.1.1 The Western Area, Northern Area and the Hancılı Basin

The structure which covers the oldest Neogene formation is the Kılçak Thrust Fault (KTF). Along the KTF, the NAOM and associated Late Cretaceous units are thrust over the MN 1-2 Kılçak Formation. There is no unit covering the fault contact to constrain the age of the fault precisely, however, the MN 17 (Gelasian) Deyim Formation unconformably overlies the folded and over turned Kılçak Formation in the vicinity of the KTF (Figure 4.17a), which indicates post MN 1-2, and pre MN 17 development of the KTF.

108

The other faults in the western part of the Çankırı Basin are the TF-4 and TF-5. Along the TF-4 the NAOM and associated Late Cretaceous units were thrusted over the Middle Miocene Çandır Formation and the thrust contact is covered by Late Miocene Sűleymanlı formation in the area indicated with 3 in Figure 4.12. Along the TF-5, the NAOM and associated Late Cretaceous units thrusted over the MN ?4-6 Çandır Formatıon and the thrust contact ıs cover by the MN 13 Sűleymanlı Formation (Figure 4.17d) in the area indicated wıth 3 and 5 in Figure 4.12. In addition it is coverd by the MN 17 Deyim Formation (Figure 4.17c) in the location indicated with 6 in Figure 4.12. This relation indicates post-MN 6 and pre-MN 13 development of the TF-5.

The Kazmaca-Hamzalı Reverse Fault (KHRF) is developed within the pre-Neogene units and it is of Middle Eocene to pre-MN 1-2 (Aquitanian) age as discussed in chapter 3.

The NF 2 is one of the sinistral transtensional faults within the Eldivan Fault zone (Figure 4.17c). NF 2 displaced the TF-5 and MN 13 Sűleymanlı and Bozkır formations (Figure 4.12a), which indicates post-MN 13 development of the NF-2.

The NF-3 is a sinistral transtensional fault developed with in Kılçak sector of the Çankırı Basin (Figure 4.05a). It displaced the MN 1-2 Kılçak and MN 17 Deyim formations, which indicate post MN 17 development of the NF-3.

The Hamzalı Faults (HF) and the Kargın-Elmapınar Fault (KEF) are transtensional faults that displaced the Kazmaca-Hamzalı Reverse Fault (KHRF) and MN 13 Sűleymanlı and Bozkır formations, which indicates post-MN 13 development of the HF and KEF faults.

Eldivan Fault Zone defines the Western Margin of the Çankırı Basin (WMCB) and includes a number of generally N-S to NNE-SSW to NE-SW striking sinistral transpressional and transtensional faults (Figure 4.12a). The youngest unit displaced by the EFZ is the MN 17 (Gelasian) Deyim Formation (Figure 4.17c), which indicates post-MN 17 development of the EFZ.

Merzi-Badiğin Fault Zone (MBF) is one of the longest fault zones that delimit the north-western margin of the Çankırı Basin (Figure 4.12). It is composed of a number of NE-SW striking dextral transtensional faults that displaced the TF-4, the rim lithologies, MRF, pre-Neogene units and MN 17 Deyim Formation, which indicates post-MN 17 (Gelasian) development of the MBF.

The Bűrtű Fault Set (BUFS) has displaced the rim, the pre-Neogene and the Late Pliocene (Gelasian) to Early Quaternary (MN 17) Deyim Formation (Figure 4.12a), which indicates its post-MN 17 development.

The Merzi Reverse Fault (MRF), Çavuşkőy Fault (ÇF) and Ayseki Reverse Fault (ARF) are the youngest compressional faults that controlled the structural development of the NW corner of the Çankırı Basin. Along the MRF, the rim lithologies cut across the MN 13 Sűleymanlı formation and the fault contact is covered by the MN 17 Deyim Formation (see location 1 in Figure 4.12a), which indicates that MRF postdates MN 13 (Messinian) and predates MN 17 (Gelasian). Likewise, along the ÇF, the Late Eocene to mid-Oligocene İncik Formation cut across the MN 13 Suleymanlı and Bozkır formations and the fault itself is covered by the MN 17 Deyim Formation (location 4 in Figure 4.12a), which indicates it has a post-MN 13 and pre-MN 17 development. Along the ARF, the pre-Neogene units cut across the Late Eocene to mid-Oligocene İncik Formation. The ARF has not been covered by any Neogene unit, however, the MN 13 Sűleymanlı formation is overturned parallel to the ARF into the Kıvçak Fold between Ayseki and Kıvçak villages (KF in Figure 3.12a), which indirectly indicates post MN 13 development of the ARF.
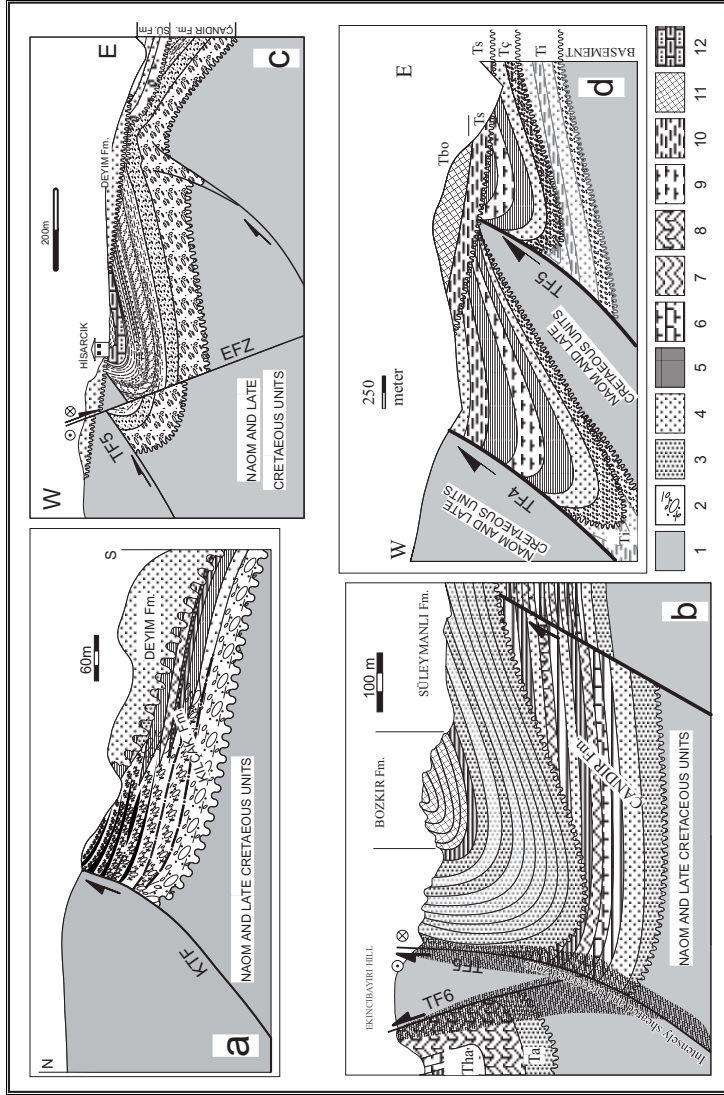
The thrust faults developed within the Hancılı Basin (TF-6, TF-7, TF-8, and TF-9, in Figure 4.05a) cut the MN 3-4 Altıntaş and MN 4-5 Hancılı formations and are locally covered by the MN 17 Deyim Formation, which indicates post-MN 5 and pre MN 17 development of these faults (see chapter 5).

The Kargın anticline and syncline (KA and KS, 4 and 5 in Figure 4.05b) are parallel to the KHRF. The strike of beds of the Dizilitaşlar and Çandır formations are parallel to each other on either limbs of the anticline. Unfolding of the Dizilitaşlar Formation according to the dip of the Çandır Formation indicates that this structure has two episodes of coaxial folding (Figure 4.18a-c). The earlier phase developed prior to the deposition of the Çandır Formation in MN ?4-6 (?Burdigalian to Serravalian). Together with the information discussed in the chapters 2 and 3, this relation indicates presence of a compressional deformation prior to Burdigalian.

In the Hancılı Basin, two sets of folds have developed (Figure 4.05) in the Neogene units. One set is oriented approximately NW-SE, parallel to the thrust faults and the longer axis of the three depressions of the Hancılı Basin (Figure 4.05a), which indicates that these folds were developed due to the activity of the thrust faults (t1 folds in Figure 4.18d). The other set of the folds is developed in the Hasayaz Depression and the folds are oriented NE-SW, parallel to the folds that developed within the Late Miocene units in the western margin of the Çankırı Basin. The folds, which developed within the Çandır Formation in the western margin of the Çankırı Basin are oriented NNE-SSW and within the same area, the folds within the Late Miocene units are oriented NE-SW. This relation ship implies sequential anticlockwise rotation of the folds within the sinistral strike-slip Eldivan Fault Zone (Figure 4.18e-f) in combination with the activity of a restraining bend (Figure 4.19d). This relation gave way to 50° of angular difference between the folds that developed within the Middle Miocene Çandır and Late Miocene Sűleymanlı formations (Figure 4.18 d-f). Sanderson and Cox (1984) have discussed how the structures within a convergent strike-slip fault zones tend to become parallel to the principal displacement zone. Therefore, the observed 50° of angular difference between the folds developed within the Çandır Formation and the Late Miocene units can not be attributed to the rotation alone but may reflect the combination of rotation about vertical axes and re-organization of fold axial trends due to local stress perturbation exerted by the restraining bend of the EFZ (Figure 4.18d-f).

In the north-western part of the Çankırı Basin, the folds developed within the Late Miocene units, namely the Tuğlu, Sűleymanlı and Bozkır formations (Figure 4.12). Here, the orientation of the major folds, which include the Sűleymanlı Anticline (SŰA) and Syncline (SS), the Topuzsaray Anticline (TA), the Yőrűk Syncline (YS), and the Kıvçak

folds (KF) (Figure 4.12a), change, their orientation gradually from about E-W to NE-SW. The tightness of the folds becomes greater in the NW than in the south (Ovacık Monocline and SŰA). This relationship indicates the response of the basin in-fill within the wedge shaped area defined by the EFZ in the west, MRF and ARF in the north-west and the Kırşehir Block in the south. As displacement occurred along the EFZ, MRF and ARF, the basin in-fill tends to rotate anticlockwise similar to the mechanism proposed for the folds developed within the Çandır and Sűleymanlı formations in the western margin of the Çankırı Basin (Figure 4.18d-g). This is further discussed later.

4.3.1.2 The Eastern and Central Areas

Structurally, the central (Figure 4.11) and eastern parts of the Çankırı Basin (Figures 4.13 and 4.14) are characterized mainly by transpressional faults, which are striking generally NNE-SSW to NNW-SSE and NE-SW and by folds and dome-like structures.

4.3.1.2.1 Eastern area

The main reverse faults in the eastern part of the Çankırı Basin are the Halaçlı Fault (HTF, Figure 14), the Saĝpazar Reverse Fault (SRF, Figure 14), the Karaçay Reverse Fault (KARF, Figure 13) and the Gűvendik Thrust Fault (GTF, Figure 4.13). Among these, the Gűvendik Thrust Fault (GTF) has developed between the underlying Gűvendik formation and overlying NAOM, indicating its post mid-Oligocene activity. There is no Neogene unit overlying the GTF. Therefore, its latest activity could not be precisely constrained. The GTF is displaced sinistrally by a NE-SW trending fault.

The Halaçlı Fault (HTF) is observed in the east of the central part of the Çankırı Basin (Figure 4.14). Along the HTF, the Gűvendik formation of Oligocene age is thrust over the Çandır Formation of MN ?4-6 age (Figure 4.19a), which indicates its post-MN 4?-6 development.

The Saĝpazar Reverse Fault (SRF) is observed between the Gűvendik formation and the Late Miocene units (Figure 4.14). Along the SRF, the post-Middle Eocene to mid-Oligocene Incik Formation has been thrusted over the Late Miocene Sűleymanlı formation in the northern part of the fault (see location 2 in Figures 4.14 and 4.19b). In the south, it becomes a blind fault (location 3 in Figures 4.14 and 4.19b). Parallel to the SRF, the Tuğlu formation is folded along the Saĝpazar Anticline (TA in Figure 4.14). The angular unconformable relationship between the Early Tertiary units (Incik and Gűvendik Formations) and the Tuğlu formation and the degree of tightness of the Saĝpazar Anticline (SA) within the Tuğlu and Early Tertiary units, in cross-section, indicates two different episodes of compressional deformation. The strike of the Tuğlu formation and of the Early Tertiary units are parallel along the SA (see Figure 4.14), which indicates co-axial deformation, prior to and after the deposition of the Tuğlu Formation.

The Karaçay Reverse Fault (KARF) is developed within the early Tertiary units (Figure 4.13). In the north the KARF, it is covered by the Tuğlu formation of MN 10-12 age and by the Çandır Formation of MN ?4-6 age in the central part (locality 9 and 11 in Figure 4.13 and 4.19c), which indicates its pre-MN ?4-6 development.
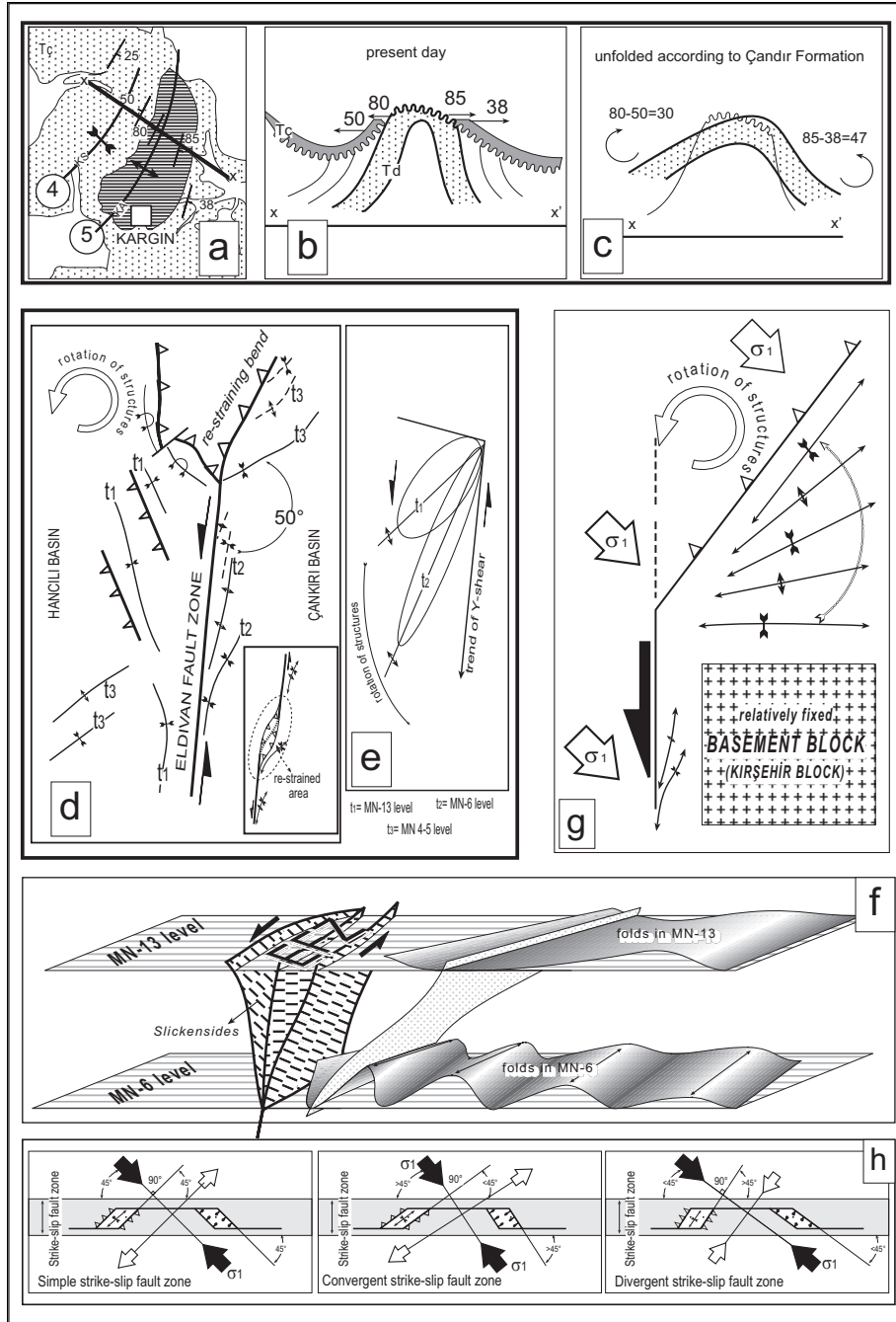
Figure 4.18 a) Simplified geological map around the Kargın village (see Figure 4.05b), b) present day cross-section. c) Unfolded Early Tertiary units (according to the dips of the Çandır Formation) still preserve an asymmetric fold. d-e) Possible mechanisms suggested for the development of the folds in the Çandır, Süleymanlı and Bozkır formations. d) The folds have a constant angle with the boundary fault and the discrepancy between trend of the folds is due to the bending of the boundary fault as it forms a restraining bend (mechanism after Biddle and Christie-Blick 1985). e) The trends of the folds are related to their age of formation in a simple shear setting. The folds are first formed in NE-SW attitude and then they are rotated counter-clockwise so that the older folds gradually became NNE-SSW in orientation. f) Block diagram depicting the relation between the Eldivan Fault Zone (EFZ) and the folds developed in the western margin of the Çankırı Basin (see Figure 4.05). g) Model proposed for the formation of the folds in the north-western part of the Çankırı Basin (see text for the explanation). h) Angular relationships between fault zone, principal stresses and the structures developed within a simple, convergent and divergent strike-slip fault zones (modified from Sanderson and Cox 1984). Along strike-slip faults, three of the angular relationships presented in this figure might be developed due to local stress perturbations as the fault zone change its strike (Biddle and Christie-Blick 1985).

It will be further discussed in chapters 6 and 7 that within the Sungurlu Fault Zone, the Gűvendik Syncline and KARF were re-folded (Figure 4.19g, see chapter 7), which indicate that the Sungurlu Fault was a sinistral fault in the pre-Neogene. Along the Master Strand of the Sungurlu Fault Zone (SFMS), the Çandır Formation of MN ?4-6 age and Tuğlu formation of MN 10-12 age are truncated and locally overturned (16 and 17 in Figure 4.13) which indicates a post-MN 10-12 activity. A paleostress inversion study along this fault (discussed in chapter 6) has demonstrated that three different fault movements took place along the SFMS. The first movement was sinistral strike-slip in nature and took place in the pre-Neogene, the second phase was normal in nature and took place in Middle Miocene, and the latest movement was dextral strike-slip in nature and postdates MN 10-12 (Tortonian).

A number of NE-SW (N40°-50°E, Figure 4.13b) trending faults displace the pre-Neogene units and the Tuğlu (MN 10-12), Süleymanlı and Bozkır (MN 13) formations in other parts of the Çankırı Basin (Figures 4.13 and 4.14). In the field, these faults are characterized by wide zones of distributed deformation dominated by a number of mezoscopic faults with high angles of dip (>60°), and oblique slickenlines with a dextral strike-slip component and a component of normal movement (transtensional faults) having pitches ranging between 20° to 60° (see Chapter 5). These faults are obscured in Gűvendik, Tuğlu and Bozkır Formations because of their gypsum content, however morphological expressions of and juxtapositions along these faults are partly preserved.

The Gűvendik Syncline (GS) is one of the most spectacular folds in the SE part of the Çankırı Basin. It is developed within the İncik Formation and has been re-oriented in the south by the SFMS. In the localities 12 and 13 (in Figure 4.13) the fold is covered by the Çandır Formation (see also Figure 4.19e) indicating that GS predates Çandır Formation of MN ?4-6 age. As discussed in chapters 2 and 5 and 7, the Gűvendik folds were developed during the westward tectonic transport on the thrust faults in the eastern rim of the Çankırı Basin, in the Late Eocene to pre-Burdigalian. Back rotation of the Gűvendik Syncline, together with KARF, according to paleomagnetic data (discussed in chapter 7), indicated that the fold was oriented NW-SE during the Eocene and Oligocene, which indicates that the σ_1 was oriented approximately NE-SW during its development in pre-MN ?4-6 times (Figure 4.19g). The Gűvendik Syncline is displaced dextrally by one of the sub strands of the Sungurlu Fault Zone between locations 18 and 18' in Figure 4.13. In addition, the Sungurlu Fault Zone is a sub strand of the Ezinepazarı-Sungurlu Splay

Fault Zone (ESFZ) of the North Anatolian Fault Zone (Figure 4.01). The ESFZ was ruptured between Mecitözű to Erzincan during the 1939 Great Erzincan earthquake (Ms. 7.9, Barka and Hancock 1984, Barka and Kadinski-Kade 1989). August 1996 and September 1999 earthquake tremors (KARDEA 1999) along the ESFZ, also gave an indication of the dextral nature of the Sungurlu Fault Zone.

The Karaçay Folds are a number of NNE-SSW oriented folds that developed within the Tuğlu formation of MN 10-12 age (Figures 4.13 and 4.19d), which indicates their post-MN 10-12 development in which σ_1 was oriented approximately WNW-ESE.

In the localities 5,6,7, and 8 in Figures 4.13 and 4.14, the İncik Formation has a circular outline. Around the location 7 in Figure 4.14, the dips of the Tuğlu formation display a radial pattern. In the localities 5,6,7 and 8, the Tuğlu and İncik formations have an angular unconformable relationship. In the central parts of these areas, the İncik formation is intensely deformed and folded and the gypsum lithologies within the unit are flow banded so that the İncik Formation has partially lost its internal structures while overlying Tuğlu Formation is less deformed. This relationship indicates that diapirism took place during and after the deposition of the Tuğlu Formation of Tortonian age (MN 10-12).

4.3.1.3 Central Areas

The central part of the Çankırı Basin is characterized by on-lap patterns of the Early Tertiary and Neogene units onto the Kırşehir Block (which is represented, in this area, by the Sulakyurt Granite and the Late Cretaceous NAOM and the Yaylaçayı Formation,) and generally NNE-SSW to NNW-SSE and NE-SW trending faults with linear to curvilinear trace (see Figure 4.11).

The NE-SW to NNW-SSE trending faults divide the central part of the Çankırı Basin into horst-graben complexes (Figure 4.11a. see also chapter 2 and 6). These faults are covered by the Sűleymanlı and Bozkır formations and locally truncated by ENE-WSW trending faults (Figure 4.11a). The mesoscopic faults that are parallel to the NNE-SSW trending major faults have very high dips and the slickenlines on these faults indicate that they are normal oblique-slip faults (see also Chapters 2 and 6). In the locality indicated by 1 in Figure 4.11a, the granites are juxtaposed with the İncik and Çandır formations along an approximately NNE-SSW striking fault. At this locality, the displacement of the base of the Çandır Formation on the hanging- and the foot-wall block is about 250 m which is the minimum vertical (normal) displacement along the fault.

In the locality 2 (Figure 4.11a), the NAOM, İncik and Çandır formations have been juxtaposed. In this locality, within the fault zone, the Çandır Formation is inversely drag folded (Figure 4.19f, see also chapter 2), which indicates reverse faulting, although, normal faulting is obvious approximately 1km south of this location along strike. In addition, overprinting slickenlines observed on the mesoscopic faults, in this area, indicate two phases of fault movement. The first movement is associated with a normal sense of movement and second movement is with a reverse movement with a sinistral component of horizontal displacement (Figure 4.19f, and see chapter 6). Similar relationships are also observed in localities 3 and 4 in Figure 4.11a. This is discussed in chapters 2 and 6.

4.4 Discussion of the Tectonic and Stratigraphical Development of the Çankırı and the Hancılı Basins During the Neogene

4.4.1 Çankırı Basin

In the folowing chapters (5 and 6) it is argued that the pre-Burdigalian tectonic evolution of the Çankırı Basin is characterized by a compressional deformation in which the orientation of σ_1 changes from WSW-ENE to NNW-SSE in the northwestern margin of the Çankırı Basin (see chapters 5 and 6). During this period, the İncik Formation of Middle Eocene to Middle Oligocene and Kılçak Formation of Aquitanian age, which is the latest product of this compressional regime, was deposited coeval with thrusting and transpressional faulting (see Chapters 2,5 and 6). As seen in the Figures 4.20 and 4.21. In the beginning of the Burdigalian, the region was dominated by an oblique extensional deformation characterized by a sub horizontal σ_3 and an oblique σ_1, (see also chapters 2, 5 and 6), during which the Çandır Formation was deposited in the Çankırı Basin and Altıntaş and Hancılı formations were deposited in the Hancılı Basin.

In Tortonian to present (possibly post-MN 6), the extensional regime was replaced by an approximately NW-SE oriented compression (see Figures 4.20 and 4.21). During this phase, σ_1 was oriented NW-SE while σ_2 was sub vertical and indicates a regional transcurrent tectonics (Figures 4.20 and 4.21). As discussed in chapter 2, the structures that were developed in the latest compressional deformation phase display a Riedel pattern, as illustrated in Figure 4.24c (see also chapter 2).

Considering the characteristics of the major structures summarized in Figures 4.20 and 4.21, It can be concluded that the compressional regime that commenced in the Tortonian is characterized by a regional transcurrent tectonics. Pre-existing thrust faults in the western margin of the Çankırı Basin were reactivated as transpressional faults, which makes approximately 75° with the σ_1 (Figure 4.24b). The pre-existing thrust faults and the reverse faults in the rim of the Çankırı Basin (possible western continuations of the ÇF, MRF, ARF) gradually converted into strike-slip faults as they were transported southwards and wrapped around the Kırşehir Block and rotated anticlockwise (Figures 4.18 and 4.22a-c). In this regime, the western boundary of the Çankırı Basin was a transpressive sinistral strike-slip fault zone (Eldivan Fault Zone-EFZ) while the northwestern margin was dominated by reverse faults (Figure 4.22d). The conjugate to the EFZ are NE-SW trending faults that displaced the basin in-fill, the basement (Kırşehir Block) and the western margin of the Çankırı Basin dextrally (Figures 4.22a-c and 4.24). In addition, the normal faults that developed in the previous extensional regime, in the western margin and central part of the basin, were inverted as transpressional faults (see chapters 2,5 and 6).
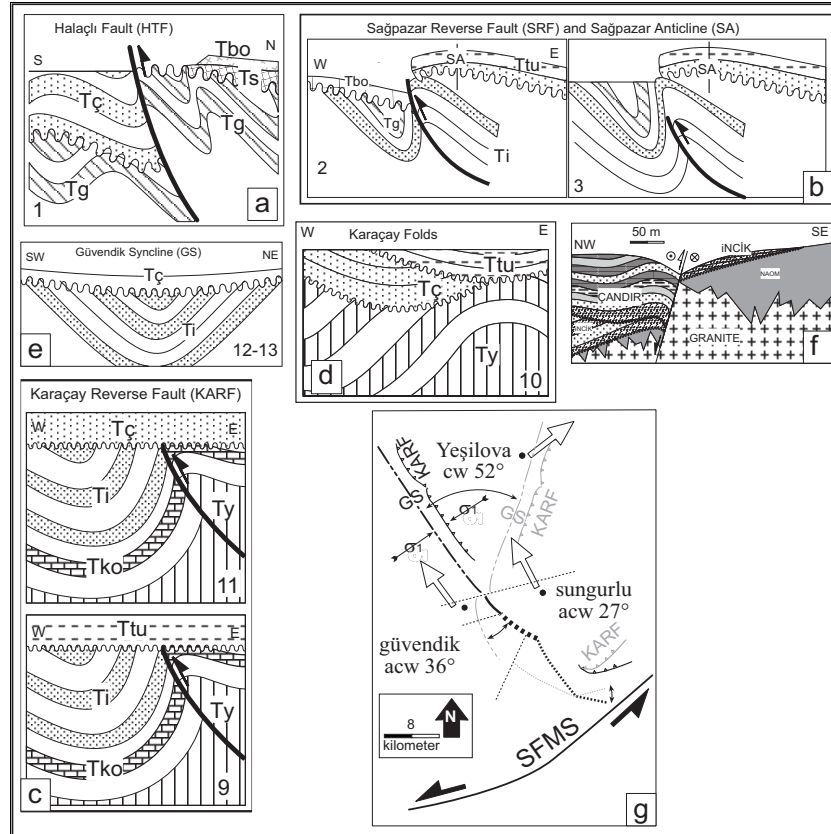
Figure 4.19 Schematic illustration of various tectonic relationships between different Neogene units: a) Between Gűvendik formation (Tg), Çandır Formation (Tç), Sűleymanlı (Ts) and Bozkır (Tbo) formations along the Halaçlı Fault (HTF) (see location 1 in Figure 4.14). b) Between Incik (Ti), Gűvendik (Tg), Sűleymanlı, and Tuğlu (Ttu) formations along the Sağpazar Reverse Fault (SRF) and Sağpazar Anticline (SA) (note emergent and blind nature of the SRF, see locations 2 and 3, in Figure 4.14). c) Tectonic and stratigraphic relationships of the Early Tertiary units (Yoncalı-Ty, Kocaçay-Tko, Incik, and Gűvendik formations) and Çandır and Tuğlu formations along the KARF (see locations 9 and 11 in Figures 4.13 and 4.14). d) Stratigraphical relationships between Yoncalı (Ty), Çandır and Tuğlu formations along one of the Karaçay Folds (see location 10 in Figure 4.13). e) Unconformable relationship between İncik and Çandır formations in locations 12 and 13 in Figure 4.13. f) Cross-section depicting an inverted normal fault near Dağhalilince village (see Figure 4.11a for its location). Note sinistral strike-slip component of the fault and inverse dragging and normal separation that is still preserved and also to the on-lap unconformities between the basement and the İncik Formation (looking to N). The down going arrow indicates normal faulting and up going arrow indicates reverse faulting due to inversion. g) Simplified map illustrating the back rotation of the Gűvendik Syncline (GS) and the Karaçay Reverse Fault (KARF) using the paleo-declination data (large arrows) discussed in chapter 7. Present day orientations are fainted. Angles are the amounts of clockwise (cw) and anticlockwise (acw) rotations. Note that the GS and KARF become relatively straight and oriented NW-SE which indicates that the σ_1 (possibly in deformation phase 2) was oriented NE-SW prior to the rotation of the GS.
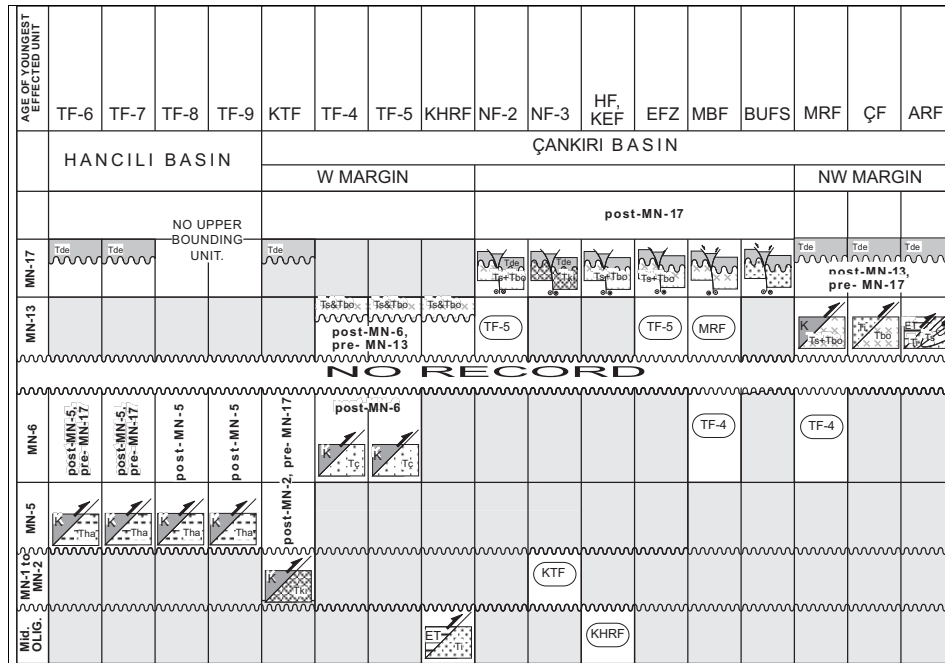
117

Figure 4.20 Summary of the temporal relationships between various structures developed in the western and north-western part of the Çankırı Basin during the Neogene (see Figure 4.03 for the abbreviations of the units). The faults indicated in ellipses are displaced by the faults in the top row. The times in the first column indicate the ages of the underlying unit, which together with the covering unit brackets the age of related faults. KHRF: Kazmaca-Hamzalı Reverse Fault, HF: Hamzalı Faults, KEF: Kargın-Elmapınar Fault, EFZ: Eldivan Fault Zone, MBF: Merzi-Badiğin Faults, BUFS: Bűrtű Fault Set, MRF: Merzi Reverse Fault, ÇF: Çavuşkőy Fault, ARF: Ayseki Reverse Fault. K: Late Cretaceous to Paleocene, ET: Early Tertiary units, Ti: İncik Formation, Tki: Kılçak Formation, Tha: Hancılı Formation, Tç: Çandır Formation, Ts: Sűleymanlı formation, Tbo: Bozkır Formation, Tde: Deyim Formation. The age of the ARF is constrained using overturned folding (last column). Note difference between the faults in the western (strike-slip) and NW margin (reverse faults) of the Çankırı Basin.

The Tuğlu and Sűleymanlı Formation are successive units in the Çankırı Basin. However, they have an angular unconformable relationship. The Tuğlu Formation is intensely deformed while the Sűleymanlı Formation is less deformed. In addition, the intensity of deformation in the Tuğlu formation is higher than the underlying Çandır and overlying Sűleymanlı and Bozkır formations. Considering the gypsum content of the Tuğlu formation, it is proposed that the deformation of the Tuğlu formation is exaggerated due to salt tectonics. That is, the deformation was preferentially located in the Tuğlu formation because of the salt. On the other hand, the Bozkır Formation also includes gypsum (coarser grained than the Tuğlu Formation and makes up approximately 25% of its total volume) and this relation invalidates the foregoing argument. Therefore, the gradual decrease in the intensity of the deformation upwards from the Tuğlu to the Bozkır formations is attributed to the syn-tectonic sedimentation of these gypsum-bearing

118

formations, which indicates that compressional deformation commenced during the deposition of the Tuğlu Formation in Tortonian.

The faults that are oriented generally NE-SW, and postdating the Late Pliocene (Gelasian, MN 17), are the latest products of the latest compressional deformation. There is no direct evidence for any present activity on them. However, deep incision of gullies (Koçyiğit et al. 1995) and the presence of unpaired terraces along most of the streams and seismic activity in nearby areas imply that they are a part of the presently active system.

MN ZONES	KARF	HTF	SRF	SA	GTF	GS	DIAPIRS	Karaçay Folds	SFMS	NE-SW FAULTS	NNE-SSW and NNW-SSE FAULTS	FAULT TYPES	TECTONIC REGIME	DURATION OF THE TECTONIC REGIME
				Eastern part							Central part			
MN 13		post-MN 13	post-MN-13 WNW-ESE COMPRESS.	post-MN-12 WNW-ESE COMPRESS. (reactivated)		post-MN 12 WNW-ESE COMPRESSION (co-axially re-folded)	end of diapirsm	post-MN 10-12 WNW-ESE COMPRESSION.	post-MN 10-12 DEXTRAL WNW-ESE COMPRESS. (reactivated)	post-MN 13 STRIKE-SLIP	post-MN 13 (inverted)	REVERSE TO TRANSPRESSIONAL — STRIKE-SLIP	TRANSCURRENT	TORTONIAN TO RECENT
MN 10-12						post-MN-12	?							
(NO RECORD)														
MN ?4 to MN-6										MN-4? to MN6 NORMAL	NORMAL OBLIQUE-SLIP	OBLIQUE-EXTENSIONAL	BURDIGALIAN TO SERRAVALLIAN
pre-MN ?4-6	post-Oligocene NE-SW COMPRESS.			end of 1st folding Tç	post-Oligocene NE-SW COMPRESS.	post-Oligocene	post-Oligocene and pre-MN-6 Tç			post-Oligocene SINISTRAL NE-SW COMPRESS.		THRUST AND TRANSPRESSIONAL (INDENTATION)	COMPRESSIONAL	PRE-BURDIGALIAN

Figure 4.21 Temporal relationships between various structures developed in the eastern and central parts of the Çankırı Basin (see Figure 4.03 for the abbreviations of the units). Thrusting (pre-Burdigalian) and extensional regimes (Burdigalian to Serravalian) are based on the information summarized in Figure 4.20 and discussed on chapters 2,3,5 and 6. KARF: Karaçay Reverse fault, HTF: Halaçlı Fault, SRF: Sağpazar Reverse Fault, KRF: SA: Sağpazar Anticline, GTF: Gűvendik Thrust Fault, GS: Gűvendik Syncline, SFMS: Master Strand of the Sungurlu Fault Zone.

4.4.2 Hancılı Basin

The Hancılı and Altıntaş formations represent lateral facies variations in the Hancılı Basin. The Altıntaş Formation is thicker in the south-western parts of each of the three depressions of the Hancılı Basin, namely the Hasayaz, Şemsettin and Demirtaş depressions (Figure 4.08). The red coloration, unsorted to poorly sorted nature of the conglomerates, the sub angular to sub rounded character of the pebbles, the lensoidal geometry of the facies of the Altıntaş Formation and rodent fossils reported by Şen *et al*. (1998) indicate continental environments and, possibly, an alluvial fan origin for the unit. The presence of a fining and thinning upward sequence indicates retreat of the source area, which is a characteristic for extensional settings (see Mial 1996). The presence of marls, fresh water molluscs and pelecypoda indicate that the Hancılı Formation was

deposited mainly in lacustrine settings. The presence of organically rich levels and very thin coal seams imply marshy and back swamp settings for the Hancılı Formation (Figure 4.07). The presence of thicker tuffaceuos layers in the western parts of the basin implies the presence of volcanic centers in the west, which are probably associated with the Middle to Late Miocene (21.8 Ma to Recent) Galatean Volcanic Province (GVP, Toprak *et al*, 1996). Locally, the Hancılı Formation onlaps directly on to the horst-like blocks of the rim lithologies (see Figure 4.05 and 4.08) and indicate that these basement blocks were temporarily submerged below the lake level during the deposition of the Hancılı Formation. Because the Altıntaş and Hancılı formations are thicker in the SW margins of the Hancılı Basin and thinner (the Altıntaş Formation may be completely missing, see Figure 4.05) in the NE margins and onlap on the horst-like blocks indicate asymmetric extensional faulting (Leeder *et al*. 1988, Gabrielsen *et al*. 1995) during the development of the Hancılı Basin. The deeper parts of the basins are interpreted to lie in the south-western parts of each depression (see Figures 4.05,4.08,4.23b and e). Considering overprinting slickenlines on the faults (TF 6-9, Figure 4.05) defining the boundaries of the three depressions within the Hancılı Basin (discussed in chapter 5) in combination with the above-mentioned information indicate that the Altıntaş and Hancılı formations were deposited in an extensional setting possibly characterized by half grabens (Leeder *et al*. 1988, Gabrielsen *et al*. 1995) associated with oblique-slip normal faults (see Figure 4.23b and e) that are striking generally NW-SE (present day orientations) (see discussion above about the western margin of the Çankırı Basin).

4.4.3 Tectonic Development of the Hancılı Basin and of the Western Margin of the Çankırı Basin

In the pre-Neogene (most likely pre-Burdigalian?) due to the northwards drift of the Kırşehir Block and indentation of its promontories into the Sakarya Continent (see chapters 4,5, and 6), the western margin of the Çankırı Basin experienced a compressional deformation that is characterized by thrust and reverse faults with strong sinistral lateral components (transpression) (Figure 4.23a and d). The indentation process continued until about the deposition of the Kılçak Formation (see chapter 5 and 6) in the Aquitanian. During this period, in addition to other pre-Early Tertiary units, the İncik, Gűvendik and Kılçak formations were deposited in the Çankırı Basin as the latest products of the indentation process (see chapter 2 and 6).

By the beginning of the Burdigalian, the compressional deformation was replaced by an extensional deformation (see chapter 2) and resulted in the development of the Hancılı Basin and deposition of the Altıntaş and Hancılı formations (in MN 3-4 to MN 4-5). These two units were not exposed in the Çankırı Basin. Therefore, it is inferred that during the extensional deformation period, the Hancılı and Çankırı Basins were isolated from each other. Therefore, they evolved, stratigraphically, independently, although, they were tectonically dependent. Paleostress inversion studies (discussed in chapters 5 and 6) indicate that the extension took place under tri-axial strain conditions, which indicates that most of the normal faults developed in this period had oblique components (Figure 4.23b and e) The pre-existing faults (TF 4 and 5) were reactivated as normal faults with a sinistral strike-slip component and the faults along the western margin of Çankırı Basin maintained their pre-existing sinistral component (Figure 4.23b and e).

The extensional deformation was replaced by a new phase of compressional deformation characterized by a regional transcurrent tectonics in MN-10-12 (Tortonian) during which the Tuğlu formation was deposited (Figure 4.23c and f). As stated earlier, intense deformation of the Tuğlu formation indicates that its deposition took place coeval

with the transcurrent tectonics. During this period the western margin of the Çankırı Basin has been deformed with a component of anticlockwise rotation and the pre-existing faults were re-activated (Figure 4.23c and f). The faults along the western margin have been reactivated into sinistral transpressional faults as the northern part of the rim of the Çankırı Basin reactivated into thrust faults as explained in Figures 4.19 and 4.23c and f. The normal faults in the Hancılı Basin and the normal faults in the central part of the Çankırı Basin (Figure 4.12a) were inverted into compressional faults (see also chapters 2 and 6). As these faults moved, the Hancılı Basin acquired its present-day geometry and became divided into 3 sub depressions. During this period, the Süleymanlı and Bozkır formations were deposited in the Çankırı Basin and they have been deformed by transcurrent movements along the western margin and by thrusting, which continued in the northern margin. During this deformation phase the western margin rotated anticlockwise.

4.5 Discussion of the Regional Implications

The beginning of the extensional tectonic regime in the Çankırı Basin is in Burdigalian (20.5 Ma). Seyitoğlu *et al*. (1992) proposed that beginning of the extensional regime in western Anatolia is Early Miocene. The eastern continuation of west Anatolian extension has not studied yet. However, the timing of the extensional deformation phase discussed for the Çankırı Basin fits with the overall timing of extension in the west Anatolia. Therefore, it can be concluded that the eastern continuation of the Early Miocene extensional regime in western Anatolia can be extended at least up to the Çankırı Basin.

The Early Miocene commencement age of the extensional regime approximately corresponds to the collapse of the Aegean orogenic wedge (see Lips 1998, Wallcot 1998). One of the causes of the orogenic collapse in the Aegean was the decrease in the convergence rates of Eurasia and Africa since 20 Ma, in combination with the detachment of the subducted slab of the Eastern Mediterranean oceanic crust below Eurasia (Lips 1998, Wallcot 1998). Therefore, we propose that, the Middle Miocene extensional regime in the Çankırı Basin, which replaces the compressional regime that is exerted by the collision of the Kırşehir Block and the Sakarya Continent along the Izmir-Ankara-Rerzincan Suture Zone in the deformation phase 2 (see chapter 3), indicates a destabilization and resultant post-orogenic collapse, and was caused by post-20 Ma decrease in the convergence rates of the Eurasia and Africa, at least until the latest compressional regime commenced in the Tortonian.

Further convergence of the Arabian Plate along the Bitlis-Zagros Suture led to the escape of the Anatolian Block along the dextral North Anatolian and sinistral East Anatolian Fault Zones (NAFZ and EFZ, Figure 4.01c) (Şengőr and Yilmaz 1981, Şengőr 1982, Şengőr *et al*. 1985). It is the NAFZ from which a number of splay faults, convex to the north, bifurcate (Figure 4.24a) and transfer transcurrent deformation into the continental interiors of the Anatolian Block (Barka and Hancock 1984). Two of these splay faults are the Sungurlu Fault Zone (SFMS), which is a sub-strand of the Ezinepazarı-Sungurlu Splays and the Kızılırmak Fault Zone (KFZ), which is the western continuation of the Laçin Fault Zone (Figure 4.01b and 4.24a, see also chapter 6). Presently, these faults have a dextral strike-slip sense of movement while the NNE-SSW striking Eldivan Fault Zone (EFZ, western boundary fault of the Çankırı Basin) has a sinistral strike-slip sense of movement. Its orientation and sense of movement indicates that EFZ is the r'-shear of the NAFZ (Figure 4.24b and c).

post-MN6

MN 10-12

MN 13 to recent?
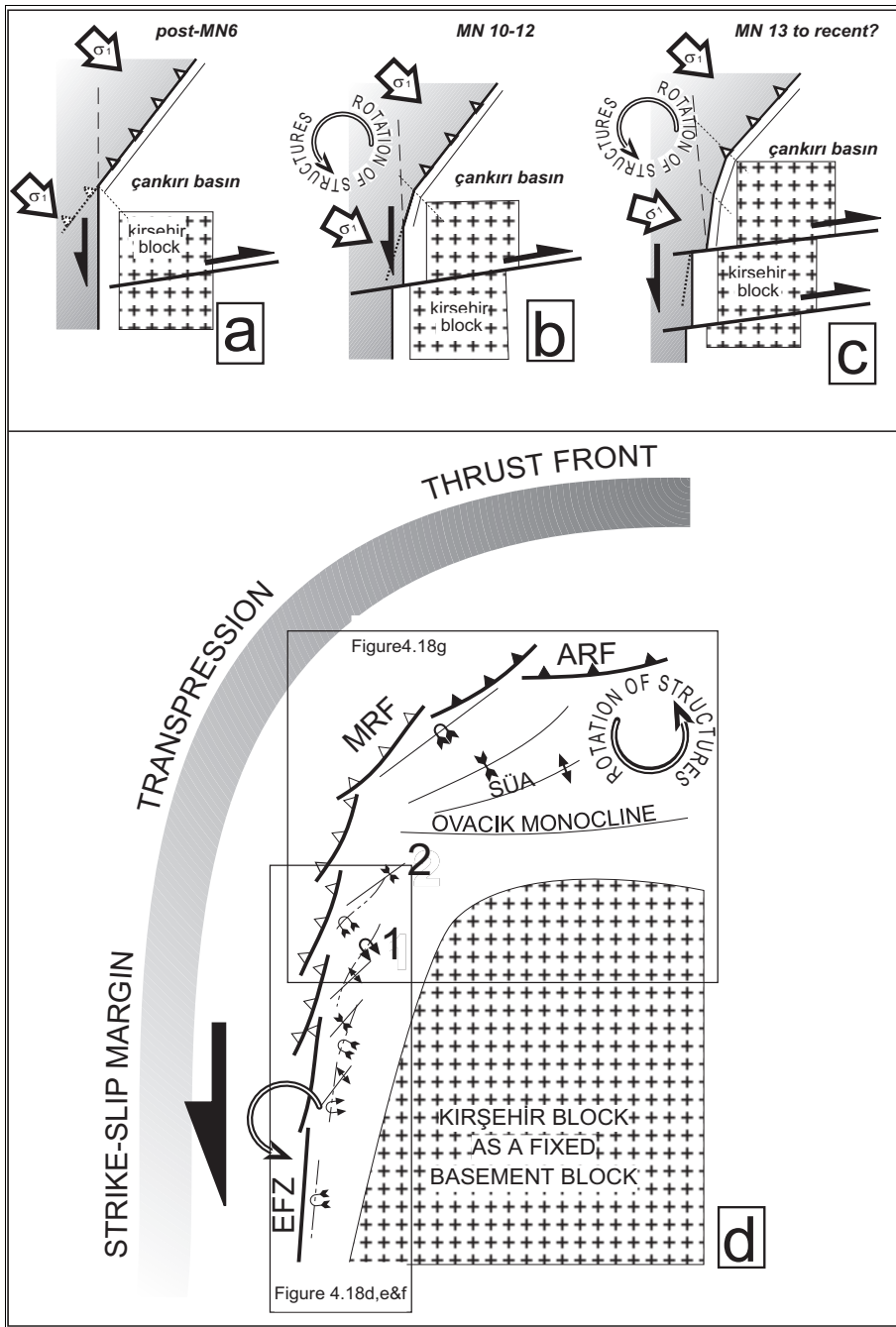
Figure 4.22 a-c) Model proposed for the sequential development of the reverse faults in the western and north-western parts of the Çankırı Basin during the Neogene. As the northern rim of the basin is transported southwards it wraps around the relatively fixed Kırşehir Block so that the reverse faults in the north-western margin are rotated anticlockwise and become transpressional faults. Contemporaneously, the rim of the Çankırı Basin and the Kırşehir Block are displaced dextrally by the NE-SW faults (i.e. Sungurlu Fault Zone, Sivritepe Fault Zone, Yağbasan-Faraşlı Fault Zones, see Figures 4.02 and 4.24) as the conjugate of the Eldivan Fault Zone. d) Summary of the model for the development of the structures in the western and north-western parts of the Çankırı Basin (see text for the explanation).

The orientations of σ_1, as discussed in chapters 5 and 6, are in good agreement with the axes obtained from two seismic fault plane solutions (Figure 4.24) for the North Anatolian Fault Zone. This relation indicates that the latest compressional deformation phase (phase 4), discussed also in chapters 5 and 6 is the same system which gave way to the regional transcurrent tectonic regime, which commenced in Tortonian and is still active. All of the active faults, including the NAFZ, its splays in the Çankırı Basin, EFZ, and other structures smaller scale faults (discussed in chapter 2 and rose diagram of which illustrated in Figure 4.24) can be explained by a riedel pattern of deformation (Figure 4.24c). Therefore, it can be concluded that the latest compressional deformation recognized in the Çankırı Basin is not a local phenomenon but it fits well into the overall regional transcurrent tectonics in the eastern Mediterranean area that resulted in the development of the NAFZ (Mckenzie 1972, Dewey and Şengőr 1979, Şengőr and Yılmaz 1981, Şengőr *et al.* 1985, Barka 1992).

4.6 Conclusions

I. From this study it can be concluded that eight different Neogene stratigraphic units can be identified and mapped in the Çankırı Basin. The units were dated using rodent fossils. The age of the units in which no rodents were found in the field are constrained by their superposition with respect to the well-dated units. The units, in the order of younging are:

1. Kılçak Formation, which is characterized mainly by fluvio-lacustrine clastics. It represents the oldest Neogene unit in the Çankırı Basin and of earliest-Early Miocene (Aquitanian, MN 1-2) age.

2. Altıntaş Formation, which is characterized mainly by red clastics and is latest-Early Miocene (Burdigalian) age.

3. The Çandır Formation, which is characterized by fluvio-lacustrine clastics and carbonates of latest-Early Miocene to Middle Miocene age (Burdigalian to Serravallian).

4. Tuğlu formation is characterized mainly by evaporites of earliest-Late Miocene age (Tortonian).

5. The Süleymanlı Formation, which is latest Miocene (Messinian) to Pliocene age and is characterized mainly by fluvio-lacustrine red clastics.

6. The Hancılı Formation, which is characterized mainly by lacustrine deposits of latest-Early Miocene to early-Middle Miocene age (Burdigalian to Langhian).
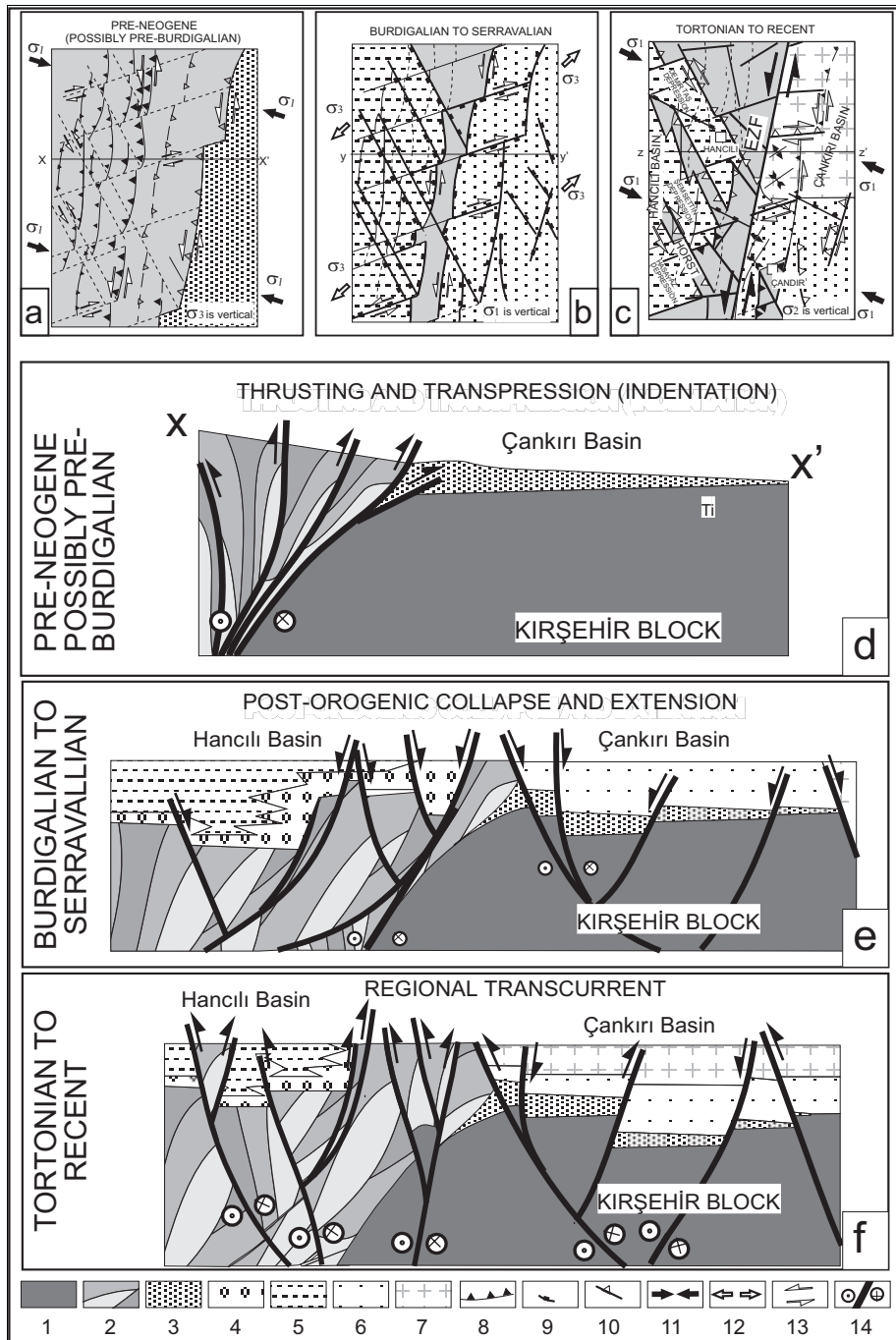
Figure 4.23 a-c) Conceptual diagrams illustrating tectonic evolution of the western parts of the Çankırı Basin. d-f) Schematic E-W cross-sections. a and d) phase of thrusting in pre-Neogene. (b and e) normal faulting during an extensional phase of deformation in Early to Middle Miocene (note reactivation of pre-existing tear faults into normal faults in this period). Note also that deposition in the Hancılı Basin and the Çankırı basin is isolated from each other. (c and f) phase of Neogene compression that commenced in Tortonian. Note that most of the normal faults are inverted into reverse faults and they have strike-slip components. 1. Kırşehir Block, 2. pre-Neogene units, 3. İncik Formation (Ti), 4. Altıntaş (Ta) Formation, 5. Hancılı (Tha) Formation, 6. Çandır Formation (Tç), 7. Süleymanlı (Ts) and Bozkır (Tb) formations. 8. thrust/reverse faults, 9. normal faults, 10. transpressional faults, 11. compression direction, 12. extension direction, 13. strike-slip faults, 14. sinistral component of oblique-slip faults in cross-sections.

7. The Bozkır Formation is latest-Late Miocene (Messinian) to Pliocene age and is characterized by thick evaporites.

8. The Deyim Formation is Late Pliocene (Gelasian) to Early Quaternary age and is characterized mainly by fluvial clastics.

II. Two different tectonic regimes were recognized in the Neogene:

1. The earlier regime commenced in the Burdigalian and is characterized by extensional deformation in which the Kılçak, Altıntaş, Hancılı, and Çandır formations were deposited.

2. The second regime is characterized by regional transcurrent tectonics and commenced in Tortonian (ca. 9.7 Ma). In this phase, the Tuğlu, Süleymanlı, Bozkır and Deyim formations were deposited.

3. In the latest tectonic regime early-formed structures, both in the Hancılı and in the Çankırı Basins were inverted into transpressive faults.

4. The latest tectonic regime in the Çankırı Basin is kinematically related to the same regime that resulted in the development of the North Anatolian Fault Zone and which is still active.
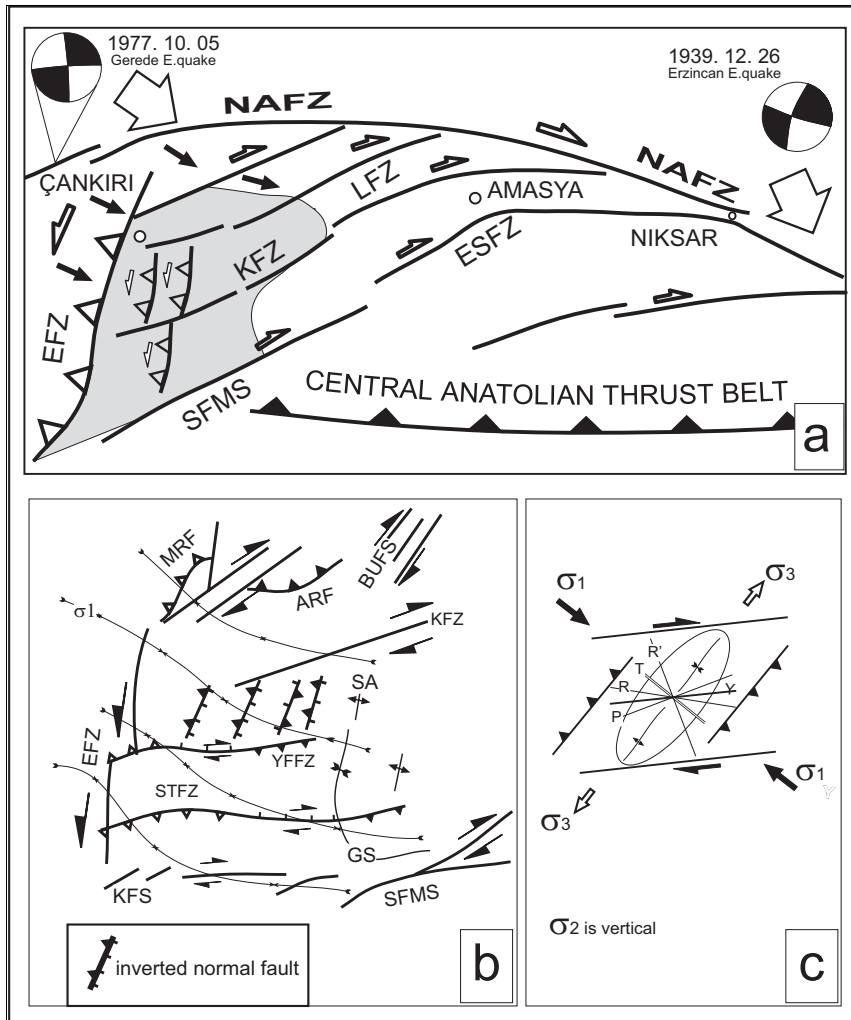
125

Figure 4.24 Simplified tectonic map of the active faults in the north central Turkey. ESFZ: Ezinepazarı-Sungurlu Fault Zone, KFZ: Kızılırmak Fault Zone, LFZ: Laçin Fault Zone, NAFZ: North Anatolian Fault Zone, SFMS: Master Strand of the Sungurlu Fault Zone. Large arrows are the horizontal components of the compression directions obtained from fault plane solutions of the Gerede and Erzincan Earthquakes (partly modified after Barka and Hancock 1984, Õzçelik 1994, Kaymakci and Koçyiğit 1995, fault plane solutions are after Jackson and McKenzie 1984). b) Simplified structural map of the Çankırı Basin area. ARF: Ayseki reverse fault, BUFS: Bűrtű Fault Set, EFZ: Eldivan fault Zone, GS: Gűvendik Syncline, KFS: Kırıkkale Fault Set, MRF: Merzi Reverse Fault, STF: Sivritepe Fault Zone, YFFZ: Yağbasan-Faraşlı Fault Zone. Note transpressional and transtensional segments of the STFZ and YFFZ as the faults change their strike. c) Riedel pattern of deformation proposed for the structures developed in the latest phase of deformation (Tortonian to Recent) in the Çankırı Basin area.

5

PALEOSTRESS INVERSION IN A MULTI-PHASE DEFORMED AREA: KINEMATIC EVOLUTION OF THE ÇANKIRI BASIN (Central Anatolia, Turkey), Part I:

The Northern Area

Abstract

The kinematic and structural evolution of the major structures effecting the Çankırı Basin, Central Turkey has been deduced from a paleostress inversion study. Four paleostress tensor configurations indicative of a four-phase structural evolution have been constructed from fault slip data collected from the Çankırı Basin. The first two phases indicate the dominant role of thrusting and folding and are attributed to the collision between the Pontides and the Taurides, the proposed interface of which is straddled by the Çankırı Basin. Phase-1 occurred in the pre-Late Paleocene, Phase-2 occurred in the Late Paleocene to pre-Burdigalian. The third phase is dominated by extensional deformation in the Middle Miocene. The fourth and latest phase has been active since the Tortonian and is characterized by regional transcurrent tectonics.

5.1. Introduction

Paleostress analysis is the estimation of the principal stress orientations using fault slip data that is obtained by field measurements of the orientations of populations of fault planes together with slip data. Slip directions are generally inferred from the orientations of frictional grooves or fibrous lineations, termed slickenlines (Fleuty 1974, Doblas 1998). However, they can also be deduced from focal mechanism of earthquakes (Angelier, 1984, Gephart and Forsyth, 1984, Carey-Gailhardis and Mercier, 1989) and from the orientations of mechanical twins in calcite (Lacombe et al., 1990, 1992).

A number of methods have been developed for the paleostress inversion and the separation of stress tensors in multi-phase deformation situations, following initial graphical and numerical methods of Arthaud (1969) and Carey and Brunier (1974) respectively. Graphical methods have been further developed by Alexandrowski (1985) (modified M-Plane Method) and Krantz (1988) (Odd-Axis Method). However, they are only applicable if special conditions are fulfilled. For instance, the faults to be analyzed using the M-Plane Method should have developed under uniaxial stress conditions in which two of the principal stress magnitudes are equal and are manifest, in plan view, in a radial or concentric pattern of faults. The Odd Axis Method is applicable in triaxial strain conditions where two pairs of conjugate fault sets develop and display orthorhombic symmetry. On the other hand, numerical methods are more robust and have been more widely used (for example see Angelier 1979, 1984, 1994, Etchecopar et al. 1981, Angelier et al. 1982, Armijo et al. 1982, Gephart and Forsyth 1984, Michael 1984, Carey-Gailhardis and Mercier. 1987, Reches 1987, Hardcastle 1989, Gephart 1990, Marret and Almandinger 1990, Will and Powell, 1991, Yin and Ranalli 1993, Nieto-Samaniego and Alaniz-Alvarez 1997).

All numerical methods are based on the Wallace (1951)-Bott (1959) assumption which is that slip occurs parallel to the maximum resolved shear stress and is also presumed to be parallel to the slickenline direction. A further assumption is that a given tectonic event is characterized by one regional homogeneous stress field. This implies that the slip direction on a fault plane is determined by a single stress deviator and that all faults which slipped during one tectonic event moved independently but in a way consistent with this single stress deviator (Will and Powell 1991). After determining the stress tensor with respect to operative fault planes, it is transformed to a regional co-ordinate system using standard computational transformations (Means, 1976, Angelier, 1994).

The assumptions, upon which the numerical methods are based, are an over simplification of the situation encountered in the field. Inhomogeneity and anisotropic material properties, fault interactions especially in strike-slip settings, presence of rotational deformation, and the non coaxial stress and strains (monoclinic or triclinic symmetry of Twiss and Unruh, 1998) can either cause local variations in the stress field or a very high deviation between the maximum resolved shear stress and the slip direction (Pollard et al., 1993). This decreases the reliability of the stress inversion procedure and makes the identification of different deformation phases

128

more difficult, but is helped if constrained by stratigraphic controls and by overprinting and cross-cutting relationships (Nemcok and Lisle 1995, Hardcastle 1989, Angelier 1994).

Fault reactivation is another source of difficulty as not all inversion procedures can cope with it. For example Angelier's (1979,1984) method is best suited for reactivated systems. But it has limitations because faults with pure dip slip and strike-slip components yield unreliable results because the intermediate stress will be perpendicular to the slip direction and it will have no effect on the inversion procedure (see Angelier 1994 for the details).

Although, the basic assumptions underlying stress inversion procedures have been criticized (e.g. Pollard et al., 1993, Twiss and Unruh, 1998), empirical observations and theoretical analyses (e.g. Dupin, et al. 1993) show that the shear stress vectors and the slip vectors on a single isolated fault plane vary little in orientation from the predicted, namely the average slip remains parallel to the average shear stress, thus agreeing with the Wallace-Bott assumption (Angelier, 1994). Stress inversion techniques have been applied to fault slip data from a variety of tectonic settings and have produced results that are consistent and interpretable (Pollard et al. 1993).

The aim of this study is to use paleostress inversion procedure to delineate the kinematic evolution of faults and related structures within the northern part of the Çankırı Basin with respect to its structural and tectonic evolution.

5.1.1 Background

The Çankırı Basin (Figure 5.01) is thought to be located in a zone where the Sakarya Continent of the Pontides and the Kırşehír Block of the Taurides collided and sutured along the Izmir-Ankara-Erzincan Suture Zone (IAESZ) which demarcates the former position of the northern branch of Neotethys (Şengőr and Yılmaz, 1981). The timing of collision is under debate. Okay (1984) argued that it occurred at the end of the Late Cretaceous. Şengőr and Yılmaz (1981) when reviewing the plate–tectonic evolution of Turkey from Precambrian to present, proposed a Late Paleocene to Middle Eocene age for the timing of the collision. Gőrűr et al. (1984) proposed a Middle Eocene origin based on their study in Tuzgőlű (Salt Lake) Basin which is located in the western margin of the Kırşehir Block and is thought to have similar stratigraphical and evolutionary history to the Çankırı Basin (Figure 5.01). It is possible that these different dates reflect a diachronous collision which may be due to irregularities at the promontories of the colliding blocks or oblique collision (Dewey, 1977)

Besides being affected by collisionary process, the Çankırı Basin was subjected to further deformation in the post-Middle Miocene being a part of the Anatolian wedge caught between the expulsive transcurrent motions on the North and East Anatolian Faults (Figure 5.01d). This has resulted a number of northwards convex dextral strike-slip faults, which bifurcate from the North Anatolian Fault Zone (Barka and Hancock 1984, Şengör et al. 1985, Kaymakcı and Koçyiğit 1995). The Kızılırmak and the Sungurlu Fault Zones are the two major splays of the NAFZ, which partly controlled the Late Miocene evolution of the Çankırı Basin (Figures 5.01d and 5.02).
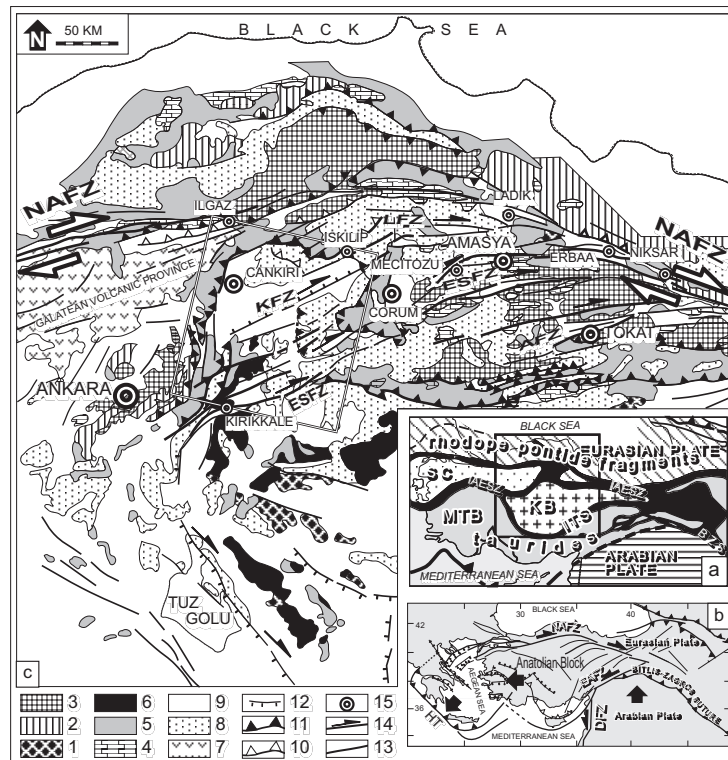
129

Figure 5.01 a) Inset map showing the geological outline of the Eastern Mediterranean area (Modified after Şengőr et al. 1984). BSZ: Bitlis-Zagros Suture, IAESZ: Izmir-Ankara-Erzincan Suture Zone, ITS: Intra-Tauride Suture, KB: Kırşehir Block, MTB: Menderes-Taurus Block, SC: Sakarya Continent. b) Active tectonic outline of Turkey and surrounding regions. DFZ: Dead Sea Fault Zone, EAFZ: East Anatolian Fault Zone, HT: Hellenic Trench, NAFZ: North Anatolian Fault Zone. Large black arrows are the movement directions of Arabian plate and Aegean-Anatolian Block (modified after Barka and Hancock 1984, Gőrűr et al. 1984, Őzçelik 1994, Kaymakci and Koçyiğit 1995). c) Detailed tectono-stratigraphical map of the central Anatolia. Box shows the location of the study area. AFZ: Almus Fault Zone, ESFZ: Ezinepazari-Sungurlu Fault Zone, KFZ: Kızılırmak Fault Zone, LFZ: Laçin Fault Zone, NAFZ: North Anatolian Fault Zone, YFFZ: Yağbasan-Faraşlı Fault Zone. 1. Pre-Late Cretaceous metamorphic basement of the Kırşehir Block, 2. Pre-Jurassic metamorphic basement of the Sakarya Continent, 3. Triassic Karakaya Complex, 4. Jurassic-Cretaceous platform carbonates on the Sakarya Continent, 5. Late Cretaceous (?) ophiolites and ophiolitic melanges, 6. Pre-Paleocene Granitoids of the Kırşehir Block, 7. Galatean Volcanic Province (GVP, Toprak et al. 1996), 8. Early Tertiary units (mainly marine), 9. Neogene and Quaternary Cover, 10. reverse faults, 11. thrust faults, 12. normal faults, 13. faults with unknown sense of movement,, 14. active strike-slip faults. 15. major towns.
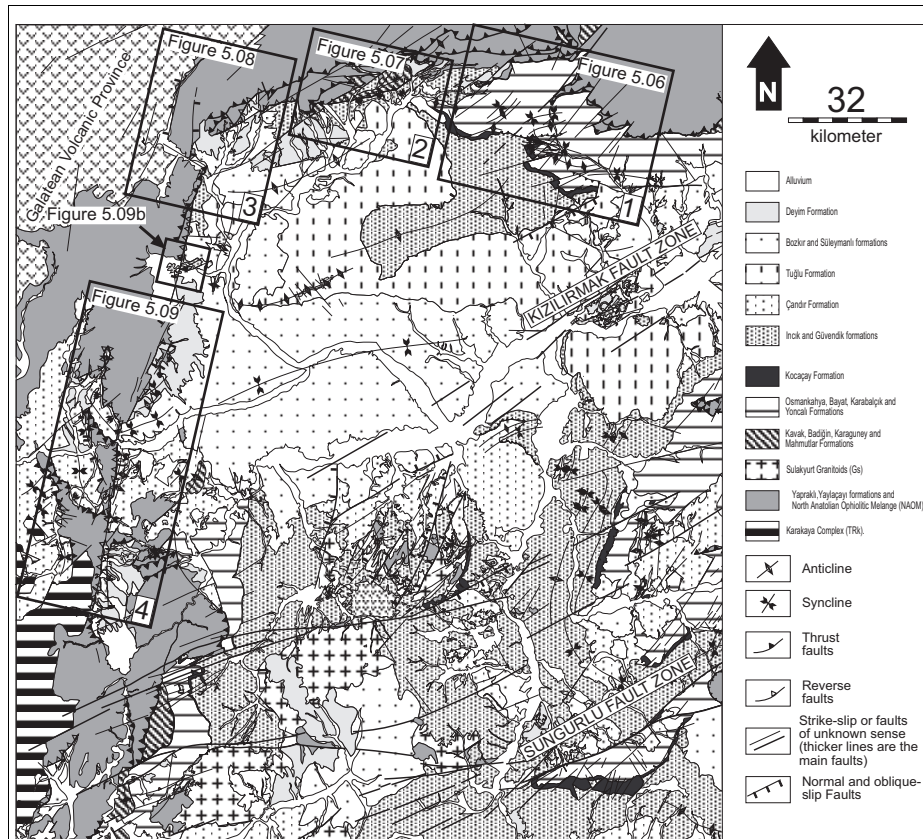
130

Figure 5.02 Geological map of the Çankırı Basin. The numbers 1-4 are the locations of the sub-areas.

5.1.2 Geological Setting

The Çankırı Basin has a Ω shape (Figure 5.01b) with the main outcrops lying in the west, north and east. In the south it is delineated by the granitoids of the Kırşehir Block of the Taurides (Figure 5.01). The rim to the Çankırı Basin is marked by an ophiolitic melange, the North Anatolian Ophiolitic Melange (NAOM, terminology after Rojay, 1993, 1995). This is thought to underlie the sedimentary in-fill of the Çankırı Basin. The basement to the melange is thought to be the Kırşehir Block to the southern part but is unknown in the north. That is, the IAESZ may lie below the Çankırı Basin rather than skirting around its northern margin as indicated in Figure 5.01.
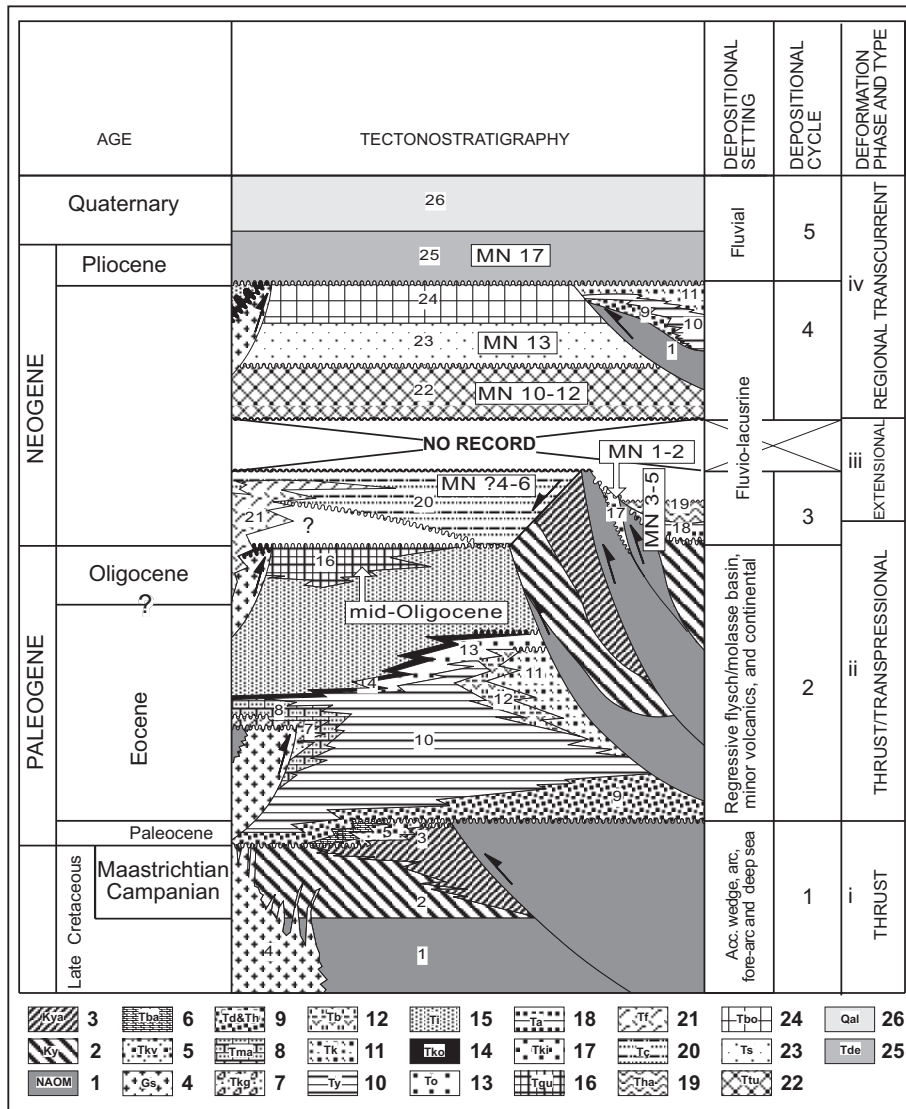
131

Figure 5.03 Generalized tectono-stratigraphic column of the units exposed in and around the Çankırı Basin. For the detailed description of the units and the MN zones in the age column see chapters 3 and 4.

132

1. North Anatolian Ophiolitic Melange-NAOM (ophiolitic melange), 2. Yaylaçayı Formation (distal fore-arc sequence), 3. Yapraklı Formation (proximal fore-arc facies), 4. Sulakyurt Granitoids of the Kırşehir Block (intruded in pre-Paleocene), 5. Kavak formation (red clastics and carbonates), 6. Badiğin formation (neritic limestones), 7. Karagűney Formation (clastics derived mainly from the Kırşehir Block) 8. Mahmatlar Formation (clastics derived from Sulakyurt Granite), 9. Dizilitaşlar and Hacıhalil Formations (mainly turbiditic clastics and intercalated limestones), 10. Yoncalı Formation (Eocene flysch), 11. Karabalçık Formation (distributary channel conglomerates and sandstones with coal seams), 12. Bayat Formation (Eocene volcanics and volcanoclastics), 13. Osmankahya Formation (mixed environment clastics and red beds), 14. Kocaçay Formation (Middle Eocene nummulitic limestone covering both basin in-fill and the Sulakyurt Granitoids), 15. İncik Formation (Late Eocene to Oligocene continental red clastics), 16. Gűvendik formation (Oligocene evaporites), 17. Kılçak Formation (fluvio-lacustrine clastics exposed only in the Kalecik sector of the of the Çankırı Basin (see Figure 5.02), 18. Altıntaş Formation (fluvial red clastics exposed only in the Hancılı Basin), 19. Hancılı Formation (Lacustrine deposits exposed only in the Hancılı Basin, 20. Çandır Formation, 21. Faraşlı Basalt (interlayed within the Çandır Formation), 22. Tuğlu formation (early-Late Miocene evaporites and Lacustrine shale/marl), 23, Sűleymanlı formation (fluvio-lacustrine red clastics), 24. Bozkır Formation (evaporites), 25. Deyim Formation (fluvial clastics), 26. Alluvium.

The fill of the Çankırı Basin is more than 4km thick and accumulated in 5 different cycles of sedimentation (Figure 5.03). The oldest cycle comprises the Late Cretaceous volcanoclastics and regressive shallow marine units and the Paleocene mixed environment red clastics and carbonates (Özçelik 1994). The subsequent cycles have been partly studied by Dellaloğlu et al. (1992) and their scheme is followed in this study. The second cycle is a Late Paleocene to mid-Oligocene regressive flysch to molasse sequence overlain by a widespread thin (<100m) nummulitic limestone of Middle Eocene age which passed into a very thick (up to 2000m) Late Eocene to mid-Oligocene continental red clastics intercalated and overlain by mid-Oligocene evaporates. The third cycle is represented by fluvio-lacustrine clastics deposited in the Early to Middle Miocene. The fourth cycle is represented by the deposits that were deposited in the Late Miocene fluvio-lacustrine conditions and are frequently alternating with evaporates. The Plio-Quaternary alluvial fan deposits and recent alluvium locally overlay all of these units (Figure 5.03). Names of the formal units are mostly adopted after Dellaloğlu et al. (1992).

The main structures shaping the current geometry of the Çankırı Basin (Figure 5.02) are the transpressional and thrust faults defining the western and northern rims of the Çankırı Basin. The eastern margin is defined by a belt of diffuse NNE striking folds. In the south, the basin in-fill onlaps on to the Kırşehir Block. The other major structures affecting the Çankırı Basin are the dextral Kızılırmak Fault zone oriented SW-NE in the central, and the Sungurlu Fault zone in the SE part, of the basin. Both are regarded as splays of the NAFZ (Figure 5.01). The southern part of the central area of the basin is dominated by a number of curvilinear faults oriented circa NE-SW (Figure 5.03).

5.2 Methodology

5.2.1 Data Collection

The relative ordering of fault motions and related deformation was established from overprinting and cross-cutting relations. The age constraints were applied through the careful documentation and analysis of the fault structures in each of the above stratigraphical horizons. To avoid problems due to relative block and fault plane interactions (see Pollard et al. 1993 and Twiss and Unruh 1998) sampling sites were as small as possible and structurally homogeneous (Hancock, 1985).In addition, the displacement should also be as little as possible (few cm) so that it should not accommodate significant strain (Hardcastle, 1989) and therefore the principal strain and stress axes should remain parallel.

Most of the Early Tertiary in-fill of the Çankırı Basin is only exposed in the three belts forming the western, northern and eastern rim of the basin (Figure 5.01). The central parts of the basin are covered mainly by evaporates that are very susceptible to gravity induced ductile deformation and were not included in the analysis. As a result, the study was limited to the northern and western margins, which forms a convex arcuate belt (see Figure 5.01). Four sub-areas were selected for detailed study. Selection of sub-areas was based on the structural trends and pattern of exposed stratigraphic units (Figure 5.02). Two of the sub-areas lie in the northern margin of the basin. In the sub-area 1 (1 in Figure 5.02) the in-fill of the basin is well exposed and the boundary is affected by dextral NE trending transcurrent faults (Figure 5.02). The second sub-area (2 in Figure 5.02) is dominated by the anastomosing ENE trending thrust faults. In addition, in this area, the Late Cretaceous to Paleocene units are better-exposed than in any other part of the basin. The third sub-area lies in the area where the rim of the Çankırı Basin changes from an overall E-W trend to a N-S one (3 in Figure 5.02). In this sub-area, the basin units are post-Middle Eocene in age. The fourth sub-area (4 in Figure 5.02) covers the western margin of the basin. It also covers the Neogene Hancılı Basin. In this area, mainly the Late Cretaceous units and the Miocene to recent units are exposed; the Early Tertiary units are missing or not exposed.

In order to have structurally homogeneous data (Hancock 1985), the size of a sampling site was kept to less than 50m diameter. The areas larger than this were subdivided into sub sites and analyzed independently. More than 600 slickenline data from 72 sites have been collected. For each fault measured in the field, the following features were noted: 1) the attitude of the plane, 2) the stratigraphic units which were displaced, 3) whenever possible, the relative order of movement, 4) amount of off-set, 5) type of the slickenline, 6) type of the shear sense indicators, 7) evidence of ductility (i.e. breccia versus mylonite), and 8) degree of planarity. Each was given a confidence value 1 to 4 (excellent to poor) (as explained in Hardcastle, 1989). If no movement sense could be deduced, the fault was not used in the analyses, which happened to circa 20% of the data.

5.2.2 Stress Inversion Procedure and Separation of Movement Phases

It was found that most of the measured faults have undergone reactivation as seen from overprinting kinematic indicators which subsequently were used to order the different phases

of movement (Figure 5.04). The maximum number of slickenline overprinting and/or overgrowth patterns observed in any fault plane was 3, which was encountered in 10% of the faults, ~25% of them have 2 overprinting sets.
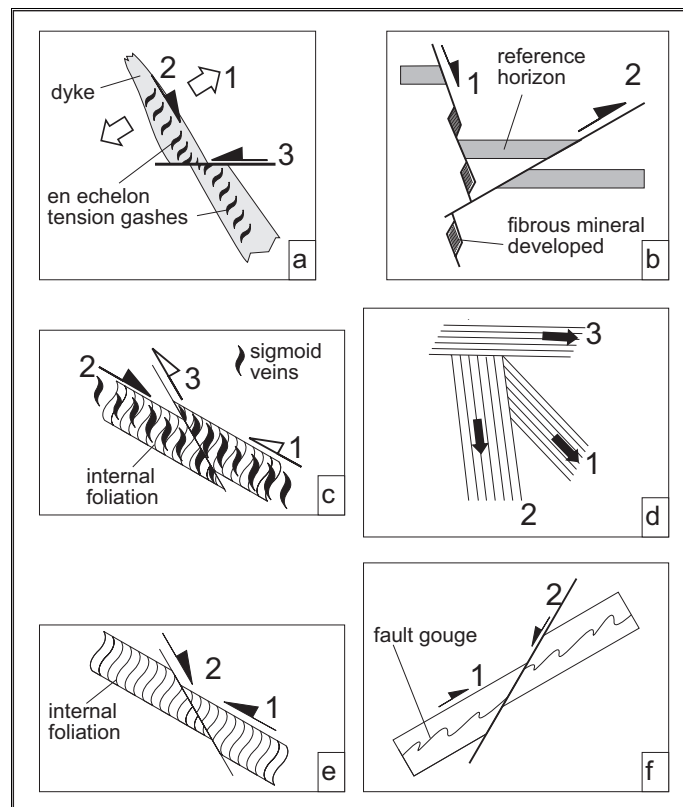

Figure 5.04 Schematic illustrations of criteria used to temporally order relative occurrences of slip data. Numbers indicates the sequence of deformation, 1st oldest 3rd youngest. a) A dyke indicating extension (1) (large opposite arrows), then tension veins indicating dextral movement (2), all displaced sinistrally (3). b) Hybrid joints with fibrous mineral development in dilational jogs having normal displacement (1) are displaced by reverse faults (2). c) Internal foliation within the shear zones with reverse movement (1) sigmoidal veins indicating an opposite sense of movement (2) are then displaced by a reverse fault (3). d) Cross-cutting slickenlines. e) Shear zone with internal foliation indicating a reverse movement (1) displaced by a fault with a normal sense of movement (2), f) folded fault gouge with reverse sense of movement displaced by a fault of opposite sense of movement. The numbers are relative to each other and do not necessarily correspond to the order of the regional deformation phases.

135

Relative age of each movement phase was determined independently for each fault from a given sub-area and carefully correlated with data from other sub-areas to form a regional sub set and then processed (see Figure 5.05) by Angelier's Method (1989) using his computational procedures. During the analyses, the data were carefully examined and data from each site were correlated to that from other sites in a sub-area such that the slip data which have same order of occurrence could be grouped together for preliminary stress inversion processing (see flowchart in Figure 5.05 for the steps followed in the stress inversion procedure). The computational procedures are namely *Direct Inversion* (INVD), *Right Dihedra* (P and T-Dihedra) and *Iterative methods*, (R4DT, R4DS, R2DT, R2DS). These procedures are based on the concept of '*reduced stress tensor*' in which the ratio (Φ) together with the orientations of the fault planes and the slickenlines are used. The ratio Φ is defined as the ratio between the differences of the magnitudes of the principal stresses ($\Phi=(\sigma2-\sigma3)/(\sigma1-\sigma3)$).Therefore, Φ ranges between 0 to 1 and defines the shape of the stress ellipsoid. (see Angelier 1994, for an overview of the stress inversion procedure).

After preliminary processing, faults giving spurious results were re-examined. If they still remained spurious they were separated from the data set and treated separately. After removal of spurious data, the stress tensor was re-computed and re-analyzed using the software developed by Hardcastle and Hills (1991) for the automated separation of stress tensors associated with the different deformation phases as indicated from the field observations. Concordant data were then taken as indicating that the computed stress tensor is most likely to be correct. The initial spurious data were re-computed by the Hardcastle and Hills (1991) method and if again spurious they were deleted. If concordant they were included and re-analyzed.

In order to determine the mean stress tensor configuration for a given movement phase in each sub-area, all the data from each site and each phase were grouped and above procedure repeated. After the mean stress orientations were determined, all of the raw data was re-processed using the Hardcastle and Hills (1991) approach and the results were compared with those obtained using the direct inversion method. Because, the minimum number of slickenline data required to construct a stress tensor is 4 in the direct inversion method (Angelier 1979), the data of sites containing less than this number was used only in the construction of mean stress tensor for the sub-area within which it was located.

After the stress tensors for each set at each site had been determined, they were correlated between sites. By combining the stratigraphic information and the relative order of the different sets, the stress tensors were arranged into ordered deformation phases.

In both the direct inversion and the Hardcastle-Hills methods, 15° was chosen as the maximum angular deviation acceptable for the computation of a given stress tensor. Faults with greater angular deviations were considered to be spurious and deleted.

The tensors computed for a sub-area should be more reliable than site based tensors. The reasons for this are obvious but include deviations due to a particular site being located at the termination of a fault or in an area where two or more structures interact. Both will cause a

136

deviation of the local stress tensor from the regional tensor (Pollard *et al*. 1993) and will tend to cancel out in the regional compilation (Angelier 1994).
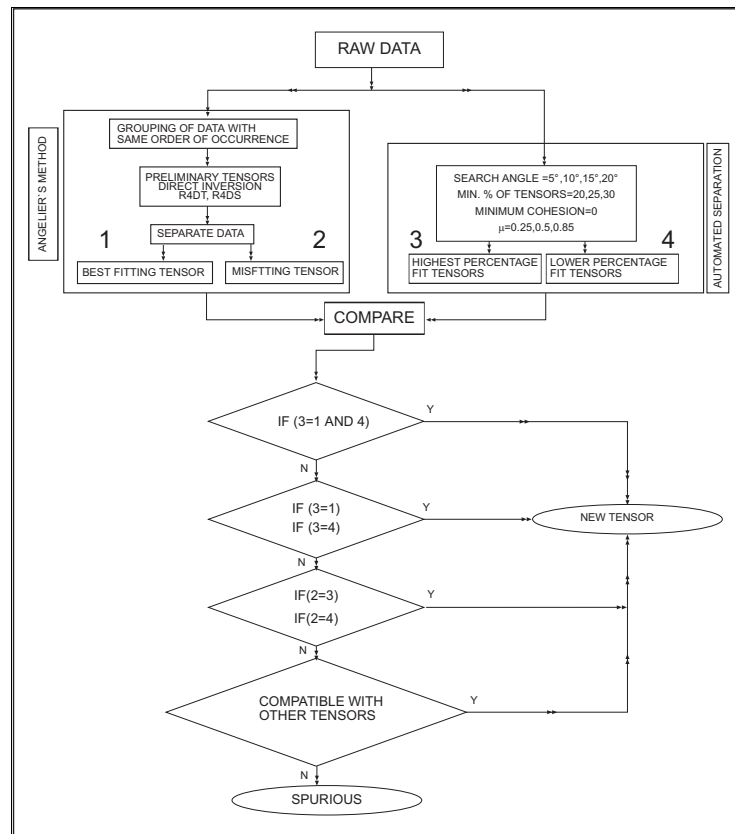

Figure 5.05 A flowchart of steps followed during the analysis of the data. The data was analyzed independently using two different methods then they were compared. After determination of the tensors and separation of the data into best fitting and tensor of miss-fitting faults, the results were compared with the automated method. If best-fitting and miss-fitting tensors of Angelier`s method fall within the highest percent fit tensors of automated method, each subset is ascribed into two separate acceptable tensors. If not, and if they fall within the lower percentage fit tensors, then further analysis was carried out until reasonable and acceptable tensors were obtained (lowest miss-fit angles that was less than 15° was obtained for all the groups. Only faults with more than 45° were accepted spurious (less than 2% of whole data). This process is repeated for each class of structures (number of relative chronology) for each phase and for determining mean regional (sub-area based) stress tensor configurations.

5.3 Results

5.3.1 Sub-area 1

The location of Sub-area 1 is shown in Figure 5.02. The main structures in this area are the ENE trending thrust faults (TF1) along which the Late Cretaceous North Anatolian Ophiolitic Melange (NAOM) was thrust over the Yaylaçayı Formation and which in turn was thrust onto the Late Paleocene to Middle Eocene Yoncalı and Karabalcık formations (Figure 5.06a). Relatively the oldest slip data which can be ascribed to the first movement of TF1 include slickenline pitches with dominant thrust fault character (>45°) with a dextral lateral component. This thrust belt is displaced dextrally by a number of later NE-SW oriented strike-slip faults that cut through both the hanging- and foot-wall blocks. Further to the south-west, the Yoncalı Formation is thrusted over the Incik Formation and over the other Late Paleocene to Middle Eocene units namely Karabalçık, Bayat, Osmankahya, and Kocaçay formations along the fault TF3 (Figure 5.06a). A number of syn-depositional unconformities had been observed in the Incik Formation during the field studies (especially near sites 81-82 and 115 in Figure 5.06a) implying that the TF2 (Figure 5.06a) operated during the deposition of the Ti, in the Late Eocene to pre-mid-Oligocene times. The main fault planes of TF-2 and TF-3 are dominated by overprinting slickenlines. Relatively, the oldest of these slickenlines have pitches ranging between 15° to 35° with a sinistral sense of movement. Likewise, the younger slickenlines have pitches less than 20° with a dextral sense of movement. These relations indicate that TF-2 and TF-3 were developed as transpressional sinistral strike-slip faults and later they were reactivated as dextral strike-slip faults.

5.3.1.1 Paleostress Inversion

Eight sites were selected (see Table 1) and from the field analyses, four phases of fault activity were recognized using the criteria outlined in Figure 5.04. In some of the sites (62,63,64) the sampled faults have 3 sets of overprinting slickenlines. These faults in turn crosscut other structures such as shear zones, *en echelon* veins and other sets of faults (as indicated in Figure 5.04), A combination of all of these relationships led to the identification of sets of 4 fault movements. Based on their relative timing, the sets of faults having similar movements were directly assigned to the deformation phases arranged from older to younger (Nemcok and Lisle 1995). These sites were used as a reference in the analysis of other sites that have fewer sets of fault movements.

From the 18 sites sampled, 12 sites have sufficient slip data for the construction of site based paleostress tensors (Figure 5.06b-e). From these sites 19 paleostress configurations have been constructed. The data from the remaining 6 sites were combined in constructing the mean stress tensor for the whole sub-area (see Figure 5.06f-i). The results are presented in Figure 5.06.

Phase1: Only four sites had sufficient data for the construction of a site based stress tensor (Figure 5.06b). The results are consistent for all four sites. The average orientations of the principal stresses and stress ratio for the sub-area are σ_1=309°N/07°, σ_2=218°N/06°, σ_3=085°N/81°, and Φ=0.345 (Figure 5.06f). The major stress is NNW-SSE and the minor

138

stress (σ_3) is sub vertical indicating thrust tectonics in this phase. The orientation of σ_1 is approximately perpendicular to the main NE-SW striking segments of TF1 and oblique to the other segments (Figure 5.06a).

Table 5.01. Field characteristics of sites in the sub-area 1. O.P. number of overprinting slickenline sets, C.C. number of crosscutting relationships either with veins, shear zones or with other faults, #MOVE. Number of movement sets encountered in each site. The numbers do not necessarily correspond to the order of deformation phases. S.LINE. Fibrous slickenfibres associated with the sampled faults (SP. Serpentine, Ca. Calcite), K. Late Cretaceous units (NAOM, Ky, Kya), Ty. Yoncalı Formation, To. Osmankahya Formation, Tko. Kocaçay Formation, Ti. İncik Formation +. exists, -. not observed.

SITE	SHEAR	VEIN	O.P.	S.LINE	C.C.	UNIT	#MOVE
60	-	-	2	SP	2	K	2
61	-	-	2	SP	2	K	2
62	-	+	3	SP,Ca	4	K	4
63	+	+	3	SP,Ca	4	K	4
64	+	+	3	SP,Ca	4	K	4
65	-	-	2	-	2	Tb	2
66	+	-	-	-	-	K	1
77	+	+	2	Ca	3	Ty	3
78	+	-	2	-	-	To	2
79	-	+	2	-	2	Tko	2
80	-	+	2	Ca	2	To	2
81	-	+	2	Ca	2	Ti	2
82	-		2	-	2	To	2
115	-	+	2	Ca	2	Ti	2
116	-	+	2	Ca	2	Ti	2
117	-	+	2	Ca	2	Ti	2
118	-	+	-	-	-	Ti	1
119	-	+	2	Ca	2	Ti	3

Phase2: The second phase was also only recognized in 4 sites (Figure 5.06c), which also give comparable results. One site, 64b gives a slight deviation. This site is very close to the intersection of TF1 and a NE-SW trending oblique-slip fault. The deviation may be due to the interaction of these faults (as explained by Pollard et al., 1993). For the sub-area as a whole, both σ_1 and σ_2 are sub horizontal and σ_3 is sub vertical, in all sites and in the sub-area based tensor, indicating thrusting during this deformation phase. The orientation of sub-area based principal stresses and stress ratio are as follows $\sigma_1=065°N/04°$, $\sigma_2=155°N/08°$, $\sigma_3=308°N/81°$ and $\Phi= 0.635$ (Figure 5.06g). The orientation of the σ_1 is almost perpendicular to the NW-SE striking segments of the TF1, TF3, and the NW striking folds east of TF2 fault.
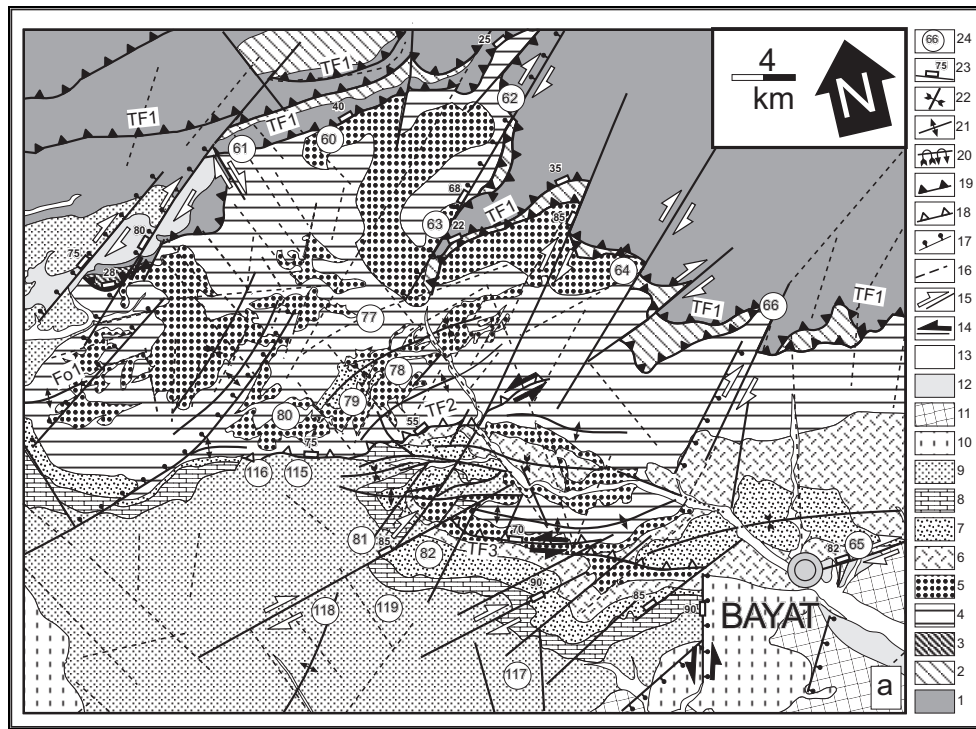
Figure 5.06 a) Geological map and sample location for the sub-area 1. 1. NAOM, 2. Yaylaçayı and Yapraklı formations, 3. Dizilitaşlar Formation. 4. Yoncalı Formation, 5. Karabalçık Formation, 6. Bayat Formation, 7. Osmankahya Formation, 8. Kocaçay Formation, 9. İncik Formation, 10. Tuğlu formation. 11. Sűleymanlı formation, 12. Deyim Formation, 13. Alluvium, 14. faults with sinistral strike-slip sense of movement, 15. faults with dextral strike-slip sense of movement, 16. photo-lineaments, 17. faults with normal sense of movement. 18. reverse faults, 19. thrust faults, 20. overturned folds, 21. anticline, 22. syncline, 23. dip of faults where they are best observed in the field. 24. sample site locations. b-e) Plots of fault planes, slickenlines and stress orientations for each site and whole data in a particular phase and sub-area, (f-i) (lower hemisphere equal area projection).
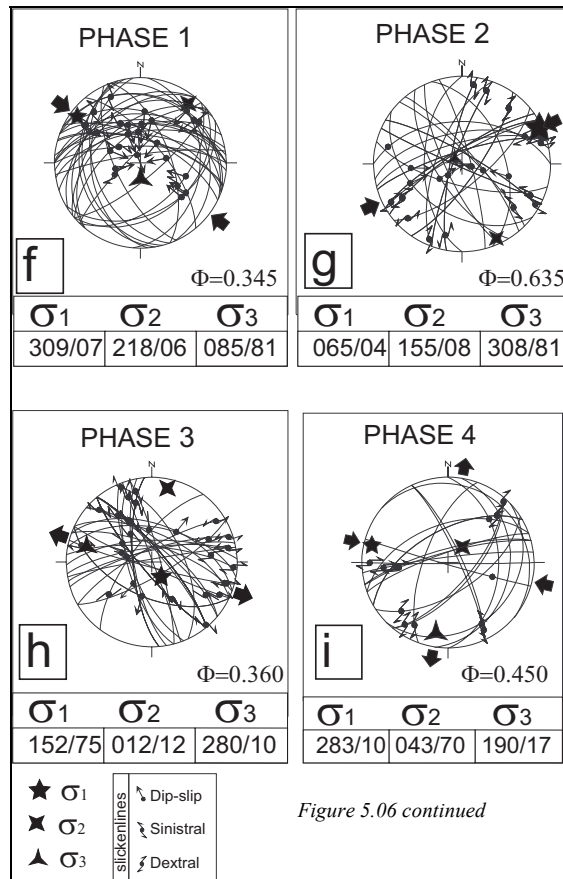
140

Figure 5.06 continued
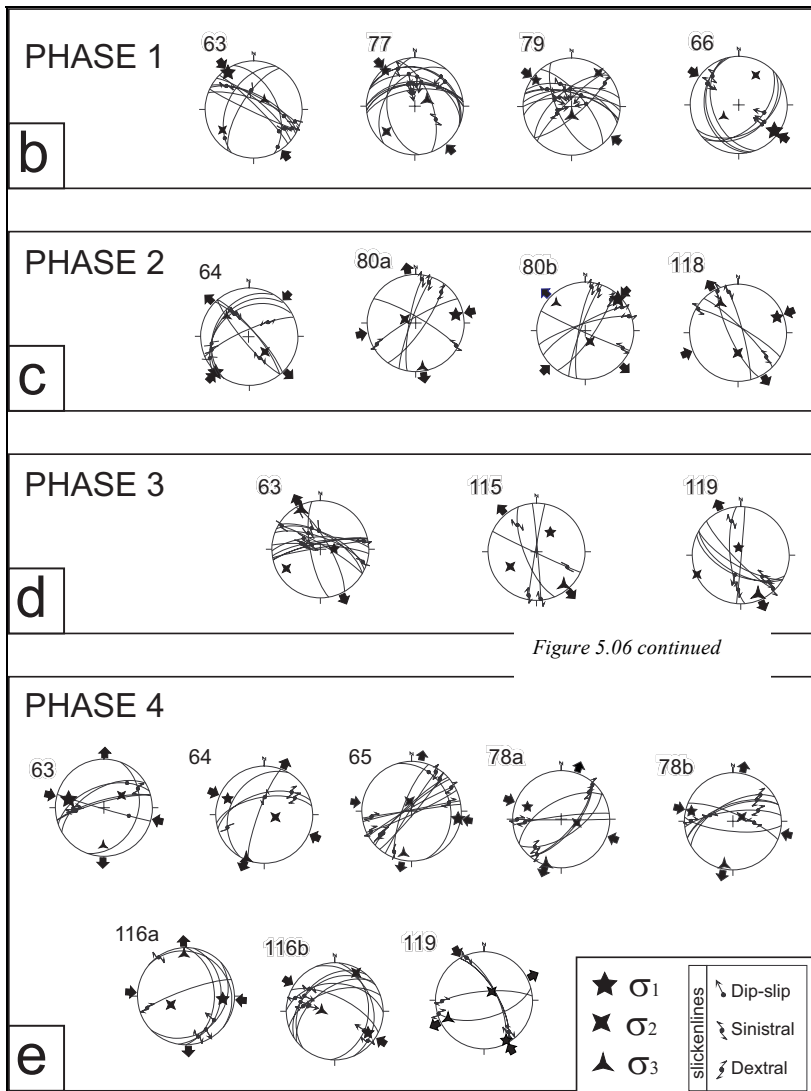
Figure 5.06 continued

Phase3: Three sites had sufficient slip data for the construction of site based stress tensors. The orientations of the principal stresses are relatively consistent between each site (Figure 5.06d). The horizontal components of the σ_3 is oriented NNE-SW. The orientation of sub-area based average stress tensors and stress ratio are as follows: $\sigma_1=152°N/75°$, $\sigma_2=012°N/12°$, $\sigma_3=280°N/10°$ and $\Phi=0.360$ (Figure 5.06h), indicating an extensional deformation in this phase.

Phase4: This phase is recognized in 7 sites (Figure 5.06e). Except for site 119, all the other sites yielded compatible results. The horizontal component of σ_1 is oriented approximately WNW-ESE which is also parallel to the sub-area based stress tensor. The

142

orientations of sub-area based principal stresses and stress ratio are σ_1=283°N/10°, σ_2=043°N/70°, σ_3=190°N/17° and Φ=0.450 (Figure 5.06i), indicating strike-slip deformation in this phase.

5.3.2 Sub-area 2

The location of this sub-area is shown in Figure 5.02. This area is also dominated by NE trending thrust faults. The Late Cretaceous units are thrust over the Paleocene units by TF1 near Badiğin and TF4 to the east (Figure 5.07a). Relatively, the oldest slickenlines observed on the TF4 indicate a dominant thrust fault character with a dextral lateral component of movement. The Paleocene units (Kavak and Badiğin formations, see Figure 5.03) are thrust over the Late Eocene to mid-Oligocene İncik Formation along the Ayseki Reverse Fault (ARF). In the central parts of the sub-area, the Paleocene units, İncik Formation and the Late Miocene units are folded and overturned parallel to the ARF (Figures 5.03 and 5.07a).

In the SE part of the study area, an E-W trending fold (Fo1), which is observed within Eocene to Oligocene units (Ty and Ti) is unconformably overlain by the relatively undisturbed Late Miocene units (op1 in Figure 5.07a).

Near Badiğin village, the TF1 and TF4 faults are displaced by a E-W trending normal fault (NF1) which in turn is displaced by NE-SW trending faults with an apparent sinistral horizontal off-set and with a vertical normal component. These faults also displaced the Late Miocene units (Süleymanlı and Bozkır formations) and the Plio-Quaternary Deyim Formation (Figure 5.07a) which indicate their post-Late Miocene activity..

5.3.2.1 Paleostress Inversion

Four deformation phases were recognized in this sub-area. The same criteria were used for ordering the deformation phases as described in Figure 5.05. The details for sites located in this sub-area are given in Table 2 and results are illustrated in Figure 5.07b-e.

Phase 1: Six sites had sufficient data to construct site based stress tensors for this sub-area. Although, the angular discrepancy between the orientations of the σ_1 constructed for each site and averaged for the sub-area is around 45°, however, there is a great discrepancy between the orientations of σ_2 and σ_3. The orientations of the σ_1 vary from NNW-SSE to WNW-ESE and it is sub horizontal in each site. The σ_2 and σ_3 are oblique, however, σ_3 is more vertical than σ_2 (Figure 5.07b). Orientation of the stresses and the stress ratio for the sub-area are σ_1=208°N/13°, σ_2=285°N/04, σ_3=030°N/70° and Φ=0.412 (Figure 5.07f). Having σ_3 sub vertical and other stresses sub horizontal indicate thrusting during this phase.

Phase 2: Only 4 sites had sufficient data for the construction of the site based stress tensors. The orientation of site and sub-area based tensors is relatively compatible. The orientation of σ_1 range from NNW-SSE to NE-SW (Figure 5.07c). The mean sub-area based principal stresses orientations and stress ratio are as follows σ_1=189°N/14°, σ_2=280°N/04°, σ_3=025°N/75° and and Φ=0.804. The orientation of the σ_1 is perpendicular to Fo1 and indicates compressive deformation (Figure 5.07g).
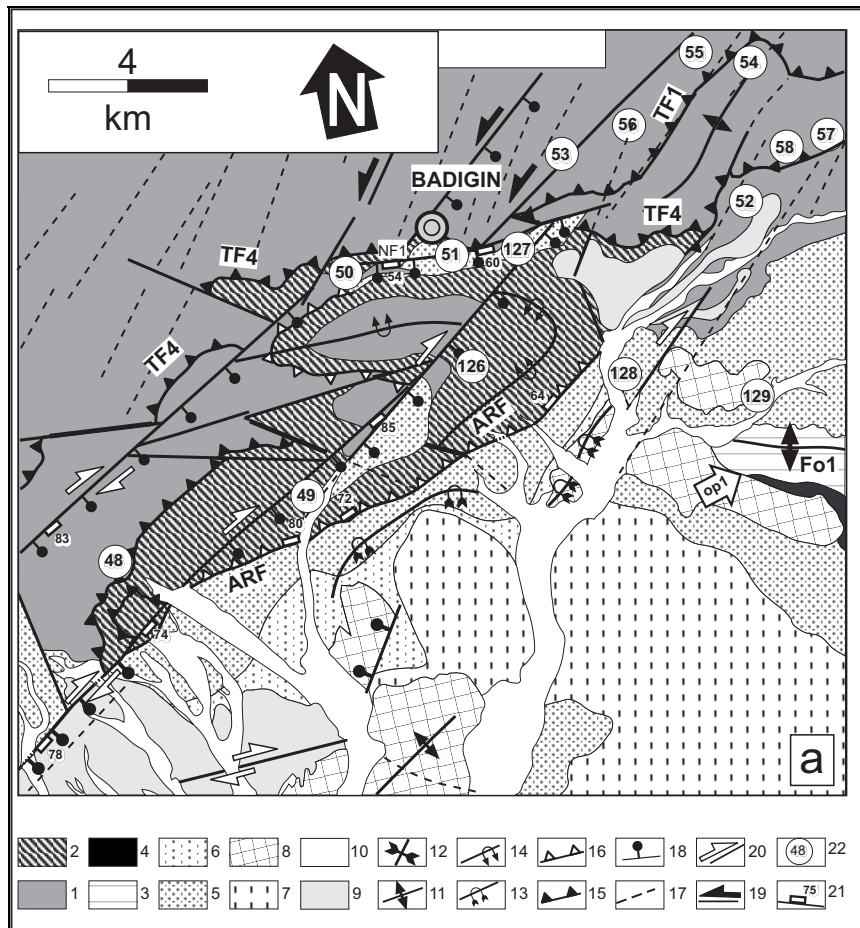
143

Figure 5.07 a) Geological map and sample location for the sub-area 2.1. NAOM, 2. Yapraklı, Kavak and Badiğin formations,3. Yoncalı Formation, 4. Kocaçay Formation, 5. İncik Formation, 6. Çandır Formation. 7. Tuğlu formation, 8. Süleymanlı formation, 9. Deyim Formation, 10. Alluvium, 11. anticline 12. syncline, 13. overturned syncline, 14. overturned anticline, 15. thrust faults, 16. reverse faults, 17. photo-lineaments, 18. faults with normal sense of movement 19. faults with sinistral strike-slip sense of movement, 20. faults with dextral strike-slip sense of movement, 21. dip of faults where they are best observed in the field. 22. sample site locations. Plots of fault planes, slickenlines and stress orientations for each site (b-e) and whole data in a particular phase and sub-area (f-i) (lower hemisphere equal area projection).
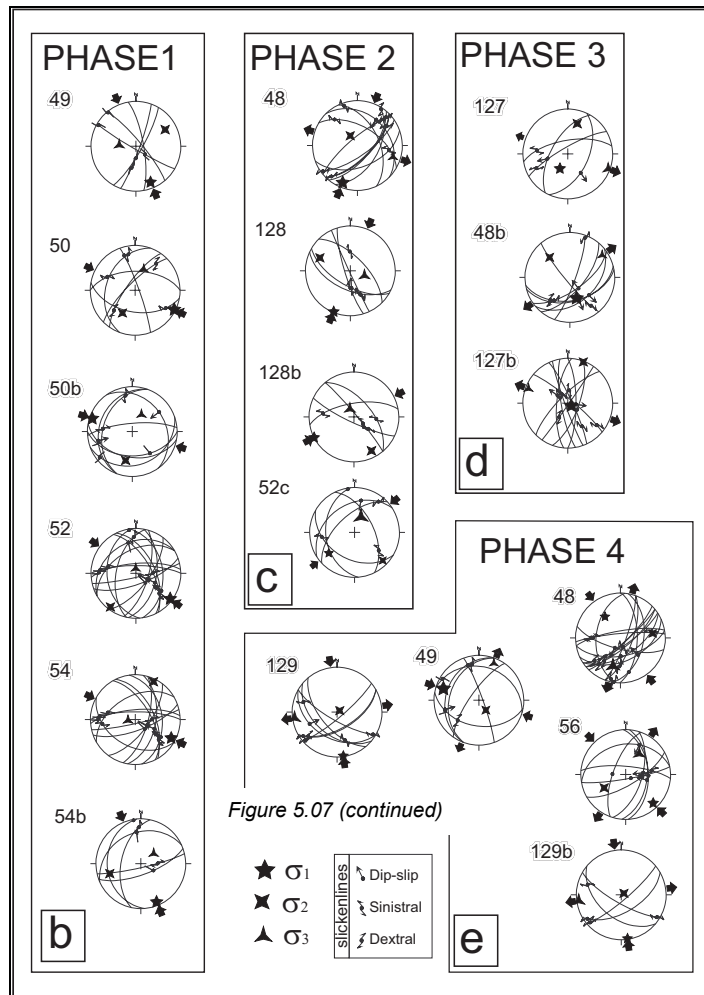
144

Table 5.02. Field characteristics of sites in the sub-area 2. Tkv. Kavak Formation. Other abbreviations are similar to Table 5.01.

SITE	SHEAR	VEIN	O.P.	S.LINE	C.C.	UNIT	#MOVE
48	+	+	2	SP,Ca	4	K	4
49	-	+	2	SP,Ca	2	K	3
50	+	+	2	SP	4	K	4
51	+	-	3	SP,TI	3	K	4
52	+	+	2	SP	2	K	3
53	-	+	-	Ca	2	K	2
54	-	-	3	Ca	3	K	3
55	-	-	2	Ca	2	K	2
56	-	-	-	-	-	K	1
57	-	+	-	Ca	2	K	2
58	-	-	-	-	-	K	1
126	-	-	-	-	-	Ti+Tkv	1
127	-	+	2	Ca	2	Ti+Tkv	2
128	-	-	2	Ca	2	Ti	2
129	-	+	2	Ca	2	Ti	2

Phase 3: Only 3 sites had sufficient slip data for the construction of the site based tensors (Figure 5.07d). In sites 127 and 48, σ_2 is oblique, implying local transtension which is not observed in the sub-area based stress tensor. Only the data from site 48 is compatible with the sub-area based tensor, others deviate from it. This relation may indicate local stress perturbations, for example site 127 is very close to the normal fault NF-1. The orientation of the mean sub-area based principal stresses and stress ratio are; σ_1=213°N/81°, σ_2=350°N/07°, σ_3=080°N/06° and Φ=0.542 (Figure 5.07h). Having σ_1 sub vertical and other stresses sub horizontal indicates an extensional deformation in this phase.

Phase 4: Five sites had sufficient slip data for the construction of site based stress tensors (Figure 5.07e). Almost in all sites, σ_2 is sub vertical and σ_1 ranges between NW-SE to NNW-SSE. This relation indicates strike-slip deformation. The orientation of the sub-area based mean stresses and stress ratio are as follows; σ_1=291°N/03°, σ_2=033°N/83°, σ_3=201°N01° and Φ=0.564 (Figure 5.07i). Having σ_2 vertical and the other stresses as horizontal indicate regional transcurrent deformation during this phase. Most of the thrust and reverse faults and folds trending NE-SW are almost perpendicular to the σ_1. In addition, the folds within the Late Miocene units (near the site 128) are perpendicular to σ_1.

Figure 5.07 (continued)

	PHASE 1			PHASE 2	
f		Φ=0.412	g		Φ=0.804
σ_1	σ_2	σ_3	σ_1	σ_2	σ_3
208/13	285/04	030/70	189/14	280/04	025/75

	PHASE 3			PHASE 4	
h		Φ=0.542	i		Φ=0.564
σ_1	σ_2	σ_3	σ_1	σ_2	σ_3
213/81	350/07	080/06	291/03	033/83	201/01

★ σ_1 ✖ σ_2 ▲ σ_3 slickenlines: Dip-slip, Sinistral, Dextral
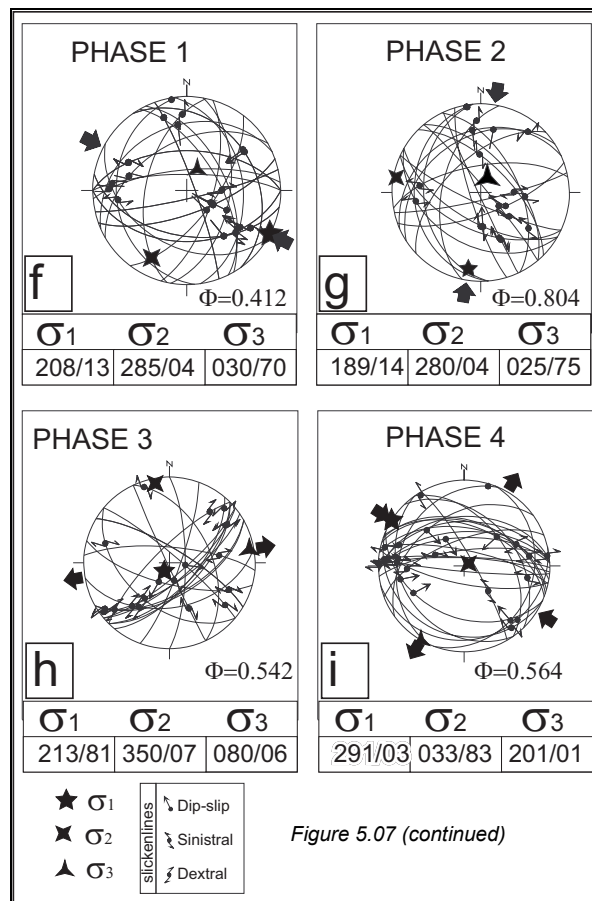
Figure 5.07 (continued)

5.3.3 Sub-area 3

This area is located at the NW corner of the Çankırı Basin (3 in Figure 5.01) where the ophiolitic melange belt (NAOM) and the thrust faults bounding the western margin of the basin change their strike from NNE-SSW to NE-SW. The area in which the sharpest change occurs is hidden below the Plio-Quaternary units (Deyim Formation) (Figures 5.01 and 5.08a). The thrust faults along which the ophiolites and the Late Cretaceous units were thrusted over the Middle Miocene Çandır Formation are covered by the Late Miocene Sűleymanlı and Bozkır formations (op1 and op2 in Figure 5.08a). This relation indicates that thrust activity along the TF4 and 5 took place after the Middle Miocene and prior to the Late Miocene. Along the Merzi

147

Reverse Fault (MRF), the NAOM is thrust over the Late Miocene Sűleymanlı Formation (op3 in Figure 5.08a) and the thrust contact is covered by the Plio-Quaternary Deyim Formation (op 3 and op 4 in Figure 5.08a). The TF5 is displaced by NF2 indicating that two distinct tectonic regimes gave rise to the development of these structures. The first one is thrusting that resulted in the development of TF5 and the second one is an extensional regime, which gave rise to NF2 that is a normal fault with strike-slip component (Figure 5.08a).

In the central eastern part of the sub-area near Çavuşkőy, the post-Middle Eocene İncik Formation was thrusted over the Late Miocene to Pliocene (?) Bozkır Formation along the Çavuşkőy Reverse Fault (ÇF) and the reverse fault contact is covered by the Plio-Quaternary Deyim Formation (op5 in Figure 5.08a) which indicates post-Late Miocene to Pliocene (?) development of the reverse fault. The Deyim Formation, in turn, is displaced by NE-SW trending dextral strike-slip faults (Figure 5.08a).

5.3.3.1 Paleostress Inversion

In this sub-area, like the previous sites, 4 phases of fault movement were observed. These movements were assigned to deformation phases and they were ordered according to their order of occurrence as explained previously (see Figure 5.04). The details of each site is given in Table 3 and the results are presented in Figure 5.08b-e.

Phase 1: Only 4 of the 14 sites had sufficient data for the construction of site based stress tensors (Figure 5.08b). The orientations of the principal stresses are consistent on a site basis and also are consistent with the constructed regional stress tensor (Figure 5.09b). The orientation of the principal stresses and the stress ratio are as follows: $\sigma_1=322°N/02°$, $\sigma_2=052dN/05°$, $\sigma_3=212°N/85°$ and $\Phi=0.413$ (Figure 5.08f) and indicate a compressive deformation. The orientation of σ_1 is almost perpendicular to the trace of TF4 and oblique to the trace of the faults TF5 and NF2.

Phase 2: Only 3 sites had sufficient slip data for the construction of site based stress tensors (Figure 5.08c). The orientation of principal stresses are consistent to each other on the site basis and when averaged for all of the sub-area in which the orientation of the principal stresses and the stress ratio are as follows: $\sigma_1=278°N03°$, $\sigma_2=008°N/03°$, $\sigma_3=142°N/86°$ and $\Phi=512$ (Figure 5.08g) and indicate a compressive deformation. σ_1 is almost perpendicular to faults TF-5 and NF2 and is oblique to faults MRF, TF4 and ÇF.

Phase 3: Only 3 sites had sufficient data for the construction of site based stress tensors. The horizontal component of the σ_3 is consistent for individual sites and with the constructed mean sub-area stress tensor (Figure 5.08d). The orientation of the regional stresses and the stress ratio are $\sigma_1=343°N/51°$, $\sigma_2=206°N/31°$, $\sigma_3=102°N/31°$ and $\Phi=0.401$ (Figure 5.08h). None of the principal stresses are oriented either vertical or horizontal and there are stress permutations (Angelier 1994) between the sites. This relation may indicate the state of the *so called* "tri-axial strain conditions" (Reches 1978a,b) and oblique extension. The orientation of horizontal component of the σ_3 is almost perpendicular to the NF2 and other marked normal faults with sinistral strike-slip component (Figure 5.08a).
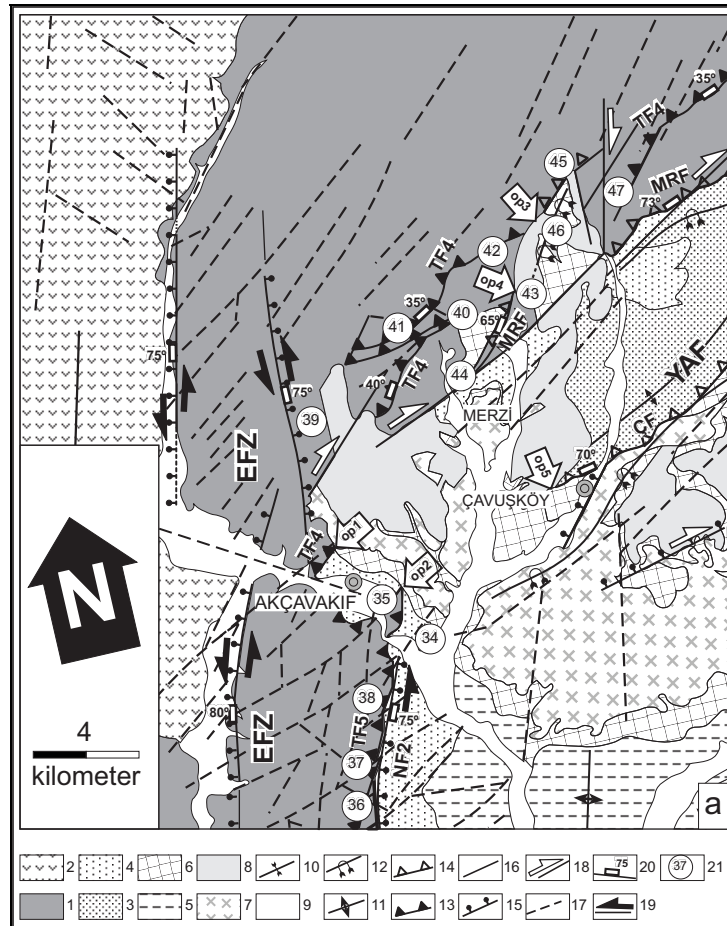
148

Figure 5.08 a) Geological map and sample location for the sub-area 3. EFZ: Eldivan Fault Zone, O.P. observation point (see text)1. NAOM, 2. Galatean Volcanic Province (see Tankut et al. 1995 and Toprak et al. 1996), 3. İncik Formation, 4. Çandır Formation. 5. Tuğlu formation, 6. Sūleymanlı formation, 7.Bozkır Formation, 8 Deyim Formation, 9. Alluvium, 10. syncline, 11. anticline, 12.overturned syncline, 13. thrust faults, 14. reverse faults, 15. faults with normal sense of movement, 16. strike-slip or faults with unknown sense of movement, 17. photo-lineaments, 18. faults with dextral strike-slip sense of movement, 19. faults with sinistral strike-slip sense of movement, 20. Dip of faults where they are best observed in the field. 21. sample site locations. Plots of fault planes, slickenlines and stress orientations for each site (b-e) and whole data in a particular phase and sub-area (f-i) (lower hemisphere equal area projection).

149

Table 5.03. Field characteristics of sites in the sub-area 3. Tç Çandır Formation, other abbreviations are similar to Table 5.01.

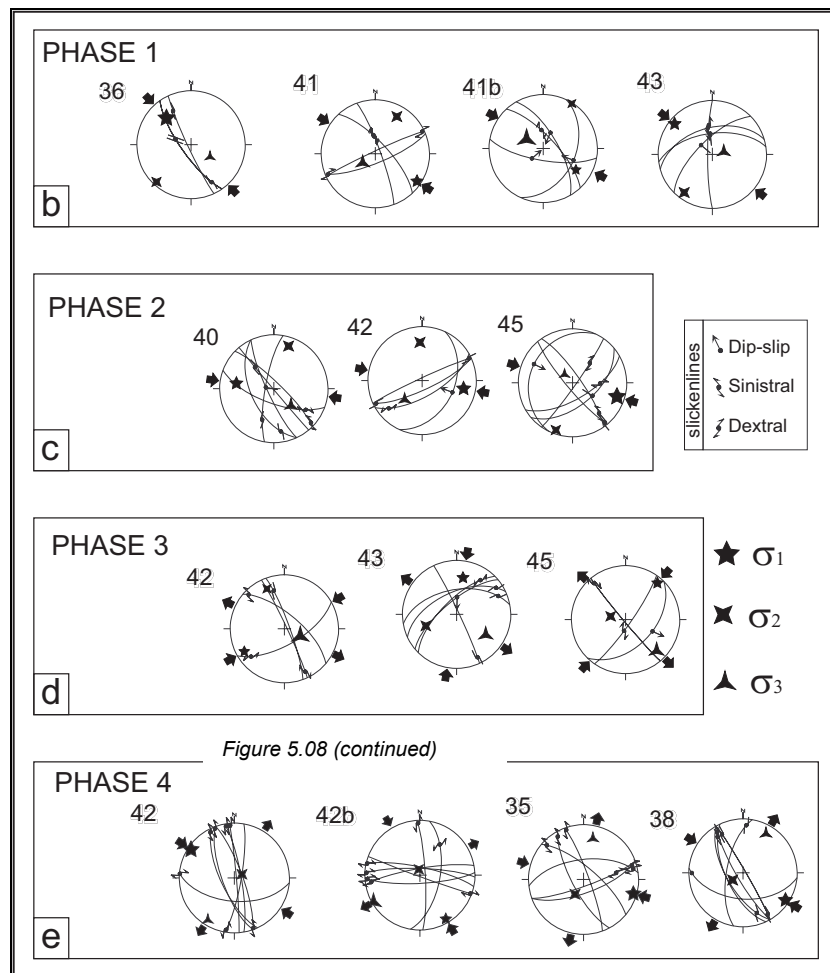| SITE	SHEAR	VEIN	O.P.	S.LINE	C.C.	UNIT	#MOVE
34	-	+	2	Ca	2	Ti	3
35	+	+	2	SP,Ca	2	K	2
36	-	-	2	SP	2	K	2
38	-	-	2	-	2	K	2
39	+	-	-	SP	2	K	2
40	+	-	2	SP	2	K	2
41	-	-	2	SP	2	K	2
42	+	+	2	Ca	2	K	3
43	+	+	3	SP,Ca	3	K	4
44	-	-	-	Ca	-	K	1
45	+	+	-	SP,Ca	2	K	2
46	-	-	-	-	-	K,Tç	1
47	+	+	2	SP	4	K,Tç	4

Phase 4: Four sites had sufficient slip data for the construction of site based stress tensors (Figure 5.08e). The orientation of site based tensors are relatively consistent to each other. In each site σ_2 is sub vertical and horizontal component of the σ_1 ranges between WNW-ESE to NW-SE. The orientations of the sub-area based mean stresses and the stress ratio are as follows: $\sigma_1=293°N/06°$, $\sigma_2=201°N/22°$, $\sigma_3=037°N/68°$ and $\Phi= 0.608$ (Figure 5.08i). The horizontal component of σ_1 is almost perpendicular to faults TF5, NF2 and MRF, and oblique to faults TF4 and ÇF.

5.3.4 Sub-area 4

This area includes the western margin of the Çankırı Basin and extends into the adjacent Hancılı Basin. The latter is separated from the Çankırı Basin by the TF5 and NF2 (Figures 5.02 and 5.09a).

Along TF 5, the Late Cretaceous units are thrust over the Middle Miocene Çandır Formation and the fault contact is covered by the Late Miocene units in the north outside of the Sub-area 4 (op1-3 in Figure 5.09b). Along the TF 6, the Late Cretaceous units are thrust over the Middle Miocene Hancili Formation. Along the faults TF 7 and TF 8 the Late Cretaceous units are thrust over the Early to Middle Miocene Altıntaş and Hancili formations. These units are locally overturned along TF 8. The fault TF 7 is covered by the Plio-Quaternary Deyim Formation indicating pre-Plio-Quaternary activity of the fault. Along the fault TF 9 the Early to Middle Miocene Altıntaş and Hancili formations are thrust over the older Late Cretaceous units. TF 10 is a set of thrust faults developed within the Late Cretaceous

150

and Paleocene units. It is covered by the Plio-Quaternary Deyim formation indicating pre-Plio-Quaternary activity of this fault set (TF 10). Two sets of overprinting slickenlines were developed on the faults formed within the Hancılı Basin (TF 6 to TF 9). The earlier set has an oblique-slip component with a strong normal component (20°-60°). The second (overprinting) set has a dextral transpressional component of movement. This relation reveals that these faults were developed first as oblique-slip transtensional faults with normal component then they are inverted into transpressional faults with dextral strike-slip component.
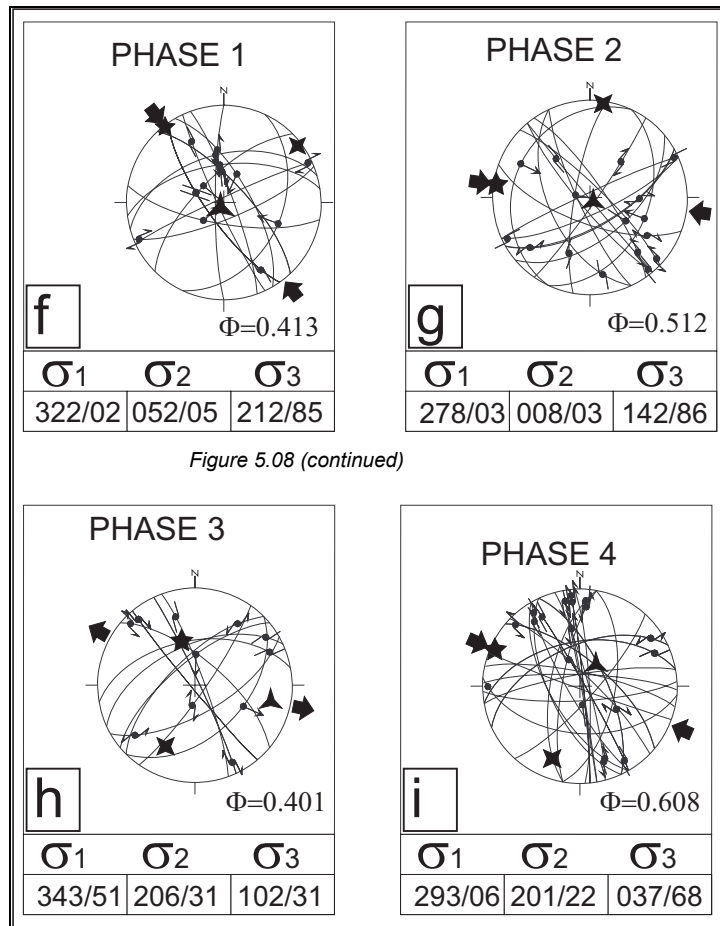

Figure 5.08 (continued)

PHASE 1

f

Φ=0.413

σ1	σ2	σ3
322/02	052/05	212/85

PHASE 2

g

Φ=0.512

σ1	σ2	σ3
278/03	008/03	142/86

Figure 5.08 (continued)

PHASE 3

h

Φ=0.401

σ1	σ2	σ3
343/51	206/31	102/31

PHASE 4

i

Φ=0.608

σ1	σ2	σ3
293/06	201/22	037/68

The fault TF 5 is displaced by a number of circa NNE-SSW striking oblique-slip faults with normal components (e.g. NF3) that strike almost parallel to the fault TF 5. The faults TF 6 to TF 9 are displaced by a number of approximately NE-SW striking strike-slip faults some of which have a normal component of movement (Figure 5.09a).

In the Çankırı Basin, the folds are oriented in two directions. The folds developed in the Çandır Formation are oriented N-S to NNNE-SSW and the ones developed in the Late Miocene units are oriented NE-SW. This relation indicates sequential rotation of fold axes within the sinistral Eldivan Fault Zone (EFZ) (see chapter 4).

The folds in the Hancılı Basin are oriented into two different directions. One set is oriented NW-SE parallel to the faults TF 6, TF 7,TF 8 and TF 9. This relation indicates folding of the units in the Hancılı Basin after the deposition of Hancılı Formation during the inversion of faults which defines the margins of the Hancılı Basin (TF 6,TF 7, TF 8 and TF 9) (see also chapter 4). Second set is oriented in a NE-SW direction, parallel to the folds in the Çankırı Basin that are observed within the Late Miocene units (Sűleymanlı and Bozkır formations).

Table 5.04. Field characteristics of sites in the sub-area 4. Ta. Altıntaş Formation, Tha. Hancılı Formation. Other abbreviations are similar to Table 5.01.

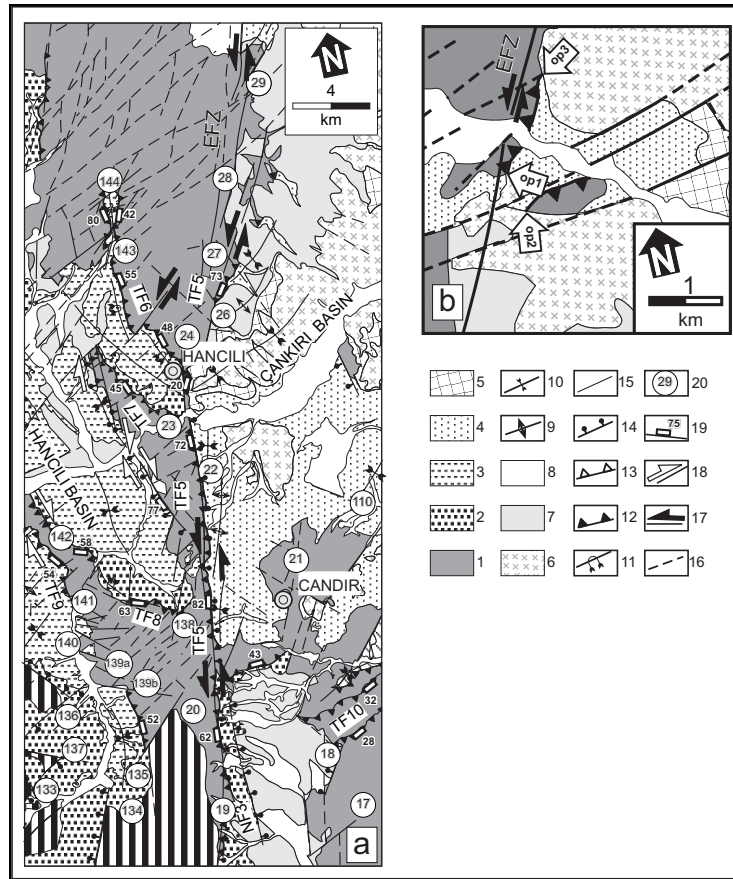| SITE	SHEAR	VEIN	O.P.	S.LINE	C.C.	UNIT	#MOVE
17	-	-	2	-	2	Ti	2
18	+	+	-	Ca	2	K	3
19	+	+	-	SP,Ca	3	K	3
20	-	+	-	-	-	K	2
21	+	-	2	-	2	K	3
22	+	+	2	Ca	2	K	3
23	-	-	-	-	-	K	1
24	+	+	2	-	3	K	4
25	-	-	-	-	-	-	-
26	+	-	-	-	2	K	2
27	-	-	-	-	-	K	1
28	-	-	-	-	-	K	1
29	-	-	-	-	-	K	1
133	-	-	-	-	-	Ta	1
134	-	+	-	Ca	-	Tha	1
135	-	+	-	Ca	2	Tha	2
136	-	+	-	Ca	2	Tha	2
137	+		2	-	2	TRK,Ta	3
138	+	+	2	-	2	K,Tha	3
139a	+	+	2	-	2	K	3
139b	+	+	2	SP,Ca	2	K,Ta	3
140	-	-	-	-	-	Ta	1
141	+	-	-	-	2	Tha	2
142	+	-	-	-	2	Tha	2
143	-	-	-	-	-	Tha	1
144	-	-	2	Ca	2	Tha	2

Figure 5.09 a) Geological map and sample location for the sub-area 4. EFZ: Eldivan Fault Zone, O.P. observation point (see text). 1. NAOM, 2. Altıntaş and Kılçak formations, 3. Hancılı Formation, 4. Çandır Formation. 5. Süleymanlı formation, 6.Bozkır Formation, 7 Deyim Formation, 8. Alluvium, 9. anticline, 10. syncline, 11.overturned syncline, 12. thrust faults, 13. reverse faults, 14. faults with normal sense of movement , 15. strike-slip or faults with unknown sense of movement, 16. photo-lineaments, 17. faults with sinistral strike-slip sense of movement, 18. faults with dextral strike-slip sense of movement, 19. dip amount of faults where they are best observed in the field. 20. sample site locations. b) Map showing the relation between thrusting of NAOM onto the Çandır Formation and covering of the fault contact by the Bozkır Formation (see Figure 5.02 for the location of the map). Plots of fault planes, slickenlines and stress orientations for each site (c-f) and whole data in a particular phase and sub-area (g-j) (lower hemisphere equal area projection).
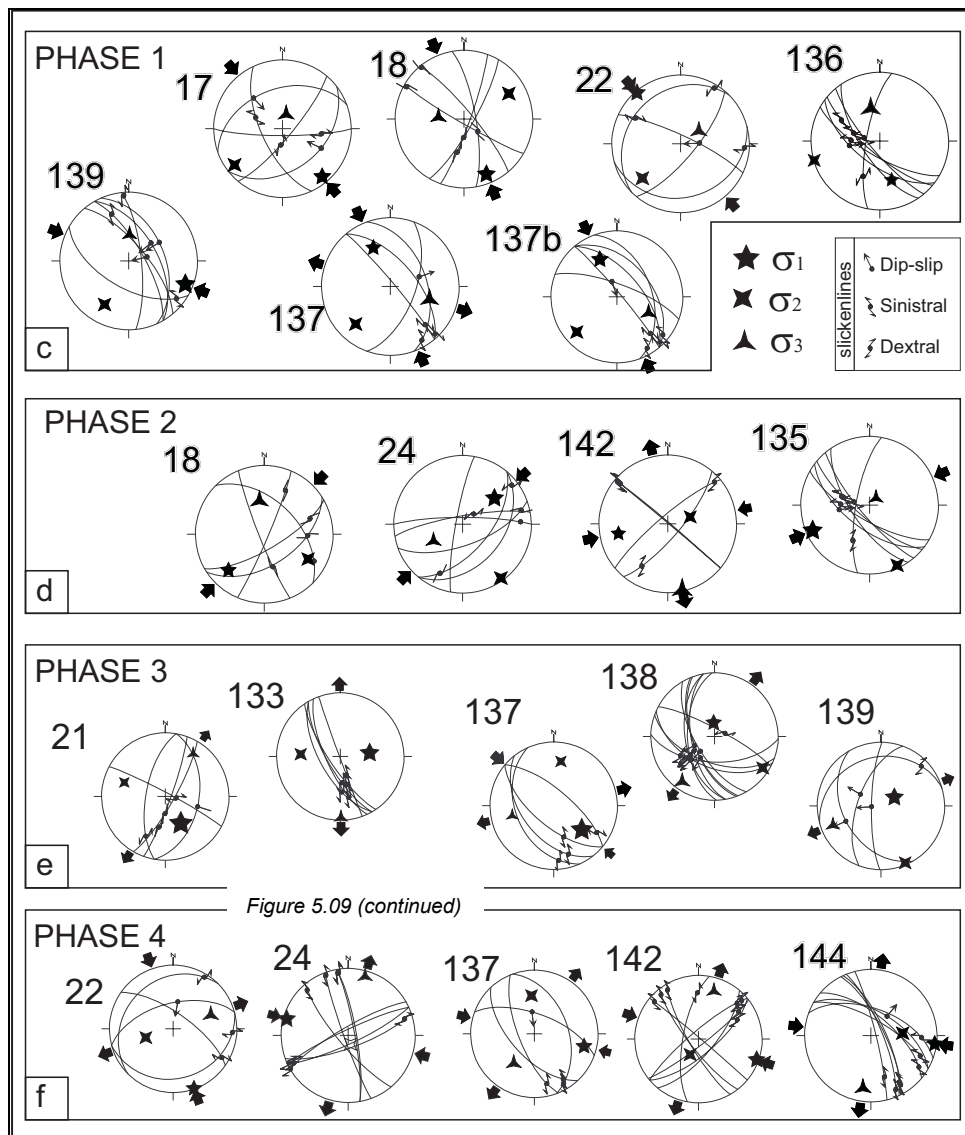
154

5.3.4.1 Paleostress Inversion

Twenty-one sites were selected for the construction of site based stress tensors. Like the previous sub-areas, 4 phases of fault movements were again recognized. These movements are assigned into deformation phases and they are ordered according to their order of occurrence as explained previously (see Figure 5.05). The detail of each site is given in Table 4 and the results are presented in Figure 5.09c-f.
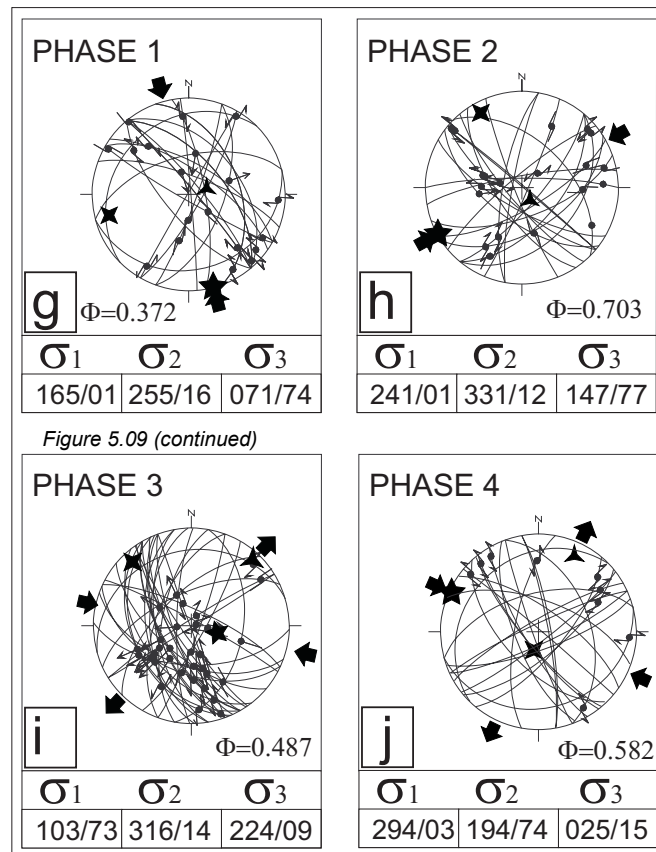
Phase 1: Seven sites had sufficient slip data for the construction of site based stress tensors. Except for Site 136 (Figure 5.09c), the orientation of the principal stresses are consistent on site basis and in all other sites, the σ_3 is sub vertical, the σ_1 is oriented in NW/NNW to SE/SSE direction and σ_2 is sub horizontal. The orientation of the mean regional principal stresses and the stress ratio are as follows: σ_1=165°N/01°, σ_2=255°N/16°, σ_3=071°N/74º and Φ= 0.372 (Figure 5.09g), indicating that thrusting occurred during this phase.

Phase2: Only 4 sites had sufficient slip data for the construction of site based stress tensors (Figure 5.09d). The orientation of σ_2 and σ_3 is variable in each site whilst σ_1 is relatively consistent and oriented in ENE-WSW to NE-SW. The orientation of the averaged sub-area based stresses and the stress ratio are as follows: σ_1=241°N/41°, σ_2=331°N/12°, σ_3=147°N/77º and Φ= 0.703 (Figure 5.09h), also indicating thrusting during this phase.

Phase3: Six sites had sufficient slip data for the construction of site based stress tensors (Figure 5.09e). In all of the sites, σ_1 is sub vertical and other stresses are sub horizontal. The horizontal component of σ_3 is relatively consistent in each site, however, other stresses are variable in orientation. This may be due to the magnitudes of the σ_2 and σ_3 being very close to each other which gives way to stress permutations (Angelier 1994). In addition, the orientation of the horizontal component of σ_3 is approximately perpendicular to the faults (TF6-9) in the Hancılı Basin from where most of the data came and indicates that these faults were normal faults prior to their inversion in the latest phase (see also chapter 4). The orientation of the mean regional principal stresses and the stress ratio are as follows: σ_1=130°N/73°, σ_2=316°N/14°, σ_3=224°N/09º and Φ= 0.487 (Figure 5.09i). Having σ_1 sub vertical and other stresses sub horizontal indicates an extensional deformation in this phase.

Phase 4: Five sites had sufficient slip data for the construction of site based stress tensors (Figure 5.09f). The orientation of the principal stresses are variable. However, σ_1 is relatively consistent in each site except site 22 and is oriented WNW-ESE while the horizontal component of σ_3 is oriented NNE-SSW. The orientation of mean sub-area based stresses and the stress ratio are as follows: σ_1=294°N/03°, σ_2=194°N/74°, σ_3=025°N/25 and Φ= 0.582 (Figure 5.09j), indicating a transcurrent deformation during this phase.

155

Figure 5.09 (continued)

156

PHASE 1

g   Φ=0.372

σ1	σ2	σ3
165/01	255/16	071/74

PHASE 2

h   Φ=0.703

σ1	σ2	σ3
241/01	331/12	147/77

Figure 5.09 (continued)

PHASE 3

i   Φ=0.487

σ1	σ2	σ3
103/73	316/14	224/09

PHASE 4

j   Φ=0.582

σ1	σ2	σ3
294/03	194/74	025/15

5.4 Discussion

The results obtained are summarized in Figure 5.10 in which both the site and sub-area stress tensors are presented. Of importance to the structural evolution of the Çankırı Basin, are the sub-area stress tensors and the discussion will concentrate on these.

Phase1. As stated above Phase-1 is characterized by compressional deformation in which the orientation of σ_1 is sub horizontal and σ_3 is sub vertical. When the results are considered it can be seen that σ_1 has a consistent NW trend in the northern and northwestern margins but to a NNW trend in the western margin. This gives an overall discrepancy of 37° (Figure 5.10a). The orientations of σ_1 in the north (sub-area 1-3) are almost perpendicular to the

157

marked thrust faults and oblique to the ones in the western margin of the basin (Figure 5.11). The units affected in this phase are the Late Cretaceous to Paleocene units; therefore, this phase had operated in the Late Cretaceous to pre-Late Paleocene.

Phase 2. This phase is also characterized by a compressional deformation in which σ_1 is sub horizontal and σ_3 is sub vertical, although some sites do indicate local strike-slip deformation in which σ_1 and σ_3 both being sub horizontal and σ_2 is sub-vertical. The averaged trend of σ_1 is very variable changing from NE-SW in the sub-areas 1 and 2 to almost N-S in the sub-area 2 to E-W in the sub-area 3 (Figure 5.11b). The angular discrepancy between the sub-areas is 87° (Figure 5.10b). The fault slip data ascribed to this phase are only observed in most of pre-Burdigalian units. Therefore, Late Paleocene to pre-Burdigalian age is ascribed to this phase.

Phase 3. This phase is characterized by extensional deformation in which σ_1 is sub-vertical and σ_3 is sub horizontal. The orientation of σ_3 changes from a WNW trends in the sub-areas 1 and 3 to ENE in sub-area 2 and to NE trend in the sub-area 4 (Figure 5.10c). This gives an overall discrepancy of 73° (Figure 5.10c). The orientation of the horizontal component of the σ_3 in each sub-area is oblique to the faults, which are thought to have been active in this deformation phase (Figure 5.11c). The fault slip data ascribed to this deformation phase were obtained mainly from Burdigalian to pre-Tortonian (Early to Middle Miocene) units in the sub-area 4, and in other sub-areas they overprint the slickenlines that are ascribed to older phases and are, in turn, overprinted by the latest phase. Therefore, a Burdigalian to Serravallian age is assigned to this phase. The length weighted rose diagram (Figure 5.11d) prepared from the normal faults thought to have developed in this deformation phase indicates 2 sets of conjugate pairs of normal faults. Considering the oblique nature of principal stresses discussed above it is proposed that these faults were developed in "so-called" tri-axial strain conditions give rise to oblique-extension (Reches 1978a,b, Krantz 1988).

Phase 4. This phase is characterized by strike-slip deformation in which σ_2 is sub vertical and σ_1 and σ_3 are sub horizontal. The orientations of the trends of σ_1 are relatively consistent in the sub-areas and trending WNW with a 17° overall discrepancy (Figure 5.10d). In Figure 5.11e the structures that possibly developed in this phase are illustrated. It is obvious that most of these structures were reactivated in this deformation phase and were inherited planes of weaknesses. However, the variation of σ_1 between sub-areas is almost negligible. This relation indicates that pre-existing planes of weakness do not play a major role in the stress inversion procedure. The slip data attributed to this phase includes the latest overprinting slickenlines and also the data collected from the faults that affected the Late Miocene and younger units. Therefore, post-Middle Miocene (Tortonian to Recent) age is assigned to this phase. This phase corresponds to the transcurrent tectonics controlled dominantly by the North Anatolian Fault Zone (NAFZ), which was developed due to collision of Arabia and Eurasia along the Bitlis-Zagros Suture (Figure 5.01), at the end of Serravallian beginning and beginning of Tortonian (11.1 Ma to Recent)
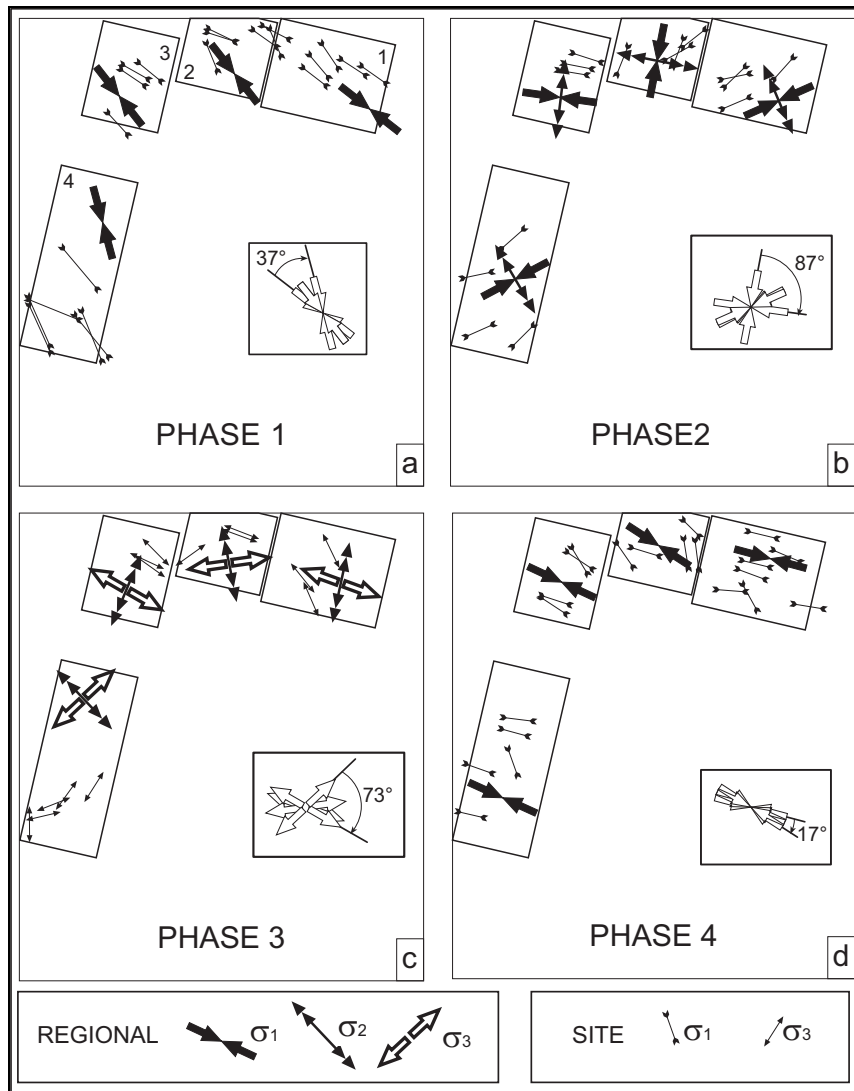
Figure 5.10 Plots of the horizontal components of σ_1 (a, b, and d), and σ_3 (c) for different deformation phases in each studied sub-areas (1-4).
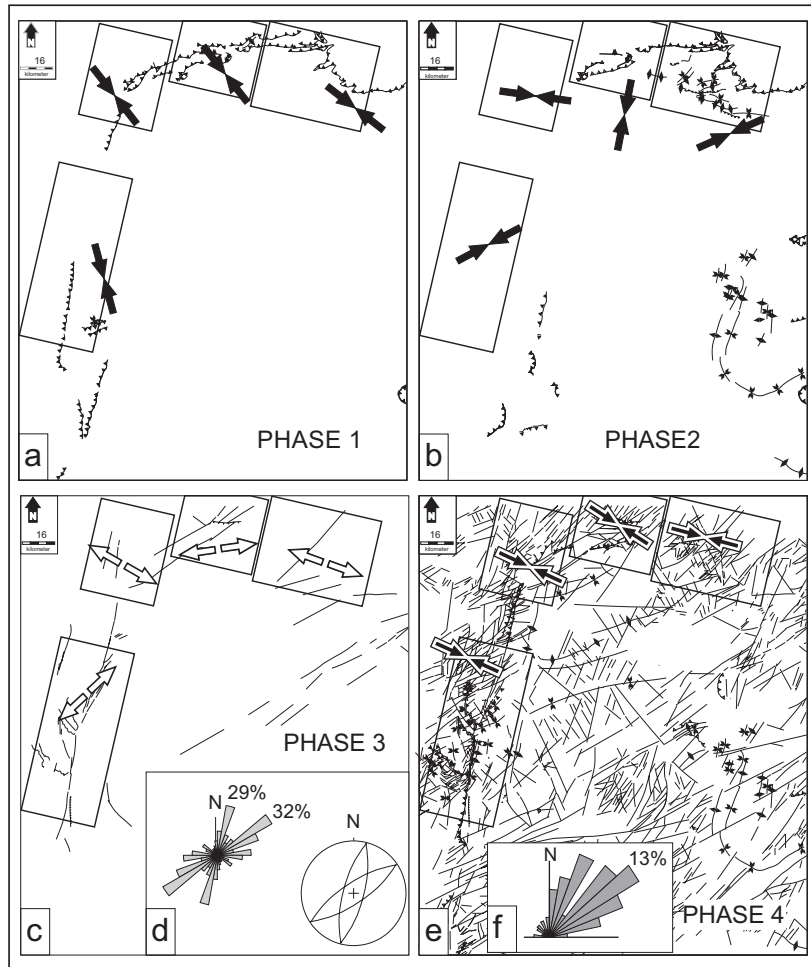
Figure 5.11 Plots of the horizontal components of the σ_1 for phases-1, 2 and 4 (converging large arrows) and the σ_3 for the phase-3 (diverging large arrows) and the structures proposed to have been developed in the corresponding phase (a,b,c and e). d) Length weighted rose diagram prepared from the faults that proposed to have been developed in the deformation phase-3 and idealized stereographic projection of largest populations note that they display 2 sets of conjugate fault pairs. f) Length weighted rose diagram prepared from the faults proposed be have been developed in the deformation phase-4.

160

5.4.1 Stress Trajectories and Models

Using the sub-area based principal stresses smoothed stress trajectories of each phase are plotted (Figure 5.12). The stress trajectories in phase-1 display a mash like pattern in which the σ_1 trajectories are oriented NW-SE while σ_2 trajectories are curvilinear and convex southeastwards (Figure 5.12a). In the phase-2, they display a radial σ_1 and concentric σ_2 patterns (Figure 5.12b). In the deformation phase-3, the σ_2 trajectories display radial pattern while σ_3 are concentric around the rim of the Çankırı Basin and exposed parts of the Kırşehir Block (Figure 5.12c). Concentric pattern of σ_3 trajectories in the deformation phase-3 indicates uni-axial extension (Carey and Brunier 1974) which is characteristic for the areas of regional doming (Means 1976) and multi directional extension (Arlegui-Crespo and Simon-Gomez 1998). In the deformation phase-4 σ_1 and σ_3 trajectories display mash like pattern oblique to the western and northern rim and to the Kızılırmak and Sungurlu Fault zones (Figure 5.12d).

The subduction of Neotethys took place northwards under the Pontides along a roughly E-W trending trench (Şengőr and Yılmaz 1981, Gőrűr et al. 1984, Koçyiğit et al. 1988, Koçyiğit 1991, Dellaloğlu et al. 1992) in the Late Cretaceous to Early Tertiary i.e. during the deformation phase-1. Considering the E-W oriented zone of convergence, the orientation of the σ_1 (in the phase-1) is oblique to the direction of convergence (Figure 5.13a). This relation may indicate that subduction had dextral strike-slip component in this part of the Tethys Ocean (Figure 5.13a) where Sakarya Continent and Kırşehir Block are eventually collided and amalgamated. As discussed in chapter 7, the western part of the Cankiri Basin has rotated about 30° anticlockwise while eastern margin rotated about 52° clockwise which resulted in Ω-shape of the basin in Eocene to Oligocene times. This relation may be the reason for the radial σ_1 pattern and concentric σ_2 pattern while σ_3 is sub vertical in the deformation phase-2 (Figure 5.13a).

In the Early Miocene, the collision and further convergence of the Sakarya Continent and the Kırşehir Block were completed after which the compressional regime was replaced by an extensional regime in the deformation phase-3 which may have been due to gravitational collapse (Dewey 1988). This gave rise to the formation of multi directional normal faulting within oblique extension setting and deposition of Altıntaş, Hancılı and Çandır Formations within graben complexes (see chapter 4). Extensional deformation driven by gravitational collapse have already been postulated for western Turkey and the Aegean area (Seyitoğlu et al. 1992, Bozkurt and Park 1997, see Lips 1998 and Walcott 1998 for Aegean references). Lips (1998) has discussed that the Early to Middle Miocene extension in the west Anatolia and the Aegean region is the result of 20 Ma to Recent decrease in the convergence rates of Africa and Eurasia which approximately corresponds to the beginning of extension in the Çankırı and Hancılı Basins in Burdigalian (20.5 Ma) during which Altıntaş Formation was deposited in the Hancılı Basin in sub-area 4. Therefore, it can be concluded that the Early to Middle Miocene extension in the Çankırı and Hancılı Basins is not a local phenomenon but the consequence of combination of gravitational collapse and 20 Ma to Recent slow convergence rates of Africa and Eurasia.
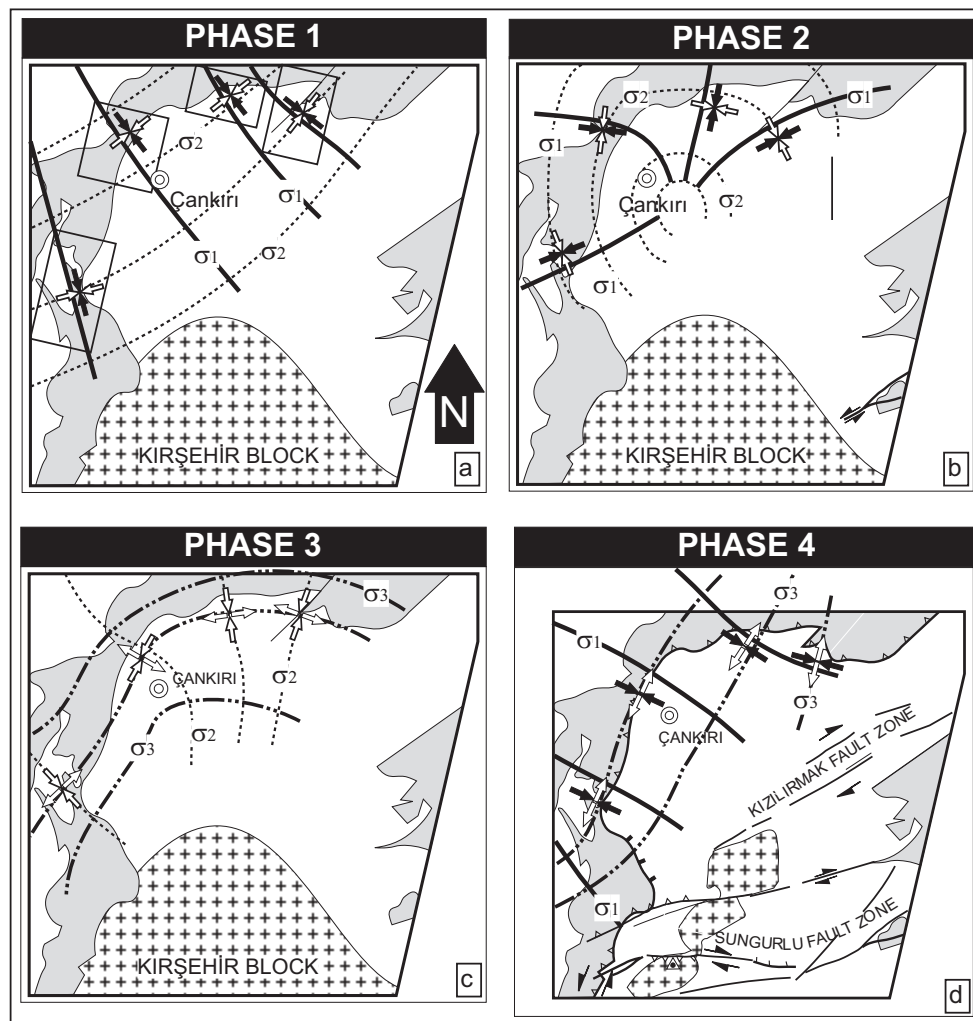
Figure 5.12 Interpreted and smoothed stress trajectories for each deformation phase.

Having σ_2 sub vertical and σ_1 oriented NW-SE during Phase 4 indicates that the Sungurlu (SFZ) and Kızılırmak Fault Zones (KFZ) have been the two major strike-slip faults which deformed the Çankırı Basin and displaced its rims dextrally. The length weighted rose
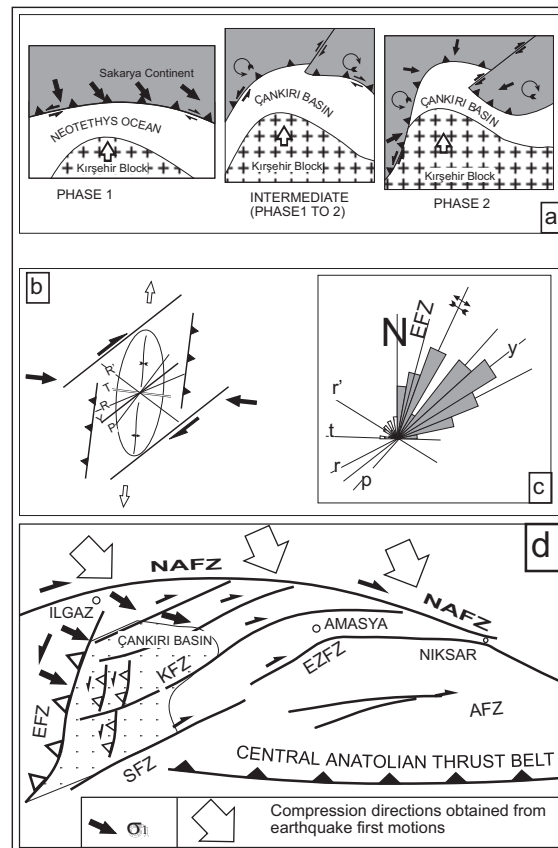
162

Figure 5.13 a) Cartoons illustrating the possible development of the Çankırı Basin through deformation phase 1 to 2. Note block rotations and response of principal stress orientations as the Kırşehir block drives northwards. b) Riedel pattern of deformation (after Biddle and Christie-Blick 1985) and plot of horizontal components of the σ₁ (convergent large arrows) proposed to explain the structures developed in the deformation phase-4. c) Length weighted rose diagram prepared from the structures proposed to have been developed in this phase and corresponding Riedel shears. r. synthetic-shear, r'. antithetic-shear, p. secondary synthetic-shear, y. principal displacement zone, t. extension fractures. Note that the orientation of the Eldivan Fault Zone (EFZ) with respect to the riedel shears. d) Schematic illustration of the structures in north-central Turkey plotted to explain the structural development of the Çankırı Basin during the deformation phase 4. AFZ: Almus Fault Zone, EFZ. Eldivan Fault Zone (which is the WBCB-western boundary fault of the Çankırı Basin), EZFZ: Ezinepazarı Fault Zone, KFZ: Kızılırmak Fault Zone, NAFZ: North Anatolian Fault Zone (modified after Barka and Hancock 1984, Şengör et al. 1985).

163

diagrams (Figure 5.11f) for the trends of these structures indicate a domination of northeasterly trends (see chapter 2) that a part of a system displaying a Riedel deformation pattern (Figures 5.11f, 5.2b and c), which commonly develops in regions of regional transcurrent deformation and along strike-slip fault zones (Biddle and Cristie-Blick 1985). During this phase, the western margin of the basin was reactivated as a sinistral strike-slip fault zone (Eldivan Fault Zone, EFZ) as the conjugate of KFZ and SFZ. Because, the western margin was dominated by pre-existing transpressional faults, it reactivated as a sinistral transpressive fault (Figure 5.13d). In addition, the orientations of the constructed principal stresses are parallel to the P (compressive) and T (tensile) axes obtained from recent earthquakes along the North Anatolian Fault Zone (Jackson and McKenzie 1984, Dewey et al 1986). This relation is consistent of our results.

5.5 Conclusions

I. Four deformation phases have been recognized and their paleostress configurations are constructed.

   1. The first phase is characterized by NW-SE oriented σ_1 and sub-vertical σ_3 indicating compressional deformation characterized by thrusting, and occurred in the Late Cretaceous to Paleocene.

   2. The second Deformation phase is characterized by radial σ_1 and concentric σ_2 pattern with sub vertical σ_3 indicative of thrusting and occurred in the Late Paleocene to pre-Burdigalian.

   3. Concentric σ_3 and sub-vertical σ_1 is indicative of extensional deformation in the third deformation phase. It occurred in the Early to Middle Miocene (Burdigalian to Serravalian).

   4. The latest phase is characterized by NW-SE oriented σ_1 pattern with a very little variation of σ_1 orientations between the sub-areas. It has been active since the Late Miocene (Tortonian to Recent).

II. The structures which have been active in the latest deformation phase display a Riedel pattern of deformation that is in accordance with the strike-slip deformation that has operated since the Late Miocene.

6

KINEMATIC AND STRUCTURAL DEVELOPMENT OF THE ÇANKIRI BASIN (Central Anatolia, Turkey): A PALEOSTRESS INVERSION STUDY. Part II: SouthernArea

Abstract

In the southern part of the Çankırı Basin, three different deformation phases have been recognized from the major structures and through using paleostress inversion techniques for fault slip data obtained in the field. The deformation phases recognized from the paleostress data are correlated with the deformation phases recognized from the major structures. The first phase is characterized by an oblique σ_2 and NNE-SSW to NE-SW trending sub horizontal σ_1 and WNW-ESE to NW-SE trending σ_3 patterns which indicates transpressional deformation, associated with a combination of thrusting and strike slip faulting. The second phase is characterized by a sub vertical σ_1 and oblique σ_2 and σ_3 which indicates oblique extension associated with normal faulting. The third deformation phase is characterized by a vertical σ_2 while the other stresses were horizontal, which indicates regional transcurrent tectonics. These phases were correlated with the deformation phases recognized from the major structures and dated accordingly.

The first phase occurred in Late Paleocene to pre-Burdigalian and is characterized by combination of thrusting and transpression. The second phase occurred from Burdigalian to Serravalian and is characterized by extensional deformation due to post-orogenic collapse. The third phase has been active since the Tortonian and corresponds to the currently active transcurrent tectonics, which is controlled by the North Anatolian Fault Zone.

6.1 Introduction

Paleostress inversion provides an estimation of the orientation of the principal stresses using fault slip orientation data. The direction of slip is inferred from the fault slip data (Angelier 1979, 1984, 1994, Petit *et al.* 1985, Means 1987, Petit and Laville, 1985, Doblas 1998), which are assumed to record the direction of maximum shear stress on a fault surface (Carey and Brunier 1974, Etchecopar *et al.* 1981, Angelier 1979, 1984, 1994, Reches 1987, Krantz 1988, Lisle 1987). The faults in three dimension may conform to the Coloumb criterion (Reches 1987). However, due to anisotropy and inherited planes of weakness, faults develop at angles to principal stress directions other than those predicted for isotropic media (Wojtal and Pershing 1991). Wallace (1951) and Bott (1959) suggested that slip on pre-existing surfaces occur parallel to the maximum resolved shear stress. After the pioneering work of Carey and Brunier (1974) who developed ther paleostress inversion technique by reversing the assumption of Wallace and Bott, a number of paleostress techniques have been developed and have been applied to fault slickenline data from a variety of tectonic settings and have produced results that are consistent and interpretable. Because of this success, paleostress inversion procedures are becoming a routine analytical technique in structural geology (Pollard *et al.* 1993).

The Çankırı Basin (Figure 6.01) is situated in north central Anatolia at the interface between the Sakarya Continent of the Pontides in the north and the Kırşehir Block of the Taurides, in the south. It is characterized by a rim of tectonic slices of Late Cretaceous ophiolitic mélange and volcano-sedimentary successions. It comprises more than 4 km thick clastics, carbonates and evaporites and has experienced multiple phases of deformation, since its first inception, in the Late Cretaceous (Şengőr and Yılmaz 1981, Dellaloğlu *et al.* 1992, Tűysűz and Dellaloğlu 1992, Koçyiğit *et al.* 1995, Kaymakcı *et al.* 1998, 2000).

The purposes of this study are to apply paleostress inversion techniques to unravel the paleostress history of the southern part of the Çankırı Basin including the Kırşehir Block (basement) and to constrain the timing of each deformation phase and relate the results to the major structures that were active during each deformation phase. This is a complementary study to the chapter 5, which covers the western and northern parts of the basin. Therefore, the sub-areas are numbered according to those outlined in chapter 5. Analytical and numerical procedures follow those outlined in detail in chapter 5.

6.2 Regional Setting

Çankırı Basin lies adjacent to the İzmir-Ankara-Erzincan Suture Zone along which the Sakarya continent of the Pontides and the Kırşehir Block of Taurides (Figure 6.01) are thought to have collided and amalgamated (Şengőr and Yılmaz 1981, Tűysűz and Dellaloğlu 1992). Besides being affected by collisionary process, the Çankırı Basin was subjected to further deformation in the post-Late Miocene being a part of the Anatolian wedge caught between the expulsive transcurrent motions on the North and East Anatolian Faults (Figure 6.01c). This has resulted in a number of northwards convex dextral strike-slip faults which bifurcate from the North Anatolian Fault Zone (NAFZ) (Barka and Hancock 1984, Şengör *et al.* 1985, Kaymakcı and Koçyiğit 1995). The Kızılırmak and

the Sungurlu Fault Zones are the two major splays of the NAFZ, which partly controlled the Late Miocene evolution of the Çankırı Basin (Figure 6.02).
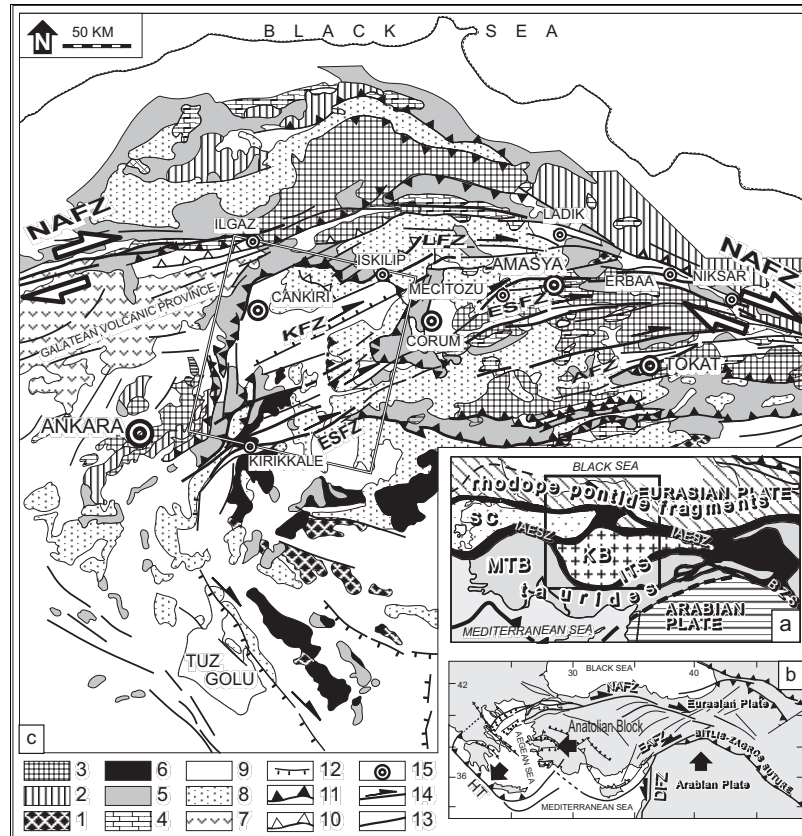

Figure 6.01 a) Inset map showing the geological outline of the Eastern Mediterranean area (Modified after Şengőr et al. 1984). BSZ: Bitlis-Zagros Suture, IAESZ: Izmir-Ankara-Erzincan Suture Zone, ITS: Intra-Tauride Suture, KB: Kırşehir Block, MTB: Menderes-Taurus Block, SC: Sakarya Continent. b) Active tectonic outline of Turkey and surrounding regions. DFZ: Dead Sea Fault Zone, EAFZ: East Anatolian Fault Zone, HT: Hellenic Trench, NAFZ: North Anatolian Fault Zone. Large black arrows are the movement directions of Arabian plate and Aegean-Anatolian Block (modified after Barka and Hancock 1984, Gőrűr et al. 1984, Őzçelik 1994, Kaymakci and Koçyiğit 1995). c) Detailed tectono-stratigraphical map of the central Anatolia. Box shows the location of the study area. AFZ: Almus Fault Zone, ESFZ: Ezinepazari-Sungurlu Fault Zone, KFZ: Kızılırmak Fault Zone, LFZ: Laçin Fault Zone, NAFZ: North Anatolian Fault Zone, YFFZ: Yağbasan-Faraşlı Fault Zone. 1. Pre-Late Cretaceous metamorphic basement of the Kırşehir Block, 2. Pre-Jurassic metamorphic basement of the Sakarya Continent, 3. Triassic Karakaya Complex, 4. Jurassic-Cretaceous platform carbonates on the Sakarya Continent, 5. Late Cretaceous (?) ophiolites and ophiolitic melanges, 6. Pre-Paleocene Granitoids of the Kırşehir Block, 7. Galatean Volcanic Province (GVP, Toprak et al. 1996), 8. Early Tertiary units (mainly marine), 9. Neogene and Quaternary Cover, 10. reverse faults, 11. thrust faults, 12. normal faults, 13. faults with unknown sense of movement,, 14. active strike-slip faults. 15. major towns.
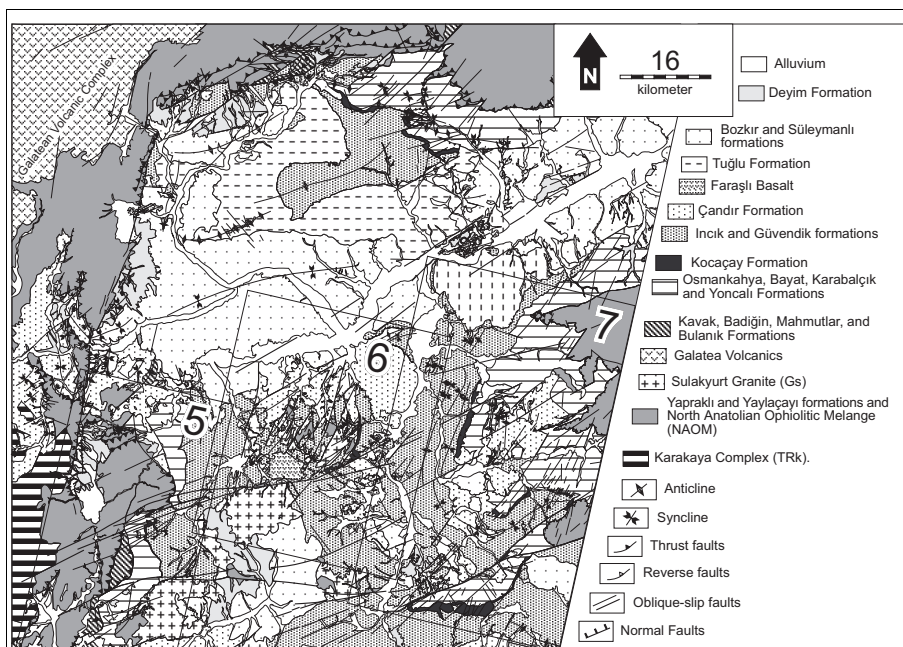
167

Figure 6.02 Geological map of the Çankırı Basin. The numbers and the boxes indicate the locations of the sub areas.

The major structures which developed and shaped the Çankırı Basin are the compressional structures (discussed in chapter 5) defining the western, northern and eastern margin of the basin. They define an arcuate pattern which give the Çankırı Basin a distinctive Ω-shape (Figure 6.02). Along these faults, an ophiolitic mélange unit and associated Late Cretaceous volcano-sedimentary successions have been tectonically transported over the basin in-fill (Akyürek *et al.* 1980, Dellaloğlu *et al.* 1992, Tűysűz and Dellaloğlu, 1992, Őzçelik 1994, Koçyiğit *et al.* 1995, Kaymakcı *et al.* 1998,2000). In the south, the granitoids of the Kırşehir Block delimit the southern margin of the basin and constitute the basement to the southern part of the basin (Dellaloğlu *et al.* 1992, Tűysűz and Dellaloğlu 1992, see chapters 3 and 4).

The other major structures that affected the Çankırı Basin are the strike-slip faults (see Figures 6.01c and 6.02), namely the Kızılırmak Fault Zone (KFZ), Yağbasa Faraşlı Fault Zone (YFFZ), Sivritepe Fault Zone (STFZ) and the Sungurlu Fault Zone all of which splay off the NAFZ which occurs to the north. These structures are oriented approximately NE-SW. They traverse the basin and displace the basin in-fill, the rim, and the basement. The south-central part of the basin is dominated by generally NNW-SSE to NE-SW oriented normal faults (Figure 6.02) (see also chapters 2-5). The southern area is dominated by the Ezinepazarı-Sungurlu Fault Zone (ESFZ), which is one of the major splays of the NAFZ (Figure 6.01d) that ruptured partly during the Erzincan Earthquake (26 December 1939).

The fill of the Çankırı Basin is more than 4km thick and accumulated in 5 different cycles of sedimentation (Figure 6.03). The cycles are discussed in detail in chapters 3 and

168

4 and only a summary is given here. The oldest cycle comprises the Late Cretaceous volcanoclastics and regressive shallow marine units and the Paleocene mixed environment red clastics and carbonates (Özçelik 1994, see also chapter 3). The subsequent cycles have been partly studied by Dellaloğlu *et al.* (1992) and their scheme is followed in this study. The second cycle is a Paleocene to Oligocene regressive flysch to molasse sequence overlain by a widespread thin (<100m) nummulitic limestone of Middle Eocene age that passes into very thick (up to 2000m) Late Eocene to Oligocene continental red clastics intercalated and overlain by the Oligocene evaporites. The third cycle is represented by fluvio-lacustrine clastics deposited in the Early to Middle Miocene. The fourth cycle is represented by the deposits that were deposited in the Late Miocene fluvio-lacustrine conditions and frequently alternate with evaporites. The Plio-Quaternary alluvial fan deposits and recent alluvium locally overlie all of these units (Figure 6.03) and form the fifth cycle.

6.3 Field Observations and Result

The southern part of the Çankırı Basin is subdivided into three sub-areas (Figure 6.02) based on the marked differences in the underlying lithologies, type and trends of the structures. This study is complementary to chapter 5. Therefore, numbering of the sub-areas is continued from the previous chapter.

6.3.1 Sub-area 5

Sub-area 5 lies in the south-western part of the Çankırı Basin where the basement and the rim come closer to each other than at any other part of the basin (Figure 6.04). They are separated from each other by the Late Cretaceous to Paleocene and early to Middle Eocene units. The main structures in the sub-area are faults and the folds (Figure 6.04).

6.3.1.1 Faults

The main faults observed in this area (Figure 6.04) are the Bedesten Faults (BTF-1, BTF-2, and BTF-3), Malıboğazı Trust Faults (MTF), Kazmaca-Hamzalı Reverse Fault (KHRF), Sivritepe Fault (STF), Kılçak Thrust Fault (KLTF), Kayadibi Fault (KDF), Babas-Ekincibayırı Fault (BETF) (Figure 6.04) and HITF. Most of these faults delimit the western rim of the basin and are dextrally displaced by the sub strands of the Yağbasan-Faraşlı (YFFZ) and Sivritepe Fault Zones (STFZ). The structural characteristics and possible age ranges of these faults are outlined in Figure 6.05.

Along the faults BTF-1 and –2 various constituent units of the NAOM are intensely deformed and sheared. No reliable slickenlines were observed along these fault planes. Along the fault BTF-3, the NAOM tectonically overlies the Late Cretaceous to Paleocene Dizilitaşlar Formation (Figure 6.04). The Dizilitaşlar Formation, in turn, has been thrusted over the Early to Middle Eocene Karabalçık and Yoncalı formations along the fault BTF-4. Along the fault BTF-5 the NAOM tectonically overlies the Early to Middle Eocene Mahmatlar Formation in the south-western most part of the basin. This relationship is important for determining the amount of E-W tectonic transport of the rim. The Mahmatlar Formation is derived mainly from the Kırşehir Block (as discussed in chapter 3) and lies adjacent to it. It is separated from the rim of the Çankırı Basin by the Late Cretaceous to Paleocene Dizilitaşlar Formation and from the Early to Middle Eocene units (Yoncalı and

169

Karabalçık formations). Therefore, the cumulative vertical offset of this fault must be larger than the total thickness of these units, which is more than 2km. In the north, along the fault
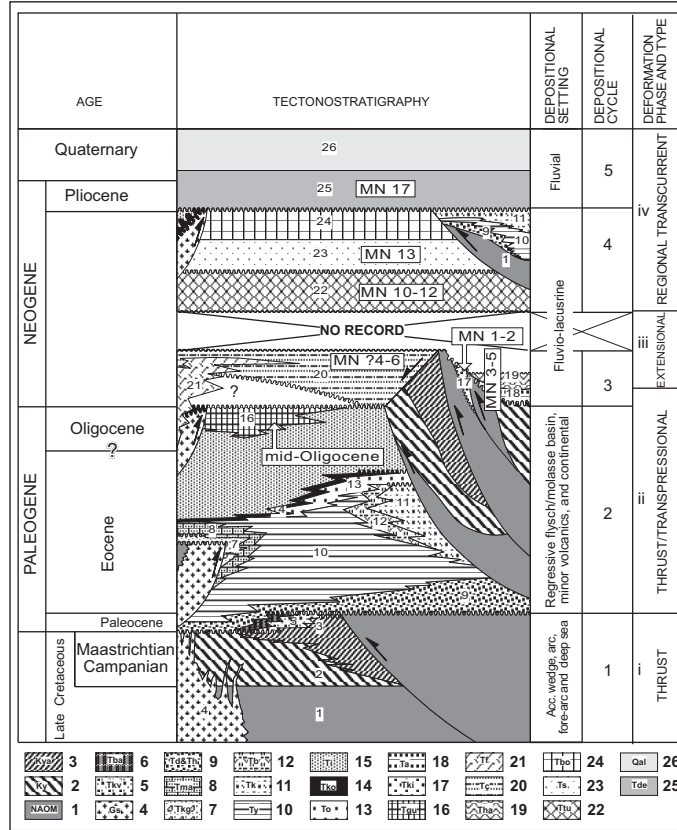

Figure 6.03 Generalized tectono-stratigraphic column for the units exposed in and around the Çankırı Basin (for the MN zones given in the age column see Chapter. 4). North Anatolian Ophiolitic Melange-NAOM, 2. Yaylaçayı Formation (distal fore-arc sequence), 3. Yapraklı Formation (proximal fore-arc facies), 1. Sulakyurt Granites of the Kırşehir Block that intruded in pre-Paleocene, 5. Kavak formation (red clastics and carbonates), 6. Badiğin formation (neritic limestones), 7. Karagüney Formation (clastics derived mainly from the Kırşehir Block) 8. Mahmatlar Formation (clastics derived from Sulakyurt Granite), 9. Dizilitaşlar and Hacıhalil Formations (mainly turbiditic clastics and intercalated limestones), 10. Yoncalı Formation (Eocene flysch), 12. Karabalçık Formation (distributary channel conglomerates and sandstones with coal seams), 12. Bayat Formation (Eocene volcanics and volcanoclastics), 13. Osmankahya Formation (mixed environment clastics and red beds), 14. Kocaçay Formation (Middle Eocene nummulitic limestone covering both basin in-fill and the granites. 15. İncik Formation (Late Eocene to Oligocene continental red clastics), 16. Güvendik formation (Oligocene evaporites), 17. Kılçak Formation 18. Altıntaş Formation (fluvial red clastics exposed only in the Hancılı Basin), 19. Hancılı Formation (Lacustrine deposits exposed only in the Hancılı Basin, 20. Çandır Formation (fluvio-lacustrine sediments), 21. Faraşlı Basalt, 22. Tuğlu formation (early-Late Miocene evaporites and Lacustrine shale/marl), 23, Süleymanlı formation (fluvio-lacustrine red clastics), 24. Bozkır Formation (evaporites), 25. Deyim Formation (fluvial clastics), 26. Alluvium. See chapters 3 and 4 for the description of these units.
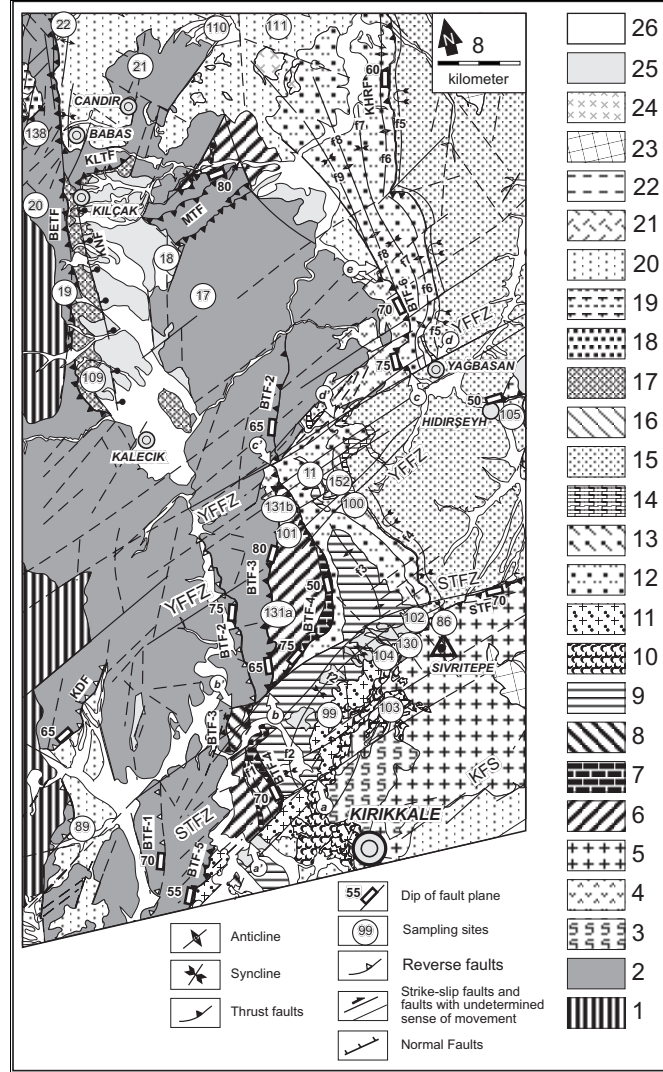
170

Figure 6.04 Geological map and sample locations for the sub-area 5. 1.Karakaya Complex, 2. North Anatolian Ophiolitic melange (NAOM), 3. ophiolitic units of the Kırşehir Block, 4. quartz-latite member of the NAOM, 5. Sulakyurt Granitoids, 6. Dizilitaşlar Formation, 7. D3-member of the Dizilitaşlar Formation, 8. Dizilitaşlar and Hacıhalil formations (undifferentiated), 9.Yoncalı Formation, 10. Karagűney Formation, 11. Mahmatlar Formation, 12. Karabalçık Formation, 13. Osmankahya Formation, 14. Kocaçay Formation, 15. Incik Formation, 16. Gűvendik formation, 17. Kılçak Formation, 18. Aslantaş Formation, 19. Hancılı Formation, 20. Çandır Formation, 21. Faraşlı Basalt, 22. Tuğlu formation, 23. Sűleymanlı formation, 24. Bozkır Formation, 25. Deyim Formation, 26. Alluvium (see Figure 6.03 for the ages of these units).

FAULTS

Faults	hanging wall Formations	foot wall Formations	covering or youngest displaced Formation	dip range and direction of the fault plane	Possible age range	Deform. style	AGE
STF	Sulakyur Granite	Ty, Tk, To İncik (Ti)	Deyim	70°S	Late Miocene to recent	TRANS-CURRENT	post-Early Miocene
KDF	NAOM	Çandır	Çandır	70°-80°W	post-Middle Miocene		
BETF	NAOM, Ky, Kya	Çandır	Süleymanlı	60°-80°W	post-Middle Miocene pre-Late Miocene		
BTF-1 BTF-2	NAOM, Yalaçayı (Ky), Yapraklı (Kya)	NAOM, Ky, Kya	NAOM	65°-75°W	Late Cretaceous to recent	TRANSPRESSION	PRE-MIDDLE MIOCENE (?)
BTF-3	NAOM, Ky, Kya	Dizilitaşlar (Td)	Dizilitaşlar	65°-80°W	post-Paleocene		
BTF-4	Td	Yoncalı (Ty), Karabalçık (Tk)	Karabalçık	50°-70°W	Early to Middle Eocene to recent		
BTF-5	Td	Ty, Tk	Mahmatlar	55°W			
BTF-6	NAOM, Ky, Kya	Tk	Çandır (Tç)	70°-75°W	Middle Eocene, pre-Middle Miocene		
MTF	NAOM	Kya	Deyim (Tde)	20°-45°S	post-Late Cretaceous pre-Late Pliocene		
KHRF	Kocaçay (Tko), Tk	İncik	Çandır	60°-90°E	Middle Eocene to pre-Middle Miocene		
KLTF	NAOM, Ky	Kılçak	Deyim	35°-70°N	post-Early Miocene pre-Late Pliocene		

Faults	Displaced youngest Formations	Max. offset	Along strike changes in def. style	dip range and direction of the fault plane	Possible age range	Deform. style	AGE
YFFZ	Bozkır and Süleymanlı	c-c'=13km d-d'=9 km	Transpression to transtension	70°N to 70°S	syn- to post- Late Miocene	Transpression/Transtension	post-Middle Miocene
STFZ	Süleymanlı	a-a'=7km b-b'=3km	transpression to transtension	70°N to 65°S	syn- to post- Late Miocene		
KFS	Süleymanlı	?	transtension	60°S to 90°S	syn- to post- Late Miocene		

FOLDS

folds	youngest folded unit	Covering unit	dip range and direction of the axial plane	possible compression direction	Age range
f1	Td		70°-90°W	E-W	post-Paleocene
f2	Ty		60°-90°N	NW-SE	post-Mid. Eocene
f3	Ty, Tk		70°-90°W	E-W	post-Mid. Eocene
f4, f5	Ti		35°-60° W	E-W	syn- to post- Mid. Eocene
F6-f9	Tk	Tç	50°-90°W	E-W	syn- to post- Mid. Eocene to pre- Middle Miocene

Figure 6.05 Figure illustrating the structural and kinematic characteristics, possible age ranges of the faults and the folds developed in the sub-area 5. BTF: Bedesten Faults, MTF: Malıboğazı Fault, KHRF: Kazmaca-Hamzalı Fault, KLTF: Kılçak Thrust Fault, STF: Sivritepe Fault, KDF: Kayadibi Fault, BETF: Babas-Termeyenice Fault, YFFZ: Yağbasan-Faraşlı Fault Zone, STFZ: Sivritepe Fault Zone, KFS: Kırıkkale Fault set.

BTF-6, the NAOM is thrusted over the Early to Middle Eocene Karabalçık Formation and its is covered by the latest-Early Miocene to Middle Miocene (MN ?4-6) Çandır Formation where it is displaced by a NW-SE trending normal fault (location e in Figure 6.04)

172

indicating post Middle Eocene and pre-latest-Early Miocene to Middle Miocene activity of this thrust fault.

The Kılçak Thrust Fault (KLTF) is the youngest well-constrained thrust fault observed in the Çankırı Basin. Along the KLTF the NAOM and the Yaylaçayı Formation has been thrusted over the Aquitanian (MN 1-2) Kılçak Formation.

The Yağbasan-Faraşlı and Sivritepe Fault Zones have displaced the rim, the basin in-fill, including the Late Miocene units, and the basement (Figure 6.04) indicating the syn- to post-Late Miocene activity on these faults.

6.3.1.2 Folds

The folds (f1-9) developed in this sub-area (see Figure 6.04) are oriented mainly in a N-S to NNW-SSE direction except f2, which has a curved trace and becomes parallel to the SFZ in the north (Figure 6.04). The folds f1 and f3 trend parallel to the fault BTF-4, which indicates their common tectonic origin. The folds (f5-9) in the north of the YFFZ are sub-parallel to the BTF-6 and trend NNW-SSE to N-S. In addition, the folds f8-9 are overridden by the BTF-6 indicating their sequential development. The folds f4 and 5 are overturned synclines developed within the İncik Formation and associated with progressive unconformities within the İncik Formation and this relation was interpreted as being due to the coupling of thrusting and deposition of the İncik Formation in the post-Middle Eocene to pre Oligocene (discussed in chapter 3). The characteristics of these folds are summarized in Figure (Figure 6.05).

6.3.1.3 Paleostress Inversion

The methodology in collection and analysis of the fault slip data is discussed in chapter 5. Therefore, we refer to chapter 5 for the techniques followed and limitations of these techniques. In order to understand, the kinematic history of this sub-area, 91 out of 105 fault slip data have been analyzed from 17 sites (Figure 6.06). The remaining 14 data were spurious. Therefore they were not used in the construction of final stress tensors. Except the sites 109 and 89 where the data was collected from Aquitanian (MN 1-2) Kılçak Formation and the NAOM respectively. All the other data were collected from Paleocene to Eocene units. The details of the data from each site are given in Table I.

In 7 sites, 2 different sets of overprinting slickenlines and slickenfibres developed in the dilational jogs and 3 different fault movements were observed in the field (Table 1). In ordering of movement sets and deformation phases the procedure discussed in chapter 5 was followed, i.e. first the movement sets were determined based on the stratigraphic units within which the data was collected and using overprinting patterns. Then, preliminary tensors were constructed using both the direct inversion (Angelier 1989) and the automated stress separation procedure (Hardcastle and Hills 1991). The results from each methods were compared and spurious data were sorted out. The procedure was continued iteratively until best-fit tensors were constructed. Finally, the determined movement sets were subsequently grouped into 3 different deformation phases (see chapter 5 for the details of the procedure).

Phase1: Phase one is recognized in only 6 sites (Figure 6.06 and Table II). The orientation of the horizontal stress is relatively consistent in each site and it is oriented ENE-WSW to NNE-SSW, except for sites 109 and 131-2 in which σ_3 is vertical, in all other sites σ_2 and σ_3 are oblique (see Table II).

173

Table 6.01 Kinematic field characteristics of the faults and their hosting units for each site in sub-area 5. Slickenlines/fibre: polished surfaces and growth fibres. # c.c.: number of cross-cutting and/or overprinting sets of kinematic indicators of any type. # phases corresponds to the number of phases of deformation encountered in each site but do not necessarily correspond to the order of phases. The numbers do not necessarily correspond to the order of the deformation phases. NAOM. North Anatolian Ophiolitic Mélange, + present, - absent.

Site	type of indicators	Associated fibres	# of c.c.	Vein	Host unit	# phases
11	Slickenlines/fibre	Calcite	2	-	Karabalçık	2
17	Slickenlines	-	2	-	İncik	2
86	Slickenlines	-	-	-	Mahmatlar	2
89	Slickenlines	-	2	-	NAOM	2
99	Slickenlines	-	-	-	Dizilitaşlar	1
100	Slickenlines/fibre	Calcite	2	+	Kocaçay	2
101	Slickenlines/fibre	Calcite	2	+	Kocaçay	2
102	Slickenlines	-	-	-	Mahmatlar	2
103	Slickenlines	-	-	-	Mahmatlar	1
104	Slickenlines	-	-	-	Mahmatlar	1
105	Slickenlines	-	-	-	Mahmatlar	1
109	Slickenlines/hyd.P.S.	-	2	+	Kılçak	2
111	Slickenlines/hyd.P.S.	-	2		Hacıhalil	2
130	Slickenlines	-	-	-	Hacıhalil	1
131-a	Slickenlines/fibre	Calcite	2	+	Hacıhalil	2
131-b	Slickenlines/fibre	Calcite	2	+	Karabalçık	2
152	Slickenlines/fibre	Calcite	2	+	Karabalçık	2

The orientation of the sub-area based mean regional stresses are as follows $\sigma_1=023°N/01°$, $\sigma_2=116°N/64°$, $\sigma_3=293°N/26$, and the stress ratio (Φ) = 0.373 (Figure 6.07 and Table II). The youngest unit which has been deformed in this phase is the MN-1 Kılçak Formation. Therefore, deformation phase-1 postdates the deposition of the Kılçak Formation in the Aquitanian (MN 1–2 in MN zones, Figure 6.03). The approximately, sub vertical orientation of the σ_2 and oblique orientation of the σ_3 indicates transpressional deformation in the deformation phase-1.

174
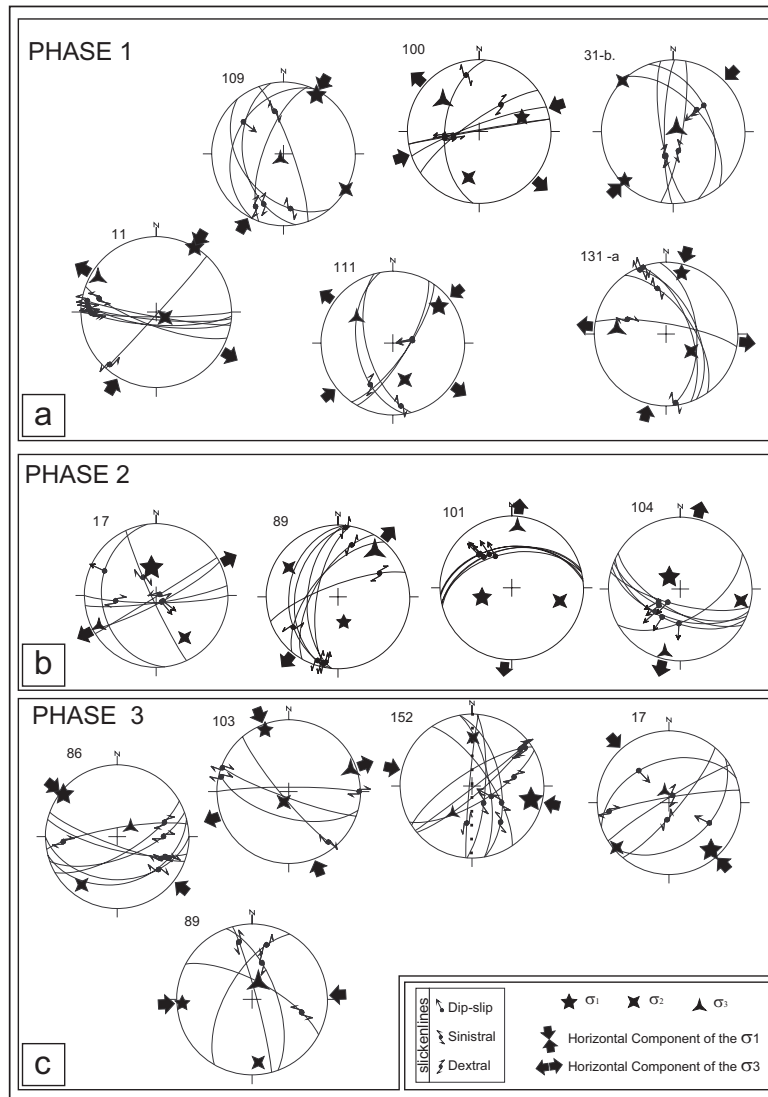
Figure 6.06 Plots of faults planes, slickenlines, and stress orientations for each site in sub-area 5 (lower hemisphere, equal area projection).

Phase 2: This phase was recognized in 4 sites (Figure 6.6). In all of the sites σ_1 is sub vertical and σ_3 is sub horizontal and σ_2 is oblique (Figure 6.06 and Table II). The orientation of the mean regional stresses are oriented $\sigma_1=303°N/67°$, $\sigma_2=075°N/16°$, $\sigma_3=170°N/17$ and $\Phi=0.325$ (Figure 6.07 and Table II). The sub vertical orientation of σ_1

175

and approximately sub horizontal orientation of the other principal stress indicate a dominantly extensional deformation.

PHASE	σ_1	σ_2	σ_3	ϕ
1	023/01	116/64	113/13	0.373
2	303/67	075/16	017/25	0.325
3	150/24	300/64	228/62	0.265
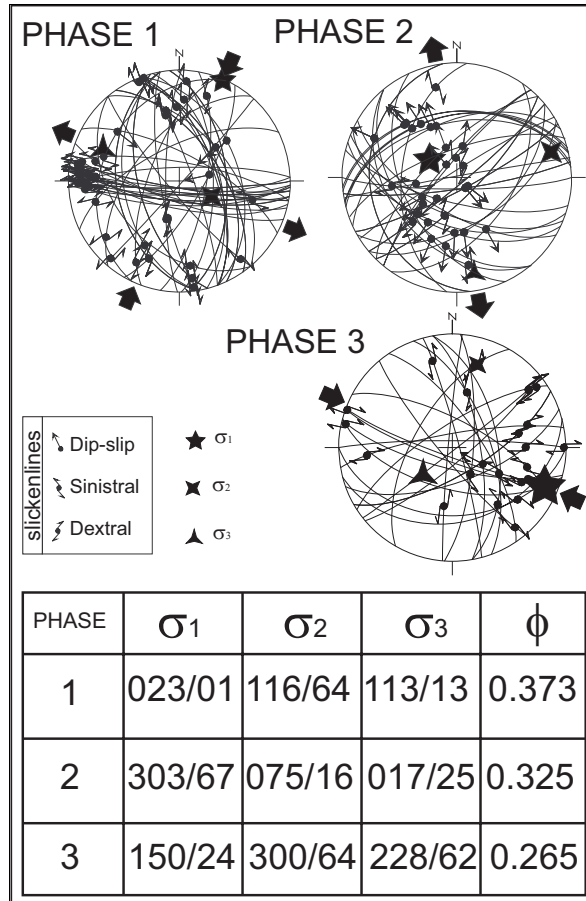
Figure 6.07 Plots of fault planes, slickenlines and stress orientations for the whole data, in sub-area 5, for each deformation phase.

Phase 3: Only 5 sites had sufficient data for the construction of site based stress tensors (Figure 6.06 and Table II). The horizontal component of the σ_1 was relatively consistent and is oriented E-W to NNW-SSE. Except for site-103 where σ_2 is sub vertical, in the other sites, σ_3 is sub vertical. The mean stresses for the sub-area are σ_1=113°N/13°, σ_2=017°N/25°, and σ_3=228°N/62° and the stress ration is Φ=0.265 (Figure 6.07). Having the regional σ_3 sub vertical, σ_2 oblique and σ_1 horizontal indicates transpression in this sub-area.

176

Table 6.02 Orientations of principal stresses and stress ratios for each site in the sub area 5.

	SITE	σ_1	σ_2	σ_3	ϕ
PHASE 1	11	031/00	121/79	301/11	0.509
	100	071/37	193/35	311/34	0.72
	109	029/07	119/00	211/84	0.385
	111	051/19	162/46	305/38	0.402
	131-a	014/13	124/55	276/32	0.639
	131-b	225/05	315/00	046/85	0.783
PHASE 2	17	350/58	146/30	242/11	0.176
	89	167/61	301/21	039/19	0.830
	101	252/54	105/31	005/16	0.465
	104	318/71	101/15	194/11	0.317
PHASE 3	17	138/13	229/05	339/76	0.245
	86	308/05	216/18	054/71	0.317
	89	267/08	174/17	021/71	0.84
	103	339/09	206/77	70/09	0.659
	152	103/17	001/33	216/52	0.147

6.3.2 Sub-area 6

6.3.2.1 Faults

The main structures shaping sub-area 6 (Figure 6.08) are the Yağbasan-Faraşlı Fault Zone (YFFZ), generally N-S to NE-SW oriented normal faults with sinistral components, the Halaçlı Fault (HTF), and the Kızılırmak Fault Zone (KFZ).

The YFFZ extends from the sub-area 5 and in this sub-area it has strike-slip fault with a normal component sense of movement as indicated by the slickenlines and slickenfibres developed in the dilational jogs.

The Halaçlı Fault (HTF) is observed in the NE corner of the sub-area. Along the HTF the Oligocene Gǔvendik Formation tectonically overlies the latest-Early Miocene to Middle Miocene (MN ?4-6) Çandır Formation. It is displaced more than 7 km dextrally by one of the faults within the Kızılırmak Fault Zone (Figure 6.08). Based on this information it can be concluded that the HTF postdates the deposition of the Çandır Formation in latest-Early Miocene to Middle Miocene and predates the Kızılırmak Fault Zone.

Along the N-S and NE-SW oriented faults (Figure 6.08), to the north of the YFFZ, the Sulakyurt Granite, Kocaçay, İncik, and Çandır Formations are displaced dominantly in normal sense with slight lateral components. In the north these faults are covered by the MN-13 Sǔleymanlı Formation and further in the north some of these faults are partly delimited by the Kızılırmak Fault Zone. As discussed in chapters 2 and 5, these faults were normal faults during the deposition of the Çandır Formation in MN ?4-6 period and later they were inverted into reverse faults in post-MN-13 times.

The Kızılırmak Fault Zone, in this part of the Çankırı Basin, is characterized by NE-SW oriented strike-slip faults with normal component (see chapter 2) that have displaced the HTF, MN-13 Sűleymanlı and Bozkır Formations which indicates post-MN 13 activity of the Fault.
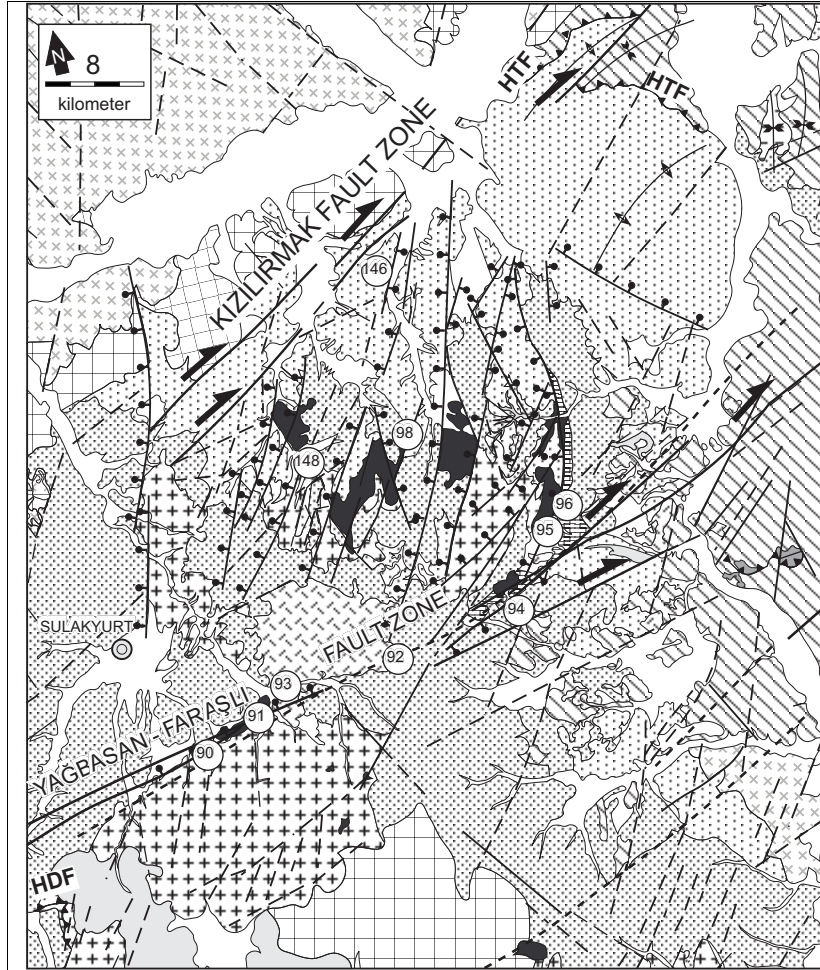
Figure 6.08 Geological and sample location (site) map for sub-area 6 (see Figure 6.04 for the description of the units).

6.3.2.2 Paleostress Inversion

From 10 sites, 43 fault slip data have been collected and 43 of them were used in the analyses. In 5 of the sites overprinting slickenlines were observed that are indicative of 2 different phases of fault movements. Ordering of the deformation phases was based on the overprinting relationships, the automated separation procedure (Hardcastle and Hills

178

1991) and correlation with the other sub-areas (see chapter 5 for the methodology). The details of the sites are given in the Table III.

Phase 1. Only 2 of the sites had enough slip data for the inversion procedure. The orientation of the site-based tensors is given in Table IV and Figure 6.09. The orientation of the sub-area based regional stresses are as follows: $\sigma_1=056°N/10°$, $\sigma_2=255°N/80°$, and $\sigma_3=147°N/03°$ and the stress ratio is $\Phi=0.600$ (Figure 6.10 and Table IV). Having σ_1 and σ_3 sub horizontal and σ_2 sub vertical in this phase indicates transcurrent deformation in this part of the basin during the deformation phase 1.

Table 6.03 Kinematic field characteristics for the sites in the sub-area 6 (the legend is same as Table 6.01)

Site	type indicators	Assoc. fibres	# of move.	Vein	unit	# phases
90	Slickenlines	-	1	-	Sulakyurt Granite	1
92	Slickenlines	-	1	-	Sulakyurt Granite	1
94	Slickenlines		1		İncik	1
95	Slickenlines		1	-	İncik	1
98	Slickenlines		1		İncik	1
146	Slickenlines/fibre	Calcite	2	y	Çandır	2
148	Slickenlines/fibre	Calcite	2	y	İncik	2

Phase 2: This deformation phase was recognized in only 3 sites (Figure 6.09). The orientations of the principal stresses are consistent. In each site σ_3 is sub horizontal and σ_1 is sub vertical. The orientation of regional stresses are as follows: $\sigma_1=180°N/59°$, $\sigma_2=357°N/31°$, $\sigma_3=088°N/01°$, and the stress ratio is $\Phi= 0,454$ (Figure 6.10 and Table IV) and indicate oblique-extensional deformation (transtension) in the area during this phase.

Phase 3: Only 2 sites had enough slip data for the construction of site based stress tensors. The orientations of the principal stresses are given in Figure 6.09 and Table IV. The orientation of the regional principal stress are: $\sigma_1=123°N/39°$, $\sigma_2=308°N/51°$, $\sigma_3=041°N/02°$, and the stress ratio is $\Phi=0.666$ (Figure 6d and Table IV). Having σ_1 and σ_2 oblique and horizontal σ_3 indicates oblique extension (transtension) in this part of the basin in deformation phase 3.

6.3.3 Sub-area 7

6.3.3.1 Faults

The main structures in the sub-area 7 (Figure 6.11) are the Uğurludağ Thrust faults (UTF 1-4), the Tuğcu Faults (TGF 1 and 2), the Sağpazar Reverse Fault (SRF), the

179

Karaçay Reverse Fault (KARF), the Gűvendik Thrust Fault (GTF), the Sungurlu Fault Zone and its main strand (MSFZ), the Gűvendik Folds (GF) and the Sağpazar Anticline (SA) (Figure 6.11).
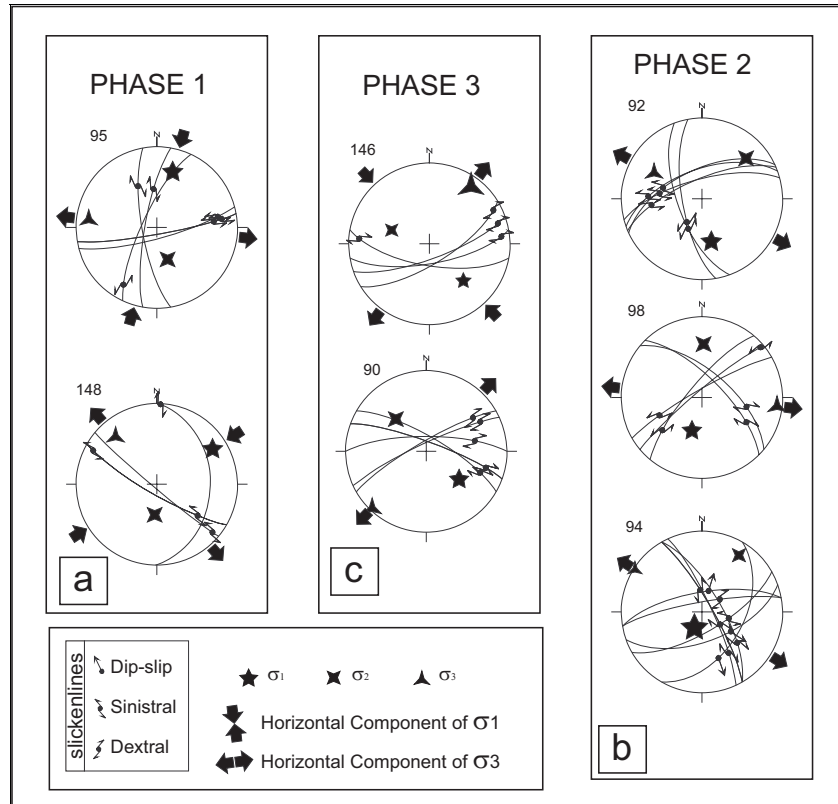
Figure 6.09 Plots of faults planes, slickenlines, and stress orientations for each site in sub-area 6 (lower hemisphere, equal area projection).

Some of these structures namely SRF, KARF, GTF, and MSFZ are explained in chapter 4; therefore, they will be only described briefly in this chapter. The basic characteristics and their tectonic implications are summarized in Figure 6.12.

The Uğurludağ Thrust Faults (UTF 1, UTF 2, UTF 3, and UTF 4) are the most prominent structures in this sub-area. Along the UTF's the NAOM and associated Late Cretaceous units are thrusted over most of the Early to Middle Eocene units namely the Yoncalı, Karabalçık, Bayat and Osmankahya Formations (Figures 6.11, 6.12). This relation indicates post-Middle Eocene activity of these faults. The UTF's are displaced dextrally by a number of NE-SW oriented faults and, therefore, the primary relation between individual UTF's were obliterated. Among these, the UTF 1 is a reverse fault with dextral strike-slip component. The kinematic characteristics of the other UTF's, namely UTF 2 and UTF 3, could not be constrained precisely.

180

PHASE 1 **PHASE 2**

PHASE 3

slickenlines			σ₁	σ₂	σ₃

PHASE	σ_1	σ_2	σ_3	ϕ
1	056/10	255/80	147/03	0.600
2	180/59	357/31	088/01	0.454
3	123/39	308/51	041/02	0.666
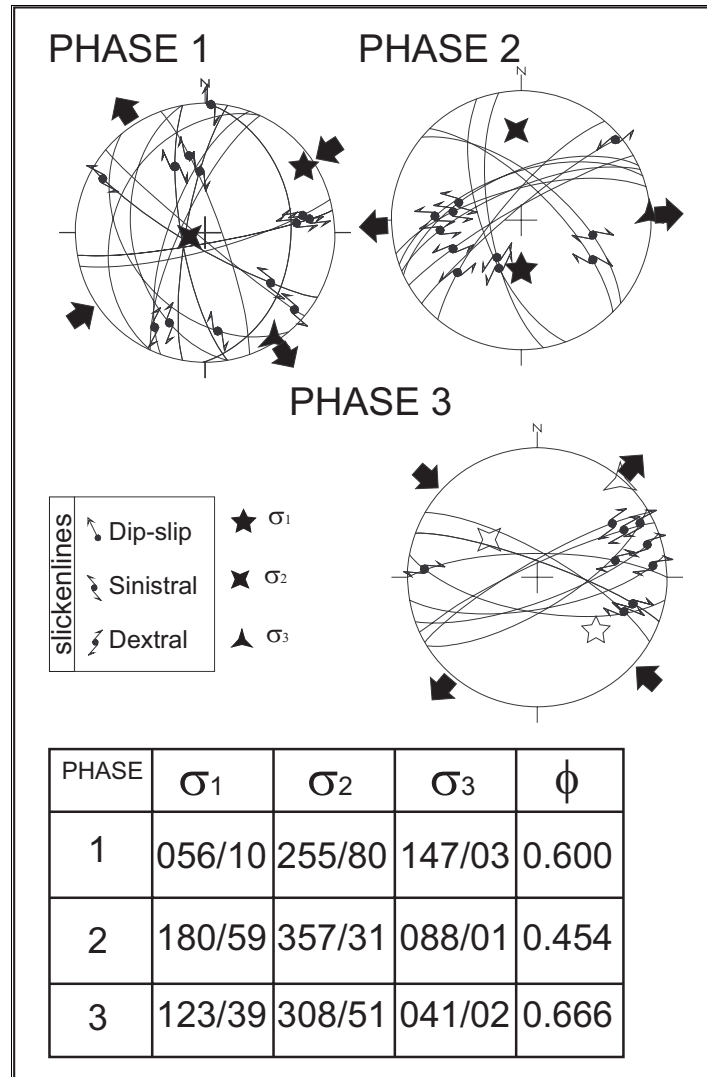
Figure 6.10 Plots of fault planes, slickenlines and stress orientations for the whole data, in sub-area 6, for each deformation phase (lower hemisphere, equal area projection).

Along the TGF-1 and TGF-2 (Tuğcu Faults), in the locations *a* and *b* to the NE of the site-148, the NAOM has been thrusted over the Çandır Formation (Figure 6.11). In the location *c* along the TGF-3, the NAOM is thrusted over the Karabalçık Formation from NE to NW and the Çandır Formation covers the thrust contact. This relation indicates that TGF-3 postdates the Early to Middle Eocene Karabalçık Formation and predates the Middle Miocene (MN 4?-6) Çandır Formation.

181

Table 6.04 Orientation of principal stresses and stress ratios for each site in the sub-area 6.

	SITE	σ_1	σ_2	σ_3	ϕ
PHASE1	95	016/29	161/56	277/16	0.458
	148	058/20	184/59	319/23	0.479
PHASE 2	92	167/45	048/27	298/33	0.457
	94	206/73	033/17	302/02	0.126
	98	197/55	002/34	097/07	0.529
PHASE 3	90	130/46	317/44	224/03	0.537
	146	137/38	290/49	036/14	0.929

The Karaçay Fault (KARF) is an NNE-SSW oriented fault along which the Kocaçay Formation is thrusted over the İncik Formation and the thrust fault contact is covered by the Çandır Formation in the south (location d in Figure 6.11) and by the Tuğlu Formation in the north (location e in Figure 6.11). This relation indicates that the thrusting predates the deposition of the Çandır Formation in the latest-Early Miocene to Middle Miocene (MN ?4-6) (see also chapter 4).

The Sağpazar Reverse Fault (SRF, Figure 6.11) is observed between the overlying İncik and the underlying Bozkır Formation. This relationship implies that the SRF postdates the deposition of the Bozkır Formation in latest-Late Miocene (MN-13) to Pliocene (see also chapter 4).

The Sungurlu Fault Zone is one of the largest structures, not only in the study area, but also in north Central Anatolia (Figure 6.01). It is distributed over much of the study area and characterized by a number of generally NE-SW striking faults that displace most of the above structures as well as the Late Miocene and Plio-Quaternary units (Deyim Formation). Along the Master strand of the Sungurlu Fault Zone (MSFZ) the Gűvendik Syncline (GS) is rotated anticlockwise together with the KARF implying a sinistral activity on the Sungurlu Fault Zone, after the deposition of the Gűvendik formation, in the Oligocene (this is discussed later and in chapters 4 and 7). Along the sub branches of the Sungurlu Fault Zone, the Gűvendik Syncline (GS), the Karaçay Folds, the GTF's and the UTF's were displaced dextrally. The youngest dextrally displaced unit is the MN 13 Bozkır Formation. These relationships indicate that the Sungurlu Fault has been active since MN 13 with a dextral sense of slip (see also chapter 4).

6.3.3.2 Folds

The Gűvendik Syncline (GS) is developed within the post-Middle Eocene to Oligocene İncik and the Oligocene Gűvendik formation. It is overlain by the MN ?4-6 Çandır Formation (see f-g in Figure 6.11). This relation indicates the post-Oligocene and pre-latest Miocene tyo Middle Miocene development of the GS after the Gűvendik formation and before the deposition of the Çandır Formation.

A number of folds are observed parallel to the Güvendik Syncline to the north of site-70. They are developed within the Incik and Güvendik formations indicating their syn- to post-Oligocene development. In the NW part of the sub-area they are covered by the Çandır and Tuğlu formations indicating their pre-Middle Miocene development (Figure 6.11).

Figure 6.11 Geological and sample location (site) map of the sub-area 7 (see Figure 6.04 for the description of the units).

183

The N-S trending Karaçay Folds that are located around sites 148-150 are developed within the Tuğlu Formation, which indicates their post-Tortonian (MN 10-12) development and approximately E-W compression (see Figure 6.12 and chapter 4).

The f11-13 folds that developed in the SE corner of the sub-area 7, formed in the Incik and Güvendik formations indicating their post-Oligocene origin.

6.3.3.3 Paleostress Inversion

From 15 sites, 132 fault slip data were obtained in the field and 116 of them were useful for the construction of final paleostress tensors and 16 of them were spurious. Good results were obtained in the Yoncalı Formation, in the sites 76 to 125 (Figure 6.11), where 3 distinct set of fibrous calcite overgrowth patterns were observed. The kinematic characteristics of each site in sub-area 7 are summarized in Table V. The oldest set of calcite fibres indicated a sinistral sense of movement for the NE-SW to E-W striking faults. The second set, which overprints the above-mentioned sinistral set, generally has a normal sense of slip and the latest set, which overprints all the other sets, has a dextral sense of slip. In addition to the calcite overgrowth patterns, using the procedure discussed in chapter 5, these movements consequently were assigned to deformation phases.

Table 6.05 Kinematic field characteristics for the sites in the sub-area 7. Hyd.P.S. hysdroplastic slickensides (legend is same as Table 6.01)

Site	type indicators	Assoc. fibres	# of move.	Vein	unit	# phases
76	Slickenlines/fibre	calcite	3	+	Yoncalı	3
120	Slickenlines/fibre	calcite	3	+	Yoncalı	3
121	Slickenlines/fibre	calcite	3	+	İncik	3
122-A	Slickenlines/fibre	calcite	3	+	Yoncalı	3
122-B	Slickenlines/fibre	calcite	3	+	Yoncalı	3
124	Slickenlines/fibre	calcite	3	+	Yoncalı	3
125	Slickenlines/fibre	calcite	3	+	Yoncalı	3
132	Slickenlines /hyd.P.S.	calcite	2	+	Osmankahya	2
148-A	Slickenlines/fibre	calcite	2	+	Yoncalı	2
148-B	Slickenlines/fibre	calcite	2	+	Çandır	2
149	Slickenlines	-	2	-	Tuğlu	2
150	Slickenlines	-	2	-	Tuğlu	2
151	Slickenlines/fibre	calcite	2	+	Candır	2

Phase 1. Only 6 sites had sufficient data for the construction of site based stress tensors (Figure 6.13 and Table VI). The orientations of the principal stresses are relatively consistent. In all except site-125, σ_2 is sub vertical, σ_1 and σ_3 are sub horizontal. σ_1 varies

between NNW-SSE to NE-SW. The orientation of the regional stresses are: σ_1=199°N/03°, σ_2=306°N/80°, σ_3=109°N/10°, and the stress ratio Φ=0.336 (Figure 6.14) and indicates a strike-slip deformation in this phase. Having σ_1 oriented NNE-SSW indicates that the NE-SW oriented faults, in this sub-area, would be sinistral in nature (as reflected in the slip data) in this phase.

Table 6.06 Orientation of principal stresses and stress ratios for the sites in the sub-area 7

	SITE	σ1	σ2	σ3	Φ
PHASE 1	76	013/18	253/57	112/27	0.262
	120	195/04	356/86	105/01	0.508
	122-A	172/14	333/75	081/05	0.492
	122-B	174/17	335/72	081/06	0.434
	125	205/02	296/33	112/57	0.386
	150	042/02	137/69	311/21	0.263
PHASE 2	120	324/62	118/26	213/11	0.986
	121	086/86	287/03	197/01	0.271
	121	186/69	328/26	066/17	0.338
	132	355/73	107/06	199/15	0.325
PHASE 3	76	107/14	303/75	198/04	0.252
	124	111/23	294/67	201/01	0.719
	148-A	271/13	014/44	169/43	0.514
	148-B	103/27	221/42	351/36	0.249
	149	142/29	349/58	239/12	0.385
	151	087/27	266/63	356/00	0.548

Phase 2. For this phase, only 4 of the sites had sufficient data for the construction of site based stress tensors (Figure 6.13). In all sites, σ_1 is sub vertical, σ_2, and σ_3 are sub horizontal and vary between WNW-ESE to NW-SE and NNE-SSW to NE-SW, respectively (Table VI). All the results are consistent with each other. Orientation of the regional stress are as follows: σ_1=080°N/77°, σ_2=299°N/10°, σ_3=207°N/08° and the stress ratio Φ=0.635 (Figure 6.14). The sub vertical nature of σ_1 indicates an extensional deformation (NNE-SSW) during this phase.

Phase 3. For this phase, 6 sites had sufficient data for the construction of the site based stress tensors (Figure 6.13). Except for site 148-A where σ_2 are σ_3 are oblique, all sites are consistent with each other and with the sub-area based regional stress tensor in which σ_2 is sub vertical σ_1 and σ_3 are sub horizontal (Figure 6.14 and Table VI). The orientation of the regional stresses are as follows: σ_1=100°N/23°, σ_2=285°N/67°, σ_3=191°N/02°, and the stress ratio Φ=0.377 (Figure 6.14) and indicates a strike-slip deformation during this phase. Having σ_2 sub vertical, σ_1 and σ_3 sub horizontal and approximately E-W oriented σ_1 indicates that the NE-SW faults would be dextral in nature in this phase as reflected in the fault slip data.

FAULTS							
Faults	hanging wall Formations	foot wall Formations	covering or youngest effected Form.	dip range of the fault plane	Possible age range	DEFORM. STYLE	AGE
NE-SW faults	Tuğlu& Süleymanlı	Tuğlu& Süleymanlı	Tuğlu& Süleymanlı	60°-90°	syn-to post Late Miocene	TRANSCURRENT	TORTONIAN TO RECENT
SRF	İncik	Süleymanl	Tuğlu& Süleymanlı	70°-90°	post-Late Miocene		
UTF 1&2	NAOM, Yalaçayı Osmankahya	Yoncalı Karabalçık Osmankahya	Yoncalı Karabalçık Osmankahya	20°-60°	Early to Middle Eocene to recent		
UTF 3	NAOM, Yalaçayı, Yapraklı	Yoncalı Çandır	Yoncalı Çandır	60°	post-Middle Mioecne	TRANSPRESSION	PRE-MIDDLE MIOCENE
TGF 1	NAOM	Karabalçık	Çandır	60°-90°	syn- to Post-Middle Eocene, pre-Middle Miocene		
TGF 2	Dizilitaşlar	Yoncalı, Karabalçık	Yoncalı, Karabalçık	60°-90°			
TGF 3	NAOM, Yalaçayı, Yapraklı	Karabalçık	Çandır	70°-90°	Middle Eocene, pre-Middle Miocene		
KARF	Kocaçay	İncikı	Çandır& Tuğlu	80°	post-Middle Eocene pre-Middle Miocene		
GTF	NAOM	Gûvendik	Gûvendik	30°-50°	post-mid-Oligocene pre-Middle Miocene		

FOLDS					
FOLDS	youngest folded unit	Covering unit	dıp range of axıal plane	possible Compression direction	Age range
GS	İncik Gûvendik	Çandır	30°-70° (asymmetric)	WNW-ESE (NE-SW*)	syn- to post-mid-Oligocene pre-Middle Miocene
GA	İncik	Süleymanlı	60°-80° (asymmetric)	WNW-ESE (NE-SW*)	
SA	Tuğlu	Deyim	80° (asymmetric)	E-W	post-Tortonian (MN10-12)
Karaçay folds	Tuğlu		80°-90°	E-W	

Figure 6.12 Figure illustrating the structural characteristics, possible age ranges of the folds and faults developed in the sub-area 7. SRF: Sağpazar Reverse Fault, UTF: Uğurludağ Thrust Faults, TGF: Tuğcu Faults, KARF: Karaçay Reverse Fault, GTF: Gûvendik Thrust Fault, GS: Gûvendik Syncline, GA: Gûvendik Anticline, SA: Sağpazar Anticline.
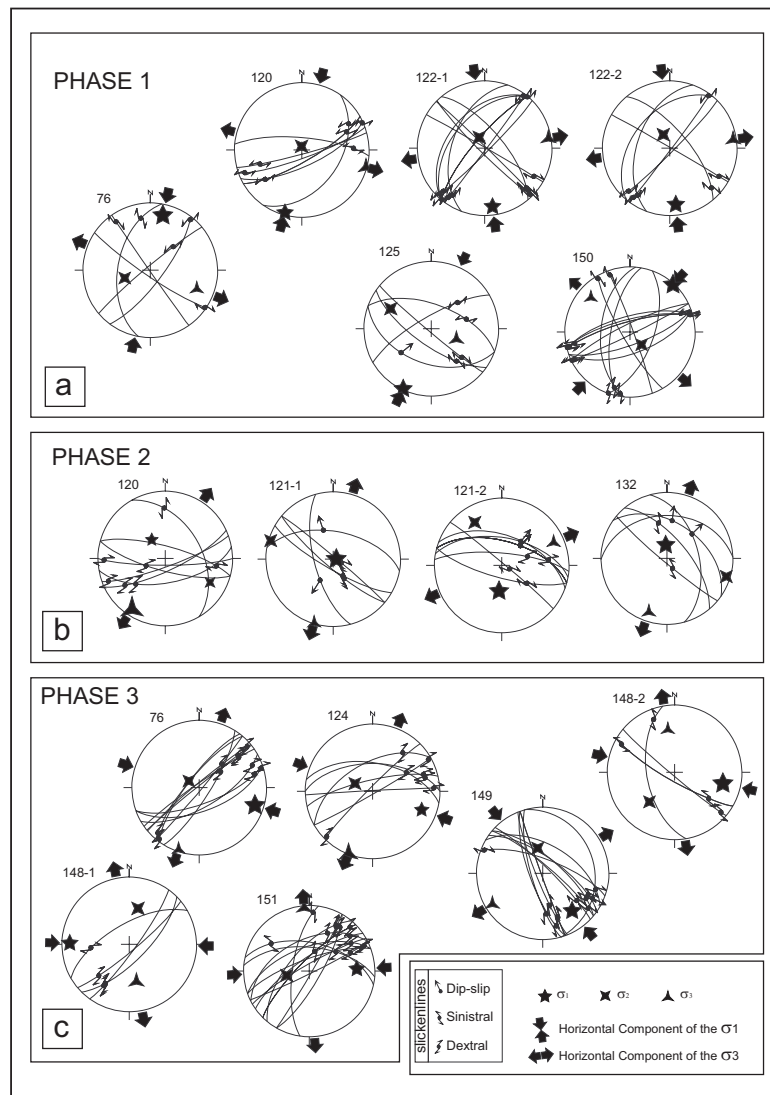
Figure 6.13 Plots of faults planes, slickenlines, and stress orientations for each site in sub-area 7 (lower hemisphere, equal area projection).

PHASE	σ_1	σ_2	σ_3	ϕ
1	199/03	306/80	109/10	0.336
2	080/77	299/10	207/08	0.635
3	100/23	285/67	191/02	0.377
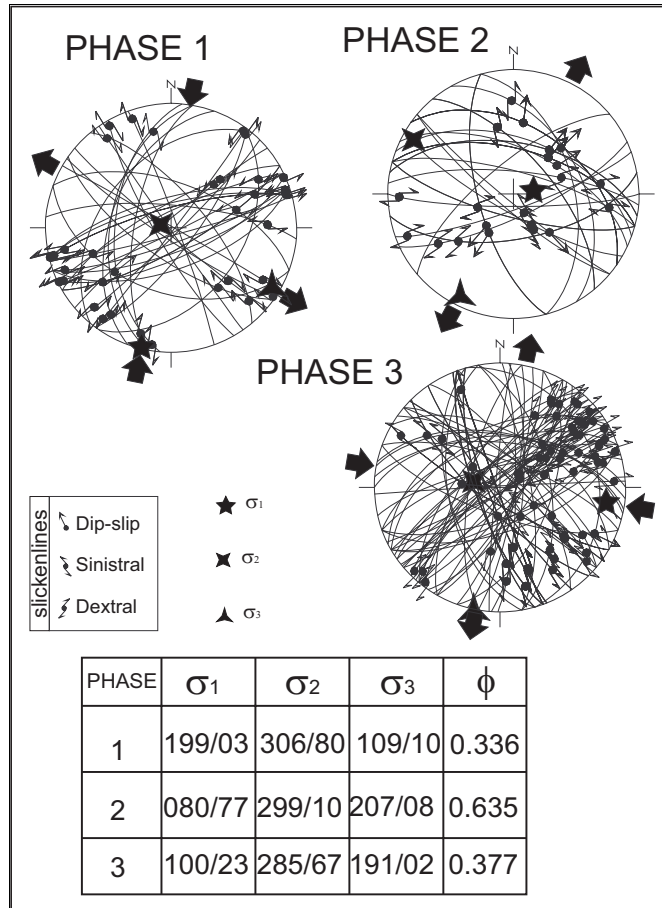
Figure 6.14 Plots of fault planes, slickenlines and stress orientations for the whole data, in sub-area 7, for each deformation phase.

6.4 Discussion

6.4.1 Temporal Relationships

The temporal relationships of the structures developed in the southern part of the Çankırı Basin are summarized in Figures 6.05 and 6.12. Two different compression phases (deformation phases 1 and 3) separated by an extensional period (deformation phase 2) have been determined using the cross-cutting relationships and covering of structures with the younger units.

188

The crosscutting relationships of the faults STF, KDF, BETF, KFZ, YFFZ, KFS, NE-SW oriented faults, SRF, and UTF1 and UTF2 indicate regional transcurrent tectonics characterized by a transpressional and/or a transtensional component in the post-Middle Miocene. Based on the cross-cutting relationships and deformation styles of the Neogene units, discussed in chapter 4, the beginning of the regional transcurrent tectonics is circa Tortonian (MN 10-12, which corresponds approximately to 9.7 to 6.6 Ma).

The thrust faults and folds covered by the Çandır Formation (mentioned above and illustrated in Figures 6.05 and 6.12) indicate a compressional tectonic regime prior to the regional transcurrent tectonics. The temporal relationships of some of these structures (Figure 6.05 and 6.12) indicated that the orientation of the σ_1 in the earlier compressional regime is WNW-ESE and of pre-latest-Early Miocene to Middle Miocene age. The growth fault patterns observed within the latest-Early Miocene to Middle Miocene (MN ?4-6) Çandır Formation, in the seismic sections (see chapter 2) and Neogene deformation styles discussed in chapter 4 also supports that earlier compressional phase was ended prior to the deposition of the Çandır Formation.

In addition to the above, growth fault patterns, as discussed in chapters 2 and 4, displacement of thrust faults by normal faults and inversion of some of these growth faults indicate that earlier compressional regime (deformation phase-1) was replaced by an extensional regime (deformation phase-2) in latest-Early Miocene to Middle Miocene (MN ?4-6, which corresponds approximately to 18.0 to13.5 Ma), which, in turn, was replaced (in the Late Miocene) by a new compressional regime and which was characterized by regional transcurrent tectonics (deformation phase-3) (see Figures 6.05, 6.12, and chapters 2,4 and 5).

6.4.2 Comparison of the Sub-areas

Phase 1: The horizontal component of the σ_1 varies from NNE-SSW to NE-SW in which the maximum deviation is between sub-area 6 and 7 and is 46° (Figure 6.15b). The σ_2 is sub vertical in each sub-area. Like the major stress (σ_1), σ_3 is also sub horizontal and the maximum angular divergence between the horizontal components of σ_3 is between Sub-area 5 and 6 and is 33°. Having σ_2 sub vertical in all sub-areas indicates transcurrent deformation in the region (Figure 6.15b).

Paleomagnetic results discussed in the chapter 7 have revealed that the western (33.4°) and southeastern parts (36° and 27°) of the Çankırı Basin has rotated anticlockwise and the eastern margin (52°) has rotated clockwise in the Early to Middle Eocene and the post-Late Eocene to Oligocene. The paleomagnetic declinations are illustrated in Figure 6.15a. Because, deformation phase 1 is thought to have occurred in the time range between the Early to Middle Eocene to pre-latest-Early Miocene (pre-Burdigalian), the paleostress data for this phase is restored according to the closest declination data (Figure 6.15c). Therefore, the regional stress for the sub-area 5 is rotated 33.4° clockwise (Figure 6.15c). There is almost no rotation in the central part of the Çankırı Basin (i.e. sub-area 6); therefore, no restoration was performed for this sub-area for deformation phase 1. The paleostress data for sub-area 7 was collected from south of the YFFZ. Therefore, the regional stresses for this sub-area were rotated 31.5° clockwise (Figure 6.15c), which is the average of the Eocene and Oligocene paleomagnetic declination data from south of the YFFZ (Figure 6.15a). Maximum angular divergence between σ_1 orientations between the sub-areas after back rotation become 76°.

189
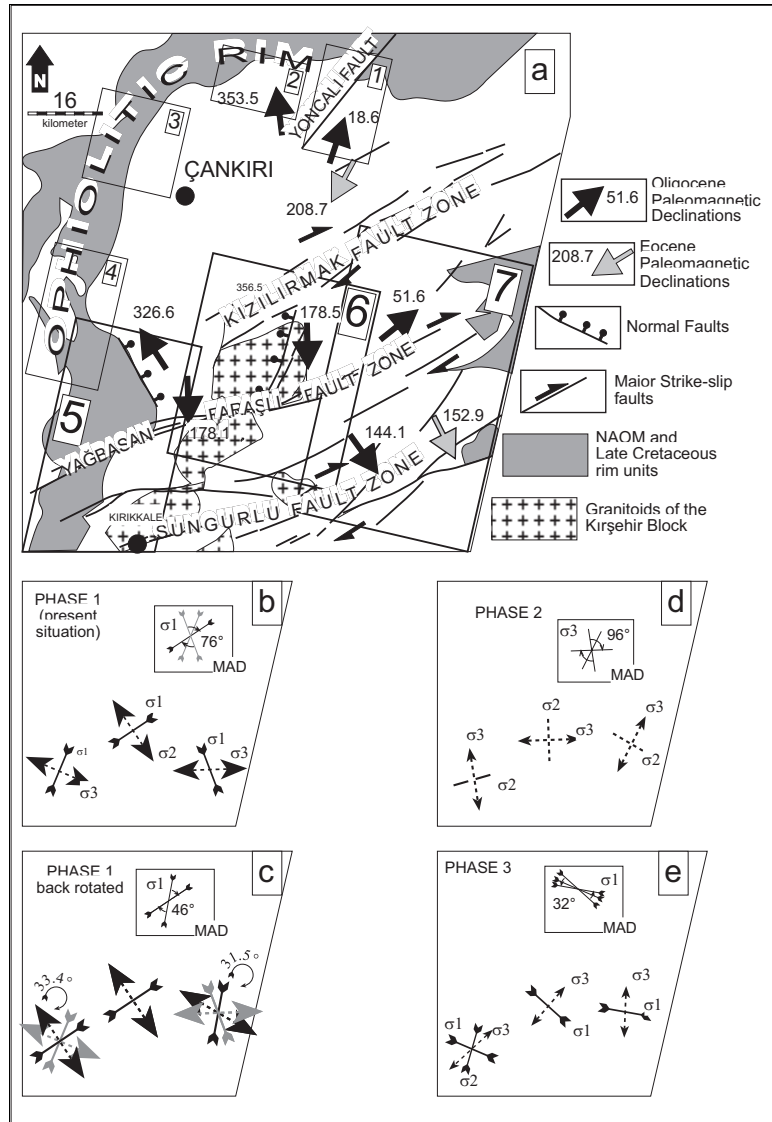
Figure 6.15 a) Simplified geological map illustrating the amount and orientations of paleodeclinatios (discussed in chapter 7). b, d and e) Present day horizontal component of the principal stress for each deformation phase. c) Back rotated (rotation amounts are indicated) horizontal components of the principal stresses for the deformation phase 1 (present day orientations are in gray). MAD: Maximum angular divergence between the stresses between sub areas.

Phase 2: This is a poor data set, but in all sub-areas, σ_1 is sub vertical. However, the horizontal component of σ_3 varies by as much as 96° (Figure 6.15d). Maximum deviation is between the Sub-area 5 and 6. Maximum angular divergence of σ_2 is between the sub-areas 5 and 7 and it is 123°. Having σ_1 sub vertical and σ_3 horizontal in each sub-area indicates extensional deformation during this phase (Figure 6.15d).

Phase 3: In this phase (Figure 6.15e) σ_1 is oblique in all the sub-areas and the other stresses are variable between the sub-areas. In sub-areas 6 and 7, σ_2 is sub vertical while σ_3 is horizontal. However, in sub-area 5, σ_3 is sub vertical while σ_2 is oblique. Maximum angular divergence in the horizontal component of σ_1 is 32° (Figure 6.15e). Maximum angular divergence between the horizontal components of the σ_3 is 46°. Having σ_1 oblique in all sub-areas and the variation in the orientation of σ_2 and σ_3 between sub-areas such that σ_3 becomes sub vertical in sub-area 5 where the NE-SW oriented strike-slip faults, namely YFZ, STFZ, STFS have reverse components, while in the other sub-areas sub vertical σ2 indicates that the faults change their character from transpressional to transtensional from west (sub-area 5) to east (mainly sub-area 6) as their strikes change from NE-SW to E-W. This means that these faults forms a restraining single bend in the sub-area 5 (see Figures 6.02, 6.06 and 6.08).

6.4.3 Stress Trajectories

Stress trajectories are the representation of the variation in the pattern of the stresses in three dimensions. Mandle (1987) has discussed the existence and continuity of principal planes of stres, axes of which are the principal stresses (σ_1,σ_2, and σ_3). Treagus and Lisle (1997) have discussed and mathematically proved that planes of principal stresses are present and they are continuous if one of the principal stresses is constantly oriented which means that the variation occurs only in two dimensions.

In relation to the Çankırı Basin, smoothed trajectories for the southern part have been plotted using the constructed paleostress orientations discussed above (Figure 6.16). In plotting the trajectories, various combinations and patterns are possible. However, during plotting of the trajectories, the smoothest pattern was aimed at bearing in mind that a trajectory of the one stress cannot cross another. In this way, the number of possibilities for trajectory patterns is decreased.

6.4.3.1 Stress Trajectories for the Southern Part of the Çankırı Basin

Only one configuration of the smoothed stress trajectories is possible (Figure 6.16 and b) for the deformation phases 1 and 3. The stress trajectories of these phases (phases 1 and 3) display a somewhat similar pattern in which the σ_1 trajectories are oriented NE-SW and they tend to diverge south-westwards while σ_3 are circular and convex south-westwards. However, for deformation phase 2, two different patterns of stress trajectories are possible (Figure 6.16c and d). In both patterns, the pattern of σ_2 is the same but σ_3 patterns vary. This is discussed in the next section.

6.4.3.2 Integration of Stress Trajectories for the Whole Çankırı Basin

Phase 3 Trajectories of the horizontal components of σ_1 and σ_3 for the last phase of deformation display a mesh like pattern in which the σ_1 trajectory is oriented approximately WNW-ESE and the σ_3 trajectories are oriented approximately NNE-SSW (Figure 6.17a). As discussed previously, in the sub-area 5, σ_3 is sub vertical while in other sub-areas, both

in the north and the south, σ_2 is vertical or sub vertical. Sub-area 5 is located within an area where NE-SW oriented strike-slip faults, namely YFFZ, STFZ, KFS change their strike. They strike at a high angle to the σ_1 orientations and have a reverse component in this sub-area (Figure 6.18a).

The rose diagrams prepared from the lineaments of the Çankırı Basin display a riedel pattern (as discussed in chapter 2). The Kızılırmak, Sungurlu, Yağbasan-Faraşlı and Sivritepe Fault Zones are 30°-45° to σ_1 (Figure 6.18a). Therefore, they constitute the y-shear (Figure 6.18b). The faults that define the western margin of the Çankırı Basin (Eldivan Fault Zone-EFZ) make an angle of approximately 75° with σ_1 (f in Figure 6.18b) and the inverted growth faults are approximately perpendicular to σ_1 (Figure 6.18a). Therefore, it is likely that the growth faults were inverted (as discussed in chapter 2). Since this phase is characterized by transcurrent tectonics, these faults may have sinistral lateral components which are indirectly indicated by the slickenlines belonging to the last phase that are close to these structures and have lateral components. In addition, it is most likely that the mechanical properties of the basement, the basin in-fill and the basin rim will be different. However, the constructed stress trajectories are not deflected by the interfaces between basement, in-fill and the basin rim. This relation implies that the pre-existing structures and material properties have not played a major role in the orientation of the principal stresses. Near Sivritepe, and north of it, the angle between STF and YFFZ and the σ_1 trajectories increases. As previously mentioned, the fault zones in this are have a transpressional character (Figure 6.18a and c). The σ_1 trajectories are also perpendicular to the Sağpazar Anticline (SA) and the Karaçay folds (Figure 6.18a) which are parallel to the expected compressional structures in a riedel system (f in Figure 6.18b).

The orientations of the σ_1 patterns are compatible with the present day stress pattern of north central Anatolia (discussed in chapter 4). The Sungurlu Fault Zone and the Kızılırmak Fault Zones are the two splays of the North Anatolian Fault Zone (Figure 6.01) which transferred transcurrent deformation into the Çankırı Basin area and displaced its rim, basement and the in-fill. The structures associated with this phase are also formed in post-Middle Miocene rocks, implying it has been active since the middle of the Tortonian (i.e. MN 10-12, which corresponds to 9.7 to 6.6 Ma)

Phase 2. Like phase 3, in the construction of the stress trajectories for this phase, the paleostress data from the chapter 5 were also used. As discussed above, phase 2 for this chapter corresponds to the phase 3 of previous chapter (5). One of the two constructed smoothed σ_3 trajectories for the southern part of the Çankırı Basin do not match with the trajectories of the northern area (Figure 6.17b). The compatible pattern have radial σ_3 trajectories with a sub concentric pattern about an axis located in sub-area 2 (Figure 6.17c). The elongations of the σ_3 curves are almost parallel to the present day geometry of the rim of the Çankırı Basin. This pattern of the stress trajectories indicates almost uni-axial stress conditions in which the magnitudes of the horizontal stresses (σ_2 and σ_3) were close to, or equal to, each other and the major compression (σ_1) is vertical. Under such regimes high angle normal faults with an unconstrained orientation develop. Therefore, they could have radial or multidirectional orientation (Carey and Brunier 1974, Arlegui-Crespo and Simon-Gomez 1998). On the other hand, the approximately E-W elongation of the σ_3 trajectories in the central part of the Çankırı Basin implies preference for the faults to form in an approximately N-S direction (see Figure 6.08), which would have high angle strike to the σ_3 trajectories.
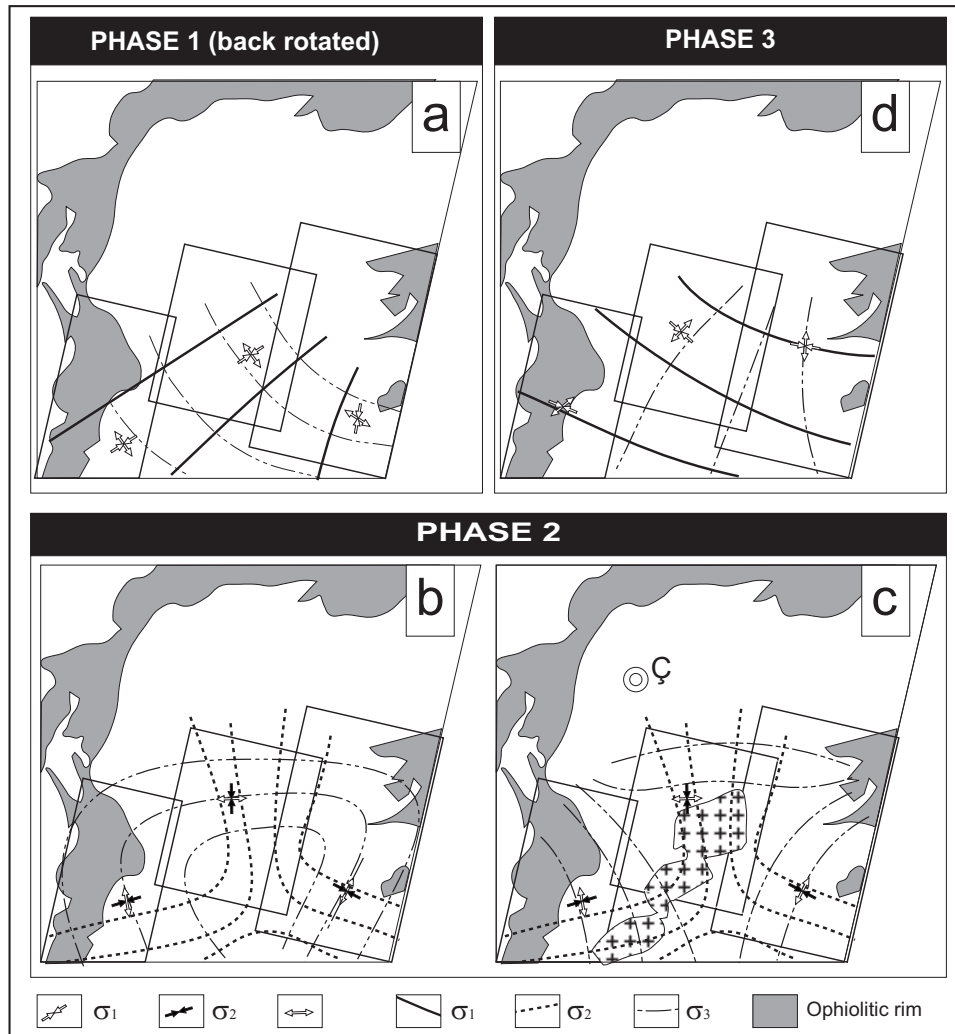
Figure 6.16 Smoothed trajectories of horizontal components of principal stresses for the southern part of the Çankırı Basin. Note that for the deformation phase 2 σ_3 has two possible patterns while keeping the σ_2 pattern fixed (see text for the discussion).

Phase 1 Like the previously mentioned phases, the data from chapter 5 have been utilized for the construction of the smoothed stress trajectories. The horizontal component of the regional σ_1 orientation, in the deformation phase 1, in this study is relatively compatible with sub-areas 1 and 4. However, there is a conflict in the orientations of other stresses, such that σ_2 is sub vertical in the southern part of the Çankırı Basin (sub-areas 5-7) while σ_3 is vertical in the north (Figure 6.17d). This apparent conflict is interpreted as being due to the presence of different stress configurations in the same phase in different

193

settings of the Çankırı Basin. It is interpreted that the configuration of the principal stresses in the sub-areas 1-4 and 5-7 are separated from each other along a possible stress discontinuity, which marks the interface between the basement (Kırşehir Block) and the in-fill of the Çankırı Basin (see chapter 2). The σ_2 trajectories to the north of this discontinuity display a concentric pattern while σ_1 is radial. The center of the circles is located somewhere to the south of Çankırı town (Figure 6.17d).

The trajectories to the south of the discontinuity display a mesh like pattern with NNE-SSW to NE-SW oriented σ_1 and NW-SE oriented σ_3, in which the σ_2 is vertical. This indicates a strike-slip deformation in this part of the basin. The σ_1 in sub-areas 5 and 7 are sub parallel to the rim of the basin, while σ_3 are perpendicular to it. These relationships can be explained by indentation (Tapponier *et al*. 1982) along an irregular margin (Zwiegel 1998). In this model, the promontory of the Kırşehir Block serves as a partly rigid indentor. The areas in the front (north) of the indentor were deformed by shortening and thrusting while the sides (western and eastern margin) of the indentor were characterized by combined transpression (Figure 6.18e). The resultant deformation would give rise to the arcuate (Ω) shape of the Çankırı Basin (Figure 6.18d). The Sungurlu Fault Zone, during this deformation phase, might have accommodated the westward movement of the eastern margin of the basin via a sinistral movement sense (Figure 6.18d).

6.4.4 Tectonic Development of the Çankırı Basin

Consequently, using the information discussed above and in the various chapters of this thesis (see chapters 2,3,4 and 5), it is concluded that the structural development of the Çankırı Basin occurred in 4 different tectonic regimes. The deformation phase-3, in this chapter, corresponds to phase-4 in chapter 5, phase-2 to phase-3, and phase 1 to phase 2, respectively. The earliest phase is not well-constrained and not detected in the southern part of the Çankırı Basin (this chapter). However, the paleostress inversion data and the structures in the southern part of the Çankırı Basin revealed three of the four deformation phases discussed in chapter 5. The latest phase is characterized by a regional transcurrent tectonics and has been active since the Late Miocene. The second phase is characterized by extensional deformation and was active in the post-Burdigalian to Late Miocene. The deformation phase 2 is characterized by compressional deformation associated with transpression and was active in the pre-Burdigalian.

The last three deformation phases recognized in the Çankırı Basin indicated that the evolution and structural development of the basin is accomplished first with indentation tectonics characterized by thrusting in its front and transpressional faulting in the sides of the indentor and occurred in the Late Paleocene to pre-Burdigalian (see also chapters 3,4 and 5). The indentation process continued until about the Early Miocene (Aquitanian) and it is replaced by an extensional tectonic regime caused by orogenic collapse. The concentric pattern of the σ_3 trajectories and sub vertical σ_1 indicates a post orogenic collapse in the Middle Miocene after a period of contraction. Location of the pole of the σ_3 trajectories on the northern tip of the Kırşehir Block indicates that the extensional deformation is driven by the rebound of the tip of the block. This area is the locus of the Middle Miocene basaltic volcanic activity (Faraşlı Basalt, see chapter 4), which might have re-organized the regional stress pattern in a way that concentric pattern of σ_3 trajectories were formed. This needs further study.

194
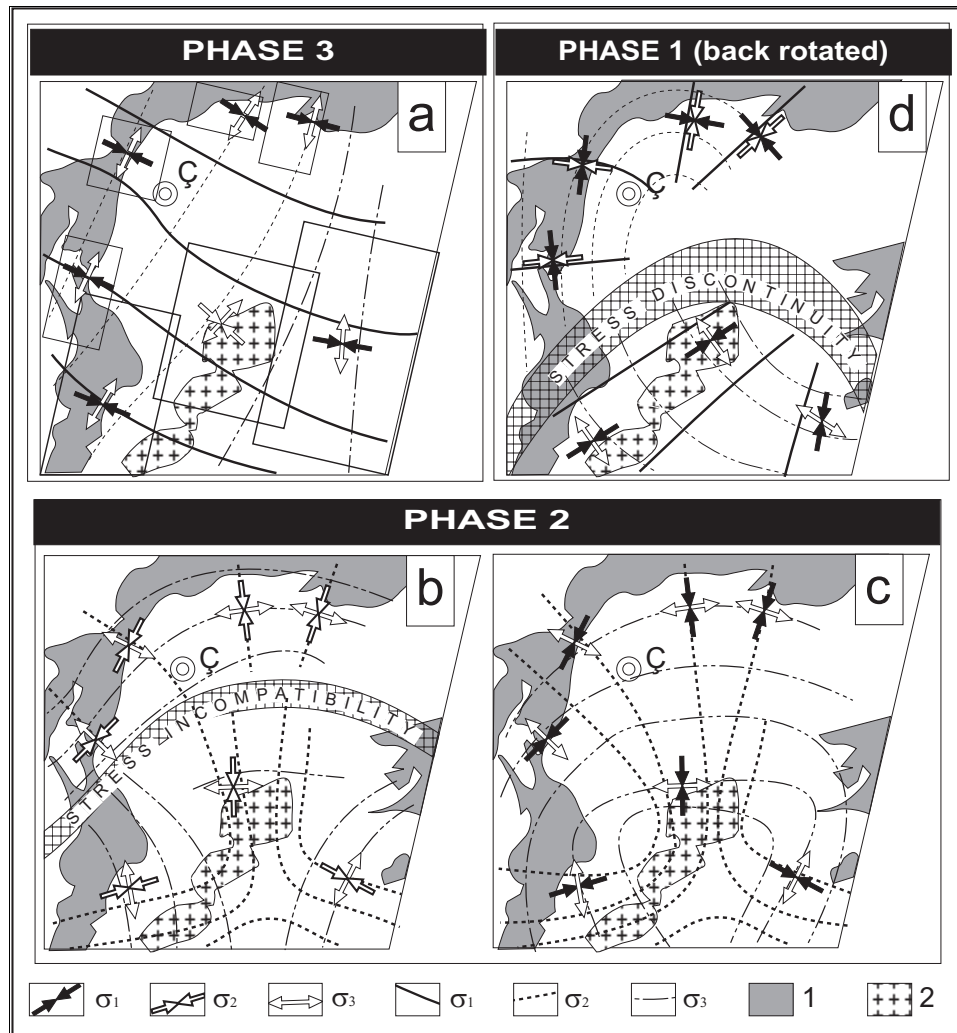
Figure 6.17 Integrated smoothed trajectories of horizontal components of principal stress for each deformation phase. Note that only concentric pattern of σ₃ (c) for the deformation phase 2 is compatible with the northern area (i.e. sub-areas 1-4). 1: ophiolitic rim of the Çankırı Basin, 2. granitoids of the Kırşehir Block. Ç: Çankırı.

The extensional tectonic regime in the Middle Miocene is replaced by a regional transcurrent tectonic regime in the Late Miocene. In this phase, a number of ENE-WSW oriented strike slip faults were developed. These faults are the splay faults of the North Anatolian Fault Zone (see chapter 4 and 5) and have dextral strike-slip sense. These faults displaced the rim, the basement and the basin fill. The Sungurlu Fault Zone, which was a sinistral fault zone in the deformation phase 1, was reactivated dextrally (compare

195
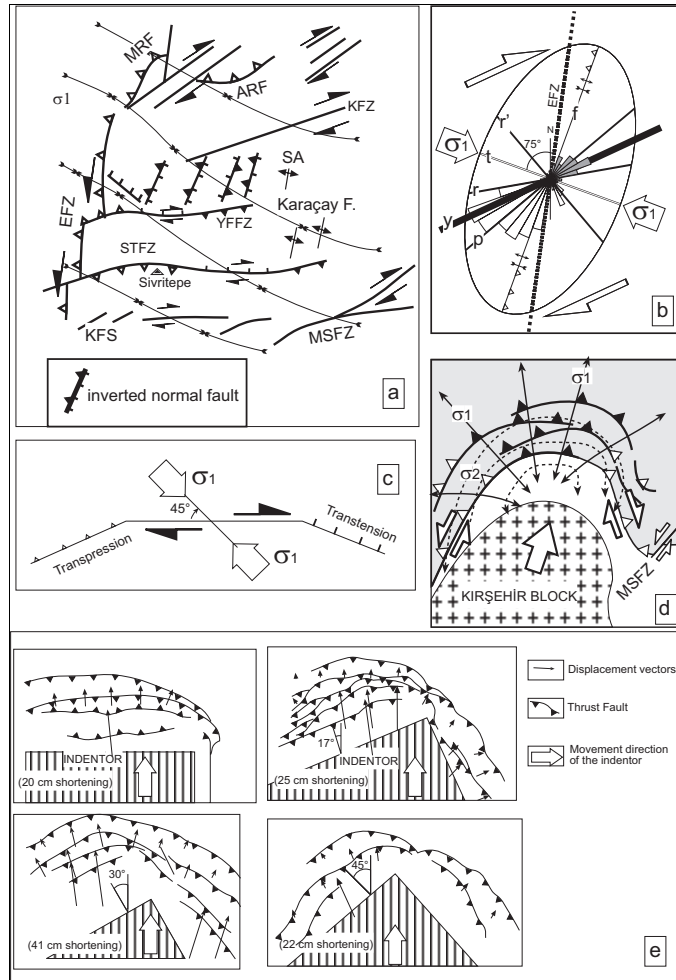
Figure 6.18 Schematic structural map of the Çankırı Basin illustrating the relation between σ_1 and type of the structures developed (reactivated/inverted) in the deformation phase 3 (presently active). MRF: Merzi Reverse Fault, ARF: Ayseki Reverse Fault, SA: Sağpazar Anticline, KFZ: Kızılırmak Fault Zone, EFZ: Eldivan Fault Zone, YFFZ: Yağbasan-Faraşlı Fault Zone, STFZ: Sivritepe Fault Zone, KFS: Kırıkkale Fault Set, MSFZ: Master Strand of the Sungurlu Fault Zone. b) Riedel pattern of deformation and rose diagrams prepared from the lineaments of the Çankırı Basin (discussed in chapter 2) (see text for the discussion). c) Sketch diagram illustrating the relationship between σ_1 and change of along strike kinematic characteristics of a dextral strike-slip fault (modified after Biddle and Christie-Blick 1985). d) Sketch diagram proposed for the patterns of faults and orientation of principal stresses during collision of an irregular indentor. Note thrusting in the front and transpressional deformation in the sides of the indentor. e) Line drawings of thrust fault patterns developed in sandbox experiments carried out by Zweigel (1998). Note the geometry of the indentor and resultant pattern of the thrust faults. Note also the amounts along the displacement vectors, which are connecting the points from their pre-deformed and deformed positions.

196

Figures 6.18a and 6.18d). The growth faults which developed in the extensional period were reactivated as reverse faults. In this phase the western margin of the Çankırı Basin (Eldivan Fault Zone) has been reactivated in a sinistral sense (Figure 6.18a). Almost no deflection of the stress trajectories occurred in the latest deformation phase and indicates that the pre-existing structures did not a play major role in the orientation of the principal stresses.

6.5 Conclusions

I. Three of the four deformation phases recognized in the northern part of the Çankırı Basin (chapter 5) are recognized in the southern part.

1. Deformation phase 1 (corresponding to deformation phase 2 of the previous chapter) is characterized sub vertical σ_2 while other stresses were sub horizontal indicating transpression in this phase. It occurred in the Late Paleocene to pre-Burdigalian.

2. The second deformation phase (corresponding to deformation phase 3 of the previous chapter) was characterized by extensional deformation with sub vertical σ_1 while the other stresses were sub horizontal to oblique. It occurred in the Burdigalian to pre-Tortonian (Early to Middle Miocene).

3. The deformation phase 3 (corresponding to deformation phase 4 of the previous chapter) is characterized by regional transcurrent tectonics in which σ_2 have been sub vertical and other stress are sub horizontal to oblique. This phase has been active since the Tortonian (Late Miocene).

II. The smoothed trajectories of horizontal components of the principal stresses were constructed in combination with the data from the previous chapter.

1. In phase 1, the northern (sub-areas 1-4) and southern sub-areas (5-7) have different stress configurations separated along a stress discontinuity, which is the interface of the Kırşehir Block and the basin in-fill. This discrepancy is interpreted as the change of the configuration of the stress ellipsoid due to the indentation of the Kırşehir Block into the Sakarya Continent.

2. The trajectories of the σ_3 in the second deformation phase display a concentric pattern, which is interpreted as the manifestation of the extensional regime resulting from a post-orogenic collapse following collision and crustal thickening in phase 1.

3. The σ_1 and σ_3 trajectories of phase 3 display a mesh-like pattern and are compatible with the current tectonic scheme of Turkey which is controlled mainly by the transcurrent North Anatolian Fault Zone.

.

<div style="text-align: right">

7

</div>

THE EARLY TERTIARY EVOLUTION OF THE ÇANKIRI BASIN (Central Anatolia, Turkey): A Paleomagnetic Study

Abstract

Paleomagnetic data in combination with paleostress data and the anisotropy of the magnetic susceptibility orientations were utilized in developing a tectonic evolutionary model of the Ω-shaped Çankırı Basin (Turkey). The results reveal clockwise rotations in the north-east and anticlockwise rotations in the west and south-east of the basin. The magnetic inclinations indicate a northward drift of the basin in-fill, suggesting an indentation model for the Kırşehir Block. It appears that the indentation started prior to the Eocene and ended before the Middle Miocene.

7.1 Introduction

The pre-Neogene tectonic history of Turkey is mainly dominated by the amalgamation of a number of tectonic blocks (micro-continents) which were once part of Laurasia and Gondwana (Şengőr and Yılmaz 1981, Gorur et al. 1984, Robertson and Dixon 1984, Sengőr et al. 1984, Dercourt et al. 1993, Channel et al. 1995, Robertson et al. 1996). Turkey is broadly divided into three tectonic belts. These are (Figure 7.01a), from north to south, the Pontides, Anatolides, and Taurides (Ketin 1966). The Pontides are the eastern continuation of the Rhodope-Pontide fragments including the Sakarya Continent (Şengőr and Yılmaz 1981, Şengőr *et al.* 1984). The Anatolides are the metamorphic northern continuation of the Taurides (Şengőr and Yılmaz. 1981) and include the Menderes Massif and Kırşehir Block. The Sakarya Continent and the Kırşehir Block each have a different geological evolution from the Late Paleozoic to the Mesozoic (Şengőr and Yılmaz 1981, Şengőr *et al.* 1984). The Sakarya Continent is separated from the rest of Pontides by the Intra-Pontide Ocean in the Early Mesozoic (Robertson and Dixon 1984, Şengőr *et al.* 1984, Tuysuz 1993), while the Kırşehir Block was separated from the Taurides by the Intra-Tauride ocean (Seymen 1981,1982, Gőrűr *et al.* 1984). However, the Kırşehir Block has the same stratigraphic characteristics and has experienced a similar evolutionary history to the Taurides. Further, it has been proposed (Şengőr and Yılmaz 1981, Gőrűr *et al.* 1984, Şengőr et al. 1984) that the two micro-continents, namely the Sakarya Continent and Kırşehir Block, were separated from each other by the main branch of the Tethys Ocean throughout the Mesozoic and both drifted from equatorial latitudes in the Late Cretaceous to their present positions (Şengőr et al. 1984, Robertson et al. 1996). Although, the timing of collision and amalgamation of these two micro-continents along the Izmir-Ankara-Erzincan Suture Zone (IAESZ, see Figure 7.01) is debated, it is generally constrained within the Late Cretaceous to Early Tertiary interval (Sengőr and Yılmaz 1981, Gorur et al., 1984, Tuysuz 1993, Kocyigit et al. 1988, Kocyigit 1991, Okay et al. 1998). According to Sanver and Ponat (1981) and Gorur et al. (1984), the Kırşehir Block has rotated 104° anticlockwise between the Cretaceous to present.

Figure 7.01 a) Inset map showing the geological outline of Eastern Mediterranean area (Modified after Şengőr et al. 1984). BSZ: Bitlis-Zagros Suture, IAESZ: Izmir-Ankara-Erzincan Suture Zone, ITS: Intra-Tauride Suture, KB: Kırşehir Block, MTB: Taurus-Menderes Block, SC: Sakarya Continent. b) regional structural situation in central Anatolia. c) detailed tectono-stratigraphical map of the central Anatolia. Box shows the location of the study area. AFZ: Almus Fault Zone, ESFZ: Ezinepazari-Sungurlu Fault Zone, KFZ: Kızılırmak Fault Zone, LFZ: Laçin Fault Zone, NAFZ: North Anatolian Fault Zone, YFFZ: Yağbasan-Faraşlı Fault Zone. 1. Pre-Late Cretaceous metamorphic basement of the Kırşehir Block, 2. Pre-Jurassic metamorphic basement of the Sakarya Continent, 3. Triassic Karakaya Complex, 4. Jurassic-Cretaceous platform carbonates on the Sakarya Continent, 5. Late Cretaceous (?) ophiolites and ophiolitic melanges, 6. Pre-Paleocene Granitoids of the Kırşehir Block, 7. Galatean Volcanic Province (GVP, Toprak et al. 1996), 8. Early Tertiary units (mainly marine), 9. Neogene and Quaternary Cover, 10. reverse faults, 11. thrust faults, 12. normal faults, 13. faults with unknown sense of movement,, 14. active strike-slip faults. faults, 12. Normal faults, 13. Faults with unknown sense of movement, 14. Strike-slip faults. Concentric circles are the major towns in the region (size of the circles are related to the population. d) active tectonic outline of Turkey and surrounding regions. DFZ: Dead Sea Fault Zone, EAFZ: East Anatolian Fault Zone, HT: Hellenic Trench, NAFZ: North Anatolian Fault Zone. Large black arrows are the movement directions of Arabian plate and Aegean-Anatolian Block (modified after Barka and Hancock 1984, Gőrűr et al. 1984, Őzçelik 1994, Kaymakci and Koçyiğit 1995)

The Late Miocene collision and further convergence of the Arabian Block in the south, and the Eurasian Plate in the north, along the Bitlis-Zagros Suture (BZS) resulted in the westward expulsion of the Anatolian Block (Figure 7.01b) along the North Anatolian (NAFZ) and East Anatolian transform fault zones (EAFZ) (Şengőr and Yılmaz 1981, Şengőr et al. 1985). The Anatolian Block continues to deform internally, which is characterized by dominant regional transcurrent deformation in the east and a dominant extensional deformation in the west (Şengőr et al. 1985). In the north central part of Anatolian Block, a number of northwards convex dextral strike-slip faults divide the region into roughly E-W oriented wedges that branch-off from the North Anatolian Fault Zone (Barka and Hancock 1984, Kaymakci and Kocyigit 1995). Deformation of these wedges is

marked by a complex rotational strain (Kaymakci and Koçyigit 1995, Oral 1994, Piper et al. 1996, Oral *et al.* 1997).

Previous paleomagnetic studies in Turkey have mainly dealt with the determination of paleolatitudes of the amalgamated micro-continents and of their apparent polar wander path (e.g. Van der Voo, 1968, Sanver and Ponat 1981, Evans and Hall 1990, Morris and Robertson 1993, Channel et al. 1995) and indicate a northwards drift of all of the tectonic blocks (including the Sakarya Continent and the Kırşehir Block), from equatorial latitudes in Late Cretaceous to their present positions. Other studies have concentrated on block rotations along the NAFZ and within the Anatolian Block (e.g. Saribudak et al. 1990,

Platzman et al 1994,1998, Michel et al. 1995, Tatar et al. 1995, Piper et al. 1996, 1997, Gursoy et al. 1997). The detected post-Late Miocene dominantly anticlockwise rotations are generally in agreement with the Geographic Positioning System (GPS) measurements (Oral et al. 1997). However, the Early Tertiary evolution of Turkey is still far from complete (Piper et al. 1996). Therefore, the aim of this study is to paleomagnetically study the Çankırı Basin and compare the paleomagnetic results with paleostress data of the Çankırı Basin to constrain its Early Tertiary evolution. The Çankırı Basin contains an almost continuous sedimentary record since the Late Cretaceous (Figure 7.02), and is situated in the collision zone of the Sakarya Continent and the Kırşehir Block and within the splay fault zone of the NAFZ.

7.2 Geological Setting

The Çankırı Basin straddles the Pontides in the north and the Kırşehir Block in the south (Figure 7.01). It lies above the Izmir-Ankara-Erzincan Suture Zone (IAESZ), which has an overall E-W trend but to the east of Ankara, the IAESZ makes a sharp bend in an Ω–shape in the Cakiri Basin. In its western, northern and eastern rim, the Çankırı Basin is surrounded by the North Anatolian Ophiolitic Melange (NAOM, terminology after Rojay 1993, 1995) and associated Late Cretaceous units. In the south it is delimited by the granites of the Kırşehir Block. The Çankırı Basin comprises a more than 4 km of sedimentary fill ranging from Late Cretaceous to present and accumulated in 5 sequences of sedimentation (Dellaloğlu et al. 1992, see also chapters 3 and 4) and summarized in Figure 7.02b.

The oldest sedimentary sequence consists of tectonically intercalated Late Cretaceous deep marine sediments alternating with mafic volcanics, volcanoclastics, proximal regressive shallow marine units and Paleocene littoral red clastics and carbonates which represent the subduction history of the northern Neo-Tethys in the region (Koçyiğit 1991, Dellaloğlu et al. 1992, Özçelik 1994, Tűysűz et al. 1995). The second sequence is a Late Paleocene to mid-Oligocene, more than 1 km thick, regressive flysch to molasse type succession intercalated with mafic to intermediate volcanics and a nummulitic limestone. The third sequence comprises a very thick (up to 2 km) Late Eocene to mid-Oligocene continental red clastics and evaporites. The fourth sequence is up to 1 km thick and represented by Early Miocene to Pliocene fluvio-lacustrine deposits. The Late Pliocene-Quaternary alluvial fan deposits and recent alluvium locally overlay all these units (Figure 7.02b) (discussed in chapters 3 and 4)

The main structures shaping the current geometry of the Çankırı Basin (Figure 7.01) are the thrust and reverse faults delineating the western and northern rims of the Çankırı Basin. The eastern margin is defined by a belt of NNE striking folds. In the south, the

basin in-fill onlaps onto the basement (Kırşehir Block). The above thrust and reverse faults developed in the Late Cretaceous to Early Tertiary during the subduction and subsequent collision of the Kırşehir Block and the Sakarya Continent and were reactivated during the post-Middle Miocene evolution of the basin (Kaymakci et al. 1998, see also chapters 5 and 6). The other major structures affecting the Çankırı Basin are the Kizilirmak, Yagbasan-Farasli (YFFZ), Sivritepe (STFZ) and Sungurlu Fault Zones that are oriented WSW-ENE and are dominantly dextral transcurrent faults. They displace the ophiolitic rim, the basement, and the basin in-fill including the Late Miocene units indicating a post-Late Miocene activity (discussed in chapters 4,5 and 6).

7.3 Paleomagnetic Results

Sampling was performed from the second, third, and fourth sequences of the basin in-fill, namely the Early to Middle Eocene part of the sequence (sequence 2), the Late Eocene to Oligocene (sequence 3), the Middle Miocene (lower part of sequence 4), and the Late Miocene (upper part of sequence 4). The ages of the studied units of sequence 2 are based on marine fauna (see chapter 3). The age of the sequence 3, is based on its stratigraphic position partly on micro-mammals as the sequence 4 (see chapter 4). Throughout this text the sequence 2 is referred to as "*Eocene*" and the sequence 3 is referred to as "*Oligocene*".

In all sites, sampling was performed using an electrical drill and a portable generator. Care was taken to avoid sampling near large faults. After removing the weathered surface to reach fresh clays, we took at least seven standard oriented paleomagnetic cores at each site. Mostly, fine-grained sediments were sampled with a low sedimentation rate. Sampling over a sufficiently large interval tends to average out secular variations in these rocks. In addition, early post-depositional processes typically smooth out the finer-scale variations of the geomagnetic field. The fold-test is done for both limbs of the fold in the eastern margin of the basin that include Yesilova and Guvendik sites. Remanent Magnetic Susceptibility (RMS) was acquired prior to folding of the Gűvendik syncline (GS, Figure 7.02a).

7.3.1. Thermal Demagnetisation

Thermal demagnetisation was performed using a magnetically shielded, laboratory-built furnace. The natural remanent magnetisation (NRM) was measured on a 2G Enterprises DC SQUID cryogenic magnetometer. At least seven specimens per site were analysed using progressive stepwise thermal demagnetisation at temperature increments of 30°C or 50°C, starting from room temperature to the limit of reproducible results.

Demagnetisation diagrams (Zijderveld, 1967) through selected data points were used to determine the NRM components (Figure 7.03). When the results show a linear decay, usually towards the origin, a magnetisation vector is determined. The magnetisation vectors were averaged using Fisher (1953) statistics to calculate mean directions per site (Table 1), from which tectonicaly induced rotations could be determined. As it is still controversial to what stable region the Çankırı Basin belonged, the results are not compared to a known reference pole, but compared to 0° as reference direction. The paleolatitude can be seen in Figure 7.04 and Table 1.
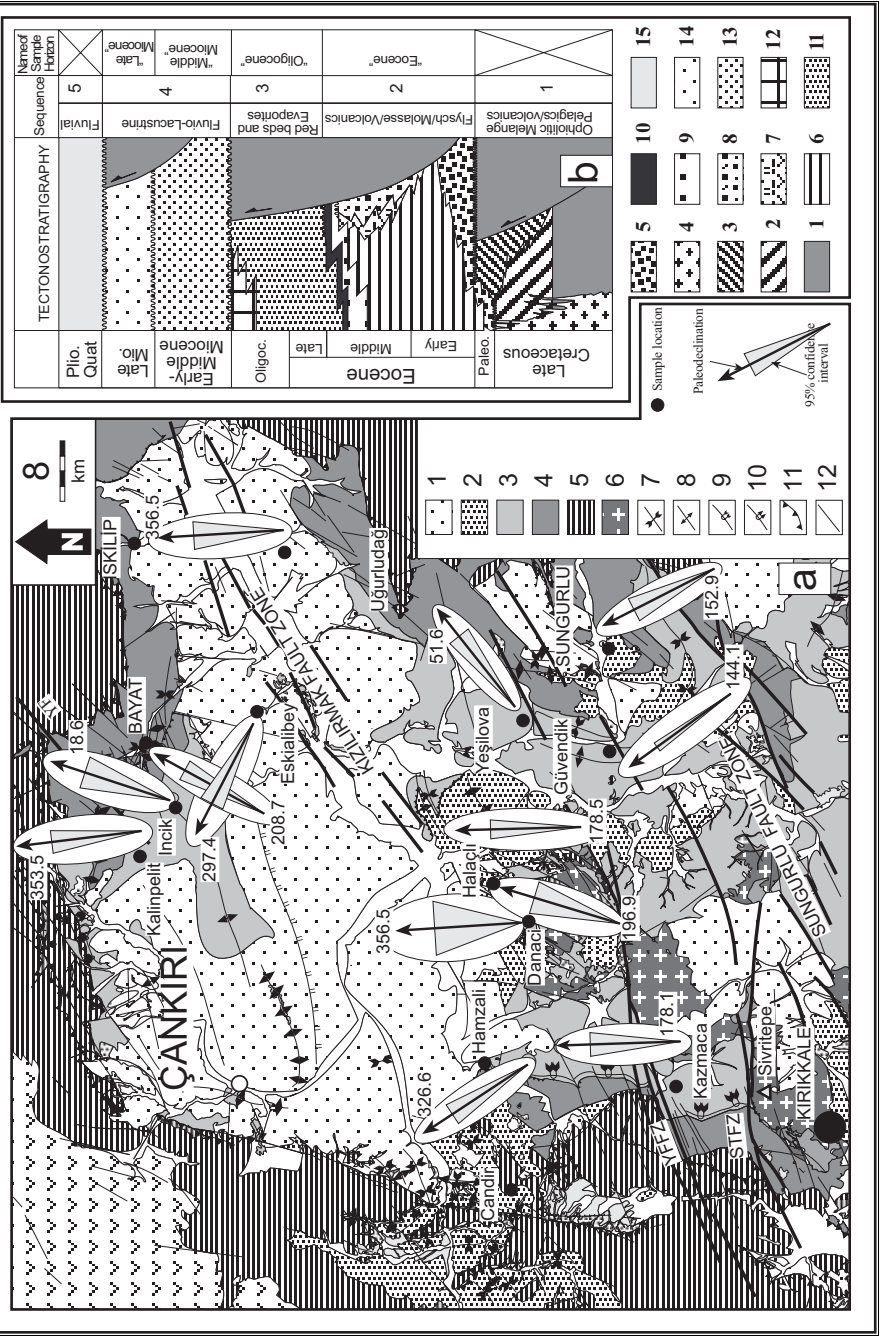
Figure 7.02 a) Geological map of the Çankırı Basin, site locations and paleo-declinations of site means with 95% confidence interval. Sites are located at the tail ends of the arrows(see Table 1 for the details). STFZ: Sivritepe Fault Zone, YFFZ: Yagbasan Farasli Fault Zone. YF. Yoncali Fault. 1. Late Miocene units, 2. Middle Miocene units, 3. Post-Middle Eocene-Oligocene units, 4. Eocene units, 5. Pre-Eocene units, 6. Granitoids of the Kırşehir Block, 7. Syncline, 8. Anticline, 9. Overturned syncline, 10. Overturned anticline, 11. Thrust faults, 12. Strike-slip and oblique-slip faults. b) Simplified tectono-stratigraphic column of the units exposed in the Çankırı Basin. Numbers in the last column of the columnar section are the sequence numbers. Note repeated thrusting that are indicated with half arrows in the columnar section. 1. Late Cretaceous North Anatolian Ophiolitic Melange (NAOM), 2. Yaylaçayı Formation (distal fore-arc sequence) 3. Yapraklı Formation (proximal fore-arc sequence), 4. Sulakyurt Granitoids (intruded in pre-Paleocene), 5. Late Paleocene to Early Eocene clastics and carbonates with progressive unconformities. 6. Yoncali Formation (regressive flysch sequence), 7. Middle Eocene volcanics, volcanoclastics and detritics (Bayat Formation), 8. conglomerate, sandstone and shale alternation and coal seam intercalations (Karabalcik Formation), 9. Early to Middle Eocene continental red clastics characterized mainly by red conglomerates, sandstones and mudstones (Osmankahya Formation), 10. Nummulitic limestone (Kocacay Formation), 11. Red beds with syn-depositional progressive and rotated unconformities (İncik Formation), 12. Gűvendik formation (Oligocene evaporites), 13. Fluvio-lacustrine red clastics (Çandır Formation), 14. fluvio-lacustrine red clastics and evaporites (Sűleymanlı and Bozkır formations), 15. Plio-Quaternary fluvial clastics.

Apart from a very small and randomly oriented laboratory-induced component removed at 100°C, a secondary component is sometimes present; it is generally removed between 100° and 200°C; it has a present-day direction before bedding tilt correction and is thus of recent origin and is assumed to be caused by weathering. A characteristic remanent magnetisation (ChRM) component is removed at higher temperatures and shows both normal and reversed polarities. Most sites reveal ChRM components demagnetised at temperatures of 570°- 600°C (Fig. 3c,e and f) residing in magnetite. Demagnetisation at higher temperatures results in randomly directed components. These samples have a relatively high NRM intensity (6-13 mA/m). Some samples are demagnetised at temperatures around 390°- 420°C (Fig. 3a), have relatively low intensities (0.8 mA/m) and the ChRM component is most likely carried by Fe-sulphides. We show an example of a completely overprinted sample with a relatively high intensity (66 mA/m) and a signal largely destroyed around 250°C (Fig. 3b). The Oligocene site of Gűvendik (Fig. 3d) has two antiparallel components; a reversed component until 510°C and a normal component from 510°C until 580°C. We used the reversed component, as it appeared to be most consistent.

Only two of the seven Eocene sites show reliable results. One site (Sungurlu), located in the south-east of the Çankırı Basin, implies an anticlockwise rotation of 27°, while the other site (Incik 2), located in the north indicates a clockwise rotation of 29°. The paleolatitude of these Eocene sites points to a near-equatorial position (6°). Of the Oligocene, all seven sites produced reliable data. The three Oligocene sites located in (south-)west of the Çankırı Basin show no rotations (Danaci and Hamzali 3) to anticlockwise rotations of 33° (Hamzali 2). In the north of the basin, a site with a large clockwise rotation of 19° (Incik 3) and a site with a small anticlockwise rotation of 7° (Kalinpelit) is found. Likewise in the east, a large clockwise rotation of 52° (Yesilova) and a large anticlockwise rotation of 36° (Gűvendik) was detected. Although the Oligocene paleolatitudes are variable, a clear trend is visible, indicating a northward movement of the Çankırı Basin. Two out of three Middle Miocene sites from the south of the Çankırı Basin were found to be reliable, with one site revealing a clockwise rotation (Halaçlı) and another site hardly indicating a rotation (Kuscalı). Of the Late Miocene, two out of three

sites are located in the northeast of the basin and imply a further northward movement. One of the late Miocene sites shows a small (Uğurludağ) anticlockwise rotation of 4° and another one (Eskialibey) a large anticlockwise rotation of 62°.

7.3.2. Anisotropy of the Magnetic Susceptibility

Analysis of the anisotropy of the magnetic susceptibility (AMS) is widely used to establish the sedimentary and tectonic history in weakly deformed sediments. Basically, the AMS of a rock is described by a second-order tensor. This tensor can be visualised by an ellipsoid having three principal axes of maximum, intermediate, and minimum susceptibility (k_{max}, k_{int}, and k_{min}, respectively). Here, we characterise the total degree of anisotropy by $P = k_{max}/k_{min}$; the magnetic foliation is defined by $F = k_{int}/k_{min}$, while the magnetic lineation is the degree of anisotropy in the magnetic foliation plane and defined by $L = k_{max}/k_{int}$ (see Tarling and Hrouda, 1993). Depositional currents can also account for lineations, but this is unlikely in the fine-grained mostly continental clays of the Çankırı Basin. In undeformed sediments, the magnetic susceptibility is characterized by an oblate ellipsoid, with the foliation coinciding with the bedding plane. In that case, the magnetic fabric is purely depositional or related to compactional loading; the k_{min} is perpendicular to the bedding plane and the k_{max} and k_{int} are scattered in the foliation or bedding plane itself. If there is deformation acting on a rock, this initially results in clustering of k_{max} in the direction of maximum extension or, equivalently, perpendicular to the maximum compression. The k_{min} is still perpendicular to the bedding plane. An increase of the strain causes the ellipsoid to have a more prolate structure. Finally, progressive strain obliterates the prolate ellipsoid into a "pencil" structure and the depositional fabric is becoming overprinted by a tectonic fabric (Tarling and Hrouda, 1993). This pencil cleavage, easily recognised in the field, was not observed in the area.

Generally, the AMS results (Table 2) of the sites from the Çankırı Basin show oblate ellipsoids with highly variable mean susceptibilities (53 - 9900 x 10^6 SI) reflecting the variable concentration of magnetic mineralogy. Error ellipses of the susceptibility axes are according to Jelinek (1978) and are given for k_{max} in Table 2. Seven sites display a well defined clustering of the k_{max}-axes, indicating the extension direction or, equivalently, the compression perpendicular to it. Three Eocene sites (Kazmaca, Sungurlu, Incik 2; Figure 7.05) expose a (N)NE-(S)SW direction of the k_{max}-axes and one Eocene site (Hamzali 1) indicates a NNW-SSE direction of the k_{max}-axes. The Oligocene site at Guvendik reveals a clear clustering of the k_{max}-axes along an E-W direction, while the Kalinpelit site implies roughly a NW-SE direction. The k_{int} and k_{min}-axes of Hamzali 2 girdle around the k_{max}-axes, indicating deformation. Finally, the Late Miocene site of Sulakyurt exhibits a ENE-WSW direction of the k_{max}-axes. The remaining sites show a large scatter in k_{max}-axes and are not interpreted.

7.4 Paleostress

Using multi-source data including satellite and aerial-photo remote sensing, seismic interpretation, paleostress inversion, and tectono-stratigraphical studies in the Çankırı Basin revealed that the basin has evolved in at least four different phases of tectonic deformation (see chapters 4,5 and 6). The first phase is characterized by thrusting with approximately NW-SE oriented σ_1 and is most likely of Late Cretaceous to Late Paleocene age. The second phase is of Eocene to Oligocene age and is characterized by

206

Site	CODE	N	D_{notc}	I_{notc}	k	a_{95}	D_{tc}	I_{tc}	k	a_{95}	rot	sense	Age	Paleolatitude		
			(°)	(°)		(°)	(°)	(°)		(°)	(°)	ac/c	(Ma)	min	mean	max
Sungurlu	SUN	8	153,1	16,4	51,8	7,8	152,9	-12,6	51,8	7,8	27	ac	Eocene	2,4	6,4	10,5
Incik 2	INC2	4	207,3	20,0	187,1	6,7	208,7	-12,5	187,1	6,7	29	c	Eocene	2,9	6,3	9,9
Kalinpelit	KAL	6	357,0	12,5	88,3	7,5	353,5	33,0	88,3	7,2	7	ac	Oligocene	13,6	18,0	22,9
Yesilova	YES	6	53,8	-17,9	83,5	7,4	51,6	22,2	83,5	7,4	52	c	Oligocene	7,5	11,5	15,9
Danaci	DAN	5	347,9	37,6	20,4	17,3	356,3	29,2	20,4	17,3	4	ac	Oligocene	6,0	15,6	27,8
Guvendik	GUV	7	120,9	-45,8	378,8	3,1	144,1	-35,6	378,8	3,1	36	ac	Oligocene	17,7	19,7	21,8
Hamzali 3	HAM3	5	184,8	-44,8	103,9	7,5	178,1	-28,1	103,9	7,5	2	ac	Oligocene	10,6	15,0	19,7
Incik 3	INC3	7	15,6	19,7	35,4	10,3	18,6	44,3	35,4	10,3	19	c	Oligocene	18,6	26,0	35,1
Hamzali 2	HAM2	7	331,7	15,7	72,4	7,1	326,6	14,4	72,4	7,1	33	ac	Oligocene	3,7	7,3	11,1
Kuscali	KUC	7	161,8	-56,2	102,4	6,0	178,5	-59,8	102,4	6,0	2,0	ac	Mid. Mio.	34,3	40,7	48,1
Halacli	HAL1	5	198,5	6,1	55,3	10,4	196,9	-21,8	55,3	10,4	17	c	Mid. Mio	5,8	11,3	17,5
Urludag	UR	6	353,1	34,9	58,8	8,8	356,5	43,9	58,8	8,8	4	ac	Late Mio.	19,4	25,7	33,3
Eskialibey	ESK	7	296,9	37,8	60,4	7,8	297,4	39,2	60,4	7,8	62,0	ac	Late Mio.	17,0	22,2	28,2
mean		2					180,8	-14,1	0,0	99,9			Eocene		7,2	
		7					357,4	32,7	8,7	21,6			Oligocene	5,6	17,8	34,8
		2					193,6	-40,9	0,0	99,9			Mid. Mio		23,4	
		2					325,8	45,5	0,0	99,9			Late Mio.		27	

Table 7.01 Results from NRM analysis from the sites sections in the Çankırı Basin; corrected (tc) and uncorrected (no tc) for bedding tilt, ages are indicated. N = number of specimens; D, I = site mean ChRM declination and inclination; k = Fisher's precision parameter; $\alpha95$ = 95% cone of confidence; rot = magnitude of rotation; (a)c = (anti)clockwise with a 0° reference direction; min/mean/max concerns paleolatitude.
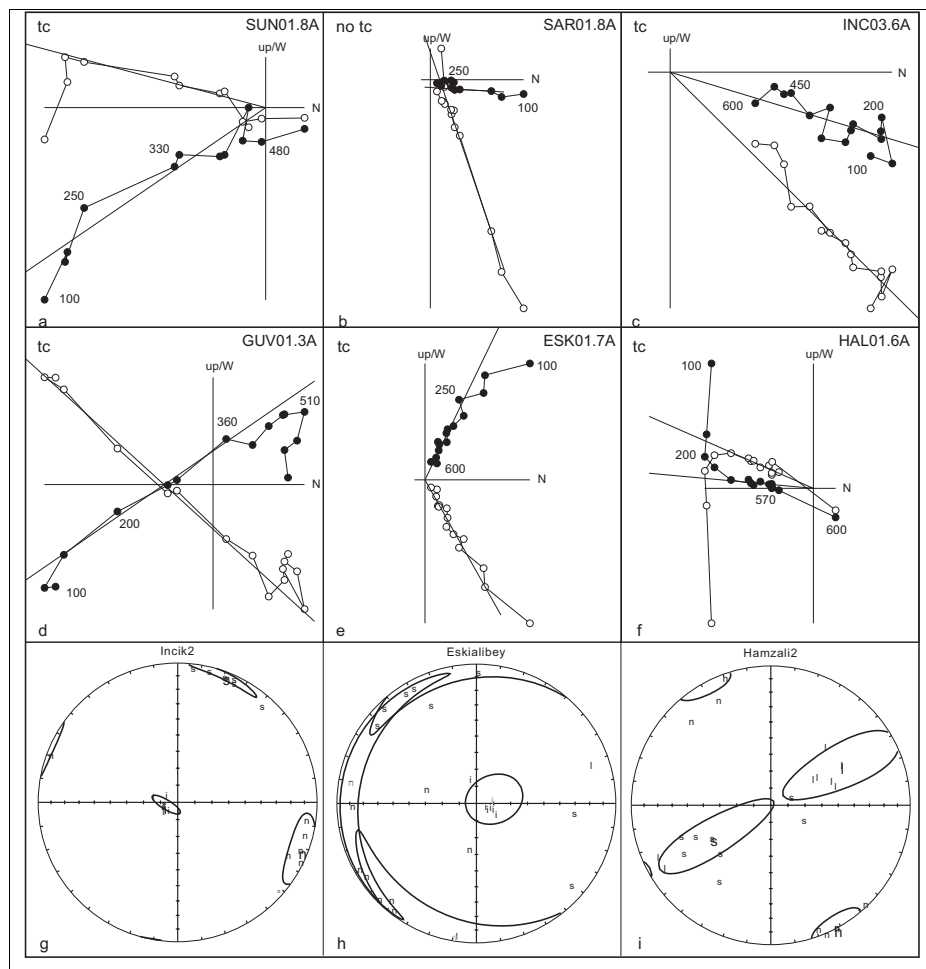
Figure 7.03 Orthogonal projections of stepwise thermal demagnetisation of selected samples from Eocene (a,b), Oligocene (c,d) and Miocene (e,f) sediments. Closed (open) circles represent the projection of the ChRM vector endpoint on the horizontal (vertical) plane. Numbers denoting temperatures in °C and tc/no tc indicates after/before bedding plane correction. g-i shows equal area projection of anisotropy of the magnetic susceptibilty with circles/squares/triangles as $k_{min}/k_{max}/k_{int}$ after bedding plane correction.

208

two different stress configurations one related to the basement and the other to the basin in-fill and the surrounding rim. The rim and the basin in-fill have a near radial σ_1 and sub vertical σ_3 pattern associated with thrusting, while the basement is characterized by a NNE-SSW oriented σ_1 and sub vertical σ_2 indicating coeval strike-slip deformation. The third phase exhibits an overall extensional deformation with concentric σ_3 and sub vertical σ_1 pattern in the Early to Middle Miocene interval. The fourth phase is characterized by a NW-SE oriented σ_1 and sub vertical σ_2 indicating regional transcurrent tectonics from the Late Miocene to present (for details on paleostress information we refer to Kaymakci et al., 1998 and chapters 5 and 6).
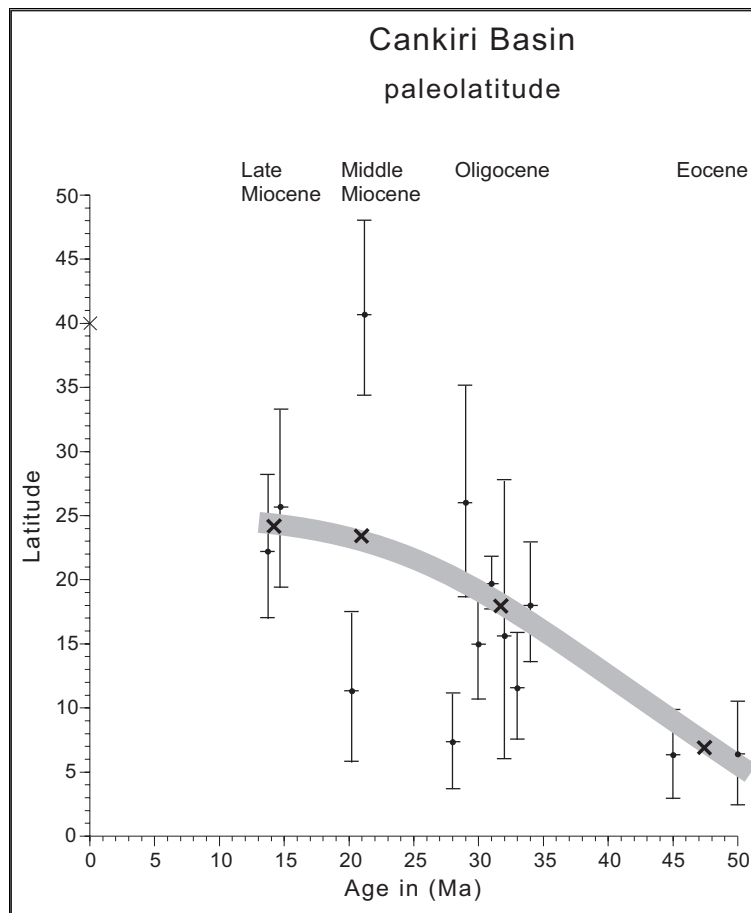
Figure 7.04 Latitude of the sites from the Çankırı Basin versus time. Crosses and grey zone represent paleolatitude-means per age (see Table 1).

Table 7.02 Results from AMS analysis from the sites in the Çankırı Basin; corrected for bedding tilt, ages are indicated. n = number of specimens; D, I = mean azimuth and dip of k_{max} axes; δD, δI = errors on mean k_{max} axes; L = magnetic lineation (k_{max}/k_{int}).

Name:	Code	N	D°	I°	D°	I°	Kmean *10⁻⁶ SI	F	L	Age (Ma)
Hamzali 1	HAM1	6	347,6	8,6	23,9	5,2	9876,5	1,0094	1,0307	Eocene
Incik 1	INC1	7	141,6	32,3	36,5	10,1	52,8	1,0118	1,0057	Eocene
Kazmaca	KAZ	7	8,9	16,7	7,8	2,2	284,7	1,0314	1,0173	Eocene
Saricalar	SAR	7	89,3	13,9	60,6	8,8	3345,3	1,0522	1,0098	Eocene
Incik 4	INC4	7	182,7	0,4	55,8	12,9	160,6	1,0067	1,0009	Eocene
Sungurlu	SUN	7	52,3	15,4	19,7	10,7	302,7	1,0365	1,0103	Eocene
Incik 2	INC2	6	111	5,8	16,4	9,3	242,1	1,0231	1,0042	Eocene
Kalinpelit	KAL	7	320,9	7,1	37,2	5,7	3783,0	1,0315	1,0064	Oligocene
Yesilova	YES	7	199,6	3,8	50,9	16,5	371,76	1,0314	1,011	Oligocene
Danaci	DAN	7	115,7	13,9	46,1	21,7	327,8	1,0043	1,005	Oligocene
Guvendik	GUV	8	88,5	5,9	17	4,4	242,7	1,0188	1,0085	Oligocene
Hamzali 3	HAM3	7	143	3,3	30	7,4	4795,4	1,0182	1,0067	Oligocene
Incik 3	INC3	8	70,6	2,8	50,8	17,2	684,0	1,0176	1,0047	Oligocene
Hamzali 2	HAM2	7	151,3	0,0	12	9,7	6653,1	1,0145	1,0105	Oligocene
Sulakyurt	SUL	7	255,3	1,8	34,7	8,4	121,85	1,0193	1,0026	Late Mio.
Urludag	UR	7	52	3,2	26,5	16,6	207,5	1,0273	1,005	Late Mio.
Eskialibey	ESK	8	280	9,8	67,9	7	259,6	1,0297	1,0032	Late Mio.
Kuscali	KUC	6	342,6	2,1	39,2	15,8	1052,3	1,0199	1,0045	Mid. Mio.
Halacli	HAL1	7	311,6	4,2	53,7	14	1105,2	1,0354	1,0032	Mid. Mio.
Mahmatlar	MAH	7	43,8	5,7	8,9	5,4	1856,7	1,0102	1,0183	Mid. Mio.

7.5 Discussion

This study has provided the first paleomagnetic results on the evolution of the Çankırı Basin. In general, the results show predominantly anticlockwise rotations in the western and clockwise rotations in the eastern margin of the basin. Furthermore, the data seem to indicate no rotation of the Kırşehir Block since the Oligocene. Magnetic inclinations of most sites indicate a northwards drift of the region from the Eocene to the Middle Miocene. Our paleomagnetic data concerns Eocene and younger rocks and therefore the data is in accordance with the latest three of the four deformation phases; in the Eocene to Oligocene (2), Early to Middle Miocene (3) and the Late Miocene to present (4). In the western margin the samples from the older parts of the Oligocene units (Hamzali-2) show more rotation than the younger samples (Hamzali-3). This relation may indicate syn-depositional deformation of the basin in-fill which is discussed in the previous chapters (see chapters 3-6) and in which the Oligocene units (Incik Formation) comprise a number of syn-depositional progressive unconformities.
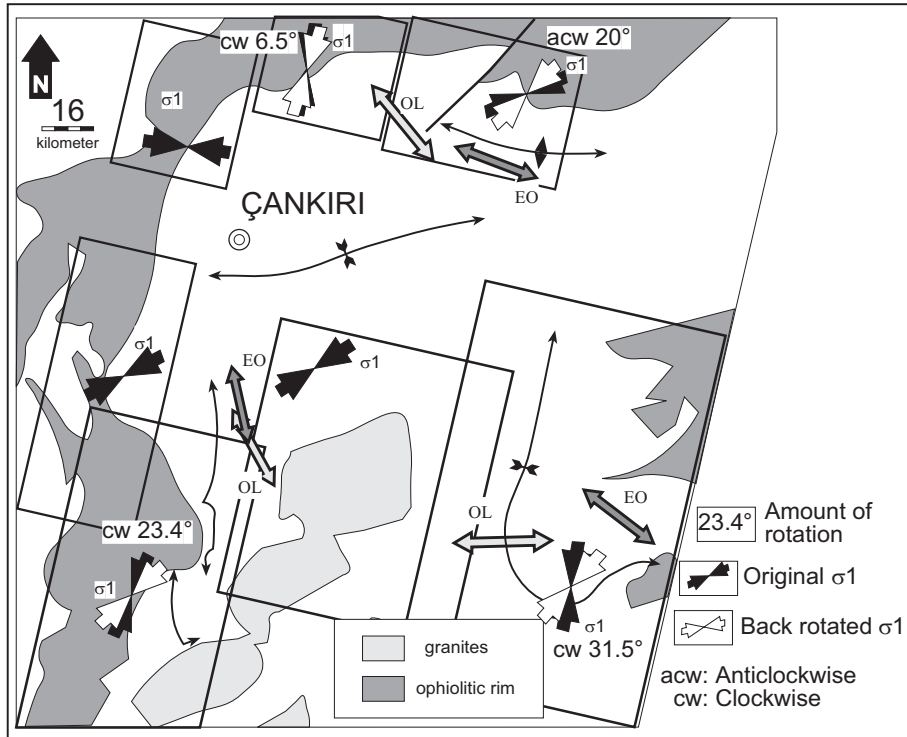
Figure 7.05 Outline maps indicating K_{max} orientations, adjacent major fold axial trends and paleostress orientations for each time interval. Boxes are sub areas which are used to generalise mean stress orientations (see chapters 5 and 6). σ_1: Major principal stress orientations. EO: Eocene, OL: Oligocen.

The Eocene and Oligocene anticlockwise rotation in the western and the clockwise rotation in the north-eastern rim together with the northward drift of the basin, support the model of a rigid indentor (Kırşehir Block) causing escape of the Sakarya Continent from the zone of intense high strain (Figure 7.06). The resulting Ω-shape of the rim of the Çankırı Basin , implies an irregular northern margin of the Kırşehir Block. This is also described from sandbox model experiments (Zweigel, 1998) and modeled by Marshak (1988). After restoring the structural trends of the basin margins on the basis of the paleomagnetic results, the southern margin of the Sakarya Continent, at the location of the Çankırı Basin, is still curved (northwards convex) prior to Eocene. This may indicate that the indentation process of the Kırşehir block pre-dates the Eocene (Figure 7.06). In the course of the indentation process, a radial pattern of σ_1 in the basin in-fill and the rim is expected, and indeed found (compare σ_1 orientations in Figure 7.05). Furthermore, the suture zone between the colliding blocks divides the region into two different tectonic regimes; where thrusting in the Sakarya Continent and coeval strike-slip deformation in the Kırşehir Block is recognised (Figure 7.05). The paleomagnetic results of the Çankırı Basin, from the Middle and (except Eskialibey) Late Miocene yielded no rotation, possibly

211

implying the end of the indentation process, which is in agreement with the paleostress and stratigraphical results discussed in chapters 3,4,5 and 6.

Finally, the trends of the k_{max} orientations, the adjacent major structural trends and the paleostress orientations constructed (discussed in chapters 5 and 6) all are in good agreement, validating the tectonic evolution of the Çankırı Basin (Figure 7.06).
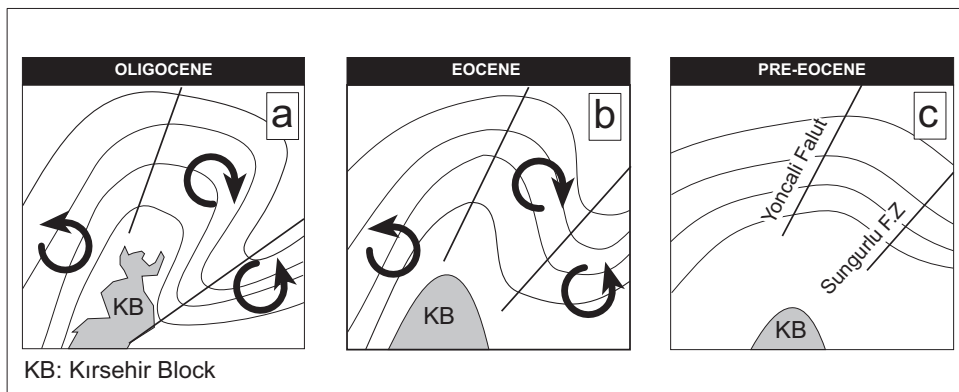
Figure 7.06 Back rotation of rim of the Çankırı Basin. Note northwards convex outline of the basin in pre-Eocene. Note pre-Eocene curved outline of the Çankırı Basin after back rotation of its margins

7.6 Conclusions

The paleomagnetic results from the Eocene to Late Miocene sediments of the Çankırı Basin show:

I.   Anticlockwise rotations in the west and clockwise rotations in the north-east and no rotation for the Kırşehir Block at least since the Oligocene.

II. The Çankırı Basin underwent a northward drift since the Eocene as indicated by inclination data. These results are also in good agreement with the proposed indentation model for the Kırşehir Block.

III. The Early Tertiary compressional period and therefore the indentation process ended before the Middle Miocene, this relation was also revealed by lack of rotations after the Oligocene.

IV. The paleostress data and AMS orientations support the proposed evolutionary history of the Çankırı Basin.

<div align="right">

8

</div>

TECTONO-STRATIGRAPHICAL EVOLUTION OF THE ÇANKIRI BASIN (Central Anatolia, Turkey)

Abstract

In this chapter the tectono-stratigraphical evolution of the Çankırı Basin is discussed based on the compilation of information presented in the previous chapters of this thesis. The Çankırı basin has evolved from Late Cretaceous to Recent through the subduction of the Northern Branch of the Neotethys (Vardar) Ocean, which led to the collision between the Sakarya Continent and the Kırşehir Block along the Izmir- Ankara-Erzincan Suture Zone. The Early Tertiary lithologies of the Çankırı Basin include units formed and deposited in various tectonic settings ranging from accretionary wedge, fore-arc to inter-arc to collisional settings in which the depocentre migrated southwards towards the Kırşehir Block. The collision of the Kırşehir Block with the Sakarya Continent in the Late Paleocene to Oligocene gave rise to an anticlockwise rotation of the western rim and a clockwise rotation of the eastern rim which subsequently resulted in the Ω-shape of the Çankırı Basin. The Neogene lithologies were deposited within an extensional setting in the Middle Miocene. A transcurrent regime was active from the Late Miocene onwards. In detail, the basin has experienced four phases of deformation, which reflect the above tectonic development. The first phase is associated with NW-SE thrusting and is attributed to the subduction phase. The second phase is characterized by a combination of thrusting in the northern area and transpressional deformation in the southern part of the Çankırı Basin in which σ_3 was vertical in the northern part of the basin, whereas in the southern areas and on the basement σ_2 was vertical. This second phase is attributed to collision between the Sakarya Continent and the Kırşehir Block during which the Çankırı Basin continued to evolve as a series of south vergent piggy-back basins. The third phase was characterized by extensional deformation and is interpreted to be the result of post-orogenic collapse enhanced by the decrease of the convergence rate between Africa-Eurasia, which began at 20 Ma. The last phase is characterized by transcurrent tectonics and has been active since ca. 11.1 Ma to Recent. The last phase is controlled by the North Anatolian Fault Zone (NAFZ) and commenced with the Eurasia-Arabia collision along the Bitlis-Zagros Suture in south-eastern Turkey and the subsequent expulsion of Anatolia to the west.

8.1 Introduction

Turkey is composed of a collage of micro-continents and continental fragments with Laurasian and Gondwana affinity, which formed during rifting through the Paleozoic to Mesozoic and were separated from each other by oceanic domains that were subducted and completely consumed through the Mesozoic and Early Cenozoic. Based on the spatial distribution of present-day ophiolitic belts in Turkey, a number of oceanic domains of differing ages have been proposed. Robertson *et al.* (1996) have discussed the various paleogeographic models for these oceans and concluded that *"...the term Paleotethys (or Paleo-Tethys) and Neotethys (or Neo-Tethys) have been used in many different ways and they are model dependent…"* In fact, all models are still controversial in that little is known about the geometry, extent, paleogeographic positions and the polarity of the subduction of these oceanic domains. Their evolution since Paleozoic is also controversial. Some of the paleogeographic reconstructions of the Tethys area in the Eastern Mediterranean since the Paleozoic are illustrated in Figure 8.01. The term Paleotethys was used mainly in two ways. According to Şengőr *et al.* (1984), Decourt *et al.* (1993) and Channel *et al.* (1996), Paleotethys is a remnant ocean of Paleozoic age that was subducted southwards under Gondwana, through the Paleozoic to Early Mesozoic. Due to its southwards subduction under Gondwana, it caused back arc rifting on the northern margin of Gondwana and gave way to the formation of the Neotethys, including a number of continental fragments, that drifted northwards in the Early Mesozoic (Şengőr *et al.* 1984). The Neotethys Ocean was geographically separated from the Paleotethys by the Cimmerian Continent and contained other isolated continental fragments, including the Sakarya Continent and the Kırşehir Block (Figure 8.01). The Cimmerian Continent and some of the other continental fragments drifted northwards and finally collided with Laurasia diachronously. According to Robertson and Dixon (1984) and Robertson *et al.* (1996), there was only a single Tethys that existed as a wide ocean and evolved continuously from Late Paleozoic to Recent with a series of rifting and subduction northwards under Eurasia (Figure 8.01a). They applied the term Paleotethys to separate the age of the oceanic crust in their models: Paleotethys implies Paleozoic oceanic floor while Neotethys implies Mesozoic oceanic floor. According to Robertson *et al.* (1991 and 1996) the northern margin of Gondwana was a passive margin at least during Late Paleozoic and micro-continents were separated by rifting from Gondwana, then drifted northwards into the Mesozoic Tethys and amalgamated as the oceanic floor separating these blocks was consumed.

The tectonic units that were involved in the Tethyan evolution of Turkey are subdivided into two groups based on their affinity to Laurasia and to Gondwana. The Rhodope-Pontide Fragments (Şengőr and Yılmaz 1981) lie in northern Turkey and have Laurasian affinity. These comprise the Strandja Zone, Istanbul Zone, Kűre Zone, Bayburt Zone and Sakarya Continent (Figure 8.02b). The continental fragments with a Gondwana affinity have been classified traditionally into the Taurides and Anatolides. The Taurides (proper) include the present day geographic areas of the Taurus Mountains and are generally non-metamorphosed. It was later recognized by Şengőr and Yılmaz (1981) that the Anatolides are the metamorphosed (in Late Cretaceous) equivalents of Taurides. They proposed that the continental fragments with the Gondwana affinity include the Taurus-Menderes Block, the Kırşehir Block and the Bitlis-Pőtűrge Fragments (Figure 8.02b).

214
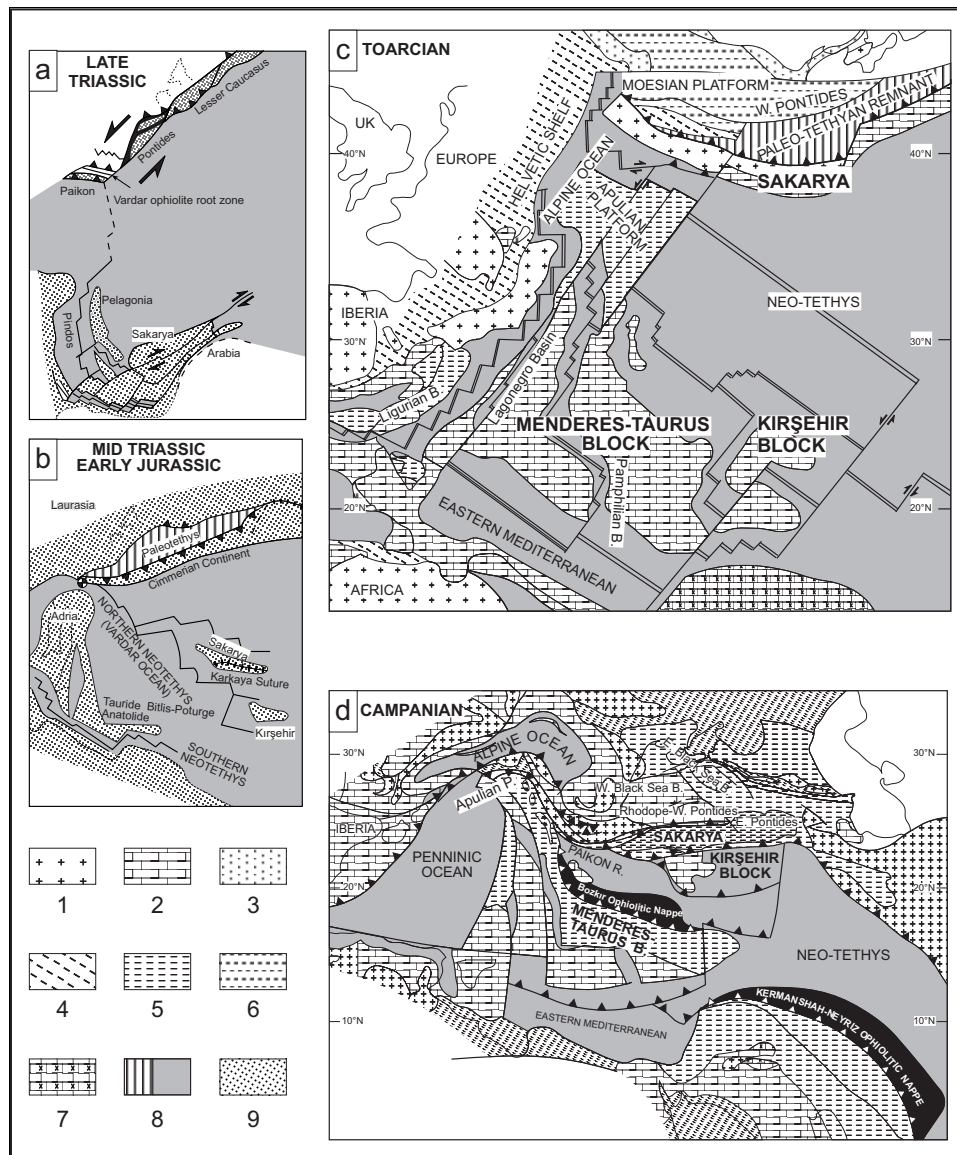
Figure 8.01 Some selected published paleogeographic reconstructions of the Eastern Mediterranean Tethys after: a) Robertson and Dixon (1984), b) Şengör et al. (1984), c-d) Channel et al. (1996). Apart from the paleogeographic positions of the continental fragments, the main difference between these models is the polarity of the subduction of the Permo-Triassic Tethys oceanic crust (Paleotethys). Note the locations of the Sakarya Continent and of the Kırşehir Block. 1. exposed continental basement, 2. carbonate platform, 3. continental deposits, 4. mixed shelf environment, 5. deep shelf, 6. marginal marine, 7. restricted carbonate platform, 8. deep sea, 9. continental crust (in a and b).

215

Little is known about the geometry, extent, paleogeographic positions and evolutionary history of these continental fragments. This is can be attributed to a lack of data as well as tosubsequent tectonic events that have obscured the early-formed structures The nett result is confusion and misinterpretations (Robertson and Dixon 1984, Şengőr *et al.* 1984, Robertson *et al.* 1996).

In addition to the evolutionary history and paleo-geographic reconstructions of the continental blocks within Tethys, the polarity of the subduction of the intervening oceanic crust, the mode of subduction and the timing of collision is still being debated. Furthermore, the processes that took place during and after the collision and amalgamation are poorly known.

The purpose of this chapter is to discuss the tectono-stratigraphical evolution of the Çankırı Basin in order to shed some light on the subduction history of the Neotethys and especially, on the collision of the Sakarya Continent and the Kırşehir Block in the Early Tertiary and to constrain its post-collisional history through the data presented and discussed in the preceding chapters. The tectono-stratigraphical evolution of the Çankırı Basin will be discussed in a regional context based on the results of the previous chapters and the literature.

8.2 Geological Outline of the Çankırı Basin

The Çankırı Basin lies within the Izmir-Ankara-Erzincan Suture Zone (IAESZ), which demarcates the former position of the Northern Neotethys ocean (Figure 8.02c along which the Sakarya Continent and the Kırşehir Block collided and amalgamated (Şengőr and Yılmaz 1981). It is an unique area in north central Anatolia to study the subduction history of Neotethys and the collisional history of the Sakarya Continent and Kırşehir Block. The IAESZ follows an approximately E-W trend and makes a northwards loop near the Çankırı Basin that resulted in the Ω-shape of the basin. The Çankırı Basin, along its western, northern and eastern margins has a rim comprising of an ophiolitic mélange unit intermingled with Late Cretaceous units, originating from the Neotethys Ocean (Floyd 1993, Tűysűz *et al.* 1995). This mélange is thought to underlay most of the northern parts of the basin while the Kırşehir Block underlies the southern part (Figure 8.02c). The Çankırı Basin has a more than 4 km thick Early Tertiary to recent basin in-fill deposited in 5 different cycles of sedimentation (discussed in chapters 3 and 4 and summarized in Figure 8.03). The Çankırı Basin experienced four different phases of tectonic deformation (see chapters 5 and 6 and Figure 8.03) and its western and southeastern margin underwent anticlockwise rotation while the eastern margin rotated clockwise in pre-Eocene to Oligocene (see chapter 7).

8.3 Brief Outline of the Tectonic units Involved in the Evolution of the Çankırı Basin

The major tectonic units in and around the Çankırı Basin are the Sakarya Continent, and the Kırşehir Block. These two blocks were separated from each other by the Northern Neotethys, Figure 8.01) and collided in Late Cretaceous to Early Tertiary (Görür *et al.* 1984, Gőncűoğlu *et al.* 1992, 1993, Dellaloğlu *et al.* 1992, Õzçelik 1994, Okay *et al.* 1996) along the IAESZ.
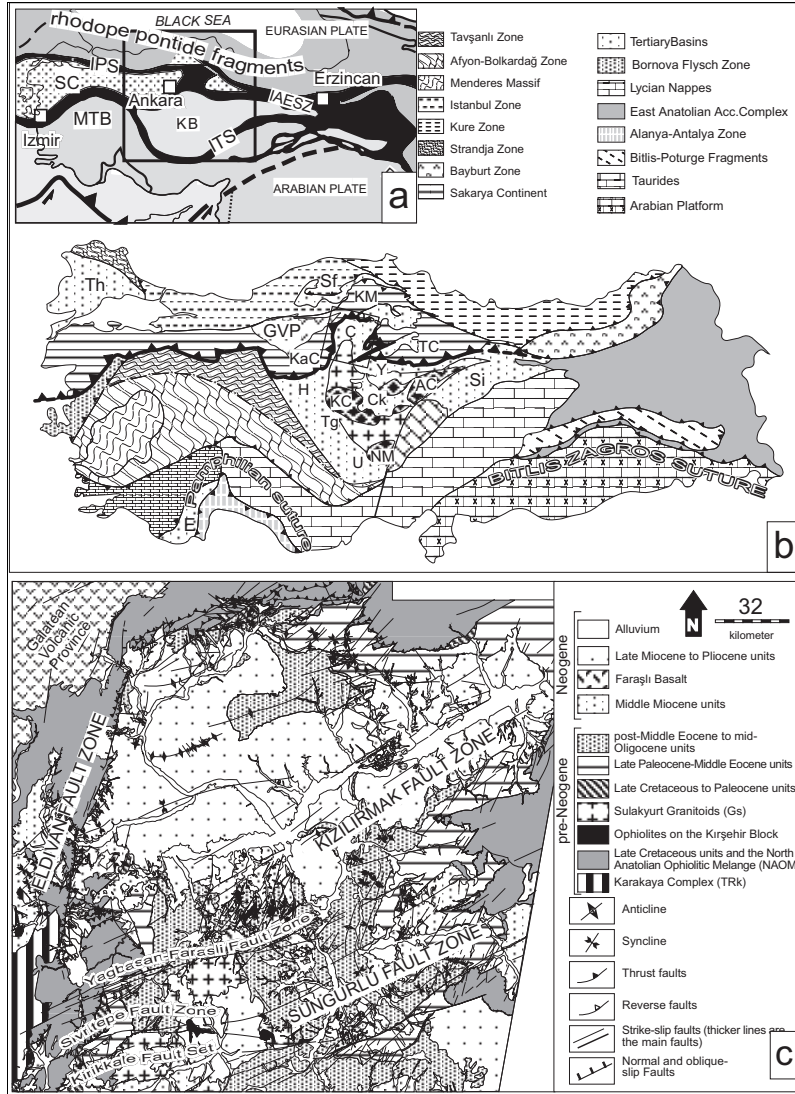
Figure 8.02 a) Main tectonic units of Turkey (after Şengőr et al. 1984). Black areas are the oceanic domains. IAESZ: Izmir-Ankara-Erzincan Suture Zone, IPS: Intra-Pontide Suture, ITS: Inner-Tauride Suture, KB: Kırşehir Block, SC: Sakarya Continent, b) Isopic zones and main Tertiary basins of Turkey (modified after Şengőr and Yılmaz 1981, Şengőr et al. 1984, Okay et al. 1996). Th: Thrace Basin, Sf: Safranbolu Basin, Ç: Çankırı Basin, GVP: Galatean Volcanic Province, Ck: Central Kızılırmak Basin, H: Haymana Basin, Tg: Tuzgölü Basin, U: Ulukışla Basin, Si: Sivas Basin, E: Elmalı Basin, KaC: Karakaya Complex, KM: Kargı Massif, TC: Tokat Complex. AC: Akdağmadeni Massif, KC: Kırşehir Metamorphics, NM: Niğde Massif. c) Simplified Geological map of the Çankırı Basin.

217

8.3.1 Sakarya Continent

The Sakarya Continent (Figure 8.02b) comprises three metamorphic complexes: the Karakaya Complex (Koçyiğit 1987) in the west, Kargı Massif (Tüysüz 1990) in the north, Tokat Complex in the east (Özcan *et al.* 1990). The Çankırı Basin lies at the junction between the three complexes. The Sakarya Continent is composed of a Paleozoic to Late Triassic basement and Liassic to Late Cretaceous cover. The lower part of the basement of the Sakarya Continent is composed of variably metamorphosed litharenites, basic volcanic rocks, shale and limestones. The upper part is composed of a Permian to Late Triassic tectono-stratigraphic assemblage comprising, from bottom to top, a very thick (more than 1km) clastic sequence, a tectono-sedimentary mixture of greywackes, spilites and Permo-Carbonifereous exotic blocks (Bozkurt 1990) set in greywackes, which passes into a relatively undisturbed Anisian to Norian (Middle to Late Triassic) sandstone, siltstone and limestone alternation (Koçyiğit 1987). In the Tokat Complex this assemblage is metamorphosed to greenschist facies (Bozkurt *et al.* 1997, Rojay and Göncüoğlu 1997).

The cover of the Sakarya Continent starts at the bottom with relatively thin (not more than 200m) but widespread Liassic clastics (Bayırköy Formation, Altıner *et al.* 1991) which passes into deep marine shales, turbidites locally intercalated with volcanics, and overlain by very thick neritic carbonates (Bilecik Group of Altıner *et al.* 1991) of Malm and Early Cretaceous age. This sequence contains a regional hiatus at the end of Jurassic and earliest Lower Cretaceous (Altıner *et al.* 1991, Koçyiğit *et al.* 1991). The Early Cretaceous is represented by pelagic limestones passing into thick tuffaceous limestones (Vezirhan Formation, Altıner *et al.* 1991), and locally into flysch and volcano-sedimentary assemblages of Late Cretaceous age (Teşrekyayla Formation of Koçyiğit *et al.* 1988).

According to Şengör *et al.* (1984), Robertson and Dixon (1984), Robertson *et al.* (1996), and Channel *et al.* (1996), the Sakarya Continent was an isolated Pontide block within the Neotethys ocean and evolved independently throughout Middle and Late Mesozoic. It drifted northwards and finally collided with the other Pontide blocks along the Intra-Pontide Suture in Early Tertiary (Figure 8.02a). However, based on paleomagnetic results on the Sakarya continent, Channel *et al.* (1996) proposed that the Sakarya continent was separated from Laurasia by a remnant ocean of Paleotethys (sensu Şengör *et al.* 1984), which implies the absence of an Intra-Pontide Ocean since the Toarcian (Figure 8.01c).

8.3.2 Kirsehir Block

The Kırşehir Block is composed of three tectonic units: metamorphics, ophiolites that have been intruded by granitoids and which make up the third unit.

8.3.2.1 Metamorphics of the Kırşehir Block

The metamorphics of the Kırşehir Block (Oktay 1973) are subdivided into three metamorphic complexes. From west to east they are the Kırşehir Metamorphics (Seymen 1981,1982), Niğde Massif (Göncüoğlu 1977), and the Akdağmadeni Massif (Göncüoğlu *et al.* 1991,1992,1993, and 1994) (Figure 8.02b). Each of these comprises three units, similar to the Menders Massif (Figure 8.02b). From bottom to top these are; the core (Gümüsler Metamorphics), schistose cover (Kaleboynu Metamorphics) and a marble cover (Aşıgediği Metamorpics, Göncüoğlu *et al.* 1993). The medium grade (upper greenschist to amphibolite facies) metamorphic core represents the oldest part of the Kırşehir Block. Its protoliths of which are composed of a former flyshoid sequence, felsic intrusives and

extrusives, clayey limestone and basic volcanics of unknown age. The schistose cover, possibly unconformably overlying the core, is composed of alternations of quartzite, marl and siltstone and was correlated with the Afyon-Bolkardağ Belt (Figure 8.02b) (Gőncűoğlu *et al.* 1992, 1993). The marble cover is composed of marble, dolomitic marble and cherty marble, which is thought to have been deposited on a carbonate platform, and is correlated with the Triassic-Jurassic to Early Cretaceous Bolkardağ (Őzgűl 1976) isopic zone of the Taurides (Gőncűoğlu 1993). Based on this information, Gőncűoğlu et al (1993) further interpreted that the top sequence (marble cover) was deposited in the northern margin of the Menderes Taurus Block (Şengőr and Yılmaz 1981) that was facing the Northern Branch of the Neotethys to the north. The cherty limestones were interpreted to indicate the timing of the collapse of the platform due to the beginning of the subduction of the Neotethys ocean, in Early Cretaceous (Gőncűoğlu *et al.* 1993). Recently, the Niğde Massif, apart from the Kırşehir Metamorphics and the Akdağmadeni Massif, has been recognized as a typical core complex (Whitney and Dilek 1997) similar to that postulated for Menderes (Bozkurt and Park 1994). Both are thought to have formed in the Early to Middle Miocene. However, it appears that the intensity of extensional deformation decreases from west to east as evidenced by the relatively small Niğde Massif.

8.3.2.2 Ophiolites on the Kırşehir Block

The ophiolites on the Kırşehir Block are exposed within distributed patches. Some of them are intruded by granites and are exposed as enclaves and roof pendants within these granites (Yalınız *et al.* 1996, Kuscu 1997, Gőncűoğlu *et al.* 1992 and 1993). They are composed of various ultramafics, dominantly serpentinized peridotites and harzburgites. Locally, wherlites, lherzolites, plagio-granites, diabase dykes with dyke-in-dyke structures, pillow basalts, boninites and associated volcano sedimentary successions, alternating with pelagic sediments including radiolarites with manganese nodules (Yalınız *et al.* 1996) are also present. According to these authors, the ophiolites in the southwestern part of the Kırşehir Block (outside the present study area) were formed from a supra-subduction setting in the Campanian to pre-Late Maastrichtian.

8.3.2.3 Granitoids of the Kırşehir Block

The granitoids of the Kırşehir Block were emplaced during and after the southward obduction of the ophiolites from the northern branch of the Neotethyan Ocean onto the Taurides during Late Cretaceous (Erler *et al.* 1991; Akıman *et al.* 1993) and before the Late Maastrichtian (Yalınız *et al.* 1996). They were generated as a consequence of crustal thickening due to arc to arc or arc to continent collision (Göncüoğlu *et al.* 1992, and 1993). In general, the Central Anatolian granitoids belong to two broad classes: granitoids with S-type characteristics and granitoids displaying both S-and I-type characteristics. They display distinctive features of H-type (hybrid) granites, and plot both in island arc and collision fields with within plate signatures on trace element discrimination diagrams (Bayhan, 1987; Erler *et al.* 1991; Akıman *et al.* 1993; Erler and Bayhan, 1995), and may be accepted as collision related granitoids. The geological evidence indicates a two-fold obduction resulting in two phases of magmatism producing two different types of plutons in addition to the ones produced within an island arc setting and which were obducted and amalgamated together with the ophiolites (Göncüoğlu *et al.* 1994). The earlier phase generated S-type syn-collisional granitoids of 95±11 Ma (Rb-Sr ischrons, ?Albian-Santonian; Göncüoğlu, 1986). This phase is thought to be due to the obduction of MORB-type ophiolites (Göncüoğlu *et al.* 1992; Yalınız *et al.* 1996) onto the protoliths of the Kırşehir Block. The second phase is due to obduction of supra-subduction zone ophiolites

219

onto the previously metamorphosed units, and is characterized by post-collisional granitoids displaying both S and I-type characteristics, generated by post-collisional extension at the end of Cretaceous to Earliest Paleocene, after the second obduction event ceased (Erler *et al.* 1991; Geven, 1992; Göncüoğlu *et al.* 1993, Erler and Göncüoğlu, 1996). Both syn-collisional and post-collisional varieties cut across the metamorphics of the Kırşehir Block (Kuscu 1997).

The radiometric data on the granitoids are rather scarce and available data indicate that all granites within the Kırşehir Block are older than Paleocene (see chapter 2). In addition, granite pebbles in the Later Maastrichtian to Paleocene successions (Görür *et al.* 1984, Göncüoğlu *et al.* 1991, 1992, Çemen *et al.* 1999) indicate their pre-Paleocene emplacement.

8.4 Brief Summary of Tectono-stratigraphic Characteristics of the Çankırı Basin

In this section a brief outline of the tectono-stratigraphy of the Çankırı Basin, discussed in detail in the previous chapters will be summarized.

8.4.1 Remote Sensing and Seismic Interpretation Data

As discussed in chapter 2, remote sensing, gravity and seismic interpretation results have indicated that the Early Tertiary in-fill of the Çankırı Basin has a south ward thinning wedge shape associated with on-lap patterns onto the basement (Kırşehir Block) and progressive unconformities, together with the southward migration of the depocenters (Figure 8.4b). Three of the four deformation phases for the Early Tertiary to Recent deposits were recognized in the seismic sections. The first phase was associated with thrusting and took place prior to the Middle Miocene. The thrust faults were displaced by normal faults of variable orientations indicating an extensional phase after thrusting. These faults are growth faults with thicker down-thrown block and thinner up-thrown block geometries. In the last phase, some of these normal faults were inverted into reverse faults. These deformation phases were correlated with the last three deformation phases of the four deformation phases recognized from paleostress inversion techniques and discussed in chapters 5 and 6.

8.4.2 Stratigraphic Data

The subduction of the Neotethyan oceanic crust in the area of the Çankırı Basin is thought to occurred along two north-dipping trenches (Tűysűz *et al.* 1995, Gőncűoğlu *et al.* 2000). The northern trench was associated with an ensialic arc that produced the Late Cretaceous to Early Tertiary volcanics of the Galatean Volcanic Province (Koçyıgit 1991) while the southern one was an ensimatic arc (Figure 8.04a). Yalınız *et al.* (1996) and Gőncűoğlu *et al.* (2000) have argued that the southern trench was associated with supra subduction zone (fore-arc) ophiolites, remnants of which are now exposed on the Kırşehir Block. They must have been produced within a relatively short time interval in Campanian to pre-Middle Maastrichtian times. Tűysűz *et al.* (1995) and Rojay *et al.* (1998) have argued that lithologies that display a seamount origin are embedded within the rim of the Çankırı Basin. The granitoids of the Kırşehir Block were produced within an island arc environment (see above) and within the Kırşehir Block itself due to partial melting during the collision and obduction of the northern Neotethys ophiolites, in Late Cretaceous (Erler *et al.* 1991; Geven, 1992; Göncüoğlu *et al.* 1993, Erler and Göncüoğlu, 1996).

220
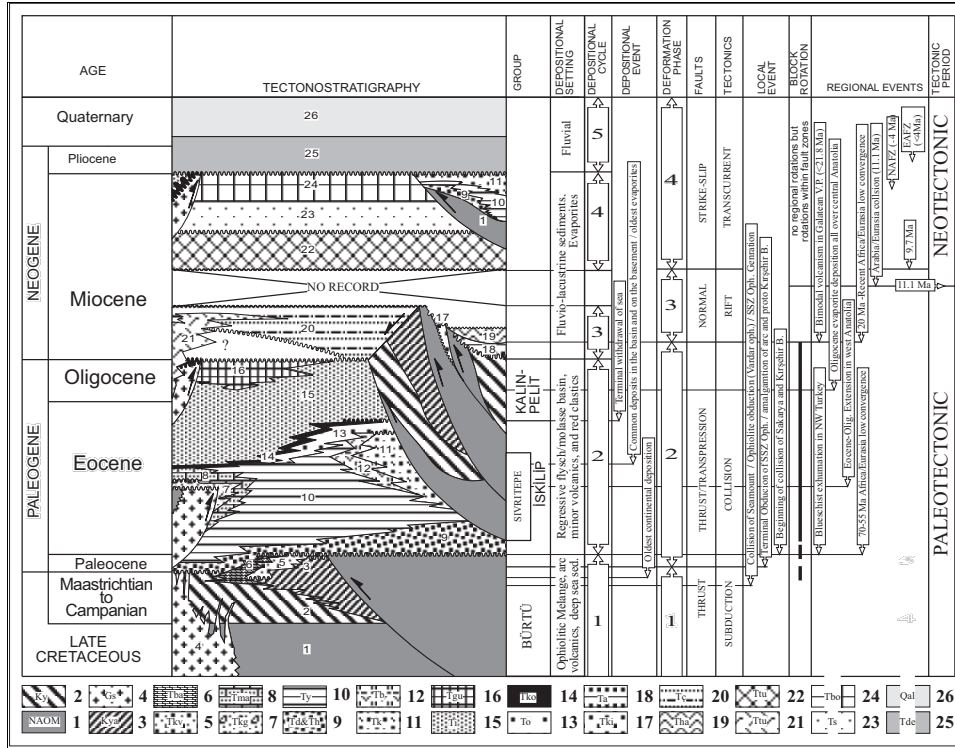
Figure 8.03 Generalized tectono-stratigraphic column of the units exposed in and around the Çankırı Basin. 1. North Anatolian Ophiolitic Melange-NAOM, 2. Yaylaçayı Formation (distal fore-arc sequence), 3. Yapraklı Formation (proximal fore-arc facies), 4. Sulakyurt Granites of the Kırşehir Block that intruded in pre-Paleocene, 5. Kavak formation (red clastics and carbonates), 6. Badiğin formation (neritic limestones), 7. Karagŭney Formation (clastics derived mainly from the Kırşehir Block) 8. Mahmatlar Formation (clastics derived from Sulakyurt Granite), 9. Dizilitaşlar and Hacıhalil formations (mainly turbiditic clastics and intercalated limestones), 10. Yoncalı Formation (Eocene flysch), 11. Karabalçık Formation (distributary channel conglomerates and sandstones with coal seams), 12. Bayat Formation (Eocene volcanics and volcanoclastics), 13. Osmankahya Formation (mixed environment clastics and red beds), 14. Kocaçay Formation (Middle Eocene nummulitic limestone covering both basin in-fill and the granitoids). 15. İncik Formation (continental red clastics), 16. Gŭvendik formation (evaporites), 17. Kılçak Formation (fluvio-Lacustrine clastics), 18. Altıntaş Formations (fluvial red clastics exposed only in the Hancılı Basin), 19. Hancılı Formation (Lacustrine deposits exposed only in the Hancılı Basin, 20. Çandır Formation (fluvio-lacustrine sediments), 21. Faraşlı Basalt 22. Tuğlu formation (evaporites and Lacustrine shale/marl), 23, Sŭleymanlı formation (fluvio-lacustrine red clastics), 24. Bozkır Formation (evaporites), 25. Deyim Formation (fluvial clastics), 26. Alluvium. NAFZ: North Anatolian Fault Zone, EAFZ: East Anatolian Fault zone. See chapters 3 and 4 for the description of the units.

It has been discussed in chapter 3, that the Late Cretaceous to Paleocene units were deposited during the subduction of the northern Neotethys. The Yaylaçayı and Yapraklı formations were deposited within the fore-arc to inter-arc basins formed during subduction in which Yaylaçayı represents the more basinal facies while the Yapraklı Formation

represents more proximal facies (Figure 8.04a). The contacts between the Yaylaçayı and Yapraklı Formation and the overlaying Malıboğazı, Kavak and Badiğin formations are syn-depositional unconformities indicative of ongoing deformation, erosion and coeval deposition. Dominance of terrestrial and shallow marine deposits indicates the narrowing of the basin and the presence of pebbles in the Kavak formation that are derived from the NAOM, Yaylaçayı and Yapraklı Formation indicates emergence and sub aerial erosion of these units.
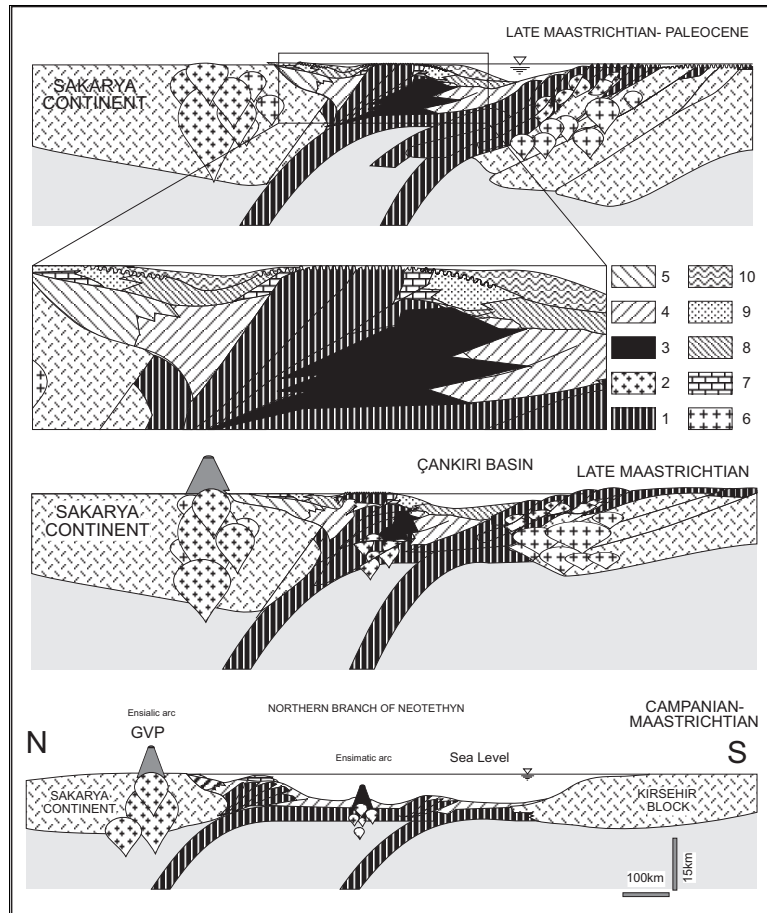
Figure 8.04a Conceptual cross-sections illustrating scenarios for the Late Cretaceous to Paleocene evolution of the northern branch of the Neotethys (NBN). 1. oceanic crust and ophiolites, 2: arc granites, 3: island arc, 4. Yaylaçayı Formation, 5. Yapraklı Formation, 6. collision type granites, 7. Malıboğazı Formation, 8. Badiğin formation, 9: Kavak formation, 10. Dizilitaşlar Formation. b) Schematic block diagrams illustrating the Late Paleocene to Oligocene evolution of the Çankırı Basin. See chapter 3 for discussion of this figure.

LATE EOCENE TO MID=OLIGOCENE

Incik

Güvendik

Lake level

Osmankahya

Karabalçık and
Osmankahya

Hacıhalil

Yoncalı

Kocaçay

Mahmatlar

EARLY TO MIDDLE EOCENE

NAOM

Yoncalı

Ophiloites

Thrust faults

Sediment transport direction
(size of the arrow is proportional
with the amount of transported sediment)

Strike-slip faults

Fault scarps

Sediment lobes (alluvial fan, fan-delta, submarine fan)

Yoncalı

Sulakyurt granitoids

Karagüney

KIRŞEHİR BLOCK

LATE PALEOCENE TO EARLY EOCENE

Sea level

Sulakyurt granitoids

KIRŞEHİR BLOCK

b   *Figure 8.04 (continued)*

The Early Tertiary units including the Hacıhalil, Yoncalı, Karabalçık, Bayat, Osmankahya, Kocaçay, İncik and Günvendik formations show migration of the depocenter towards the south (i.e. to the Kırşehir Block; see chapter 3). They are also associated with syn-depositional unconformities that are indicative of contemporaneous deformation and

223

sedimentation. The syn-depositional unconformities (discussed in chapter 3) indicate that thrusting and sedimentation were coeval during the Early Tertiary.

The oldest granite pebbles were observed within the Late Paleocene to Early Eocene Karagűney and Karabalçık formations in the SW part of the Çankırı Basin (see chapter 2). This information is very important for the timing of un-roofing of the granites of the Kırşehir Block. In addition to this, in the same time period, the Çankırı Basin received detritus both from its ophiolitic rim and the Kırşehir Block, which indicates the emergence of the Kırşehir Block, and consequently the basin becoming relatively restricted. The Early to Middle Eocene Kocaçay Formation, which is characterized by nummulitic limestones, together with the Osmankahya Formation, that is characterized by continental clastics, are the two oldest basin filling units that cover both the in-fill and the Kırşehir Block. After the deposition of the Kocaçay Formation, the sea terminally regressed and deposition continued under continental conditions from post-Middle Eocene to Oligocene. During this time interval deposition of red clastics (Incik Formation) alternated with and was subsequently overlain by evaporites (Gűvendik formation). An unconformable contact with the granitoids of the Kırşehir Block and presence of their pebbles within the Late Paleocene units indicate that un-roofing of the granitoids took place prior to Late Paleocene (see also chapter 3). Therefore, Middle Miocene core complex development proposed for the Niğde Massif (Whitney and Dilek 1997) cannot apply to the northern parts of the Kırşehir Block (see also Göncűoğlu *et al.* 1991,1994, Çemen *et al.* 1999).

8.4.3 Paleostress Data

As discussed in chapters 5 and 6, more than 1000 fault slip data from 152 sites were obtained and analyzed. Their analysis revealed that the Çankırı Basin experienced four different phases of tectonic deformation. Based on cross-cutting relationships of the mesoscopic structures and overprinting slickenlines, these deformation phases were ordered and they were dated on the basis of stratigraphical data (see Figure 8.05 and chapters 5 and 6).

Deformation Phase 1 took place in pre-Late Paleocene, and was characterized by approximately NW-SE trending σ_1 and vertical σ_3 that indicates thrusting. Smoothed trajectories of the horizontal components of σ_1 and σ_2 were oriented NW-SE and NE-SW respectively (Figure 8.05a).

The second deformation phase took place in the Late Paleocene to pre-Middle Miocene, and smoothed trajectories of σ_1 display a radial pattern towards the Çankırı Basin while the vertical stress was different in the northern and southern parts of the basin. In the northern parts σ_3 was oriented vertical while in the southern part, and especially on the Kırşehir Block, it was σ_2 that was vertical (Figure 8.05b). This relationship is interpreted as an indication of thrusting along the rim and in the northern parts of the basin while strike-slip deformation was dominant in the south and on the Kırşehir Block (see chapter 6). The interface between these two stress fields formed a stress discontinuity between the basin in-fill and the Kırşehir Block. Back rotation of the deduced stress tensors, in accordance with the paleomagnetic data, did not significantly alter the pattern of stress trajectories (Figure 8.05b). It is assumed that the distribution of the paleostress resulting from the second deformation phase reflects the collision of the Sakarya Continent and the Kırşehir Block and the indentation of the Kırşehir Block into the Sakarya Continent.

224
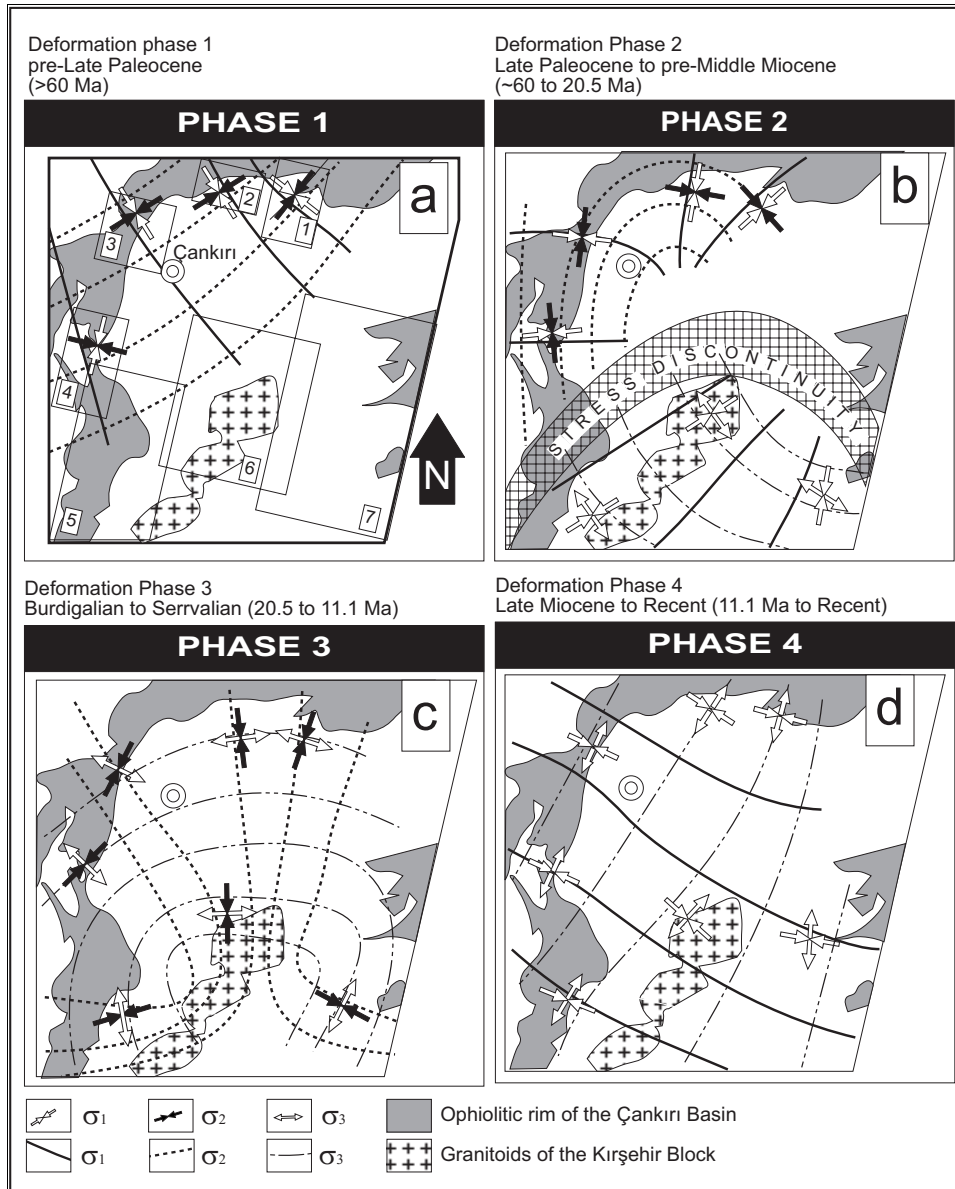
Figure 8.05 Smoothed trajectories of the calculated paleostresses for the four deformation phases experienced by the Çankırı Basin (discussed in chapters 5 and 6).

The third phase of deformation took place in latest-Early Miocene to Middle Miocene (approximately 20 to 13 Ma) and is characterized by sub vertical σ_1 and sub horizontal σ_3,

225

indicating extensional deformation in this phase. The smoothed trajectories of horizontal component of σ_3 display a concentric pattern that, more or less, follows the outline of the Çankırı Basin (Figure 8.05c).

The fourth deformation phase has been active since the Late Miocene (approximately 11 Ma to Recent) and is characterized by horizontal σ_1 and σ_3 indicating transcurrent tectonics and fitting with the current tectonic setting that is mainly controlled by the North Anatolian Fault Zone (Figure 8.05d).

8.3.4 Paleomagnetic Data and Significance of Ω-shape of the Çankırı Basin

Bends within orogens have been classified into two groups by Carey (1955) and the mechanisms by which they occur were discussed by Marshak (1988). Primary bends possibly form when younger orogens are moulded into the irregular margins of pre-existing cratons. Secondary bends, or oroclines, result from the impression of a later strain on a previously straight orogenic belt.

Paleomagnetic studies have been used to test the way in which oroclines develop. This is based on the assumption that a secondary bend in an orogen results from the rotation of rocks in the orogen around vertical axes (Marshak 1988), provided that acquisition of magnetic declinations predates rotation (Van der Voo and Channel 1980, Eldredge *et al.* 1985). On the other hand, Marshak (1988) discussed two possibilities that paleomagnetic analysis cannot recognize. *'…first, the paleomagnetic analysis of bends that form by rearrangement without rotation of fault-bounded blocks in an orogen. Second, the paleomagnetic method cannot distinguish between bends that formed during the development of the orogen (but subsequent to magnetization of the deformed rocks) and bends that truly formed after the structural grain of the orogen had been established…'* This problem can be overcome by increasing sample frequency, sufficient to resolve each tiny detail of the rotation history, which is often not possible for example, due to breaks in sedimentation, lack of good samples at desired stratigraphical levels and poor exposures (van der Voo and Channel 1980).

In relation to the Çankırı Basin, the question to be addressed by paleomagnetism is how and when the basin attained its Ω-shape. The answer to this also helps to understand the timing, mode and mechanism of the collision of the Sakarya Continent and the Kırşehir Block.

Indentation is one of the main causes for the rotation of orogenic blocks and the formation of oroclinal bends (Zweigel 1998). The mode, geometry and amount of rotation of the orogenic blocks are dependent on the type and geometry of the indentor. This is illustrated in Figure 8.06.

The paleomagnetic results, discussed in chapter 7, indicate that the western margin of the Çankırı Basin was rotated 33° anticlockwise, the eastern margin was rotated 52° clockwise while the southeastern margin was rotated approximately 36° anticlockwise within the Eocene to Oligocene time interval. No rotation was identified after the Middle Miocene. These relations indicate that the basin attained its Ω-shape by rotation induced by the indentation prior to the Middle Miocene. The curved outline of the Çankırı Basin, after back rotation of the detected Oligocene and Eocene paleo-declinations, indicates that rotational deformation commenced prior to Eocene (see chapter 7). Assuming an initial straight E-W trending outline of the rim of the Çankırı Basin, it is concluded that the collision of Sakarya Continent with the Kırşehir Block commenced prior to the Eocene.
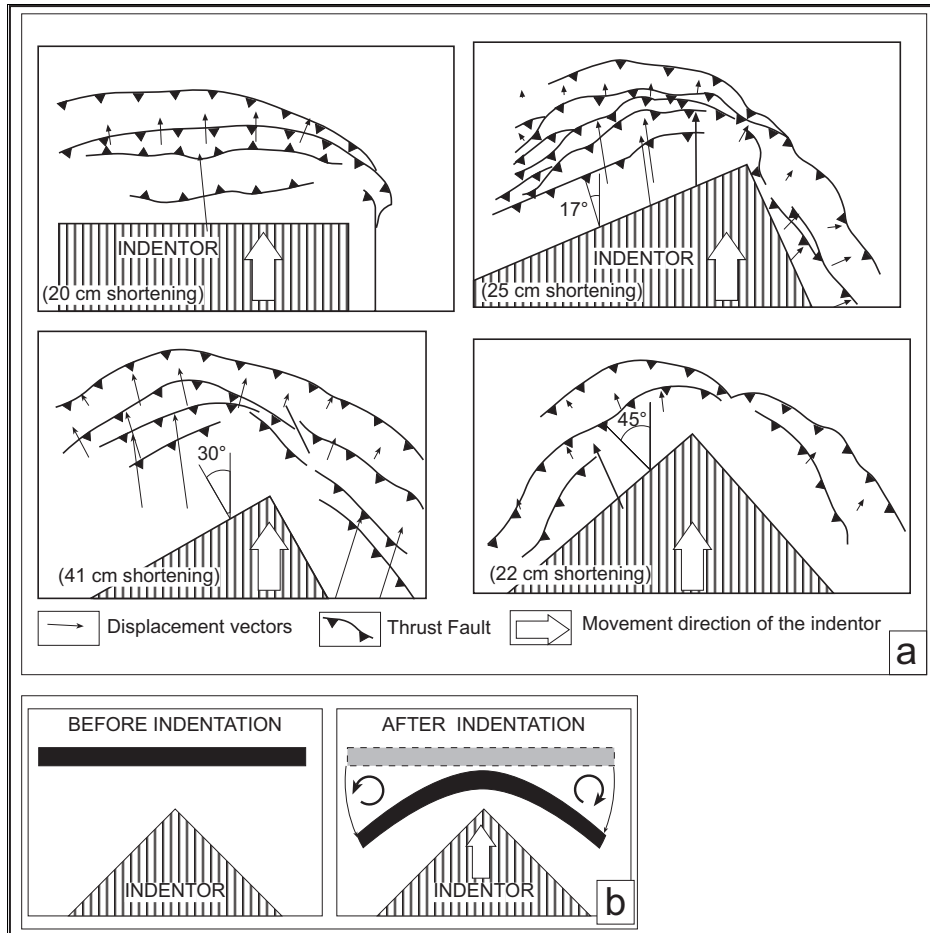
Figure 8.06 Line drawings of thrust fault patterns developed in sandbox experiments during indentation, carried out by Zweigel (1998). Note the effects that the geometry of the indentor has on the resultant pattern of the thrust faults. Note also the magnitude of the displacement vectors, which connect the points from their undeformed and deformed positions also depends on the indentor geometry. b) Simplified sketch depicting the pattern of rotation due to indentation in the sand box.

8.5 Pre-Neogene Tectono-stratigraphical Evolution the Çankırı Basin: Evolution of the Neotethys in Central Anatolia

In this section the tectonic evolution of the Kırşehir Block and of the Sakarya Continent will be discussed with respect to the evolution of the Çankırı Basin. In addition to the results of this thesis, the models that will be presented are also based on data from Şengőr and Yılmaz (1981), Robertson and Dixon (1984), Görür et al (1984), Şengőr *et al.* (1984) Gőncűoğlu *et al.* (1991,1992,1993, and 1994), Koçiğit (1991), Tűysűz *et al.* (1995), Channel; *et al.* (1996), Robertson *et al.* (1996), Yalınız *et al.* (1996)

227
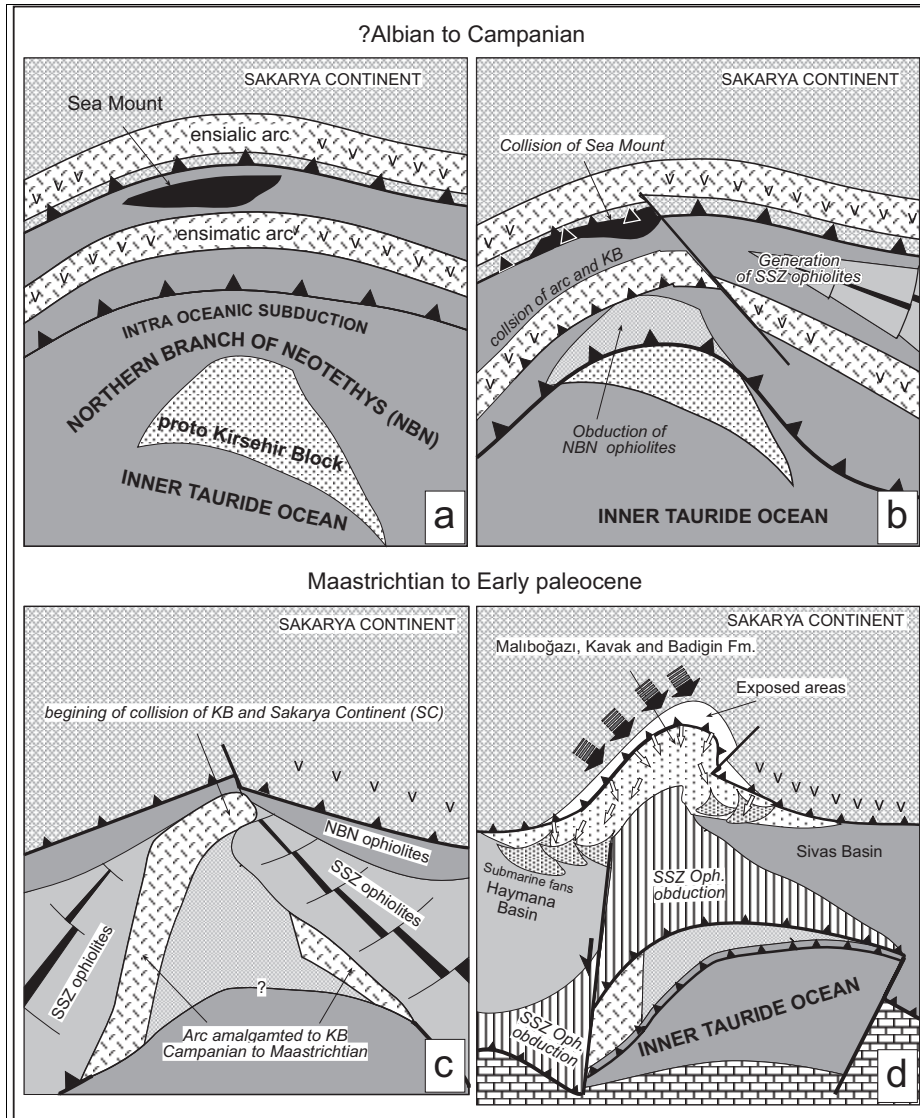
Figure 8.07 Paleogeographic reconstructions for the evolution of the Sakarya Continent and the Kırşehir Block together with the intervening areas. (a-b) based on Gőkten (1983), Gőrűr et al. (1984), Okay (1984, 1992), Gőncűoğlu et al. (1991,1992,1993,1994), Őzcelik (1994), Tűysűz et al. (1995), Yalınız et al. (1996). Anticlockwise rotation of the Kırşehir Block is based on Sanver and Ponat (1980). Collision of the ensimatic arc and the Kırşehir Block, and supra subduction zone ophiolite (SSZ) generation and their obduction is based on Yalınız et al. (1996), Yalınız (1997) and Gőncűoğlu et al. (2000). The areas in the south, south-east and south-west of the Kırşehir Block are after Gőrűr et al. (1984) and Okay (1984, 1992). See text for the discussion.

228

Figure 8.07 (continued)
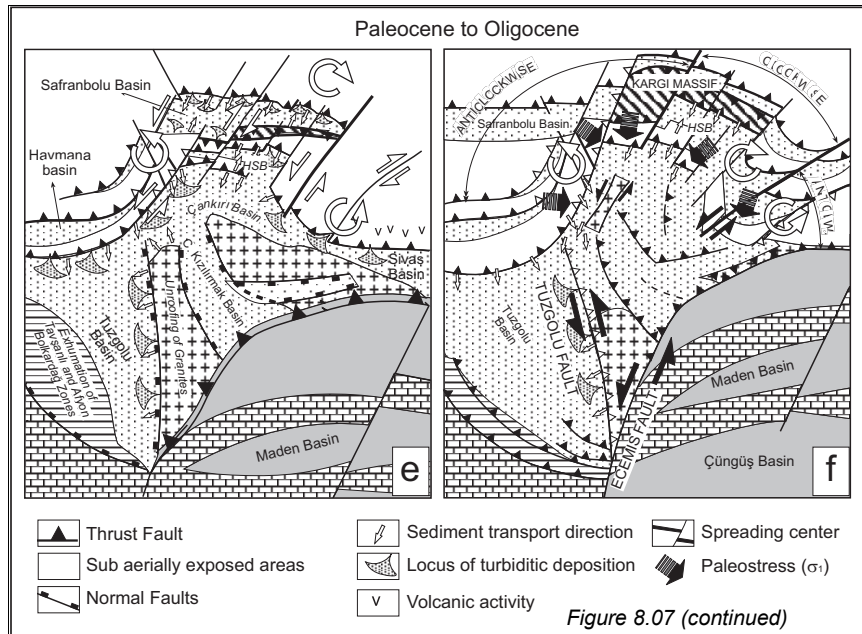
8.5.1 Santonian to Paleocene Events

As discussed in chapter 3 and illustrated in Figures 8.04 and 8.07, the subduction of the Neotethys Ocean in the Çankırı Basin area occurred along two north-dipping trenches. The northern one was associated with an ensialic arc located on the Sakarya Continent (Galatean Arc of Koçyiğit 1991) and the southern one was an intra-oceanic subduction zone associated with an ensimatic arc. The Kırşehir Block was located south of these arcs and drifted northwards with an associated anticlockwise rotation (Sanver and Ponat 1981). Tűysűz *et al.* (1995) have discussed that within the NAOM, seamount material was accreted in the Cenomanian to Late Cretaceous interval. The collision of this oceanic island (seamount) took place in the Campanian to Early Maastrichtian, that is during the deposition of Yapraklı and Malıboğazı formations (Figure 8.07a and b). The Late Cretaceous (but pre-Late Maastrichtian, Yalınız *et al.* 1996) MORB type ophiolites located to the south of the ensimatic arc were obducted onto the Taurides, including the Kırşehir Block, and led to the collision of the ensimatic arc with the Kırşehir Block (Figure 8.07b and c). The collision of the Kırşehir Block and the arc gave way to the generation of the collision related granites (Albian-Santonian, 95 ± 11 Ma) and to metamorphism of the passive margin deposits, both in the Taurides (Tavşanlı and Afyon-Bolkardağ belts, Figure 8.02b) and on the Kırşehir Block (Gőncűoğlu *et al.* 1991, 1993, 1994, Erler 1991, Akıman *et al.* 1993, Erler and Gőncűoğlu 1996). During the Campanian to pre-Late Maastrichtian, accretion of the seamount occurred and gave rise to the generation of supra-subduction zone (SSZ) ophiolites (Yalınız *et al.* 1996) on the remnant oceanic crust (to the north of the arc), possibly on either side of the Kırşehir Block (Figure 8.07b and c). The process continued as the promontory of the Kırşehir Block collided with the Sakarya Continent. It caused a decrease in the rate of northwards drift of the Kırşehir Block and served as an abutment while the pull of the subducting slab caused extension within the remnant

229

oceanic crust (Yalınız et all. 1996). In the Maastrichtian to Paleocene time interval, the supra subduction zone ophiolites obducted on to the Kırşehir Block (Figure 8.07c and d). The collision of the promontory of the Kırşehir Block caused uplift and sub aerial emergence of the collision front of the Sakarya Continent including the accreted material in the front (e.g. NAOM and associated Late Cretaceous units, Figure 8.07d), which gave way to a clastic influx from emerged areas into the Çankırı Basin (e.g. Dizilişlar Formation), and Tuz Gőlű basin (Figure 8.08). In the mean time, the Kırşehir Block was subjected to an extension possibly due to over-thickening of the Kırşehir Block during collision and obduction of the SSZ ophiolites which was enhanced by the decrease of convergence rates between Africa and Eurasia in the Paleocene (see Lips 1998). The latest Maastrichtian to Paleocene extension caused exhumation of the metamorphic belts of the Taurides (the Tavşanlı and Afyon-Bolkardağ belts; Okay *et al.* 1996) and started the un-roofing of the granitoid bodies within the Kırşehir Block accompanied by the development of the Central Kızılırmak Basin and the Tuzgőlű Fault at the western margin of the Kırşehir Block which developed as a normal fault (Çemen *et al.*1999) as the Kırşehir Block rotated anticlockwise and drifted northwards and gave way to the development of the Tuzgőlű Basin. In the Çankırı Basin, compressional deformation was still active in the same time due to the northwards drift and final convergence of the Kırşehir Block with the Sakarya Continent. In the Paleocene, piggy-back basins began to develop as the promontory of the Kırşehir Block indented the Sakarya Continent and possibly triggered rotation of the margins of the Çankırı Basin (Figure 8.07d). The paleo-stress patterns for this time period for the western and northwestern part of the Çankırı Basin are almost perpendicular to the thrust faults (see Figures 8.05a and 8.07d).

8.5.2 Paleocene to Oligocene Events

The basins that are located in central and north central Anatolia and developed in Paleocene include the Safranbolu, Haymana, Tuz Gőlű, central Kızılırmak, and Sivas basins (see Figures 8.02b and 8.07e and f) besides the Çankırı Basin. Except in the Haymana and Sivas basins, the oldest basin filling units that are unconformable (at least partly) with the underlying basement and the ophiolitic Late Cretaceous units were deposited within continental settings, passing upwards into marine settings (Figure 8.08). In the Haymana and Sivas Basins, Late Cretaceous and Paleocene strata are transitional. The basal unconformities and the continental deposits in the other basins may indicate a regional tectonic event or a drastic global sea level drop in the Paleocene. Considering the Late Cretaceous deep marine facies, some of which deposited below CCD (carbonate compensation depth) such as manganese bearing radiolarian cherts and cherty pelagic limestones (see chapter 3 and Yalınız *et al.* 1996), it is most likely that continental deposition in the Paleocene was the result of a regional tectonic uplift at the end of the Maastrichtian and in the Paleocene rather than a global sea level drop only. The basal conglomeratic units in the Safranbolu Basin (Tűysűz *et al.* 1989), in the central Kızılırmak Basin (Gőncűoğlu et al 1991), and in the Tuzgőlű Basin (Gőrűr *et al.* 1984) can be correlated with the Late Paleocene to Middle Eocene Hacıhalil Formation of the Çankırı Basin. In all of these basins, the basal continental sequence is followed upwards and laterally by alternations of turbiditic sandstone, siltstone and shale (Yoncalı Formation) intercalated with various conglomeratic lenses and marine pelagics and overlain locally by neritic limestones (Figure 8.08) indicating that marine conditions prevailed until Middle Eocene. These sequences, with local unconformities, are followed upwards by continental red clastics and evaporites of post-Middle Eocene to Oligocene age.
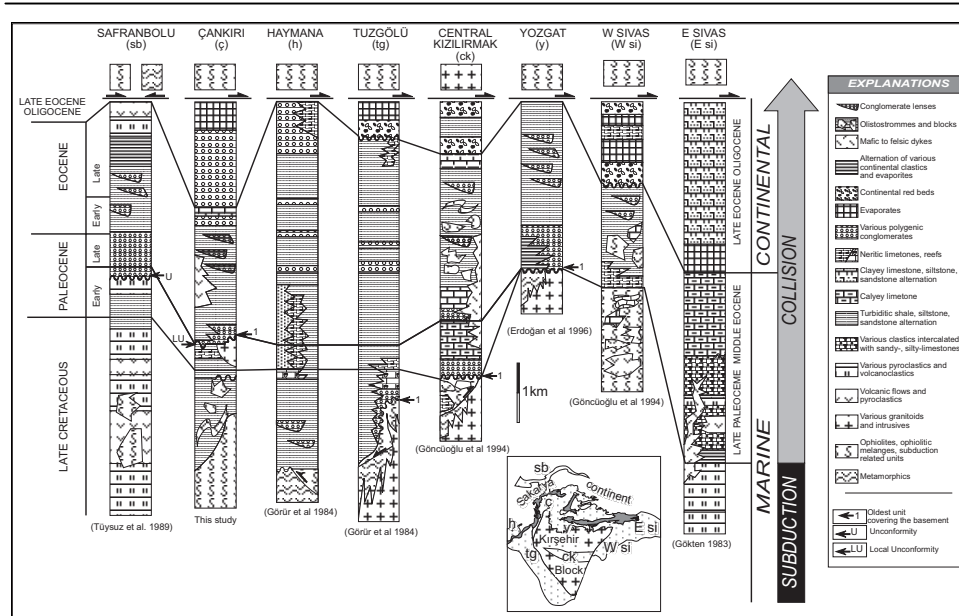
Figure 8.08 Correlation chart for the major Tertiary basins located within and around the Kırşehir Block. Note relatively younging of unconformable bottom contacts of Early Tertiary units in the Safranbolu and Çankırı Basins indicated with U and LU. Note also the Late Cretaceous to Tertiary continuous sedimentation in all of the Basins (with local unconformities) except in the Tuz Gőlű, Central Kızılırmak, Çankırı and Yozgat basins, which have unconformable relations with the Kırşehir Block (indicated with 1).

In the Çankırı and Sivas basins the basin in-fill has a regressive character and becomes younger southwards, while on-lapping on the Kırsehir Block (e.g. see Yozgat area in Figure 8.08). This indicates southward migration of the depocenter and in addition to the progradation of the margins of the Çankırı Basin away from the basement (Figure 8.07e and f). Paleostress patterns (Figures 8.06b and 8.07e and f), indicate that convergence of the Kırşehir Block took place until the Oligocene. The relative young age of the Paleocene formations of the Çankırı Basin (see Figure 8.04b) with respect to their time equivalents in the Safranbolu Basin (Figure 8.08) indicates that the sequential development of the basins (Figure 8.07e and f) also migrated southwards. First, the Safranbolu Basin developed then it was followed by the Hacıhalil sub-basin (HSB, in Figure 8.07e and f), and finally by the Çankırı Basin (see Figures 8.04b and 8.07e and f). Combining data for sedimentation, thrusting and the southwards migration of the depocenters (from Paleocene to Oligocene) indicates that the Safranbolu, Çankırı and Sivas (Carter *et al.* 1991) basins formed an array of south migrating piggy-back basins. The Haymana (Gőrűr *et al.* 1984) and Sivas basins (Gőkten 1983, Tekeli *et al.* 1984, Carter *et al.* 1991) evolved transitionally (Gőrűr *et al.* 1984) from fore-arc to foreland piggy-back basins.

The Aquitanian (Early Miocene) Kilçak Formation is the youngest unit that was deposited during thrusting. In addition, the Burdigalian? to Serravalian Çandır Formation was deposited in an extensional tectonic regime (see chapter 3,4 and 6) and

unconformably overlies Oligocene red clastics (Incik Formation) and evaporites (Gűvendik formation). Therefore, it is proposed that thrusting and piggy-back basin development may have been continuous until the Aquitanian (pre-20.5 Ma).

8.6 Neogene Development of the Çankırı Basin and Its Implications for the Evolution of North Central Anatolia

The Neogene tectono-stratigraphic evolution of the Çankırı Basin can be divided into two stages: 1. Burdigalian to Serravalian (Middle Miocene, MN-3 to MN-6 zones, 20.5-13.5 Ma) and 2. Post-Serrvalian (MN-10 zone, 9.7 Ma to Recent). No deposits between the MN 7 to MN 9 zones (13.5 to 9.7 Ma) were encountered in the Çankırı Basin, which may indicate non-deposition in this time interval.

8.6.1 Middle Miocene Extension (20.5 to 13.5 Ma)

As discussed in chapters 2 and 4, the Çankırı Basin experienced extensional deformation in the Middle Miocene (ca. 20.5 to 11.1 Ma) following Late Paleocene to Aquitanian compressional deformation associated with thrusting. The Middle Miocene extension event in the Çankırı Basin is not a local phenomenon as it is also observed in the Aegean region and west Anatolia (see Lister *et al.* 1984, Bozkurt and Park 1994,1997, Jackson 1994, Hetzel *et al.* 1995, Lips 1998, and Walcott 1998) and in the Menderes and Niğde Massifs. Stages of extremely slow convergence rates alternate with relatively fast convergence periods of Africa and Eurasia over the last 100 Ma. Lips (1998) proposed that the 20 Ma to Recent slow convergence rate of Africa and Eurasia is the main cause of extension in the Aegean region. He argued that the general decrease in convergence rates between Africa and Eurasia would cause retreat of the subducting slab (roll-back). Combination of slab roll-back and slab detachment has been proposed as a possible cause of extension in the Aegean region (Spakmamn *et al*. 1988, Wortel and Spakman 1992, Meijer 1995, Walcott 1998). Rapid growth (and thickening) of the orogen will occur during fast convergence rates whereas a decrease in convergence rates with subsequent roll back will destabilize the orogenic wedge and lead to the collapse of the orogen under its own weight (Dewey 1988).

The latest phase of volcanic activity in the Galatean Volcanic Province (Toprak *et al.* 1996) commenced in the latest-Early Miocene to Late Miocene during which the Faraşlı Basalt was also extruded in the Çankırı Basin (Figure 8.09). Tankut and Tűrkmenoğlu (1988) have discussed the geochemical signatures of the Middle Miocene volcanics of the Galatean Volcanic Province (Figure 8.09) and have shown that they have a bi-modal distribution which indicates a contribution of subducted lithosphere in the alkaline lavas which themselves originated from a primordial deep mantle source. They concluded that this is indicative of extension in the Middle Miocene. This conclusion implies that the Neotethyan oceanic crust, which was attached to the Kırşehir Block, was detached from it in Middle Miocene (Figure 8.09b). This process, together with the 20 Ma to Recent decrease in convergence rates of Africa and Eurasia caused extension in the Aegean to west Anatolian region. Although, this extensional regime resulted in the development of the core complex in the west Anatolia and in the Aegean region, however, in the east (i.e. in the Çankırı Basin area and to the north and east of the Niğde massif) no core complex development is observed. This relation indicates eastwards decrease of the intensity of the extensional deformation.
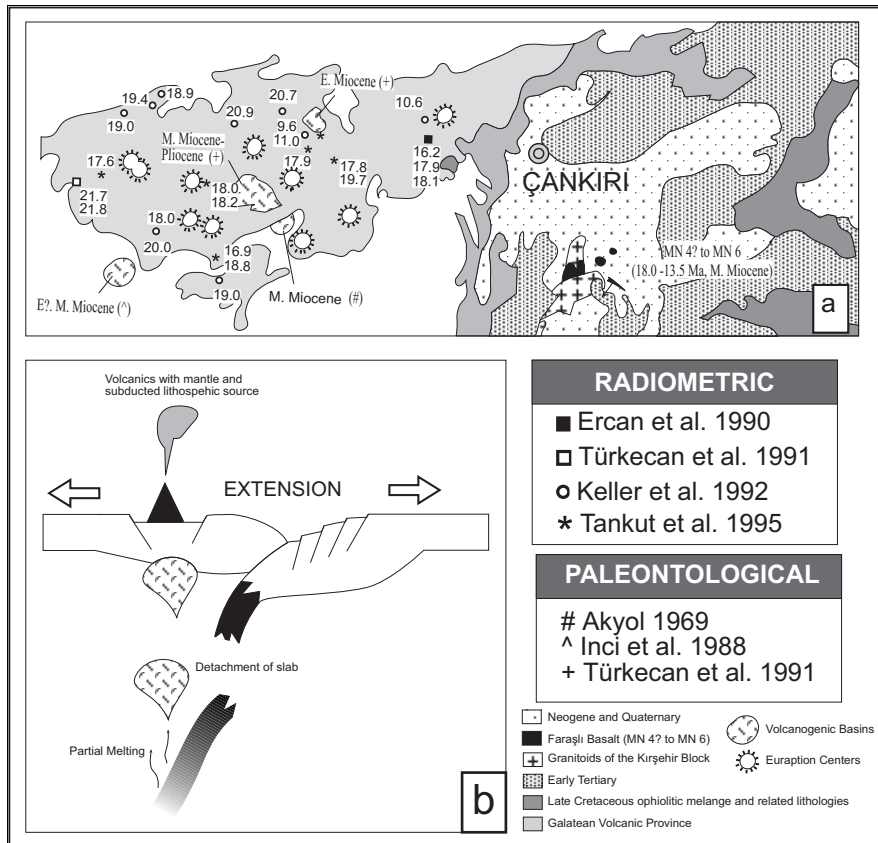
Figure 8.09 a) Distribution and ages of the Neogene volcanics in the Galatean Volcanic Province and the Çankırı Basin (modified after Toprak et al. 1997), b) Model proposed for the development of Middle Miocene extension and generation of Neogene bi-modal volcanism in the Galatean Volcanic Province (after Tankut and Turkmenoğlu 1988). See text for the discussion.

The third deformation phase identified in the kinematic studies (discussed in chapter 5 and 6) corresponds approximately to the timing of latest volcanic activity in the region (Figure 8.09a). Multidirectional normal faults and a concentric pattern of σ_3 trajectories in the Çankırı Basin implies that the magnitudes of σ_2 and σ_3 were similar ($\sigma_2 \geq \sigma_3$). This kind of stress tensor is often observed in regions of up-doming. However, the oblique nature of σ_2 and σ_3, as discussed in chapters 5 and 6, indicates so called tri-axial-strain conditions in which stress permutations and differently oriented faults commonly develop (Krantz 1988). Therefore, it is most likely that extension in the Çankırı Basin area was coupled with the rebound of the northern tip of the Kırşehir Block underlying the Çankırı Basin, which modified the regional stress tensor and gave rise to the resultant σ_3 trajectories (Figure 8.05).
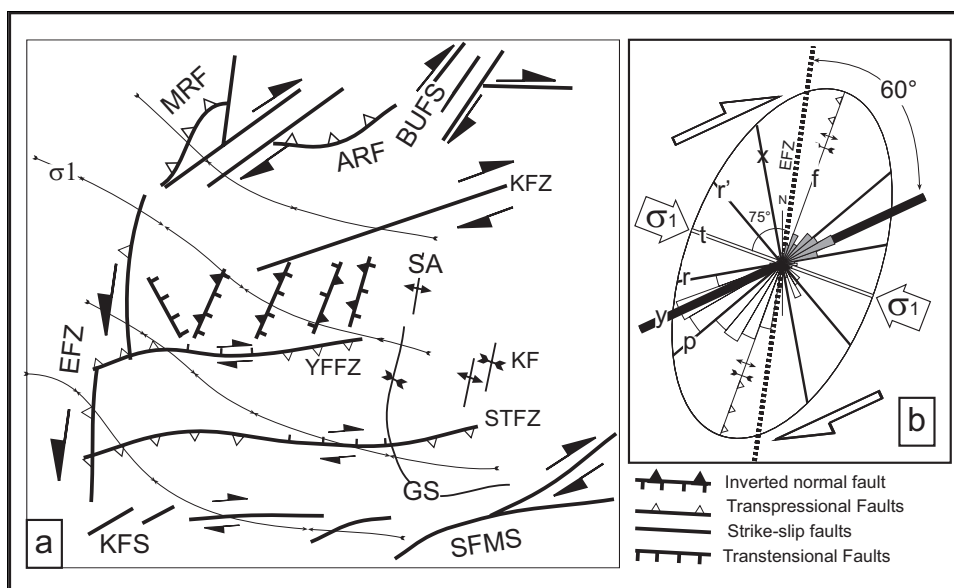
Figure 8.10 A simplified map showing the major structures developed and reactivated in deformation phase 4 (Late Miocene to Recent). Note reactivation of the normal faults in the center of the basin and change of character of faults as they change their orientation with respect to σ₁. ARF: Ayseki Reverse Fault, BUFS: Bűrtű Fault Set, EFZ: Eldivan Fault Zone, GS: Gűvendik Syncline, F: Karaçay Folds, KFS: Kırıkkkale Fault Set, KFZ: Kızılırmak Fault Zone, MFSZ: Master strand of the Sungurlu Fault Zone, MRF: Merzi reverse Fault, STFZ: Sivritepe Fault Zone, YFFZ: Yağbasan-Faraşlı Fault Zone. b) Riedel pattern of deformation proposed for the structures developed in the Çankırı Basin. Rose diagram is prepared from the faults developed in the Çankırı Basin and studied at the perimeter of it (see also chapters 2, 5 and 6).

8.6.2 Post-Middle Miocene Transcurrent Tectonics (11.1 Ma to Recent)

The Late Miocene development of the Çankırı Basin is controlled mainly by NE-SW to ENE-WSW oriented strike-slip faults, which displace the in-fill, the rim of the basin as well as the basement (Figure 8.02c). These faults have a dextral strike-slip sense of movement and their cumulative amount of displacement may reach up to 13 km (see chapter 6). The other major structures, which played a role in the Late Miocene development of the Çankırı Basin are the faults that define the western margin of the Çankırı Basin (Eldivan Fault zone-EFZ Figure 8.10a). These structures, together with other minor structures of the Çankırı Basin display a riedel pattern of deformation (Figure 8.10b), in which all riedel shear types have been developed. The major structures that operated since the Late Miocene and the orientation of the principal stresses (phase 4) are illustrated in Figures 8.05d and 8.10). As seen in the Figure 8.10a, the character of the active structures in the latest deformation phase is controlled by their orientation with respect to the orientation of the principal stresses.

234
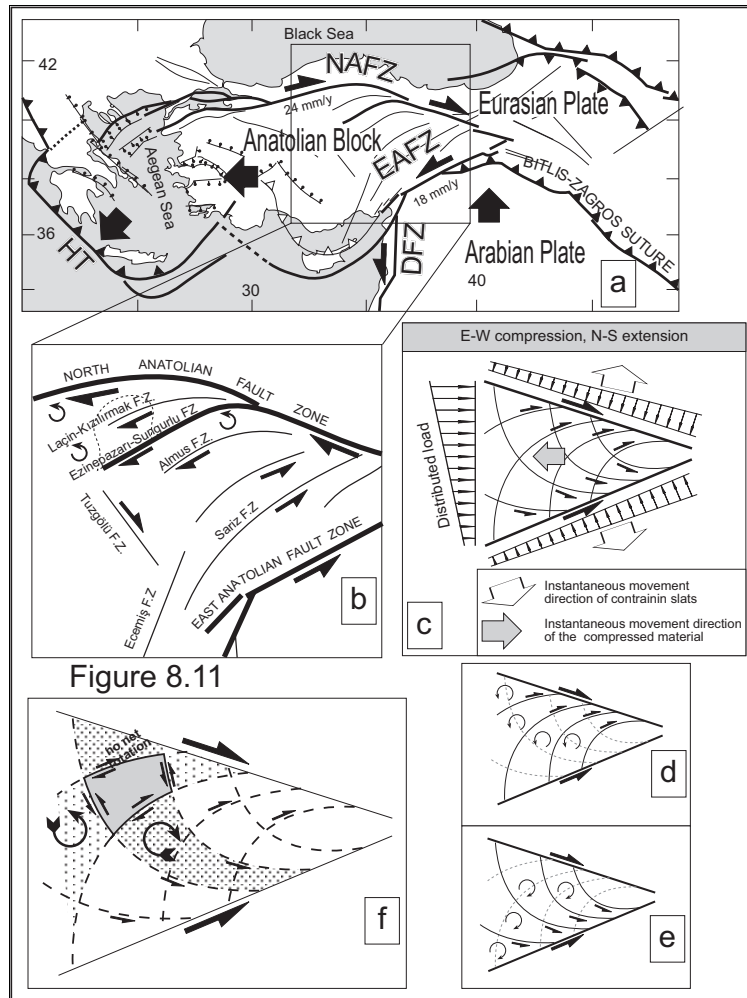
Figure 8.11

Figure 8.11 a) Major active structures in the eastern Mediterranean area. DFZ: Dead Sea Fault Zone, EAFZ: East Anatolian Fault Zone, HT: Hellenic Trench, NAFZ: North Anatolian Fault Zone. b) Splay faults off the NAFZ. c) Modified prandtl compressed cell mechanism for plastic deformation (after Varnes 1962) of the splay fault zone of NAFZ for E-W compression and N-S extension. As the wedge shaped slats (NAFZ and EAFZ in this case) compress the contained plastic material (Anatolian Block), it will yield by shear failure (no vertical movement is allowed), and the compressed material tends to escape westwards along the slip lines. d) In the case if the facing (western) distributed load is asymmetric, it will cause domination of dextral northwards convex faults over the sinistral ones and the blocks within the slip lines with dextral sense of displacement will rotate anticlockwise. e) On the other hand, domination of sinistral faults will cause clockwise rotations of the blocks. f) In areas where both of the slip lines (sinistral and dextral) compete, the bounding piece of the block will not rotate.

235

The main publications on the driving mechanism and exact timing of transcurrent tectonics in Turkey include Şengőr (1982), Barka and Hancock (1984), Şengőr *et al.* (1985), Barka and Gűlen (1988), Şaroğlu (1988), Koçyiğit (1991). The most recent studies include application of geodetic surveys based on GPS (Global Positioning Systems; Oral 1994, Oral *et al.* 1997).

Şengőr *et al.* (1985) and Dewey *et al.* (1986) have argued that collision and further northwards convergence of the Arabian Plate into the Eurasian Plate along the Bitlis-Zagros Suture at the end of Serravalian (ca 11.1 Ma) gave rise to the westwards expulsion of the Anatolian Block (Figure 8.11a) towards the Hellenic Trench, serving as the unconstrained margin of the block. The expulsion of the Anatolian Block was accomodated by the dextral North Anatolian and sinistral East Anatolian Faults. Geological, geodetic, and seismic data indicate that the current displacement rate along the NAFZ is 24 mm/y (18 mm/y for the EAFZ).

A number of splay faults bifurcate from the NAFZ and transfer transcurrent deformation throughout the Anatolian Block (Figure 8.11b). Of these, the Ezinepazarı-Sungurlu, and Kızılırmak-Laçin Fault Zones traverse the Çankırı Basin and displace its units dextrally (Figure 8.10a). Based on the geometry, dextral nature and deformation styles of the wedges between the splay faults, Kaymakcı and Koçyiğit (1995) have proposed the prandtl compressed cell (Varnes 1962) mechanism (Figure 8.11c) for the deformation of the area caught between these splays. In the case of E-W compression and N-S extension of the Anatolian Block (Şengőr *et al.* 1985), this mechanism predicts anticlockwise rotations (Figure 8.11d) in the wedges caught between dextral splay fault sets (Şengőr and Barka 1992) and clockwise rotations (Figure 8.11e) along the sinistral splays. There will be no net rotation in blocks controlled by both dextral and sinistral splays due to competition of opposite senses of rotation exerted by each splay set (see Figure 8.11f). Differential rotation of these blocks causes development of incompatible basins (Şengőr and Barka 1992), which is enhanced by a change in the rate of net strike-slip offset along the main fault zone (NAFZ in this case) due to block rotation. Paleomagnetic studies carried out close to, but outside, the NAFZ (Paltzman *et al.* 1994, 1998, Tatar *et al.* 1995, Piper *et al.* 1996) have reported anticlockwise rotations of wedges between the splay faults as well as for the whole Anatolian Block in general. Similar results were also detected in GPS studies (Oral 1994). As presented in chapter 6, a very large amount of local anticlockwise rotation (60°) is detected within the Kızılırmak Fault Zone (Eskialibey site in chapter 7). However, in the other Middle Miocene and Late Miocene sites (which are away from the major faults) no rotation was detected at all. This relationship can be explained by the mutual counter effect of the dextral splays against the sinistral faults (the latter being the EFZ at the western margin of the Çankırı Basin; Figure 8.11f).

8.7 Conclusions of This Thesis

The research presented in this thesis has led to the following conclusions:

I.   The integration of remotely sensed data including satellite images, aerial photos, reflection seismics and gravity data helped to reveal the architecture of the Çankırı Basin. A 3-D volume model was produced from seismic sections with the help of a 3-D GIS (Geographic Information System). Using various digital image processing techniques, the Landsat TM images were enhanced and interpreted. On the enhanced images, litho-stratigraphic units of the Çankırı basin were recognized and delineated and subsequently verified in the field. Integration of the volume model and gravity images helped to identify and delineate buried fold and thrust structures in the northern and eastern part of the Çankırı Basin as well as diapirism and the outline of the Kırşehir Block under its cover.

II.   Stratigraphical studies constrained the tectono-stratigraphical framework of the basin. It was found that the tectono-stratigraphical evolution of the Çankırı Basin is divided into two major periods, namely Late Cretaceous to pre-Neogene and Neogene:

    1.   During the Late Cretaceous to pre-Late Paleocene, subduction of the Neotethys took place northwards under the Sakarya Continent of the Pontides. In this period, the North Anatolian Ophiolitic Mélange (NAOM) was accreted as the subduction complex into which the Yaylaçayı Formation was incorporated locally and deposited in fore-arc to inter-arc settings. The Yapraklı, Malıboğazı, Kavak, Badiğin and Dizilitaşlar formations were deposited in the shallower parts and after the Çankırı Basin had narrowed and became restricted, some parts were uplifted and became sub-aerially exposed.

    2.   In the Late Paleocene to pre-Burdigalian period, the Çankırı Basin consisted of piggy-back basins that migrated southwards (i.e. towards the basement). Consequently, the basin in-fill displays a wedge-like geometry that thins southwards. This period is further subdivided into two parts based on the depositional settings. In Late Paleocene to Middle Eocene deposition took place in marine settings that display a regressive character. From post-Middle Eocene onwards deposition took place in continental settings and is characterized by red beds and alternating evaporites.

    3.   Deposition during the Neogene is characterized by fluvio-lacustrine associations in extensional (Burdigalian to pre-Tortonian) and regional transcurrent tectonic regimes (from Tortonian onwards).

III.   Paleostress inversion studies revealed that the Çankırı Basin evolved during four phases of deformation. Phase 1 occurred in the pre-Late Paleocene and was characterized by thrusting in which σ_3 was sub vertical and σ_1 was oriented approximately NW-SE. Phase 2 occurred in the Late Paleocene to pre-Burdigalian (ca. pre-20.5 Ma) and was characterized by a combination of thrusting in the northern part and transpression in the southern part of the Çankırı basin. In this phase σ_1 was oriented more or less radial and σ_3 was sub vertical in the north while σ_2 was sub vertical in the southern part. Phase 3 occurred in the

237

Burdigalian to pre-Tortonian (ca 20.5-11.1 Ma) and was characterized by multi directional extension in which σ_1 was oriented sub vertical and the other stress were sub horizontal to oblique. Phase 4 has been active since the Tortonian (ca. 11.1 Ma to Recent) and is characterized by regional transcurrent tectonics in which σ_2 is vertical and other stresses are horizontal to sub horizontal with σ_1 oriented NW-SE. This is compatible with the current tectonic scheme for central and western Turkey, which is dominated by the North Anatolian Fault Zone.

IV.   Paleomagnetic studies have revealed that the Çankırı Basin was subjected to rotational deformation in the pre-Middle Miocene. In the Eocene to Oligocene the western and southeastern margin of the Çankırı Basin rotated anticlockwise (33° and 36°respectively) while the eastern margin rotated clockwise (52°). Rotation of the margins of the Çankırı Basin away from the basement is interpreted to be the manifestation of indentation of the Kırşehir Block into the Sakarya Continent. No rotation occurred after the Middle Miocene.

V.   The Çankırı Basin represents a very good example for a continuum in basin development ranging from subduction to collision related basin formation to post-collisional extensional to regional transcurrent settings. It began its development as a fore-arc to inter-arc basin during the subduction of the Neotethys, in the Late Cretaceous to pre-Late Paleocene. After the Neotethys was completely closed and oceanic domains were consumed, the Çankırı Basin continued its development as a series of foreland piggy-back basins in the Late Paleocene to pre-Burdigalian, during the collision of the Sakarya Continent and the Kırşehir Block. In the Middle Miocene, the Çankırı Basin became an extensional basin similar, albeit on a smaller scale, to the Aegean and west Anatolian regions, Finally, transcurrent tectonics controlled by the North Anatolian and East Anatolian fault zones have dominated the Çankırı Basin since the Tortonian.

REFERENCES

Akıman, O., Erler, A., Göncüoğlu, M.C., Güleç, N., Geven, A., Türeli, T.K. and Kadıoğlu, Y.K., 1993. Geochemical characteristics of granitoids along the western margin of the Central Anatolian Crystalline Complex and their tectonic implications. *Geol. Journal* 28, 371-382.

Akyol, E., 1969. *Ankara-Kızılcahamam-Çeltikci civarında bulunan kőműr zuhurlarının 1/25000 őlçekli detay jeolojik etűdű hakkında rapor.* MTA. Rap. No. 4405 (unpublished).

Akyűrek, B., Bilginer, E., Akbaş, B., Hepşen, N., Pehlivan, S., Sunu, O., Soysal, Y., Dağer, Z., Çatal, E., Sőzeri, B., Yıldırım, H. and Hakyemez, H., 1984. The geology of the Ankara-Elmadağ-Kalecik region*: Chamber of Geological Engineers of Turkey Bull.* 20, 31-46.

Akyűrek, B., Bilginer, E., Çatal, E., Dağer, Z., Soysal, Y. and Sunu, O., 1980. *Eldivan-Şabanőzű (Çankırı)-Hasayaz-Çandır (Kalecik, Ankara) dolayının Jeolojisi.* MTA Rap. No: 6741 (unpublished).

Alexandrowski, P., 1985. Graphical determination of principal stress directions for slickenside lineation populations: an attempt to modify Arthoud's method. *Jour. Struct. Geol.* 7, 73-82.

Allen, P.A. and Allen, J.R., 1990. *Basin Analysis, Principles and applications.* Blackwell Sci. Publ. Oxford, London, 450p.

Altıner, D., Koçyiğit, A., Farinacci, A., Nicosia, U. and Conti, M.A., 1991. Jurassic, Lower Cretaceous stratigraphy and paleogeographic evolution of the southern part of northwestern Anatolia. *Geologica Romana.* 28,13-80.

Angelier, J., 1979. Determination of the mean principal directions of stress for a given fault population. *Tectonophysics.* 56, T17-T26.

Angelier, J., 1984. Tectonic analysis of fault slip data sets. *J. Geophys. Res.* 89, 5835-58-48.

Angelier, J., 1989. From orientation to magnitudes in paleostress determination using fault slip data. *Jour. Struct. Geol.* 11, 37-50.

Angelier, J., 1994. Fault slip analysis and paleostress reconstruction. In: Hancock, P.L. (ed.) *Continental deformation.* Pergamon Press, Oxford. 53-100.

Angelier, J., Tarantola, A., Valette, B. and Manoussis, S., 1982. Inversion of field data in fault tectonics to obtain the regional stress-1. Single phase fault populations: a new method of computing the stress tensor. *Geophys. J.R. Astr. Soc.* 69, 607-621.

Arlegui-Crespo, L.E. and Simon Gomez, J.L., 1998. Reliability of paleostress analysis from fault striations in near multidirectional extension stress fields. Examples from the Ebro Basin, Spain. *Jour. Struct. Geol.* 20, 827-840.

Armijo, R., Carey, E. and Cisternas, A., 1982. The inverse problem in microtectonics and the separation of tectonic phases. *Tectonophysic.* 82, 145-169.

Arthaud, F., 1969. Méthode de détermination graphique des directions de reccourcissement d'allongement et intermédiare d'une population de failles. *Bull. Soc. Geol. Fr.* 11, 739-757.

Ayan, M., 1963. Contribution a l'etude petrographique et géologique de la region située au nord-est de Kaman. M.T.A. Bűlteni. 115, 332.

Ayan, T., 1969. *Çankırı-Yerkőy havzası petrol imkanları: Jeolojik ve Tektonik etűdű.* Egeran Műşavirlik Műhendislik Firması. TPAO Rap. No: 469 (unpublished).

Aziz, A., 1975. *İskilip civarı ile gűney ve gűneybatısının detay jeolojisi ve petrol olanakları.* M.T.A. Arş. Rap. No: 6132 (unpublished).

Barka, A. A., 1992. The North Anatolian fault zone, *Annales Tectonicae*, VI suppl. 164-195.

Barka, A.A. and Gűlen, L., 1988. New constraints on age and total off-set of the North Anatolian Fault Zone: implications for tectonics of the Eastern Mediterranean region. METU*, Jour. Pure and Appl. Sci.* 21/1-3, 39-63

Barka, A.A. and Hancock, P.L., 1984. Neotectonic deformation patterns in the convex-northwards arc of the North Anatolian Fault Zone. In: Dixon, J.E. and Robertson, A.H.F. (eds.) *The Geological Evolution of the Eastern Mediterranean.* Spec. Publ Geol. Soc. London 17, 763-774.

Bayhan, H., 1987. Cefalıkdağ ve Baranadağ plutonlarının petrografik ve kimyasal-mineralojik özellikleri. *Türkiye Jeol. Kur. Bűlteni.* 30/31, 11-16.

Bayhan, H., 1989. Keskin sokulumunun (Ankara) petrografik ve kimyasal-mineralojik özellikleri. *Hacettepe Üniversitesi Yerbilimleri.*15, 29-36.

Benda, L., 1971. Grundzűge einer pollenanalytischen Gliederung des tűrkischen Jungtertiars. (Kanozoikum und Braunkohlen der Tűrkei, 4). *Beicip. Geol. Jb.* 133, 1-46.

Biddle, K.T. and Christie-Blick, N., 1985. Deformation and basin formation along strike-slip faults. in: Biddle, K.T. and Christie-Blick, N. (eds) *Strike-slip deformation, basin formation and sedimentation* Spec. *Publ. Soc. Econ. Paleont. Miner.* No. 37. 1-45.

Bingől, E., 1992. *1:2000000 őlçekli Tűrkiye Jeoloji Haritası*, MTA. Yayını.

Birgili, S., Yoldaş, R. and Űnalan, G., 1974. *Çankırı-Çorum havzası jeolojisi ve petrol olanakları őn raporu.* TPAO Rap. No: 1216 (unpublished).

Bott, M.P.H., 1959. The mechanics of oblique-slip faulting. *Geol. Mag.* 96(2), 109-117.

Bouma, A.H., 1962. Sedimentology of some flysch deposits: A graphic approach to facies interpretation. Elsevier, Amsterdam. 168 p.

Bozkurt, E. and Park, R.G., 1994. Southern Menderes Massif: an incipient metamorphic core complex in western Anatolia, Turkey. *Journal of the Geological Society*, London. 151, 213-216.

Bozkurt, E. and Park, R.G., 1997. Evolution of a mid-Tertiary extensional shear zone in the southern Menderes Massif, western Turkey. *Bull. Soc. Geol. Fr.* 168(1), 3-14.

Bozkurt, E., 1990a. *Geology of the Almus Fault Zone (AFZ), Almus-Tokat*. M.Sc. Thesis, Middle East Technical University, Ankara, Turkey. 118p.

Bozkurt, E., 1990b. Karakaya Napi icinde yeni bir Karbonifer ve Permiyen bulgusu. *M.T.A. Bűltetini.* 110, 181-188.

Butler, R.F., 1992. *Paleomagnetism: Magnetic Domains to Geologic Terranes*, Blackwell, Boston. 319 p.

Carey, E. and Brunier, B., 1974. Analyse théorique et numérique d'une modèle méchanique élémentaire appliqué a l'étude d'une population de failles. *C.r. Acad. Sci., Paris*. Ser. D 279, 891-894.

Carey-Gailhardis, E. and Mercier, J.L., 1989. A numerical method for determining the state of stress using focal mechanisms of earthquake populations: application to Tibetan teleseisms and microseismicity of southern Peru. *Earth Planet. Sci. Lett.* 82,165-179.

Carter, J.M.L., Hanna, S.S. Ries, A.C. and Turner, P., 1991. Tertiary evolution of the Sivas Basin, central Turkey. *Tectonophysics* 195, 29-46.

Çemen, I., Göncüoglu, M.C. and Dirik, K., 1999. Structural evolution of the Tuzgölü Basin in central Anatolia, Turkey. *Jour. Geol.* 107,693-706.

Channel, J.E.T., Tűysűz, O., Bektas, O. and Şengör, A.M.C., 1996. "Jurassic-Cretaceous paleomagnetism and paleogeography of the Pontides (Turkey). *Tectonics* 15(1), 201-212.

Chavez, P.S. Jr. and Kwarteng A.Y., 1989. Extracting spectral contrast in Landsat Thematic Mapper Image data Using selective Principal Component Analysis. *Photogramm. Eng. Remote Sens*. 55(3), 339-348.

Collinson, J.D., 1996. Alluvial Sediments. In: Reading, H.G. (ed.) *Sedimentary environments: Process, Facies, Stratigraphy*. Blackwell Science Ltd. Oxford. 37-82.

Daily, M., 1983. Hue-saturation-intensity split-spectrum processing of Seasat Radar imagery, *Photogramm. Eng. Remote Sens*. 49, 349-355.

De Bruijn and Saraç, G., 1992. Early Miocene rodent faunas from eastern Mediterranean area. Part II.

Mirabella (Paracricetodontinae, Muroidea). *Proc. Kon. Neder. Akad. Wetensch.* Amsterdam. B 95, 25-40.

De Bruijn, Fahlbusch, V., Saraç, G., Űnay, E., 1993. Early Miocene rodent faunas from eastern Mediterranean area. Part III. The genera *Deperetomys* and *Cricetodon,* with a discussion on the evolutionary history of the *Cricetodontini. Proc. Kon. Neder. Akad. Wetensch.* Amsterdam. B 96, 151-216.

De Bruijn, H. and Konigswald, W., 1994. Early Miocene rodent faunas from eastern Mediterranean area. Part V. The genus *Enginia* (*Muroidea*) with a discussion of the structure of the incisor enamel. *Proc. Kon. Neder. Akad. Wetensch.* Amsterdam. B97, 381-405.

De Bruijn, H., Daams, R., Daxner-Höck, G., Fahlbusch, V., Ginsburg, L., Mein, P. and Morales, J., 1992. Report of the RCMNS Working Group on fossil mammals. Reisensburg 1990. *Newsletter on Stratigraphy* 26, 65-118, Berlin, Stuttgart.

De Bruijn, H., van den Hoek Ostende, L., Kristkoiz-Boon, E., Rummel, M., Theocharopoulos, C. and Unay, E., 2000. The rodents,lagomorphs and insectivores from the middle Miocene locality Candir 2 (Anatolia), (in review).

Decourt, J., Ricou, L.E. and Vrielynck, B., 1993. Atlas Tethys, Paleoenvironmental maps, *Beicip-Franlab.* 1993.

Dellaloğlu, A.A., Tűysűz, O., Kaya, O.H. and Harput, B., 1992. *Kalecik (Ankara)-Eldivan-Yapraklı (Çankırı)-İskilip (Çorum) ve Devrez Çayı arasindaki alanın jeolojisi ve petrol olanakları,* TPAO Rap. No. 3194 (unpublished).

Demirer, A., Őzçelik, Y. and Őzkan, R., 1992. *Çankırı-Çorum basenindeki Eosen volkanitlerinin petrografisi.* TPAO Rap. No. 1810 (unpublished).

Dewey, J.F. and Şengőr, A.M.C., 1979. Aegean and surrounding regions: complex multiplate and continuum tectonics in a convergent zone. *Bull. Geol. Soc. Am*. 90, 84-92.

Dewey, J.F., 1977. Suture zone complexities: a review. *Tectonophysics*. 40, 53-67.

Dewey, J.F., Hempton, M.R., Kidd, W.S.F., Şaroğlu, F. and Şengőr, A.M.C., 1986. Shortening of continental lithosphere: the neotectonics of Eastern Anatolia – a young collisional zone. In: Coward, M.P. and Ries, A.C. (eds) *Collision Tectonics*, Geol. Soc. Spec. Publ. No.19, 3-36.

Doblas, M., 1998. Slickenside kinematic indicators. *Tectonophysics.* 295,187-197.

Dresen, G., 1992. Stress distribution and the orientation of Riedel shears. *Tectonophysics.* 188, 239-247.

Duphin, J.M., Sassi, W. and Angelier, J., 1993. Homogeneous stress hypothesis and actual fault slip:

240

a distinct element analysis. *Jour. Struct. Geol.* 15, 1033-1043.

Eldredge, S., Bachtadse, V. and Van der Voo, R., 1985. Paleomagnetism and the orocline hypothesis. *Tectonophysics.* 119,153-179.

Ercan, T., Yeğingil, Z., Bigazzi, G., Oddone, M. and Özdoğan, M., 1990. Kuzeybatı Anadolu obsidiyen buluntularının kaynak belirleme Çalışmaları. *Jeoloji Mühendisliği.* 9, 5-11.

Erdoğan, B., Akay, E. and Uğur, M.S., 1996. Geology of the Yozgat region and evolution of the collisional Çankırı Basin. *Int. Geol. Review.* 38, 788-806

Erler, A. and Bayhan, H., 1995. Orta Anadolu Granitoidleri'nin genel değerlendirilmesi ve sorunları. *Hacettepe Üniversitesi Yerbilimleri.* 17, 49-67.

Erler, A. and Göncüoğlu, M.C., 1996. Geologic and tectonic setting of the Yozgat Batholith, Northern Central Anatolia crystalline complex, Turkey. *Int. Geol. Review.* 38,714-726.

Erler, A., Akıman, O., Unan, C., Dalkılıç, F., Dalkılıç, B., Geven, A. and Önen, P., 1991. Kaman (Kırşehir) ve Yozgat yörelerinde Kırşehir Masifi magmatik kayaçlarının petrolojisi ve jeokimyası. *TUBITAK-Doğa.* 15, 76-100.

Etchecopar, A., Visseur, G. and Daignieres, M., 1981. An inverse problem in microtectonics for the determination of stress tensors from fault striation analysis. *Jour. Struct. Geol.* 3, 51-65.

Evans, I. and Hall, S.A., 1990. Paleomagnetic constraints on the tectonic evolution of the Sakarya Continent, northwestern Anatolia. *Tectonophysics.* 182, 357-372.

Fisher, R.A., 1953. *Dispersion on a sphere. Proc. R. Soc.* London. 217, 295-305.

Fleischman, K.H. and Nemcok, M., 1991. Paleostress inversion of fault-slip data using the shear stress solution of Means (1989). *Tectonophysics.* 196, 195-202.

Fleuty, M.J., 1974. Slickensides and slickenlines. *Geol. Mag.* 112, 319-322.

Floyd, P.A. 1993. Geochemical discrimination and petrogenesis of alkalic basalt sequences in part of the Ankara Melange, central Turkey. *Jour. Geol. Soc.* London. 150, 541-550.

Gabrielsen, R.H., Steel, R.J. and Nottedt. C., 1995.Subtle traps in extensional terranes: A model with reference to the North Sea. *Petroleum Geoscience.* 1, 223-235.

Gençalioğlu-Kuşcu, G., 1997. *Petorgraphy and geochemistry of silicic volcanics in the Akdağmadeni region, Central Anatolia, Turkey.* Ph.D. Thesis, University of Keele, U.K, 344 p.

Gephart, J.W. and Forsyth, D.W., 1984. An improved method for determining the regional stress tensor using earthquake focal mechanism data: Application to the San Fernando earthquake sequence. *J. Geophys. Res.* 89, 9305-9320.

Gephart, J.W., 1990. Stress and direction of slip on fault planes. *Tectonophysics* 8, 845-858.

Geven, A., 1992. *Mineralogy, petrography and geochemistry of Cefalıkdağ plutonic rocks (Kaman-Central Anatolia).* METU, Geol. Eng. Dept. Ph.D. thesis, 165p. (unpublished).

Gillespie. A.R., Kahle, A.B. and Walker, R.E., 1986. Color enhancement of highly correlated images. I. Decorrelation and HIS contrast stretches. *Remote Sensing of Environment,* 20, 209-235.

Gökten, E., 1983. Şarkışla (Sivas) guney-güney-doğusunun stratigrafisi ve jeolojik evrimi. *TJK. Bült.* 26,167-176.

Göncüoğlu, M.C. Dirik, K., Erler, A. and Yalınız, K., 1994. *Orta Anadolu Masifnin doğu bölümünün jeolojisi, Bölüm-4. Orta Anadolu masifinin Sivas Baseni ile ilişkisi.* ODTU-AGUDOS Rap. (unpublished).

Göncüoğlu, M.C. Erler, A., Toprak, V., Olgun, E. Yalınız, K., Kuşcu, I., Köksal, S., ve Dirik, K., 1993, *Orta Anadolu masifinin orta bölümünün jeolojisi, Bölüm 3; Orta Kızılırmak Tersiyer Baseninin jeolojik evrimi.* ODTU-AGUDOS Rap. (unpublished).

Göncüoğlu, M.C., 1977. *Geologie des westlischen Niğde massivs.* Univ. Bonn, Ph.D. thesis (unpublished)

Göncüoğlu, M.C., 1986. Orta Anadolu Masifinin güney ucundan jeokronolojik yaş bulguları. *MTA Dergisi,* 105/106, 83-96.

Göncüoğlu, M.C., Erler, A., Toprak, V., Yalınız, K., Olgun E., ve Rojay, B., 1992. *Orta Anadolu Masifi batı bölümünün jeolojisi, Bölüm 2: Orta Kesim.* TPAO Rapor No. 3155 (*unpublished*).

Göncüoğlu, M.C., Toprak, V., Kuşcu, I., Erler, A., ve Olgun, E., 1991. *Orta Anadolu Masifi batı bölümünün jeolojisi, Bölüm 1: Güney Kesim:* TPAO Rap. No: 2909 (unpublished).

Göncuoğlu, M.C., Yalınız, K. and Kaymakci, N. 2000. Izmir-Ankar-Erzincan Kenet Kuşagından yeni Jeokimyasal veriler. *Türkiye Petrol Jeologları Derneği Bülteni* (in review).

Görür, N., Oktay, F.Y., Seymen, I. and Şengör, A.M.C., 1984. "Palaeotectonic evolution of the Tuzgölü basin complex, Central Turkey: Sedimentary record of a neotethyan closure", In: Dixon, J.E. and Robertson, A.H.F. (eds.) *The Geological Evolution of the Eastern Mediterranean,* Blackwell Sci. Publ., Oxford, London, 824p.

241

Grasso, D.N., 1993. Applications of the HIS color transformation for 1:24,000-scale Geological Mapping: a low cost SPOT alternative. *Photogramm. Eng. Remote Sens.* 59, 73-80.

Güleç, N., 1994. Rb-Sr isotope data from the Ağaçören granitoid (East of Tuzgölü): Geochronological and genetic implications. *Turkish Jour. Earth Sciences-Doğa.* 3, 39-43.

Gűndoğdu, M.N. Bros, R. Kuruç, A. and Bayhan, H., 1988. Bayındır feldispatoidli siyenitinin Rb, Sr tűmkayaç sistematiği (Kaman-Kırşehir*). Hacettepe Univ. Yerbilimlerinin 20. yılı Semp.* Bildiri özleri 55 (abstract).

Gűrsoy, H. Piper, J.D.A., Tatar, O. and Temiz, H., 1997. A paleomagnetic study of the Sivas Basin, central Turkey: crustal deformation during lateral extrusion of the Anatolian Block. *Tectonophysics.* 271, 89-105.

Hancock, P.L., 1985. Brittle microtectonics: principles and practice. *Jour. Struct. Geol.* 7(3/4) 437-457.

Hardcastle, K.C. and Hills, L.S., 1991. BRUTE3 and SELECT: QuickBasic 4 programs for determination of stress tensor configurations and separation of heterogeneous populations of fault-slip data. *Comput. and Geoscience.* 17, 23-43.

Hardcastle, K.C., 1989. Possible paleostress tensor configurations derived from fault-slip data in eastern Vermont and eastern New Hampshire, *Tectonics* 8(2), 265-284.

Hayden, R., 1982. The application of a colour transformation for the enhancement of multispectral images and for the combination of multispectral data, Summaries: *International Symposium on Remote Sensing of the Environment, "Remote Sensing of Arid and Semi-Arid Lands,* 3-9 November Cairo, Egypt, 78 (abstract).

Hetzel, R.U. Ring, C. and Dora, O.O., 1995. Bivergent extension in orogenic belts: the Menderes Massif (southwestern Turkey). *Geology.* 23, 455-458.

Inci, U., Helvacı, C. and Yağmurlu., 1988. Stratigraphy of the Beypazarı Neogene basin, central Anatolia, Turkey. *Newl. Stratigraphy* 18,165-182.

Innocenti, F., Mazzuoli, G., Pasquare, F., Radicati di Brozola, F. and Villari, L., 1975. The Neogene calcalkaline volcanism of Central Anatolia: geochronological data on Kayseri-Niğde area. *Geol. Mag.* 112, 349-360.

Jackson, J. and McKenzie, D., 1984. Active tectonics of the Alpine-Himalayan Belt between western Turkey and Pakistan. *Geophys. J.R. Astr. Soc.* 77, 185-264.

Jackson, J.J., 1994. Active tectonics of the Aegean region. *Annu. Rev. Earth and Planet. Sci.* 22,239-271.

Jelinek, V., 1978. Statistical processing of anisotropy of magnetic susceptibility on groups of specimens. *Studia Geophys. Geod.* 22, 50-62.

Johnson, H.D. and Baldwin, C.T., 1996. Shallow clastic seas. In Reading, H.G. (ed.) *Sedimentary Environments: Process, Facies and Stratigraphy.* Blackwell Science, Oxford. 232-280.

KARDAE, 1999. http://www.boun.edu.tr/kardae

Kaymakci, N. and Koçyiğit, A., 1995. "Mechanism and basin generation in the splay fault zone of the North Anatolian Fault Zone: E.U.G. 8th. *Conference on the Earth Sciences, Strasbourg,* (abstract).

Kaymakci, N. White, S.H. and van Dijk P.M., 1998. Paleostress inversion in a multi-phase deformed area: Çankiri Basin (central Anatolia). *3rd International Turkish Geol. Symp: Progress in understanding the Geology of Turkey.* 31 August-4 Sept. (1998) METU, Ankara, Turkey (abstract).

Kaymakci, N. White, S.H. and van Dijk P.M., 2000. Paleostress inversion in a multi-phase deformed area: Kinematic and structural evolution of the Cankiri Basin (central Turkey): Part 1. In: Bozkurt,E. Winchester, J.A. and Piper, J. (eds) *Tectonics and Magmatism in Turkey and its Surroundings.* Geol. Soc. London, Special Publ. 173, 445-473.

Kazancı, N. and Varol, B., 1990. Development of a mass flow-dominated fan-delta complex and associated carbonate reefs within a transgressive Paleocene succession, Central Anatolia, Turkey. *Sed. Geol.* 68,261-278.

Keller, J., Jung, D. Eckhardt, F.J. and Kreuzer, H., 1992. Radiometric ages and chemical characterization of the Galatean andesitic massif, Pontus, Turkey*. Acta Volcanologica* 2, 267-276.

Kendall, A.C. and Harwood, G.M., 1996. Marine evaporites: arid shorelines and basins. In Reading, H.G.(ed.) *Sedimentary Environments: Process. Facies and Stratigraphy.* Blackwell Science, Oxford 281-324.

Ketin, I., 1966. Tectonic units of Anatolia (Asia Minor). *Min. Res. Expl. Inst. Bull.* 66, 23-34.

Kocurek, G.A., 1996. Desert Aeolian systems, In Reading, H.G.(ed.) *Sedimentary Environments: Process, Facies and Stratigraphy.* Blackwell Science, Oxford. 125-154.

Koçyiğit, A., 1987. Hasanoğlan (Ankara) yőresinin tektonostratigrafisi, Karakaya orojenik kuşağının evrimi. *Hacettepe Univ. Yerbilimleri.* 14, 269-293.

Koçyiğit, A., 1989. Suşehri basin: an active fault-wedge basin on the North Anatolian Fault Zone, Turkey, *Tectonophysics.* Vol.167, p. 13-29.

Koçyiğit, A., 1991. An axample of an accretionary forearc basin from north Central Anatolia and its implications

242

for the history of subduction of neotethys in Turkey, *Geol. Soc. Am. Bull*. 103, 22-36.

Koçyiğit, A., Kaymakci, N., Rojay, B.F. Őzcan, E., Dirik, K. and Özçlik Y. 1991. *Inegől-Bilecik-Bozűyűk arasinda kalan alanin jeolojisi*. TPAO Rap. (unpublished).

Koçyiğit, A., Őzkan, S. and Rojay, B.F., 1988. Examples from the fore-arc basin remnants at the active margin of northern neotethys; Development and emplacement age of the Anatolian Nappe, Turkey, *METU, Jour. Pure Appl. Sci*, 21(1-3), 183-120.

Koçyiğit, A., Tűrkmenoğlu, A., Aksoy, E., Beyhan, A. and Kaymakci, N., 1995. "Post-collisional tectonics of Eskişehir-Ankara-Çankırı segment of İzmir-Ankara-Erzincan Suture Zone (IAESZ): Anakara Orogenic Phase", *Turkiye Petrol Jeologlari Dernegi Bűlt*. 6(1), 69-86.

Krantz, R.W., 1988. Multiple fault sets and three-dimensional strain: theory and application. *Jour. Struct. Geol*. 10, 225-237.

Krijgsman, W. 2000. Magnetostratigraphic dating of the Çandır fossil locality (middle Miocene, Turkey). *MTA Bull*. Spec. Publ. (in review).

Krijgsman, W., 1996. *Miocene Magnetostratigraphy and cyclostratigraphy in the Mediterranean: Extension of the astronomical polarity time scale*. Ph.D. Thesis, Utrecht University, The Netherlands, 207p.

Krijgsman, W., Duemeijer, C.E., Langereis, C.G., de Bruijn, H., Saraç, G. and Andriessen, P.A.M., 1996. Magnetic polarity stratigraphy of Late Oligocene to Middle Miocene mammal-bearing continental deposits in Central Anatolia (Turkey). *Newsl. Stratigr*. 34(1), 13-29.

Kuşcu, İ., 1997. *Mineralogical and geochemical comparison of skarns in the Akdağmadeni, Akçakışla and Keskin districts, Central Anatolia, Turkey*. Ph.D. Thesis, Middle East Technical University, Ankara, 192p.

Lacombe, O., Angelier, J., and Laurent, Ph., 1992. Determining paleostress orientations from faults and calcite twins: a case study near the Sainte-Victoire Range (southern France). *Tectonophysics*. 201, 141-156.

Lacombe, O., Angelier, J., Laurent, Ph. Bergerat, F. and Tourneret, C., 1990. Joint analysis of calcite twins and fault slips as a key for deciphering polyphase tectonics: Burgundy as a case study. *Tectonophysics*. 202, 83-93.

Lavreau, J., 1992. De-hazing Landsat Thematic mapper images. *Photogramm. Eng. Remote Sens*. 57, 1297-1302.

Leeder, M.R., Ord, D.M. and Collier, R.E.L., 1988. Development of alluvial fans and fan deltas in neotectonic settings: implications for the interpretation of basin fills. In: Nemec, W. and Steel, R.J (eds.) *Sedimentology and Tectonic settings*. 173-198.

Lips, A.L.W., 1998. Temporal constraints on the kinematics of the destabilization of an orogen; syn- to post-orogenic extensional collapse of the Northern Aegean region. Ph.D. Thesis, Utrecht University, the Netherlands. *Geologica Ultraiectina* No.166, 222p.

Lisle, R.J., 1987. Principal stress orientations from faults: an additional constraint, *Ann. Tecton*. 1, 155-158.

Lister G.S. Banga, G. and Feenstra, A., 1984. Metamorphic core complexes of Cordilleran type in the Cyclades, Aegean Sea, Greece. *Geology*. 12, 221-225.

LYNX 1997. http://www.lynxgeo.com/

Lynx Geosystems Co., 1997. Users Guide. Vancouver, Canada.

MacKenzie, D. 1972. Active tectonics of the Mediterranean region. *Geophys J. R. astr. Soc*. 30, 109-185.

Mandl, G., 1987. Discontinuous fault zones. *Jour. Struct. Geol*. 9,105-110.

Marret, R. and Almandinger, R.W., 1990. Kinematic analysis of fault slip data. *Jour. Struct. Geol*. 12, 973-986.

Marshak, S., 1988. Kinematics of orocline and arc formation in thin-skinned orogens. *Tectonics*. 7, 73-88.

McClay, K.R., 1989. Analogue models of inversion tectonics. In Cooper, M.A and Williams, G.D (eds.): *Inversion tectonics*. Spec. Publ. Geol. Soc. London 44. 41-62.

Means, W.D., 1976. *Stress and strain*. Springer, New York. 283p.

Means, W.D., 1987. A newly recognized type of slickenside striation. *Jour. Struct. Geol*. 9, 585-590.

Meijer, P. Th. 1995. Dynamics of active continental margins: the Andes and the Aegean region. Ph.D. Thesis, Utrecht University *Geologica Ultraiectina*: No. 130, 218p.

Mial, A.D., 1978, Fluvial Sedimentology, *Mem. Can. Soc. Petr. Geol*. 5, Calgary, 899p.

Mial, A.D., 1996. *The Geology of Fluvial Deposits*. Springer Verlag, New York. 586 p.

Michael, A.J.1984. Determination of stress from slip data: faults and folds. *J. Geophys. Res*. 89, 11.517-11.526.

Michel, G.W., Waldhőr, M. Neugebauer, J. and Appel, E., 1995. Squential rotation of stretching axes and block rotations: a structural and paleomagnetic study along the North Anatolian Fault. *Tectonophysics*. 243, 97-118.

243

Morris, A. and Robertson, A.H.F., 1993. Miocene remagnetisation of carbonate platform and Antalya Complex units within the Isparta Angle, SW Turkey. *Tectonophysics.* 220, 243-266.

Nemcok, M. and Lisle, R.J., 1995. A stress inversion procedure for polyphase fault/slip data sets. *Jour. Struct. Geol.* 17, 1445-1453.

Nemec, W., 1990. Deltas-remarks on terminology and classification. In: Colella, A. and Prior, D.B. (eds.) *Coarse-grained deltas.* Spec. Publ. Int. Ass. Sediment. 3-12.

Nieto-Samaniego, A.F. and Alaniz-Alvarez, J., 1997. Origin and tectonic interpretation of multiple fault paterns. *Tectonophysics.* 270, 197-206.

Norman T., 1972. Ankara doğusunda Yahşihan bőlgesinde Űst Kretase-Alt Tersiyer yaşlı arazinin jeolojisi. *MTA yayınları* Ankara, 169p.

North American Stratigraphic Code 1983. North American Commission on Stratigraphic Nomenclature. *AAPG.* 67/5, 841-875.

O`Leary, D.W., Friedman, J.D. and Pohn, H.A., 1976. Lineament, linear, lineation: some proposed new standards for old terms. *Bull. Geol. Soc. Am.* 87, 1463-1469.

Ocakoğlu, F. and Çiner, A., 1997. Fay denetimli bir havzada sedimanter dolgunun niteligi ve evrimi: Çankırı havzası kuzeyinden Lűtesiyen yaşlı bir őrnek. *Hacettepe Univ. Yerbilimleri.* 19, 89-108.

Okay, A.I. Harris, N.B.W. and Kelley, S.P., 1998. Exhumation of blueschists along a Tethyan suture in northwest Turkey. *Tectonophysics.* 284, 275-299.

Okay, A.I., 1984. Distribution and characteristics of the northwest Turkish blueschists, In: Dixon, J.E. and Robertson, A.H.F. (eds.), *The Geological Evolution of the Eastern Mediterranean*, Blackwell Sci. Publ., Oxford, London. 824p.

Okay, A.I., Satır, M., Maluski, H., Siyako, Monie, P., Metzger and R., Akyűz, S., 1996. Paleo- Neo-Tethyan events in northwest Turkey: geological and geochronological constraints. In Yin, A., Harrison, M. (eds.) *Tectonics of Asia.* Cambridge University Press, Cambridge. 420-441.

Okay, A.I., Şengőr, A.M.C. and Gőrűr, N., 1994. Kinematic history of the opening of the Black Sea and its effect on the surrounding regions. *Geology.* 22, 267-270.

Oktay, F.Y., 1973. *Sedimentary and tectonic history of the Ulukışla area, southern Turkey.* Univ. College, London, Ph.D. thesis, 414 p. (unpublished).

Oral, M. B., 1994. *Global Positioning System (GPS) Measurements in Turkey (1988-1992): Kinematics of the Africa-Arabia-Eurasia Plate Collision Zone.* Ph.D. thesis, Mass. Inst. Tech. 344 p.

Oral, M.B., Reilinger, R.E. Toksoz, M.N. King, R.W., Barka, A.A., Kinik, I. and Lenk, O., 1997. Global positioning system offers evidence of plate motions in Eastern Mediterranean. *EOS, Trans. Amm. Geophys. Union.* 76(2), 9-11.

Ori, G.G, and Friend, P.F., 1984. Sedimentary basins formed and carried piggyback on active thrust sheets. *Geology.* 12, 475-478.

Ozansoy, F., 1957. Tűrkiye Tersiyer memeli faunaları ve stratigrafik revizyonları. *MTA Dergisi.* 49, 11-22.

Özcan, A. Göncüoðlu, M. C., Turhan, N. Uysal, S., Şentürk, K. and Işık, A., 1990. Late Paleozoic evolution of the Kütahya-Bolkardað belt, *METU Jour. Pure Applied Sci.* 21, 211-220.

Őzçelik, Y. and Őztaş, Y. 2000. *Çankırı havzasının jeolojisi ve petrol olanakları.* (TPAO rap. In preparation).

Őzçelik, Y. and Savun, C., 1993. *İskilip-Osmancık-Çorum-Sungurlu arasındaki alanın jeolojisi ve petrol olanakları.* TPAO Rap. No. 3290 (unpublished).

Őzçelik, Y., 1994. *Tectono-stratigraphy of the Laçin area (Çorum-Turkey)* M.Sc. Thesis, METU. Geol. Eng. Dept. 133 p (unpublished).

Őzgűl, N., 1976. Torosların bazı temel jeolojik özellikleri. *TJK Bűlt. 19*, 65-78.

Park, R.G. and Jaroszwski, W., 1994. Craton tectonics, stress and seismicity. In Hancock, P.L. (ed.) *Continental Deformation.* Pergamon Press. 200-223.

Pasquare, G., Poli, S., Vezzoli, L. and Zanchi, A., 1988. Continental arc volcanism and tectonic setting in Central Anatolia, Turkey. *Tectonophysics.* 146, 217-230.

Petit, J-P. and Laville, E., 1985. Morphology and microstructure of hydroplastic slickensides in sandstone. Program. *Conference on Deformation Mechanisms in Sediments and Sedimentary Rocks. University college, London* (abstract).

Petit, J-P., Proust, F. and Tapponier, P., 1983. Criteres de sens de mouvement sur les miroires de failles en roches non calcaires. *Bull. Soc. Geol. Fr.* 7, XXV, 589-608.

Piper, J.D.A., Moore, J., Tatar, O., Gűrsoy, H. and Park, R.G., 1996. Paleomagnetic study of crustal deformation across an intracontinental transform: the North Anatolian Fault Zone in Northern Turkey. In: Morris, A. and Tarling, D.H. (eds.), *Paleomagnetism of the Eastern Mediterranean Regions.* Spec. Publ. Geol. Soc. London. 105, 299-310.

Platzman, E.S., Platt, J.P., Tapirdamaz, C., Sanver, M. and Bundle, C.C., 1994. Why are there no clockkwise rotations along the North Anatolian Fault. *J. Geophys. Res.* 99. 21.705-21.716.

244

Platzman, E.S., Tapirdamaz, C. and Sanver, M., 1998. Neogene anticlockwise rotation of central Anatolia (Turkey): Preliminary paleomagnetic and geochronological results. *Tectonophysics.* 299, 175-189.

Pollard, D.D., Saltzer, S.D. and Rubin, A.M., 1993. Stress inversion methods: are they based on faulty assumptions*?. Jour. Struct. Geol.* 15(8), 145-154.

Postma, G. and Roep, T.B., 1985. Resedimented conglomerates in the bottom set of a Gilbert-type gravel delta. *J. sedim. Petrol.* 55, 874-885.

Postma, G., 1983. Water escape structures in the context of depositional model of a mass-flow dominated conglomeratic fan delta (Abrioja Fromation, Pliocene, America basin, SE Spain). *Sedimentology.* 30,91-104.

Reading, H.G. and Collinson, J.D., 1996, Clastic coasts. In Reading, H.G. (ed.) *Sedimentary Environments: Process, Facies and Stratigraphy*. Blackwell Science, Oxford. 154-231.

Reading, H.G., 1996. Introduction. In: Reading, H.G.(ed.) *Sedimentary Environments: Process, Facies and Stratigraphy*. Blackwell Science, Oxford. 1-4.

Reches Z., 1987. Determination of the tectonic stress tensor from slip along faults that obey the Coloumb yield criterion. *Tectonics.* 6, 849-861.

Reches, Z. and Dieterich, J.H., 1983. Faulting in rocks in three dimensional strain fields I. Failure of rocks in polyaxial, servo-control experiments. *Tectonophysics.* 95, 111-132.

Reches, Z., 1978a. Analysis of faulting in three-dimensional strain field. *Tectonophysis,* 47, 109-129.

Reches, Z., 1978b. Faulting o f rocks in three-dimensional strain field-II, Theoretical analysis. *Tectonophysisc* 95, 133-156.

Richard, J.A., 1993. *Remote sensing digital image analysis, an introduction*. Springer Verlag, New York. 2nd Ed. 1-36.

Robertson, A.H.F. and Dixon, J.E., 1984. Introduction: aspects of the geological evolution of the Eastern Mediterranean 1-74. In:J.E.Dixon and A.H.F. Robertson (eds*.), The Geological Evolution of the Eastern Mediterranean*, Blackwell Sci. Publ., Oxford, London. 824p.

Robertson, A.H.F., Clift, P.D., Degnan, P. and Jones, G., 1991. Paleogeographic and paleotectonic evolution of the Eastern Mediterranean Neotethys. *Paleogeography, Paleoclimatology, Paleoecology.* 87, 289-344.

Robertson, A.H.F., Dixon, J.E., Brown, S., Collins, A., Morris, A., Pickett, E., Sharp, I. and Ustaomer, T., 1996. Alternative tectonic models for the Late Paleozoic-Early Tertiary development of the tethys in the Eastern Mediterranean region. In: A. Morris and D.H. Tarling (eds*.), Paleomagnetism of the Eastern Mediterranean Regions*. Spec. Publ. Geol. Soc. London. 105, 239-263.

Rőgl, F. and Steininger, F.F., 1984. Neogene Paratethys, Mediterranean and Indo-pacific Seaways. In: Brenchley, P. (ed.) *Fossils and Climate*. John Wiley and Sons Ltd. 171-200.

Rojay, B., 1993. *Tectonostratigraphy and neotectonic characteristics of the southern margin of Merzifon-Suluova basin (Central Pontides, Amasya)*, Ph.D. Thesis, METU Geol. Eng. Dept. 215 p (unpublished)

Rojay, B.F. and Gőncűoğlu, M.C., 1997. Tectonic setting of some pre-Liassic low grade metamorphics in Northern Anatolia. *Hacettepe Univ. Yerbilimleri.* 19, 109-118.

Rojay, B.F., 1995. Post-Triassic evolution of central Pontides: Evidence from Amasya region, Northern Anatolia. *Geologica Romana.* 31, 329-350.

Rojay, B.F., Yalınız, K. and Altıner, D., 1998. Age and origin of some pillow basalts from Ankara melange and their tectonic implications to the evolution of northern branch of Neotethys, Central Anatolia. *IESCA-95*, Izmir, 46-47.

Sanderson, D.J. and Marchini, W.R.D., 1984. Transpression. Jour. Struct. Geol. 6, 449-458.

Saner, S., 1980.Paleogeographic interpretation of the Jurassic and younger sediments of the Mudurnu-Gőynűk Basin based on the depositional features of Jurassic and younger ages. *Tűrkiye Jeoloji Kurumu Bűlt.* 23, 39-52.

Sanver, M. and Ponat, E., 1981. Kirsehir ve dolaylarina iliskin paleomagnetik bulgular. Kirsehir Masifinin rotasyonu. *İstanbul Yerbilimleri.* 2, 2-8.

Saribudak, M., Sanver, M. Sengor, A.M.C. and Görűr, N., 1990. Paleomagnetic evidence for substantial rotation of the Elmacik flake within the North Anatolian Fault Zone, NW Turkey. *Geophys. J. Int.* 102, 563-568.

Şaroğlu, F., 1988. Age and off-set of the North Anatolian Fault. *METU, Jour. Pure Appl. Sci.* 21(1-3), 65-79.

Seagal, P. and Pollard, D.D., 1980. Mecahanics of discontinuous faulting. *J. Geophys. Res.* 85, 4337-4350.

Şen, Ş, Seyitoğlu, G., Karadenizli, L., Kazancı, N., Varol, B. and Araz, H., 1998. Mammalian biochronology of Neogene deposits and its correlation with the litthostratigraphy in the Çankırı-Çorum Basin. *Eclogae. Geol. Helv.* 91, 307-320.

Şengőr, A.M.C. and Barka, A.A., 1992. Evolution of escape-related strike-slip systems: implications for disruption of collisional orogens (abstract). 29th

International Geological Congress, Kyoto, Japan, 232 (abstract).

Şengör, A.M.C. and Yilmaz, Y., 1981. "Tethyan evolution of Turkey: a plate tectonic approach", *Tectonophysics.* 75, 181-241.

Şengőr, A.M.C. Yılmaz, Y. and Sungurlu, O., 1984. Tectonics of the Mediterranean Cimmerides: nature and evolution of the western termination of palaeo-Tethys. In: Dixon, J.E. and Robertson, A.H.F. (eds.) *The Geological Evolution of the Eastern Mediterranean.* Geol. Soc. London Spec. Publ. No.17. 77-112.

Şengör, A.M.C., 1982. *Tűrkiye'nin neotektoniğinin esasları.* TJK. Konferans serisi. No. 2, 40 p.

Şengör, A.M.C., Şaroğlu, F. and Gőrűr, N., 1985. "Strike-slip deformation and related basin formation in zones of tectonic escape: Turkey as acase study", In: Biddle, K.T. and Christie-Blick, N. (eds.) *Strike-Slip Deformation Basin Formation and Sedimentation.* Society of Econ. Palaeo. and Miner. Spec. Publ. No. 37, 227-264.

Şenyűrek, M.S., 1960. Ankara Üniversitesinde muhafaza edilen fosil fil kalıntılarına dair bir not. *Belleten*, XXIV, 96.

Seyitoğlu, G., Scot, B. and Rundle, C., 1992. Timing of Cenozoic extensional tectonics in West Turkey. *Jour. Geol Soc.* London. 149, 533-538.

Seymen, I., 1981. Kaman (Kirsehir) dolayinda Kirsehir Masifinin metamorfizmasi. *Tűrk. Jeol. Kur İc Anadolunun Jeolojisi Sempozyumu*, Ankara. 12-16.

Seymen, I., 1982. *Kaman dolayinda Kirsehir Masifinin Jeolojisi.* İ.T.Ű. Maden Fak. Docentlik Tezi. 164 p.

Soha, J.M. and Schwartz, A.A., 1978. Multispectral histogram normalization contrast enhancement, proc. *5th Canadian Symposium on Remote Sensing.* Victoria, BC. Canada, 86-93.

Spakman, W., Wortel, M.J.R. and Vlaar, N.J. 1988. The Helenic subduction zone: a tomographic image and its geodynamic implications. *Geophys. Res. Lett.*, 15, 60-63.

Steininger, F.F., 1999. The continental European Miocene: Chronostratigraphy, Geochronology and Biochronology of the Miocene "European Land mammals Mega-Zones" (ELMMZ) and the Miocene "Mammal-Zones(MN-Zones)". In: Steinger, F.F. (ed.), *The Miocene Land Mammals of Europe* 9-24.

Steininger, F.F., Berggren, W.A., Kent, D.V., Bernor, R.L., Şen, Ş. and Agusti, J., 1996. Circum-Mediterranean Neogene (Miocene and Pliocene) Marine-Continental Chronologic Correlations of European Mammal Units. In: Bemor, R.L., Fahlbusch, V. and Mittmann, H.W. (eds.) *The Evolution of western Eurasian Mammal*

Funas. Columbia Univ. Press, New York, Chichester, West Sussex.

Sylvester, A.G., 1988. Strike-slip faults. *Bull. Geol. Soc. Am.* 100. 1666-1703.

Talbot, M.R. and Allen, P.A., 1996. Lakes. In Reading, H.G. (ed*.) Sedimentary environments: Process, Facies, Stratigraphy.* Blackwell Science Ltd. Oxford. 83-124.

Tankut, A. and Tűrkmenoğlu, A., 1988. Incompatible trace element composition of Neogene mafic lavas around Ankara. *METU, Jour. Pure Appl. Sci.* 21,501-521.

Tankut, A., Satır, M., Gűleç, N. and Toprak, V., 1995. *Galatya volkaniklerinin petrojenezi*: Ankara, TUBITAK, Project No. YBAG-0059 (unpublished).

Tapponier, P., Peltzer, G., Le Dain, A.Y., Armijo, R. and Cobbold, P., 1982. Propagating extrusion tectonics in Asia: new insights from simple experiments with plasticine. *Geology* 10,611-616.

Tarling, D.H. and Hrouda, F., 1993. *The magnetic anisotropy of rocks.* Chapman and Hall, London. 217 p.

Tatar, O., Piper, J.D.A., Park, R.G. and Gűrsoy, H., 1995. Paleomagnetic study of block rotations in the Niksar overlap region of the North Anatolian Fault Zone, Central Turkey. *Tectonophysics* 244, 251-266.

Taylor, M.M., 1974. Principal components color display of ERTS imagery. *Third Earth Resources Technology Satellite-1 Symposium, National Aeronautics and Space Administration.* Special Publication No. 351(1), 1877-1897.

Tekeli, O., Aksay, A., Űrgűn, B., ve Işık, A., 1984. Geology of the Aladağ Mountains. *Geology of Taurides Symp.* 143-158.

Tekkaya, İ, Atalay, Z., Gűrbűz, M., Űnay, E., ve Ermumcu, M., 1975. Çankırı-Kalecik bőlgesi karasal Neojeninin biyostratigrafi araştırması. *TJK Bűlt.* 18, 77-80.

Toprak, V. and Gőncűoğlu, C., 1993. Tectonic control on the development of the Neogene-Quaternary Central Anatolian Volcanic Province, Turkey. *Geological Jour.* 28, 357-369.

Toprak, V., Savaşçın, Y., Gűleç, N. and Tankut, A., 1996. Structure of the Galatean Volcanic Province, Turkey. *International Geol. Rev.* 38, 747-758.

Treagus, S.H. and Lisle, R., 1997. Do principal surfaces of stress and strain always exist?. *Jour. Struct. Geol.* 19, 997-1010.

Tűrkecan, A., Hepşen, N., Papak, I., Akbaş, B., Dinçel, A., Karataş, S., Özgűr, I., Akay, E., Bedi, Y., Sevin, M., Mutlu, G., Sevin, D., Űnay, D. and Saraç, G., 1991. Seben-Gerede (Bolu), Gűdűl-Beypazarı (Ankara) ve Çerkes-Orta-Kurşunlu (Çankırı) yőrelerinin (Kőrőğlu

246

Dağları) jeolojisi ve volkanik kayaçların petrolojisi, Ankara. *MTA Rap. No.* 9193 (unpublished).

Tűysűz, O. and Dellaloğlu, A.A., 1992. Çankırı Havzasının Tektonik birlikleri ve jeolojik evrimi. *Tűrkiye 9. Petrol Kongresi Kitabı (extended abstract).*

Tűysűz, O., 1985. *Kargı Masifi ve dolayındaki tektonik birliklerin ayırdı ve araştırılması (petrolojik inceleme).* Istanbul Univ. Jeoloji Műh. Ből. Doktora Tezi. 431p.

Tűysűz, O., 1990. Tectonic evolution of a part of the tethyside orogenic collage: The Kargı Massif, Northern Turkey. *Tectonics* 9,141-160.

Tűysűz, O., 1993. Karadenizden Orta Anadolu'ya bir jeotravers. *TPJD Bult.* 5(1), 1-33.

Tűysűz, O., Dellaloglu, A.A. and Terzioglu, N., 1995. A magmatic belt within the Neo-Tethyan suture zone and its role in the tectonic evolution of northern Turkey. *Tectonophysics.* 243, 173-191.

Tűysűz, O., Yiğitbaş, E., Serdar, H.S. Gűrpınar, O., 1989. *Orta Pontidlerin gűney kesiminin jeolojisi.* TPAO Rap. No. 2596 (unpublished).

Twiss, R.J. and Unruh, J.R., 1998. Analysis of fault slip inversion; do they constrain stress or strain rate? *J. Geophys. Res.* 103,B6, 12205-12222.

Ünalan, G., 1982. stratigraphy of Ankara mélange (SW) Ankara. *In symposium on Geology of Central Anatolia. Ankara, Turkey.* Proceedings. 46-52.

Űnay, E., 1994. Early Miocene rodent faunas from eastern Mediterranean area. Part IV. The Gliridae. *Proc. Kon. Neder. Akad. Wetensch.* Amsterdam. B 97, 445-490.

Van der Voo, R. and Channel, J.E.T., 1980. Paleomagnetism in orogenic belts, *Rev. Geophys.* 18, 455-481.

Van der Voo, R., 1968. Paleomagnetism and the Alpine tectonics of Eurasia, part 4. Jurassic, Cretaceous and Eocene pole positions from NE Turkey. *Tectonophysics.* 6, 251-269.

Varnes, D.J., 1962. Analysis of plastic deformation according to Von Mises' theory with application to the south Silverton area, San Juan County, Colorado. *U.S. Geol. Surv. Prof. Pap.* 378-B: 49p.

Walcott, C.R., 1998. The Alpine evolution of the Thessaly (NW Greece) and late Tertiary kinematics. . Ph.D. thesis, Utrecht University, the Netherlands, *Geologica Ultraiectina* No.162, 176 p.

Walker, R.G. and James, N.P., 1992. *Facies Models: Response to Sea-level Change.* Geol. Ass. Can. Waterloo, Ontario. 238 p.

Wallace, R.E., 1951. Geometry of shearing stress and relation to faulting. *Jour. Geol.* 69, 118-130.

Whitney, D.L. and Dilek, Y., 1997. Core complex development in central Anatolia, Turkey. *Geology.* 25(11), 1023-1026.

Will, T.M. and Powell, R., 1991. A robust approach to the calculation of paleostress fields from fault plane data. *Jour. Struct. Geol.* 13, 813-821.

Wojtal, S. and Pershing, J., 1991. Paleostress associated with faults of large offset. *Jour. Struct. Geol.* 13, 49-62.

Wortel, M.J.R. and Spakman, W., 1992. Structure and dynamics of subducted lithosphere in the Mediterranean region. *Proc. KNAW.* 95, 325-347.

Wright, V.P. and Burchette, T.P., 1996. Shallow-water carbonate environments. In: Reading, H.G. (ed.) *Sedimentary Environments: Process, Facies and Stratigraphy.* Blackwell Science, Oxford. 325-394

Yalınız, K., 1995. *Geochemistry and tectonic setting of Sarıkaraman ophiolite, central Anatolia, Turkey.* Ph.D. Thesis, METU, Geol. Eng. Dept. 174 p. (unpublished).

Yalınız, M.K. Floyd, P.A. and Göncüoğlu, M.C., 1996. Supra-subduction zone ophiolites of Central Anatolia: Geochemical evidence from the Sarıkaraman Ophiolite, Aksaray, Turkey. *Mineral. Mag.* 60, 697-710.

Yin, Z.M. and Ranalli, G., 1993. Determination of tectonic stress field from fault slip data, toward a probabilistic model. *J. Geophys. Res.* 98,12165-12176.

Yoldaş, R., 1982. *Tosya (Kastamonu) ile Bayat (Çorum) arasındaki bőlgenin jeolojisi.* Doktora Tezi. Istanbul Univ. Fen. Fak. Genel Jeoloji Kűrsűsű.

Zijderveld, J.D.A., 1967. Demagnetisation of rock: analysis of results. In: D.W., Creer, K.M. and Runcorn, S.K. (eds), *Methods in paleomagnetism,* Elsevier, Amsterdam. 254-286.

Zweigel, P., 1998. Arcuate accretionary wedge formation at convex plate margin corners: results of sandbox analogue experiments. *Jour. Struct. Geol.* 20, 1597-1609.

247